MODELING, SIMULATION AND OPTIMIZATION OF SOLAR POWER GENERATION AND TRANSMISSION IN UGANDA

A Thesis

Submitted to the Directorate

of Higher Degrees and Research

Kampala International University

Kampala Uganda

In partial fulfilments of the requirements for the degree of
Doctor of Philosophy in Science Renewable Energy

By
Ounyesiga Living
2020-08-01254

BSc. Physics and Mathematics, MSc. Physics

April 2024

DECLARATION (A)

I, Living Ounyesiga declare that this thesis entitled 'Modeling, Simulation and Optimization of Solar Power Generation and Transmission in Uganda' is my original work under the guidance of my supervisors and has not been presented for a degree or any other academic award in any University or Institution of higher learning.

Signature: **Date:**



17/04/2024

……

OUNYESIGA LIVING

2020-08-01254

DECLARATION (B)

We confirm that the work reported in this Proposal was carried out by the candidate under our supervision as the university supervisors

Supervisor I

Signature



17/07/24

Eng. Associate professor Stephen Ndubuisi NNAMCHI **DATE**

Supervisor II

Signature



17/03/24

Associate professor Ukagwu KELECHI **DATE**

Supervisor III

Signature



17/03/2024

Dr. Mundu M. MUSTAFA **DATE**

Supervisor IV

Signature

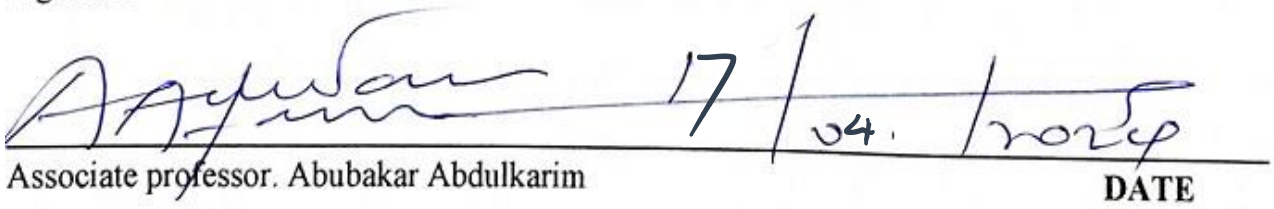

Associate professor. Abubakar Abdulkarim **DATE**

DEDICATION

I dedicate this thesis to my incredibly supportive and encouraging family, which includes my mother, father, wife, children, and siblings. They supported me during my whole PhD program and immensely contributed to the person I am today.

ACKNOWLEDGEMENT

My sincere gratitude goes to the Almighty God for the knowledge, wisdom, guidance and protection rendered to me. He is really worth to be praised and given thanks because with him all things are possible. In a special way, I would like to thank the Chairman, Board of Trustees of Kampala International University Hon. Dr. Alhajji Hassan Basajjabalaba for granting me the sponsorship for the PhD programme. I'm really indebted to Associate professor. Eng. Dr. Stephen Ndubuisi Nnamchi under whose guidance and direction this study was carried out. His encouragement was a great spring of insights and incentive for me and I'm extremely appreciative for his unwavering service, submissions, feedback, ideas, and advice throughout my thesis work. I further greatly appreciate his pragmatism and insightful intelligence, and I have found it enjoyable working with him. To my co-supervisors: Associate professor. Dr. John Ukwagu Kelechi, Dr. Mundu Mustafa M, Associate professor Abubakar Abdulkarim thank you too for steering me from the early stages of problem formulation to the illumination and careful presentation of concepts in this thesis. I am thankful to all my doctoral colleagues, more specially; Omuna Daniel who provided assistance and encouragement during my outstation study trips. I would also like to thank all the Doctoral Committee Members especially Abubakar Abdulkarim, for their helpful contribution in my research work. I would also like to greatly appreciate the. Associate professor Hanington Twinomuhwezi Dean School of Natural asnd Applied Sciences (SONAS), Dr. Mpezamihigo Mouhamad, Vice Chancellor and Prof. Janice Busingye Deputy Vice Chancellor Finance and administration, Bright Masereka , Diana Nakabugo, Rachel Arinda, Job Kahororo, Daniel Emmanuel Okello, Justin Ocom, Dennis Okot and Managing Director Uganda Electricity Transmission Company Limited (UETCL), and the Directorate of Higher Degrees and Research (DHDR) western campus team for their support and assistance throughout my time at Post Graduate (PG) for the doctoral programme, My special appreciation and gratitude go to professor Kabwegyere Tarsis Bazana and his family for the concrete foundation they laid for me and their inspiration in my academic career To all my colleagues and workmates, the Departmental exam coordinators (DECs), Teaching and Learning coordinators (TLCs), Heads of Department (HODs) past and present in the School of Engineering and Applied Sciences. May God reward you all

TABLE OF CONTENTS

DECLARATION (A) i

DECLARATION (B) ii

DEDICATION iii

ACKNOWLEDGEMENT iv

LIST OF FIGURES xiii

NOMENCLATURE xvi

LIST OF ACRONYMS xviii

LIST OF PUBLICATION xx

ABSTRACT xxi

CHAPTER ONE 1

INTRODUCTION 1

1.0 Introduction. 1

1.1 Background of the study 1

1.1.1 Historical Perspective 2

1.1.2 Theoretical Perspective 4

1.1.2.1 Solar power generation 4

1.1.2.2 Electric power transmission 6

1.1.3 Conceptual Perspective 7

1.1.3.1 Transmission line losses modeling 7

1.1.3.2 Corona and Ohmic losses. 8

1.1.3.3 Coupling of power potentials in transmission line models. 8

1.1.3.4 Degradation constant. 9

1.1.3.5 Solar power generation models 9

1.1.4 Contextual Perspective 9

1.2 Statement of Problem 10
1.3 Objective of the Study 11
1.3.1 General Objective 11
1.3.2 Specific Objectives 11
1.4 Research Question 11
1.5 Significance of the study 12
1.6 Scope of the Study 13
1.6.1 Geographical Scope 13
1.6.2 Content Scope 13
1.6.3 Time scope 13
1.7 Justification of the study 14
1.7.1 Environmental Sustainability: 14
1.7.2 Contribution to knowledge creation. 14
1.7.3 Economic impact. 14
1.7.4 Social implication. 14
CHAPTER TWO 15
LITERATURE REVIEW 15
2.0 Introduction 15
2.1 Conceptual framework 15
2.2 Review of related literature on specific objectives 16
2.2.1 Minimization of electric power losses in transmission lines 16
2.2.2 Modeling of coupled and uncoupled transmission lines 18
2.2.3 Differential and empirical modelling of solar power generation. 20
2.3 Research Gaps in Literature Review 21
2.3.1 Minimization of electric power losses in transmission lines 22

2.3.2 Modeling of coupled and uncoupled transmission lines. 22
2.3.3 Differential and empirical modelling of solar power generation. 23
2.4 History on available solar power plants in Uganda 23
2.4.1 Soroti solar Power station 24
2.4.2 Tororo power station 25
2.4.3 Mayuge solar power plant 26
2.4.4 Busitema solar power plant 27
2.5 Literature on the Equipment 28
2.5.1 Digital Solar power meter 28
2.5.2 Digital thermocouple 29
2.5.3 An anemometer 30
2.5.4 Digital multimeter 31
CHAPTER THREE 33
METHODOLOGY 33
3.0 Introduction 33
3.1 Study area 33
3.2 Research Philosophy 36
3.3 Research Methods 37
3.3.1 Minimization of electric power losses in transmission lines 37
3.3.1.1 Description of the algorithm 37
3.3.1.2 Formulation of power losses in transmission lines 38
3.3.1.3 Proof of optimality of the objective function-transmission losses 40
3.3.1.4 Derivatives of the Hessian matrix 41
3.3.1.5 Upper diagonal elements of Hessian matrix 41
3.3.1.6 Lower diagonal elements of Hessian matrix 42

3.3.2 Modeling of coupled and uncoupled transmission lines 45
3.3.2.1 Introduction 45
3.3.2.2 Description of flow chart for analysis of Bujjagali-Kawanda transmission line. 45
3.3.2.3 Model formulation 47
3.3.2.4 Coupling of transmission models 49
3.3.2.5 Boundary conditions 49
3.3.2.6 Initial conditions 50
3.3.2.7 Numerical Solution of Dimension Equations 50
3.3.2.8 Thermal properties of Air 52
3.3.2.9 Thermal properties of the transmission lines 53
3.3.3 Development of differential and empirical solar power generation models. 54
3.3.3.1 Model formulation 55
3.3.3.2 The Navier Stokes Equation 56
3.3.3.3 The Navier Stokes Equation for solar power generation 57
3.3.3.4 The Modified Navier Stokes Equation for solar power generation 57
3.3.3.5 The numerical solution 59
3.3.3.6 The boundary conditions (BC) 60
3.3.3.7 Initial condition 62
3.3.3.8 Empirical Solar power generation 62
3.3.3.9 Thermophysical properties of air 63
3.3.3.10 Error analysis and validation 63
3.3.3.11 Description of the algorithm 64
3.3.3.12 Experimentation 66
3.4 Sources of data 66
3.5 Data Collection Instruments 67

3.7 Data Collection procedure 67
3.8 Data Analysis Techniques 67
CHAPTER FOUR 69
RESULTS AND DISCUSSION 69
4.0 Introduction 69
4.1 Presentation of Results 69
4.1.1 Minimization of electric power losses in transmission lines 69
4.1.2 Modeling of coupled and uncoupled transmission lines 78
4.1.3 Development of differential and empirical solar power generation models. 87
4.2 Discussion of results basing on the specific objectives 96
4.2.1 Minimization of electric power losses in transmission lines 96
4.2.1.1 Unmodified and modified power transmission models 96
4.2.1.2 Discussion of power losses in the transmission lines 97
4.2.1.3 Optimality test 98
4.2.2 Modeling of coupled and uncoupled transmission lines 99
4.2.2.1 Simulation of transmission potentials 99
4.2.2.2 Space potentials 99
4.2.2.3 Time potentials 99
4.2.2.4 Estimation of power and power losses in transmission line 100
4.2.2.5 Validation of transmission potentials 100
4.2.2.6 Application of results 101
4.2.3 Development of differential and empirical solar power generation models. 101
4.2.3.1 Development differential models for solar power generation 101
4.2.3.2 Development of empirical models for solar power generation 102
4.2.3.3 Applications of the developed models 103

CHAPTER FIVE 104

SUMMARY, CONCLUSIONS AND RECOMMENDATIONS 104

5.0 Summary 104

5.1 Conclusions 104

5.1.1 Minimization of electric power losses in transmission lines 104

5.1.2 Modeling of coupled and uncoupled transmission lines 104

5.1.3 Development of differential and empirical solar power generation models. 105

5.2. Recommendations 106

5.2.1 Minimization of electric power losses in transmission lines 106

5.2.2 Modeling of coupled and uncoupled transmission lines 106

5.2.3 Development of differential and empirical solar power generation models. 107

5.2 Contributions to Knowledge 108

5.5 Prospects for Future Research 108

References 110

APPENDICES APPENDIX I: INTRODUCTION LETTER FROM DIRECTOR HIGHER DEGREES AND RESEARCH FOR FIELD DATA COLLECTION AT UGANDA ELECTRICITY TRANSMISSION COMPANY LIMITED 124

APPENDIX II: ACKNOWLEDGMENT OF RECIEPT OF ALLOWANCE LETTER BY UGANDA ELECTRICITY TRANSMISSION COMPANY LIMITED 125

APPENDIX III: PERMISSION LETTER BY TO COLLECT DATA FROM UGANDA ELECTRICITY TRANSMISSION COMPANY LIMITED 126

APPENDIX IV: INTRODUCTION LETTER FROM DIRECTOR HIGHER DEGREES AND RESEARCH FOR EXPERIMENTAL SET UP AND DATA COLLECTION AT BUSITEMA SOLAR POWER STATION 127

APPENDIX V: INTRODUCTION LETTER FROM DIRECTOR HIGHER DEGREES AND RESEARCH FOR EXPERIMENTAL SET UP AND DATA COLLECTION AT MAYUGE SOLAR POWER STATION 128

APPENDIX VI: INTRODUCTION LETTER FROM DIRECTOR HIGHER DEGREES AND RESEARCH FOR EXPERIMENTAL SET UP AND DATA COLLECTION AT SROTI SOLAR POWER STATION 129

APPENDIX VII: INTRODUCTION LETTER FROM DIRECTOR HIGHER DEGREES AND RESEARCH FOR EXPERIMENTAL SET UP AND DATA COLLECTION AT TORORO SOLAR POWER STATION 130

APPENDIX VIII: AVERAGE DAILY EXPERIMENTAL VALUES (215 DAYS) 131

APPENDIX X: EXPERIMENTAL ASSESSMENT PHOTOGRAPHS 189

LIST OF TABLES

Table 2.1 Design capacity of solar plants in Easter Region of Uganda..... 23
Table 4.1 Input data for the optimization of power losses in the transmission lines (UETCL, 2022) 76
Table 4.2 Optimization results of power losses in the transmission lines based on modified and unmodified models..... 76
Table 4.3 Optimality tests based on the Hessian matrix in Equation (3.8)..... 77
Table 4.4 Input data for system simulation..... 84
Table 4.5 Statistical validation of coupled transmission model 86
Table 4.6 Empirical power generation coefficients. 87
Table 4.7 Coefficients of boundary conditions. 88
Table 4.8 Statistical description of the experimental data. 88
Table 4.9 Validation of simulated with the empirical solar power generation. 89
Table 4.10 Validation of solar power design capacity with the empirical solar power generation. 90

LIST OF FIGURES

Figure 1.1: The Solar Cell's Operating Principle 5
Figure 2.1: Conceptual Framework 15
Figure 2.2: Soroti PV Power Plant 25
Figure 2.3: Tororo power station 26
Figure 2.4: Mayuge solar power plant 27
Figure 2.5: Busitema solar power plant 28
Figure 2.6: The snapshot (left) and photograph (right) of digital solar power meter. 29
Figure 2.7: The snapshot of 6802 Ii Durable Precision Dual Channel Digital Thermometer with 2 K-ty 30
Figure 2.8: The snapshot diagram of digital an anemometer. (Zhang et al., 2022) 31
Figure 2.9: The snapshot diagram of digital Multimeter (Asadi & Eguchi, 2020) 31
Figure 3.3: Map of the study area (Masaka West - Mbarara North) and the transmission lines .. 34
Figure 3.2: Map of the study area (Bujagali - Kawanda) and the transmission lines 35
Figure 3.3: Solar power plants in eastern Region 36
Figure 3.4: Flowchart for the minimization of power losses in the transmission lines Source: Present study (2023) 38
Figure 3.5: Flowchart for data acquisition and processing in coupled model. 46
Figure 3.6: Transmission line control volume 47
Figure 3.9 Experimental set up 66
Figure. 4.1 Power losses in Bujagali – Kawanda transmission line. 70
Figure 4.2 Power losses in Masaka West - Mbarara North transmission line. 71
Figure 4.3 Power losses in Bujagali – Kawanda transmission line. 71
Figure 4.4 Power losses in Masaka West - Mbarara North transmission line. 72
Figure 4.6 Power losses in Masaka West - Mbarara North transmission line as a function of air density. 73
Figure 4.7a. Unmodified 3-D plot of power losses for 220 kV Bujagali-Kawana transmission line 74
Figure 4.7b. Modified 3-D plot of power losses on 220 kV Bujagali-Kawana transmission line 74
Figure 4.8a. Unmodified 3-D plot of power losses for 132 kV Masaka West-Mbarara North transmission line 75

Figure 4.8b. Modified 3-D plot of power losses for 132 kV Masaka West-Mbarara North transmission line 75
Figure 4.9 Current in the Bujjagali-Kawanda transmission line based on the coupled power model..... 79
Figure 4.10 Voltage in the Bujjagali-Kawanda transmission line based on the coupled power model..... 79
Figure 4.11 Temperature in the Bujjagali-Kawanda transmission line based on the coupled power model..... 80
Figure 4.12. Power in the Bujjagali-Kawanda transmission line based on the coupled power model..... 80
Figure 4.13. Historic current in the Bujjagali-Kawanda transmission line based on the coupled power model..... 81
Figure 4.14. Historic voltage in the Bujjagali-Kawanda transmission line based on the coupled power model..... 81
Figure 4.15. Historic temperature in the Bujjagali-Kawanda transmission line based on the coupled power model..... 82
Figure 4.16. Historic power in the Bujjagali-Kawanda transmission line based on the coupled power model..... 82
Figure 4.17. Power and power losses Bujjagali-Kawanda transmission line 83
Figure 4.18 Historic deviation or error in variables (current, voltage and power) 84
Figure 4.19 Solar power generation (W) based on the first order generation model Source: Present study (2023) 91
Figure 4.20 Solar power generation (W) based on the second order generation model **Source:**
Figure 4.21 Empirical solar power generation at Busitema study area 93
Figure 4.22 Empirical solar power generation at Tororo study area 94
Figure 4.23 Empirical solar power generation at Soroti study area..... 94
Figure 4.24 Empirical solar power generation at Mayuge study area 94
Figure 4.25 Empirical solar power generation based on first model for Eastern region of Uganda 95
Figure 4.26 Empirical solar power generation based on second model for Eastern region of Uganda 95

Figure 4.27 Empirical solar power generation based on third model for Eastern region of Uganda 96

NOMENCLATURE

Physical Quantity	Symbol	Dimension (s)	Unit (s)
Phase voltage	V	$ML^2T^{-3}I^{-1}$	V
Nominal voltage	V_m	$ML^2T^{-3}I^{-1}$	V
Transmission current	I	$M^0L^0T^{-1}Q$	A
Thermal resistivity	ρ	$M^{-1}L^{-2}T^3K$	°K-m/W
Disruptive voltage	V_0	$ML^2T^{-3}I^{-1}$	V
Transmission frequency	f	$M^0L^0T^{-1}$	Hz
Air density	γ	M^1L^{-3}	kgm^{-3}
Length of transmission line	L	M^0L	m
Radius of transmission cable	R	M^0L	m
Spacing between the transmission cables	D	M^0L	m
Cross-section area	A	M^0L^2	m^2
Temperature	T	$M^0\ L^0\ T^0K^1$	
Circuit length	l_m	L	m
Power	p_m	$M\ L^2\ T^{-3}$	W
Specific heat capacity of the transmission line	cp	$M^0L^2\ T^{-2}K^{-1}$	cp
Wind speed	U	$M^0\ L^1T^{-1}$	ms^{-1}
Ambient temperature	T_a	$M^0L^0T^0K^1$	K
Cell temperature	T_c	$M^0L^0T^0K^1$	K
Irradiance	H	ML^2T^{-1}	Wm^{-2}
Solar power simulated,	P_{sim}	ML^2T^{-3}	W
Solar power generated	P_{gen}	ML^2T^{-1}	W
Solar power at standard test condition	P_{stc}	ML^2T^{-1}	W
Latitude of the coordinates	ϕ_i	L	m
Longitude of the coordinates	λ_i	L	m
Radius of transmission cable (m)	r	L	m
Spacing between the transmission cables (m)	d	L	m
Number of solar panels	N_p	$M^0L^0T^0$	(-)
The thermal conductivity	k	$M^1\ L^1\ T^{-3}K^{-1}$	W/m·K

Heat transfer coefficient of the surrounding air	h	$M^1L^2\ K^{-3}$	W/m²K
Thermal aging/ deterioration constant	k_T	$M^0L^0T^0$	(-)
Electrical diffusivity	D_e	$M^{-1}L^{-3}\ K^3A^2$	m^2/s
Voltage aging	k_V	$ML^2T^{-3}I^{-1}$	V
The resistivity of the transmission line	σ	$M^0L^0T^{-1}$	Hz
Current aging	k_I	$M^0L^0T^{-1}Q$	A
Coupling coefficients of temperature	β_T	$M^0L^0T^0$	(-)
Efficiency of solar cell	η	$M^0L^0T^0$	(-)
Number of solar panels	N_p	$M^0L^0T^0$	(-)
Power coupling coefficients	a_H	$M\ L^2\ T^{-3}$	W
Kinematic viscosity	ν	$L^2\ T^{-1}$	m^2/s

LIST OF ACRONYMS

ABC	Artificial Bee Colony
AfDB	African Development Bank
ANN	Artificial Neural Network
BC	Boundary Conditions
B-K	Bujagali-Kawanda
CABC	Chaotic Artificial Bee Colony
CdTe	Cadmium telluride
CIGS	Copper indium gallium selenide
CSP	Concentrated solar power
CTNM	Conductor thermal network model
DC	Direct Current
ERA	Electricity Regulatory Authority.
EU	European Union
FACTS	Flexible Alternating Current Transmission Systems
HVDC	high voltage direct current
IPSO	Improved Particle Swarm Optimization
JREC	Japan Renewable Energy Consumption
MLR	Multiple Linear Regression
MPPT	Maximum Power Point Tracking
MW-MN	Masaka West-Mbarara North
NASA	National Aeronautics and Space Administration
NOCT	Nominal Operating Cell Temperature,
PSO	Particle Swarm Optimization
PV	Photovoltaic
PWM	Pulse Width Modulation
RMSE	Root Mean Square Error
SDGs	Sustainable Development Goals
SSA	Salp Swarm Algorithm
TCSCs	Thyristor-Controlled Series Compensators
TLBO	Teaching Learning Based Optimization Algorithm

TML	Transmission line model
UETCL	Electricity Transmission Company Limited
UNMA	Uganda National Meteorological Authority
UPFCs	Unified Power Flows Controllers

LIST OF PUBLICATION

1. Living, O., Nnamchi, S. N., Mundu, M. M., Ukagwu, K. J., & Abdulkarim, A. (2024). Coupled modelling and simulation of power transmission lines: A systematic analysis of line losses. *Electric Power Systems Research*, *226*, 109954.

2. Living, O., Nnamchi, S. N., Ukagwu, K. J., Abdulkarim, A., & Jagun, Z. O. (2023). Minimization of Electric Power Losses on 132 kV and 220 kV Uganda Electricity Transmission Lines. *Energy and Power Engineering*, *15*(02), 127-150.

3. Modelling and simulation of solar power generation: New developments in design and operational models (Under review Elsevier Heliyon Science direct)

ABSTRACT

This study addresses key challenges in the optimization and modeling of power systems, encompassing three main areas. Firstly, it analyses the traditional minimization of power losses in transmission lines, dominated by artificial intelligence techniques that lack a guarantee of global optimum. The gradient technique was introduced to efficiently minimize power losses by modifying the traditional power loss model. Empirical validation on specific transmission lines in Uganda demonstrates the superiority of the modified model in minimizing power losses. Secondly, this study highlights the dominance of lumped models in transmission systems, lacking space considerations and hindering the simulation of transmission losses. To address this, a proposed distributed or coupled system of thermal and power equations, accounting for both space and time was validated through simulations and empirical data from the Bujjagali - Kawanda transmission line. Lastly, the research focuses on the alarming underperformance (about 35%) in solar power generation in eastern Uganda, attributing it to the absence of extrinsic factors in the nominal cell operating temperature (NOCT) model. The study empirically introduced the missing factors and develops a mathematical model of second-order differential with empirical solar power generated in Busitema, Mayuge, Soroti, and Tororo study areas. The unmodified (modified) models for Bujagali – Kawanda 220 kV and Masaka West – Mbarara North 132 kV transmission lines in Uganda showed maximum power losses of 0.406023685 (0.39112869) and 0.451933075 (0.445513943) kW/km/phase respectively. Secondly, the transmission percentage losses ranged from 0.03 to 0.06%, which is consistent with the 3.6% recommended by the Electricity Regulatory Authority, Uganda. Thirdly, based on the RMSEs (0.6437, 0.6692, 0.2008, 0.1804, respectively), the gaps between designed and operational solar power generation were minimized. Furthermore, Mayuge recorded the highest solar power generation of 9.028 MW compared to Busitema (8.622 MW), Soroti (8.901 MW), and Tororo (8.345 MW), suggesting that it has a conducive site for installing future solar plants. The above results are useful for operation, design and management of solar power generation and transmission in Uganda and elsewhere.

CHAPTER ONE

INTRODUCTION

1.0 Introduction.

This chapter presents the background of the study, statement of the problem, general objectives, and specific objectives, significance of the study and scope of the study

1.1 Background of the study

Solar power generation and transmission in Uganda have been identified as crucial solutions to address the country's energy challenges (Ikwaba Paul & Uhomoibhi 2013). The country is characterized by a significant portion of the population being unconnected to the grid, particularly in Eastern and Northern Uganda (Twaha et *al.,* 2016). These regions also happen to have the highest potential for solar energy (Ikwaba Paul & Uhomoibhi 2013). Solar energy has been recognized as the most promising and abundant resource in Uganda (Twaha *et al.,* 2016). Furthermore, Uganda's geographical location along the equator allows it to enjoy a high insolation of close to eight (8) hours of sunshine daily throughout the year. Solar energy in Uganda has the potential to be utilized for various applications, including electricity generation, water heating, cooking, and drying agricultural and animal products. The development and implementation of solar power generation and transmission in Uganda have received significant attention from various stakeholders. The Ministry of energy and mineral development, the World Bank, and the government of Uganda have shown great interest in supporting the development of solar power mini-grid and off-grid systems in the country (Kitunzi Mutunzi & Vyakarnam, 2019). This interest stems from the recognition that solar power can help to bridge the energy supply-demand gap and contribute to achieving sustainable development goals (González-García *et al.,* 2022). Therefore, this study considered modeling, simulation and optimization of solar power generation and transmission in Uganda. Where a gradient technique for optimizing power loss models, modifying the traditional model that combines Ohm and Corona losses was employed. The modified model is consistent with the gradient method, efficiently minimizes power losses on transmission lines. The modified model outperforms the unmodified model, demonstrating its potential for efficient design and operation of power transmission lines. Also a coupling system of thermal and power equations for transmission lines, based on space and time balance is carried out, the finite

difference method and Crank Nicolson technique were used to solve the system of transmission line equations. The results align with the recommended 3.6% by the Electricity Regulatory Authority, Uganda. Lastly the study also aimed at reducing the disparity between solar power generation and design capacities, focusing on extrinsic factors like wind speed and irradiance. By transforming the nominal cell operating temperature, NOCT model into an explicit model, the study developed a solar power generation model, multiple differential models, and simulations. The second-order differential model validated with empirical solar power generation in Busitema, Mayuge, Soroti, and Tororo study areas, indicating the potential for future solar plant installations.

This background of the study is expanded into four categories: historical, theoretical, conceptual, and contextual perspective providing researchers, engineers, personnel planning for solar power installation, and the government with a comprehensive understanding of the study.

1.1.1 Historical Perspective

Globally, renewable energy sources are abundant, sustainable and environmental friendly. Growing environmental concerns, technological advancements, and the demand for sustainable energy sources have all contributed to a considerable evolution in the modeling and simulation of solar power generation and transmission over time. (Kumar *et al.,* 2013). In the early 1950s to 1970s, solar energy was predominantly employed for space applications, such as powering satellites and spacecraft. To comprehend the behavior of solar panels and their efficiency of energy conversion, simple mathematical models were created (Pengyuan *et al.,* 2022). Also in the 1960s and 1970s, the development of computer technology led to the development of more sophisticated solar power models. These models were able to take into account a wider range of factors, such as the effects of weather and climate on solar power generation, and the interactions between solar power systems and other energy systems (Barrera *et al.,* 2020). The cost of solar PV panels and other solar power system components was on the decline between the 1980s and 1990s, which sparked an increase in interest in solar power development. As a result, models and simulation tools for solar energy development continued to grow (Aarakit *et al.,* 2021).

A variety of variables, such as the growing accessibility of high-quality solar radiation data, have fueled the growth of solar power modeling and simulation in recent years. the creation of novel solar power technologies, such as solar-thermal hybrid systems and concentrated solar power (CSP), the growing need for large-scale solar energy projects, including solar farms and solar

power plants (Pelay *et al.,* 2020). A variety of modeling and simulation tools for solar energy are accessible. In order to construct and optimize solar power systems, to evaluate the potential for the development of solar energy in various parts of the world, and to examine the effects of solar power on the environment, researchers, engineers, and developers employ these tools (Tozzi & Jo, 2017).

The growth of a country like Uganda's economy, society, and industry depends on energy. Uganda serves as an example of how solar energy has developed from an underutilized resource to a significant part of the nation's energy mix. While supportive policies and technology improvements have made solar power more widely available and economically viable, challenges have sparked the creation of modeling tools to optimize solar systems (du Can *et al.,* 2018). The use of solar energy in Uganda appears to have a bright future, with more expansion and advancement anticipated in the years to come. In order to support the growth of solar power generation in Uganda and other nations in a sustainable, dependable, clean, and economical manner, this study aimed to model and simulate solar power generation and transmission in Uganda. This action was carried out in compliance with the targets of Uganda 2040 developmental goals and the Sustainable Development Goals (SDGs), particularly SDG 7 ensuring universal access to energy as stated by Mukisa *et al.,* (2022).

Solar energy utilization in Uganda is still very low but the existing solar data clearly indicates that the solar energy resource in some regions in Uganda is high throughout the year, the average solar radiation is 5.1 kWh/m^2/day (Corkish, 2013). The use of solar photovoltaic began in the early 1980s, mainly driven by donor-funded programs, for lighting and vaccine refrigeration in health centers. Later, the Uganda Railways Cooperation, government parastatal bodies, installed 35kW at 29 locations for communications and signaling. The Uganda Post and Telecommunications Cooperation also installed 30kW at 35 remote telecommunication sites throughout the country. Some of the earlier initiatives include: PV systems installed by Uganda Rural Development and Training in Kagadi through a credit scheme supported by a Dutch organization. Solar Electric Light Fund (SELF) funded by the United States Department of Energy, which installed 125 solar home systems to low-income families in Kasese, Solar Energy Uganda Limited in partnership with the Solar Light Churches for Africa also installed a number of PV systems (Avellino *et al.,* 2018). Solar plants installed in different parts of the world, including Uganda, are mainly based on the

size of the solar power potential in Uganda solar power potential of places like Tororo plant is 32,000 panels with 10 MW, Soroti plant is 32,680 panels with 10 MW, Kabulasoke plant is 68,000 solar panels with 20 MW (Belyaev & Shapeev, 2018). In the recent study (Nnamchi *et al.,* 2021) did comparative study that investigated quantification of solar power potential in the eastern Uganda. However, the assessing of the region with the maximum solar power potential and transmission to regions with low solar power potential was left out, this creates a gap for this study in Uganda that will involve development of power generation and power transmission models for Uganda and globe. Power transmission is usually marked with power losses sequel to ohmic and corona effects on the transmission lines. However, ohmic losses could be alleviated by transmitting at a low current whereas corona losses could be minimized by transmitting at a voltage close to the disruptive voltage (at which the dielectric or insulating property of air vanishes). Power generation model was developed by simulation in order to select the best area for solar power installation in eastern region. The decision for siting of future mega solar power plant should be based on technical analysis drawn from the generation and transmission models rather on rule of thumb or on sentiment. This study will aimed at solar power generation and transmission in eastern region.

1.1.2 Theoretical Perspective

1.1.2.1 Solar power generation

Solar power generation is based on the understanding of the fundamental principles of physics that govern the conversion of sunlight into electricity. The theoretical foundation of solar power generation is the photovoltaic effect, which was first discovered by Alexandre -Edmond Becquerel in 1839 (Brusso, 2019). It describes the phenomenon where certain materials, typically semiconductors like silicon, generate an electric current when exposed to sunlight. Theoretical models explain how photons (particles of light) interact with electrons in the semiconductor material to produce an electric current. Semiconductor physics is crucial in solar power generation (Rivera & Kaminer, 2020). The theoretical framework includes concepts like the band gap energy, electron-hole pairs, and the movement of charge carriers (electrons and holes) within the semiconductor material. This knowledge is used to design efficient photovoltaic cells. Theoretical models help in predicting and improving the efficiency of solar cells. Efficiency is a critical factor in determining how much sunlight is converted into electricity. The Shockley-Queisser limit, for

example, provides an upper theoretical limit for the efficiency of a single-junction solar cell. This model was developed in the 1960s and it predicts the maximum theoretical efficiency of a single-junction solar cell under ideal conditions. A solar cell with a band gap of 1.12 eV has a Shockley-Queisser limit of 33.7% (Rühle, (2016). The detailed balancing model is another popular theoretical model for solar cell efficiency. This model accounts for all of the different types of losses that might happen in a solar cell, including thermalization, recombination, and reflection. Under different situations, the efficiency of solar cells in the real world can be predicted using the comprehensive balance model. The angle at which sunlight strikes solar panels is another factor to take into account. The conversion efficiency is better when sunlight hits the panels at the ideal angle. In order to optimize energy capture, solar tracking devices are made to track the sun's movement throughout the day using theoretical concepts from optics and trigonometry (Shockley & Queisser, 2018). Photovoltaic (PV) cells Figure 1.1 convert sunlight into electricity through the photovoltaic effect, forming the basis of solar panels. These cells, typically made of semiconductor materials like silicon, excite electrons when photons strike their surface, creating an electric current. PV cells consist of multiple layers, each promoting photon absorption, electron movement, and charge collection. The resulting DC electricity is converted into AC electricity, suitable for residential, commercial, or industrial systems (Oku, 2016).

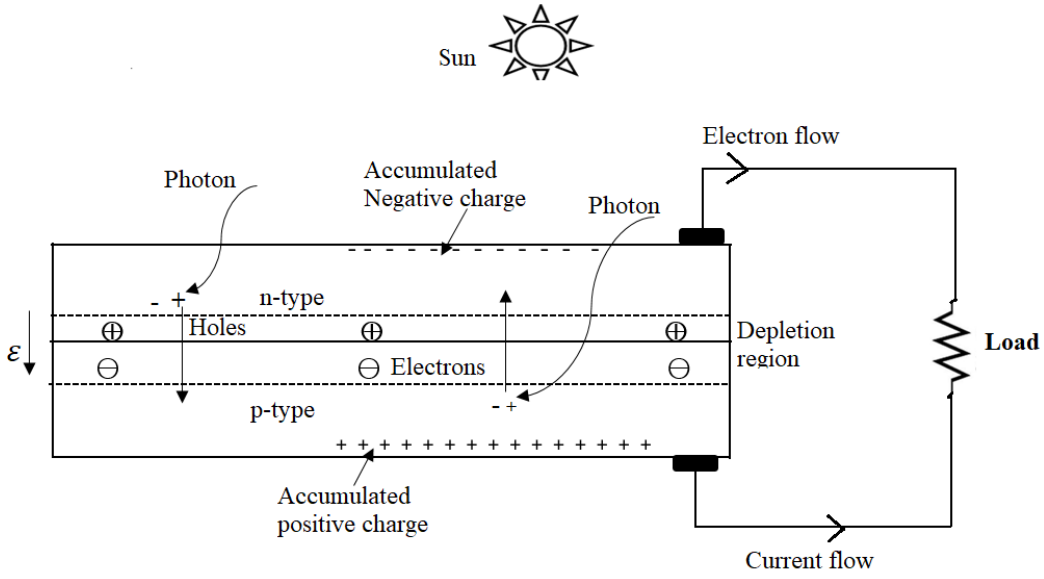

Figure 1.1: The Solar Cell's Operating Principle

Source: Present study (2023)

The above discussion considers only internal factors of mobility (diffusion) and recombination of charge carriers, thus this study will include the influence of external factors (cell/ambient temperatures, wind speed and irradiance) in solar power generation.

1.1.2.1 Electric power transmission

Electric power transmission is based on the fundamental principles of physics that govern the flow of electricity through conductors these principles include Ohm's law, Kirchhoff's laws, and Maxwell's equations (du Can *et al.,* 2018). The foundation of modern electric power transmission that was laid in 1882 when Thomas A. Edison's Pearl Street Station, a direct current, DC generator and radial line transmission system used primarily for lighting, was built in New York City (Wang, *et al.*, 2019). The development of American AC transmission, which utilized short radial lines between generators and loads, began in 1885 after George Westinghouse purchased French AC systems patents (Okba *et al.*, 2012; Doukas *et al.*, 2011). The electromagnetic field theory, as outlined by Maxwell's equations, is the foundation for the transmission of electric power. These equations describe how electric and magnetic fields behave, which is crucial for comprehending how electromagnetic waves travel through transmission lines (Suntola, 2017). Understanding the fundamental ideas, theories, and mathematical models governing the effective and dependable flow of electrical energy from power producing sources to consumers or distribution points is necessary for transmission of electrical power. For the purpose of ensuring the secure and efficient transmission of electric power, these viewpoints make use of electrical engineering, physics, and power systems analysis (DoE, 2017). Impedance is one of the key theoretical ideas in the transmission of electric power, it is a measurement of the resistance to an electrical current's flow in a conductor (Kersting, 2018). Power factor is also a key theoretical idea in the transmission of electric power. Power factor is a gauge of how efficiently power is being used in a circuit, it is a dimensionless quantity with a zero to one range, power factor of one implies that all of the electricity is being used for work, whereas a power factor of 0 indicates that all of the electricity is being wasted (Czarnecki, 2013; Weedy *et al.*, 2012). Analyzing corona discharge, coordinating insulation, and providing surge protection are all necessary for high-voltage transmission lines. At high voltage levels, these models seek to reduce losses and keep the integrity of the system (Velásquez, 2023). The theoretical aspects of both transmission system behavior in steady-state and transient states are discussed. In contrast to transient analysis, which focuses on short-term events like failures and switching operations, steady-state analysis is concerned with the system's

behavior over the long term. Razzaghi *et al.*, (2013) and Zhou *et al.*, (2021) presented Lumped-parameter models and distributed-parameter models are examples of theoretical models for transmission lines. Taking into account factors like resistance, inductance, and capacitance, these models depict how electrical signals, voltage, and current behave along the transmission line. Mestriner (2020) analyzed that the theoretical perspectives on high-voltage transmission lines include analysis of corona discharge, coordination of the insulation, and surge protection, these models aim to minimize losses and maintain the integrity of the system at high voltage levels.

Thus, it is upon the aforementioned theoretical perspective that, this study developed solar power generation model based on external factors of cell/ambient temperature, wind speed and irradiance. Also developed power transmission line models for minimizing power losses in Uganda.

1.1.3 Conceptual Perspective

The study conceptualizes on the following areas as discussed. Transmission line losses Modeling, corona and Ohmic losses, power coupling, deterioration constant, solar power generation, Extrinsic variables (wind speed, U, ambient temperature, T_a, and solar irradiance, H), power potentials of current and voltage, photovoltaic (PV) system modeling

1.1.3.1 Transmission line losses modeling

Electricity transmission over great distances is unavoidably accompanied with transmission line losses. These losses happen as a result of the insulation's dielectric losses as well as the conductors' resistance. The length of the line, the voltage level, the amount of transmitted current, the type of conductors used, and the insulation employed are just a few of the variables that affect the amount of transmission line losses. Transmission line losses are a type of energy conversion. Some of the energy is lost as heat as the electric current travels through the conductors. The conductors' resistance, which measures how much they oppose the flow of current, is to blame for this heat loss. Heat loss increases with conductor resistance. There are dielectric losses in the insulation in addition to heat losses in the conductors. When the insulating material's molecules become polarized by the conductors' electric field, dielectric losses result. The molecules vibrate as a result of the polarization, producing heat. The type of insulating material employed and the frequency of the electric current affect how much dielectric loss occurs.

1.1.3.2 Corona and Ohmic losses.

Transmission line losses typically take the form of ohmic losses. They result from the conductors' resistance to the flow of electrical current. An indicator of a conductor's resistance to current flow is its resistance. The ohmic loss increases with the conductor's resistance. Corona losses are created when air molecules near a transmission line's conductors become ionized. When an electric field is powerful enough to separate air molecules' electrons, ionization results. The conductors are surrounded by an ion and electron cloud as a result, which can provide a glowing appearance and a hissing noise. Corona losses rise with both conductor surface area and voltage level. Additionally, they rise with height and in humid environments. Corona losses are brought on by the ionization of the air molecules around the conductors, whereas ohmic losses are brought on by the resistance of the conductors. Corona losses only happen at high voltages, but ohmic losses are always present.

1.1.3.3 Coupling of power potentials in transmission line models.

This study developed coupled and uncoupled transmission line models capable of simulating lossy and lossless transmission parameters. Coupling of transmission parameters (current voltage and temperature) would help to explain the intricate physical phenomena among the potentials in space and time. The three coupling coefficients are the temperature, $\beta_T(1/\mathrm{K})$, phase voltage, $\beta_V(1/\mathrm{V})$ and current, $\beta_I(1/\mathrm{A})$ and their corresponding reciprocals; $1/\beta_T$ (K), $1/\beta_V$ (V) and $1/\beta_I$(A) result in diffusive coupling. Current, voltage, and temperature are three fundamental potentials in electrical and thermal systems. They link together in a variety of ways, so modifications to one potential may have an impact on the others. Coupling of current and voltage, Ohm's law, which states that the voltage across a conductor is proportional to the current flowing through it, links current and voltage. Accordingly, a rise in current will cause a rise in voltage, and vice versa. Connection between temperature and voltage, The Seebeck effect, which claims that a voltage is produced when two different metals are subjected to a temperature difference, links temperature and voltage. Thermocouples, which are temperature sensors that gauge the difference in temperature between two places, employ this effect. The Joule effect, which asserts that heat is produced when current runs through a conductor, explains how temperature and current are connected. Incandescent light bulbs employ this phenomenon by heating the filament to the point

of glowing as a result of the current passing through it. As a result, the coupling of current, voltage, and temperature for transmission models was a focus of this study.

1.1.3.4 Degradation constant.

The loss in the line caused by conductor resistance, dielectric loss, and corona loss is taken into account by the degradation constant in a transmission line model. There are genuine and fictitious components to this complex number. The phase shift is represented by the imaginary portion of the degradation constant, while the real portion of the deterioration constant represents the attenuation of the signal during transmission through the line. In transmission line modeling and analysis, the degradation constant is a crucial variable. It is employed in the efficient and effective construction and operation of transmission lines as well as in the assurance of accurate signal transmission over vast distances.

1.1.3.5 Solar power generation models

Solar power generation models could be intrinsic or extrinsic models. The intrinsic model considers the generation, mobility (diffusion) and recombination of charge carriers as discussed in 1.1.2.1, thus neglecting the influence of external factors (cell/ambient temperatures, wind speed and irradiance). Obviously, the impact of these factors cannot be undermined, so there is a silent need to develop a differential model that develops solar power generation as a substantial derivative of the aforementioned factors. Therefore solar power generation model developments considering external factors was considered in this study, the study develops a differential solar power generation model for the simulation of solar power generation and the development of multiple explicit empirical power generation models for improvements in the design/operations of PV systems such that the discrepancies become infinitesimal.

1.1.3 Contextual Perspective

Solar power generation and transmission in Uganda has the potential to play a significant role in the country's efforts to increase access to affordable and clean energy and growth of the country. Uganda substantial renewable energy resources (bioenergy, through biomass and biogas, water/ hydro, solar, geothermal and wind energy potential) that are distributed evenly across the country with an average daily solar radiation of 5.5 kWh/m² (Avellino *et al.*, 2018). However, hydropower remains the dominant source for electric energy production. With regards to electricity capacity

Hydroelectricity accounts for about 79.7%, Bagasse Co-generation accounts for about 8.2%, Solar power accounts for about 4.6%. Solar power transmission is a key challenge to the development of solar power in Uganda (Aarakit *et al.,* 2021). The country's transmission grid is underdeveloped and cannot currently handle the large amount of electricity that could be generated from solar power. The government is investing in expanding and upgrading the transmission grid to accommodate the increasing integration of solar power. Despite the challenges, solar power has the potential to play a significant role in Uganda's future energy mix (Mugisa, 2013). The country's abundant solar resources, declining costs, and government support are all factors that are driving the growth of solar power in Uganda. Solar power generation and transmission has the potential to play a significant role in Uganda's development. It can help to reduce electricity costs, increase access to electricity, create jobs, and protect the environment (Fashina *et al.,* 2019). Thus, this study carried out modelling and simulation of solar power transmission and generation in Uganda.

1.2 Statement of Problem

Solar Energy situation in different regions of Uganda is facing critical challenges to satisfy the existing grid demand. It has been noted with concern that for many years so many families especially in Uganda have suffered from the problem of increasingly prices of energy which leads to overdependence on fossil fuel for energy consumption and this leads to destruction of forests, loss of biodiversity, aggravated consequences of global warming. Recent solar studies by Nnamchi *et al.,* (2022) have shown that there are districts in the four regions of Uganda that have track records of insolation higher than the one where the contemporary Photovoltaic plants are installed, thus, if harnessed will give more power to meet the present grid demand. Considering the fact that nature does not distribute insolation uniformly; areas with high insolation ought to be identified for future for technical installation Photovoltaic plants. However, the studies by Nnamchi *et al.,* (2022) show that few contemporary Photovoltaic plants are situated in places with lesser insolation. Hence, the existing grid demand is difficult to meet. Technical installation is better for solar power generation than political installation (interest overridden) which can led to low grid power output. If more power is generated on the grid by the art of deforestation will be avoided, but if less power on the grid, then, the available power will be very expensive and deforestation will be alternative source of cheap power. It is very important to optimize power transmission, it is vital to know where there is need for power transmission to be encouraged. Generation and transmission need to be done from areas of high insolation to lower insolation. Siting Photovoltaic

plants with low insolation and transmitting to higher isolation will result in colossal loss of generation and transmission costs. In- case of areas with equal isolation capacity there is no need for transmission. Improper proper study on power generation leads to wrong power transmission. Therefore, there is need to utilize cheap solar energy technology which provides a cheap sustainable source of power all-round the year through overview of energy generation and transmission from the regions of maximum to lower solar irradiance (insolation). Upon this background, this study addresses the problems of solar energy generation and transmission in the eastern Uganda.

1.3 Objective of the Study

The observable main objective of this research is as follows:

1.3.1 General Objective

The main objective of the study is to model, simulate and optimize solar power generation and transmission in Uganda.

1.3.2 Specific Objectives

The specific objectives are as follows:

(i) To develop well-poses and optimizable power loss model for design and operation of solar power transmission in Uganda.

(ii) To develop a robust (lossy and lossless) system of coupled differential models to simulate transmission line losses in space and time for the Ugandan Power Transmission Company.

(iii) To formulate a differential equation for solar power generation and multiple empirical models for improving Photo Voltaic (PV) system design and operations.

1.4 Research Question

(i) What is the significance of transforming the ill-posed to well-posed model that can optimize transmission line losses?

(ii) Is coupled transmission model suitable for describing and simulating lossy and lossless transmission line parameters?

(iii) Why are there discrepancies between design and operation capacities in solar power generation for Eastern Uganda?

1.5 Significance of the study

The study's significance lies in its potential to provide Uganda with sustainable solar power by generating and transmitting electricity to low-irradiance locations that will impact the economic, environmental and social lives of Ugandans as follows:

(i) **Energy Access:** Particularly in remote and off-grid locations without access to traditional grid infrastructure, solar power helps increase access to electricity in Uganda. As a result, social services like healthcare and education are strengthened, economic growth is supported, and life quality is improved.

(ii) **Energy Security**: Uganda may lessen its dependency on imported fossil fuels and lower the dangers brought on by volatile international oil prices by diversifying its energy mix. In addition to improving energy security and lowering susceptibility to outside shocks, solar power offers a dependable and domestic energy source.

(iii) **Environmental Sustainability:** In Uganda's efforts to address climate change and lessen its carbon footprint, solar power generation generates electricity without releasing greenhouse gases or other dangerous pollutants into the atmosphere. The nation's ecosystems and natural resources, such as its waterways and forests, are preserved with its assistance.

(iv) **Cost-Effectiveness**: Uganda's year-round abundance of sunshine makes solar power an affordable option for producing electricity. Solar infrastructure is a desirable alternative for both grid-connected and off-grid applications because of its comparatively cheap operating costs after it is deployed.

(v) **Job Creation and Economic Growth:** Employment opportunities are offered by the developing of Uganda's solar energy industry at every stage of the value chain, including distribution, manufacture, installation, and maintenance. By drawing

investments, encouraging innovation, and assisting regional companies, it also promotes economic growth.

(vi) **Energy Independence:** By utilizing its large solar resources, Uganda can meet its energy needs domestically and lessen its dependency on foreign energy sources. Investing in solar power infrastructure makes Uganda less dependent on imported fossil fuels and increases its energy independence.

(vii) **Rural Electrification:** In Uganda, a large percentage of the population lacks access to electricity, solar power generation and transmission are essential to efforts to electrify rural areas. Remote communities may now affordably and reliably obtain electricity thanks to off-grid solar solutions like mini-grids and solar home systems, which raise living standards and promote economic growth.

1.6 Scope of the Study

The scope of the study is categorized into three areas, as clearly presented below.

1.6.1 Geographical Scope

Geography: This study was carried out in Uganda, It has a latitude of 1.3733° N and a longitude of 32.2903° E. Uganda is situated at equator which is suitable for optimum solar power generation

1.6.2 Content Scope

Content Scope: The study comprises three modules: 1. Modification of traditional power loss function by incorporating the Corona and Ohms losses**,** 2. development of mathematical models for coupled and uncoupled transmission lines, 3. development of differential solar power generation model and multiple empirical models for improving PV systems.

1.6.3 Time scope

This study was done in within the period of three years. It began with the preparation and presentation of the concept, followed by a thorough literature review, development and presentation of research proposals, the conducting of experiments in solar power plants located in

the eastern region (Busitema, Mayuge, Tororo, and Soroti), gathering of data, data analysis, thesis drafting, publication, and progress presentations.

1.7 Justification of the study

The anticipated findings of the study on the generation and transmission of sustainable solar energy would influence Ugandans' social, economic, and environmental well-being in addition to creating new knowledge.

1.7.1 Environmental Sustainability:

Investing in solar energy benefits the fight against air pollution, the preservation of ecosystems, and the advancement of sustainable development. Solar power generation generates electricity without producing greenhouse gases or pollutants, which contributes to efforts to mitigate climate change and prevent environmental degradation.

1.7.2 Contribution to knowledge creation.

Contribution to the knowledge to a new and improved models on power transmission line and solar power generation for sustainable solar power distribution in Uganda, in depth study of the transmission line losses within the Uganda Electricity Transmission Company Limited (UETCL) and solar power generation

1.7.3 Economic impact.

The adoption of solar energy in Uganda offers the potential to boost its economy, diversify its energy supply, generate employment opportunities, and aid small-scale enterprises. Additionally, it improves energy availability in remote areas, frees up resources for other initiatives, and is in line with global trends, luring foreign investment and fostering sustainable development.

1.7.4 Social implication.

The adoption of solar power in Uganda offers significant social benefits, including improved access to electricity, fostering education, and supporting public health. It also provides off-grid solutions, empowers remote communities, and improves livelihoods. The shift aligns with global sustainability goals, promoting environmental awareness and a cleaner living environment for Ugandans.

CHAPTER TWO

LITERATURE REVIEW

2.0 Introduction

This chapter presents conceptual framework and review of related literature. The related literature to this study has been structured according to the specific objectives based on the variables of the study; solar power generation and transmission line losses.

2.1 Conceptual framework

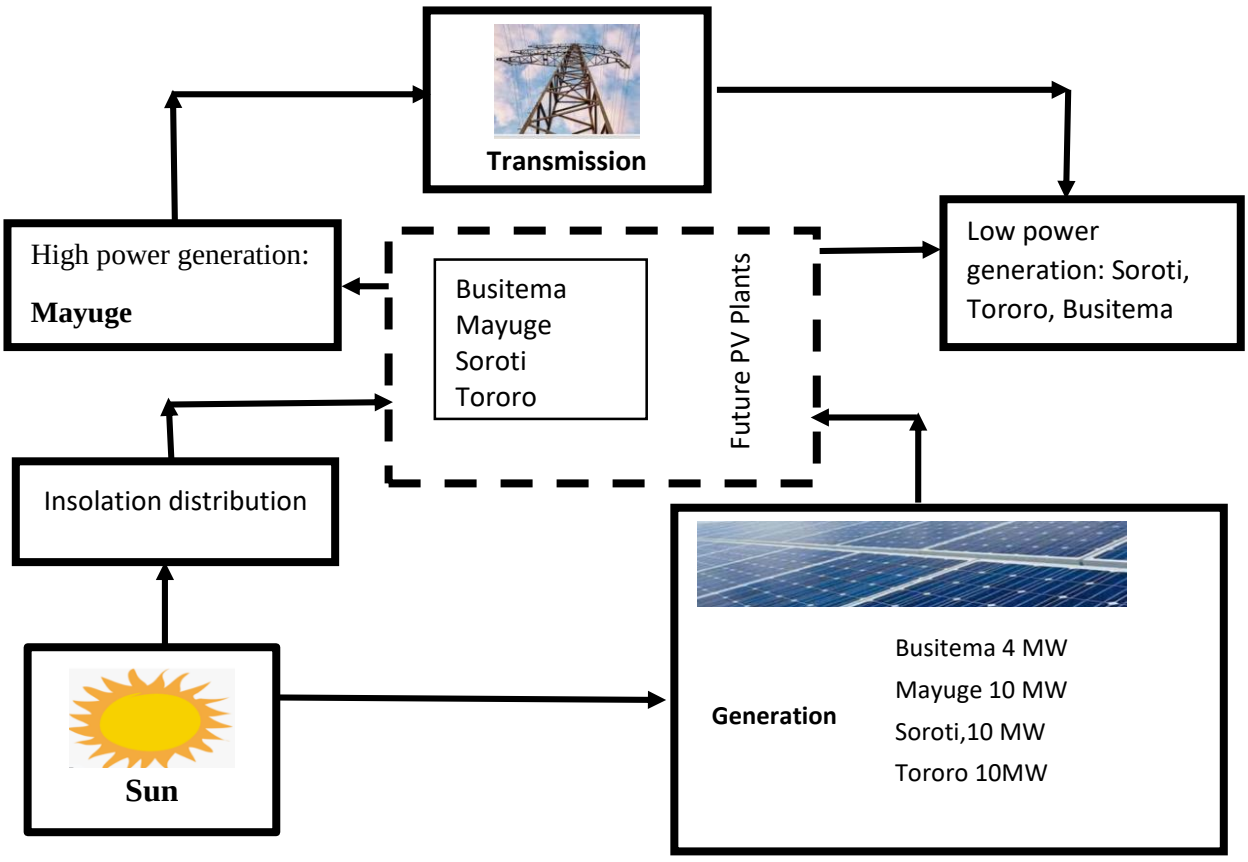

Figure 2.1: Conceptual Framework

Source: Present study (2023)

This conceptual framework links Sun (insolation distribution) to solar power generation and then to power transmission through modeling, simulation and optimization

2.2 Review of related literature on specific objectives

This sub-section presents a review of similar studies conducted by other scholars.

2.2.1 Minimization of electric power losses in transmission lines

The method for generating or converting electricity is demanding and labor-intensive. It is concerning, then, if much of it is lost. Transmission losses must be greatly reduced for transmission lines to operate efficiently. This reduction in losses requires accounting for the material or equipment causing the losses, which is known as ohmic loss, and the environmental factors (air density, disruptive voltage, etc.) that cause the power to be lost in the transmission line, which is known as Corona loss. At the design and testing phases, power losses, whether reactive or active, could be reduced (Ogar *et al.,* 2017; Jenkins & Thornycroft, 2018). The length of transmission lines, the resistivity of the conducting materials, and increasing transmission current, however, are responsible for the ohmic loss (Wain-Martin., *et al.,* 2020). Power losses in the transmission line may increase if the conducting materials' cross-section area is likewise reduced (Yahaya, *et al.,* 2013). It is well known that a sizable difference in the phase and disruptive voltages, transmission frequency, and diameter (or radius) of the conducting materials can cause additional losses (Weedy *et al.,* 2012; Anumaka, 2012). On the other hand, as air density decreases, losses from weather or environmental factors rise (Riba *et al.,* 2019). Therefore, there are three types of losses that can be associated with transmission: material losses; intrinsic losses resulting from the nature of the current; and thermal, electrical, and electromagnetic effects/atmospheric disasters. Transmission equipment includes capacitors and inductors in the transmission circuits (Alibakhshikenari *et al*., 2020; Mahdy, 2020). The reason for these ridiculous variables is that power is inherently lost to the surroundings when it is converted to heat, and it is also caused by thunderstorms forcing power through the air around the transmission lines, causing them to lose their dielectric qualities (Lalbakhsh *et al.,* 2022). Nonetheless, installing thunder arresters might be a remedial or preventative step (Pourakbari-Kasmaei & Lehtonen 2020). Compared to copper, which has superior electrical and mechanical qualities than aluminum, the use of aluminum (animal grades) is more prone to power losses. By reducing reactive power in the transmission equipment and

limiting the amount of eddy current generated in the inductors by building the inductor core as laminates parallel to the magnetic field, equipment losses might be reduced (Yamaguchi *et al.,* 2000).

Significantly. Methods of artificial intelligence that use non-gradient optimization techniques In order to find the best algorithm for minimizing power loss in transmission lines, Particle Swarm Optimization (PSO) and Salp Swarm Algorithm (SSA) were presented by Patil *et al.*, (2020). Baharozu *et al.,* (2015) developed PSO by selecting the load bus voltages, generator active and reactive powers, and line flow capacities as penalty functions in the objective function. Comparative analysis is done between PSO and IPSO-based optimal power flow solutions for IEEE 48, 118, and 300 bus systems (Patil *et al.,* 2020; Naima *et al.,* 2015; Kumar *et al.,* 2013) combined genetic algorithm technology with particle swarm optimization in the western Algerian power system; Kumar *et al.*, (2013) presented that the Chaotic Artificial Bee Colony (CABC) Algorithm was more effective than the Artificial Bee Colony (ABC) Algorithm in minimizing active power losses. ABC reduced to 8,6203MW while CABC reduced to 8,4891MW; In comparison to the current methods, the suggested technique demonstrated superior convergence and reduced power losses more effectively. From 11.61 MW to 8.7036 MW, or 25% less overall in active power losses, the method decreased losses. However, deep neural networks and artificial intelligence-based optimization approaches are commonly used to minimize power losses in transmission lines. The challenge lies in determining the global minimum/maximum among minima/maxima. Nonetheless, the global minimum and maximum can be found using the gradient approach to minimize power losses in the transmission line. A flow model (mathematical equation) was analyzed by Bamigbola *et al.,* (2014) to predict current and voltage parameters in the transmission lines; they then revolutionized and simulated the transmission model to obtain valid transmission losses; Sharma *et al.*, 2012; Kuchanskyy and Zaitsev, 2020 and noted that phase change in double circuit lines can reduce corona loss; Bisiriyu *et al.*, (2009) and Rozegnał *et al.,* (2021) achieved loss minimization in transmission line by optimum length and radius of the transmission cable; Numerous studies have been conducted on corona loss in power transmission lines, looking at things like high and low losses, conducting material deterioration, and the effects of different conditions on the conductor's performance. The conductor's performance is also affected by corona electrical surface gradients such shock potential, gaseous effluents, radio interference, and auditory noise. However, because it is impossible to determine the ideal variables

or minimization values, the gradient approach of optimization with the conventional Corona and Ohms transmission loss model is not practical. In order to test the optimality of the unmodified and modified models on various power transmission lines, this work proposes to change the classic power losses objective function by adding a third dimensionally consistent factor, a product of Corona and Ohms losses.

2.2.2 Modeling of coupled and uncoupled transmission lines

Transmission line losses are unavoidable and require careful monitoring to maintain supply and demand in the grid. Due to their dependence on time rather than space, the majority of transmission models (non-differential and lumped models) barely take transmission line losses into consideration. There are differential and non-differential versions of transmission line models (usually the J-Marti model). In order to calculate transmission line losses, differential models can be a coupled or uncoupled distributed problem, boundary value (space) problem, or initial value (or lumped) problem.

The literature has around forty-eight transmission line models (TLM). The differential transmission model, which stresses local acceleration and convective factors, was introduced (Renner & Steeb, 2015; Costa *et al.,* 1999) and is noteworthy in that it is not a robust model because it does not include a diffusion term. Besides, a differential transmission model does not incorporate Ohmic and Corona losses. First-order linear transmission model conventionally proposed Maffucci and Miano, 2013. The standard linear model was attempted to be transformed into a diffusion transmission model Belhocine and Marinescu, 2017, although the diffusion transmission model was not correctly represented. Hu *et al.,* (2018) developed the conductor thermal network model (CTNM), which is a lumped model of temperature. The transmission line's voltage and current, however, were not taken into account. Similar to Costa *et al.,* (1999), Maffucci and Miano, 2013 and Belhocine and Marinescu, 2017, Daafouz *et al.,* (2014) proposed a linear transmission line first-order model, however they disregarded resistance. The first- and second-order linear transmission line models were presented independently by Mamis & Koksal (2000). Such a composite model would have been thorough in its analysis of transmission line systems. These models neglected Corona and Ohmic losses. Uncoupled lossy transmission line models a second-order linear model in terms of lossy voltage and current were proposed by (Bamigbola *et al.,* 2014). First- and second-order boundary transmission line models for current and voltage were presented

separately by Caballero *et al.,* 2015. First-order transmission model with lossless coupling was used by (Ghazizadeh and Sadeh 2012). Abadi *et al.,* (2020) applied Using first-order space and time transmission line models without line losses. First-order distributed parameters and second-order lumped models were proposed by Hussein & Mahmoud, 2023. Suffering of taking transmission line losses into account, a distributed transmission line model without line losses in the first order was employed by Besedin and Menushenkov, 2018.

In terms of voltage and current, Chu (2019) used coupled first-order distributed transmission line models. We did not take losses or line temperature into account. A lossless single-phase transmission line was used in the study of a first order linear distributed model by Dambhare & Chandorkar, 2009. With no consideration for transmission line losses, Heilmann *et al.,* (2022) used an uncoupled second-order distributed transmission line model. Without taking transmission line losses into account, Colqui *et al.,* (2021) created a first-order lumped and coupled model. First-order lumped-line voltage and current models were introduced by (Kurokawa *et al.,* 2009). There was no consideration of line temperature or losses. Taking into account current and voltage disjointedly, da Silva *et al.,* (2013) employed first-order lumped line models without line losses. Combining coupled temperature, current, and line losses, Iranmehr *et al.,* (2020) and Xu *et al.,* (2022) employed a first-order thermal transmission line model. Without accounting for transmission line losses, Zhou (2021) studied a coupled first-order linear lumped model. Garcia *et al.,* (2016) developed a first-order distributed lossless model. Research was done on an uncoupled second-order space model without line losses by Da Costa *et al.,* (2013). Cheldavi, 2004 looked at an uncoupled first-order space model without line losses. Liu, (2021) examined voltage and current characteristics of uncoupled lossy distributed transmission line models that were based on high voltage direct current (HVDC) transmission lines. First-order lumped uncoupled model without line losses was analyzed by Caballero *et al.,* 2015. In terms of both current and voltage, Ni (2023) investigated linked first-order space models devoid of line losses. Without line losses, Kengne (2023) studied nonlinear distributed uncouple transmission line models.

Different authors have explored various models, including distributed-coupled, first-order transmission line models, first-order lumped models, linear uncoupled models, and linear transmission line first-order lumped models. The study presents coupled and uncoupled models

capable of simulating lossy and lossless transmission parameters (current, temperature and voltage) with space and time.

2.2.3 Differential and empirical modelling of solar power generation.

The performance of a photovoltaic (PV) system is influenced by ambient conditions, cell temperature, wind speed, and irradiance. High temperatures decrease solar output power, while high wind speeds improve cooling. Irradiance increases power generation by increasing output current. Efficiency of the solar cell also affects power generation. These factors form implicit and explicit linear correlations in empirical models.

Different findings have been found in literature as discussed below. Using the Standard model with nominal working cell temperature, Chung (2020) accurately predicted insolation, however, the model was unable to predict solar power generation capacities. Accordingly, Salilih & Birhane (2019) assessed the electrical performance of a photovoltaic system under various loads using the nominal operating cell temperature-Standard formula and found that 4 ohms produced the best performance. In order to improve the accuracy of NOCT temperature prediction, Sun (2020) appropriately designed a new nominal cell operating temperature, or NOCT, for an unglazed photovoltaic-thermal (PVT) module using water as the working fluid. Specifically, Sarniak (2020) demonstrated a NOCT model and found that half-cells experienced lower power loss than regular cells. Al-Amri & Abdelmagid (2021) developed a NOCT model to predict solar cell temperature in high concentration photovoltaic systems. Atia *et al.,* (2023) studied degradation of monocrystalline silicon PV modules using the model. El Hammoumi *et al.,* (2022) examined the effect of cell temperature on energy generation. Koehl *et al.,* (2011) used ambient temperature, global solar irradiation, and wind speed to develop PV-module temperature. Kamkird *et al.,* (2012) modified the model.

Furthermore, since wind speed, irradiance, and ambient temperature all directly affect solar power output, detailed empirical models are meant to enhance the prediction of cell temperature. Though extrinsic variables may be beneficial, the operational solar output power of PV systems rarely matches the design since the classical design/operational models are implicit in nature. The model correlation term, based on temperature, overlooks wind speed and irradiance, causing a discrepancy in solar power generation data from Eastern Uganda Solar Plants. This discrepancy necessitates a re-engineering of the design/operations models, introducing explicit power

generation. When compared to traditional techniques, Schwingshackl *et al.,* (2013) showed that adding wind data to the NOCT models enhances the prediction of cell temperature. Similarly, Mattei *et al.,* (2006) found that the cell temperature model that relies solely on thermal characteristics rather than wind speed or irradiance is not very effective at forecasting cell temperature. Olukan & Emziane (2014) remarkably adjusted the NOCT model without including the wind speed; still, they observed a reliable cell temperature forecast. Nguyen *et al.,* (2021) improved cell temperature prediction by modifying the NOCT model with wind speed, thermal inertia, and irradiance. Barykina & Hammer (2017) applied Faiman model, Brito *et al.,* (2018) found increased lifetime of PV modules with increased irradiance, and Ayaz *et al.*, (2014) found explicit models compatible with mono-crystalline and thin film semiconductors. The use of explicit models in solar power generation has been shown to minimize differences between design and operation. Studies have shown that cooling of PV panels affects output voltage and efficiency (Agyekum *et al.,* 2021). Multiple explicit cell temperature models have been developed, resulting in high precision in module temperature without wind speed. Weather conditions also impact efficiency, with an increase in cell temperature reducing panel efficiency (Akhsassi *et al.,* 2016). Dual explicit NOCT models have shown improvement in cell temperature prediction compared to implicit NOCT models (Kaldellis *et al.,* 2014). Researchers have modified the NOCT model to include wind speed, thermal inertia, and irradiance, achieving high accuracy in cell temperature prediction (Nguyen *et al.,* 2021). They also developed explicit models based on weather, material optics, and thermophysical properties for PV system design. Floating and land-based PVs showed better performance, and explicit models increased current and solar power generation (Araneo *et al.,* 2014). Al-Dahidi (2020) developed a triple explicit NOCT model using Multiple Linear Regression and Artificial Neural Networks for better prediction of PV cell temperature and solar power generation. Ndegwa *et al.,* (2020) found explicit NOCT models stronger than double and implicit models. This study developed a differential and empirical solar power model, focusing on ambient temperature, wind speed, and irradiance. The model uses first-order and second-order substantial derivatives for modeling and simulation. A numerical solution is sought using the Crank Nicolson explicit technique.

2.3 Research Gaps in Literature Review

This subsection presents the main gaps basing on the empirical literature review outlined in 2.2

2.3.1 Minimization of electric power losses in transmission lines

The identified research gap in the literature is the inefficiency of the traditional power loss model, which combines Ohm and Corona losses. The unmodified model, as described in literature, fails to support the minimization of power losses on transmission lines. The Hessian matrix that was used in optimization indicates that the unmodified (traditional) models is geared towards maximizing power transmission losses instead of minimizing them. Also in literature there use of artificial intelligence/machine learning optimal techniques but these techniques have short coming of guarantying global minimum amidst minima Thus, this study addresses this gap by proposing a gradient search technique cannot guarantee the use of trapping in local minimum. The modified model is consistent with the gradient method of optimization, leading to optimal variables and values that result in minimized power losses. The comparison of the unmodified and modified models for specific transmission lines in Uganda (Bujagali – Kawanda 220 kV and Masaka West – Mbarara North 132 kV) demonstrates that the modified model performs better, showcasing lower power losses. Therefore, the traditional power loss model are ill-posed for optimization of transmission line losses while the present study transforms the ill-posed to well-posed model, which can optimize transmission line losses

2.3.2 Modeling of coupled and uncoupled transmission lines.

The identified gap in the outline literature is the limitation of existing transmission models, there are numerous lumped models in the literature. Lumped models focus on describing the time dependence of transmission potentials such as temperature, current, and voltage but do not incorporate the space aspect. This omission of the space counterpart in lumped models hinders the simulation of transmission losses. The gap is addressed by proposing a distributed or coupled system of thermal and power models in this present work. Unlike lumped models, the coupled system takes into account both space and time, allowing for a more comprehensive simulation of transmission losses. The development of the coupled system of equations is based on balancing thermal and power fluxes around a control volume that represents the transmission lines. The Finite Difference Method, specifically using the Crank Nicolson technique, is employed to solve the coupled system of equations. The results from the simulation show transmission percentage losses ranging from 0.03 to 0.06%, aligning with the 3.6% recommended by the Electricity Regulatory Authority in Uganda. Additionally, the simulated model results are validated by comparing them to field data obtained from the Uganda Electricity Transmission Company Limited on the Bujjagali

- Kawanda transmission line. Therefore the previous study presented Lumped models that focus on historic transmission potentials such as temperature, current, and voltage, which are uncoupled while The present study considers the development of a coupled model that reflects all transmission potentials of current and voltage in both time and space. The space term accounts for the line losses

2.3.3 Differential and empirical modelling of solar power generation.

Approximately 35% of solar power output is significantly underperforming, which is the pointed out gap in the literature a review, particularly the discrepancy between the operating and design capacities of solar plants. This underperformance is attributed to the use of a nominal cell operating temperature (NOCT) model that relies solely on ambient and cell temperatures, neglecting important extrinsic factors such as wind speed and irradiance. The absence of these extrinsic factors in the NOCT model leads to a substantial drop in the generated solar power. To address this gap, the study proposes the development of a solar power generation model that incorporates the missing extrinsic factors. The implicit NOCT model is transformed into an explicit model by empirically introducing wind speed and irradiance. Multiple differential models are then developed, and simulation and experimentation with a pilot solar rig are conducted to create an alternate model for predicting solar power generation.

The results demonstrated how well the second-order differential model reduces the difference between designed and actual solar power generation. The model was validated using empirical solar power data from various study fields. The study areas of Busitema, Mayuge, Soroti, and Tororo's Root Mean Square Errors (RMSEs) show how well the model predicts the production of solar power. Therefore the previous studies did not developed differential solar power generation models, considers only NOCT models without extrinsic factors of wind speed and irradiance. The present study develops NOCT solar power generation model, first-order and second-order differential models that incorporates extrinsic factors, transforming these models into explicit models, and conducting simulations and experiments.

2.4 History on available solar power plants in Uganda

Table 2.1 Design capacity of solar plants in Easter Region of Uganda

S#	Power Plant	Power capacity (MW)*	Lat*	Long*	2020	2021	Average data	Source
1	Busitema Solar power station	4	0.54722	34.0236	3.082	3.142	3.112	UETCL, 2023 ,2023
2	Busitema Solar power station (upgraded)	10	0.54722	34.0236	7.705	7.854	7.780	UETCL ,2023
4	Mayuge Solar Power Station (Emerging Power – Bufulubi)	10	0.495	33.4075	7.858	7.744	7.801	UETCL ,2023
5	Soroti Solar Power Station	10	1.685	33.6581	7.379	7.160	7.269	UETCL ,2023
6	Tororo Solar North	10	0.63889	34.1192	7.205	7.247	7.226	UETCL ,2023

2.4.1 Soroti solar Power station

This power station was installed in Soroti District in December 2016 and commissioned in 2017 it generates the capacity of 10MW. It is located in Eastern Region, southeast of the city of Soroti, about 282 kilometers north-east of Kampala, the country's capital and largest city. 1°41'06.0"N, 33°39'29.0"E are the geographical coordinates of Soroti Solar Power Station with Latitude:1.685000 and Longitude:33.658056. This solar power station was Uganda's first grid-connected solar plant, with 32,680 photovoltaic panels. The power station is situated on a 33-acre plot of land (Lee, 2020).



Figure 2.2: Soroti PV Power Plant

Source: ERA Strategic Plan 2020-2021

2.4.2 Tororo power station

This power station is located in Tororo District, 12 kilometers southwest of the town of Tororo in Uganda's Eastern Region. It's about 230 kilometers east of Kampala, Uganda's capital and largest city, by vehicle. Tororo Solar Power Station's geographic coordinates are 0°37'50.0"N, 34°06'40.0"E. The power plant has a 10 MW capacity, the installation began in 2016 and was commissioned in 2017 (Kavuma *et al.*, 2022).



Figure 2.3: Tororo power station

Source: ERA Strategic Plan 2020-2021

2.4.3 Mayuge solar power plant

The power plant is situated on leased land covering 100 acres in Bufulubi Village, Imanyiro sub-county, Mayuge District, in Uganda's Eastern Region, roughly 110 kilometers east of Kampala. Solar Power Station's geographic coordinates are 00°29′42″N 33°24′27″E. The solar power station has 30,600 solar panels that monitor the sun to maximize power generation. On June 6, 2019, the finished power station was commissioned. At the time, solar plants on Uganda's system contributed a total of 50 megawatts, including Soroti Solar Power Station (10 megawatts), Tororo Solar Power Station 10 megawatts and Bugema Solar Power Station 4 megawatts. (van der Ven, 2020).



Figure 2.4: Mayuge solar power plant

Source: ERA Strategic Plan 2020-2021

2.4.4 Busitema solar power plant

According to Othieno, (2016) the Busitema Solar Power Station is a 4 megawatt solar power plant in Uganda. The power plant is situated on the main campus of Busitema University, a public university, in the Busia District of Eastern Uganda. It is roughly 184 kilometers (114 miles) east by road of Kampala, the country's largest city and capital (González-García *et al.*, 2022). The Egyptian government has donated this solar installation to the Ugandan government. This came after the two nations signed bilateral agreements in 2016. The signing of a Memorandum of Understanding in May 2018 by Presidents Yoweri Museveni of Uganda and Abdel Fattah el-Sisi of Egypt came next (González-García *et al.*, 2022). According to Petrovic and Williams (2023) the power plant's goals are to boost Uganda's renewable energy supply, provide electricity to the Eastern Region, and provide a teaching resource for university students pursuing renewable energy programs. This power plant was the fourth solar power plant linked to the national electricity grid of Uganda. The others were the Soroti Solar Power Plant, which started operations in December 2015, the Tororo Solar Power Plant, which started operations in October 2017, and the Mayuge Solar Power Plant, which has a 10 megawatt capacity and started operations in June 2019 (González-García *et al.*, 2022).



Figure 2.5: Busitema solar power plant

Source: ERA Strategic Plan 2020-2021

2.5 Literature on the Equipment

This sub-section presents the equipment that was used in this study and the reasons why it was chosen.

2.5.1 Digital Solar power meter

A digital solar power meter (Figure 2.6) is an electronic device that measures the watts per square meter (W/m^2) of the sun intensity. It is sometimes referred to as an irradiance meter, a sun light meter, or a solar radiation meter. The current solar intensity reading is displayed on a digital display in digital solar power meters, which are often handheld. The circuit that gauges the flow of current is connected to the solar cell. Digital solar power meters typically use a photovoltaic cell to convert sunlight into electricity. A digital signal is created from the current reading, which is then displayed on the meter's display. Some digital solar power meters also include extra characteristics, like the capacity to record data for subsequent study or the ability to measure the highest solar intensity over a period of time (Diaz *et al.*, 2023).

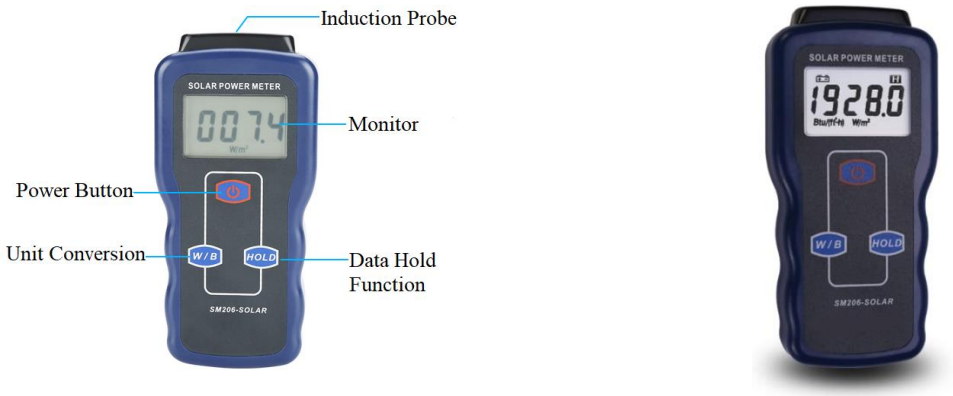

Figure 2.6: The snapshot (left) and photograph (right) of **digital solar power meter.**

Source: Present study (2023)

2.5.2 Digital thermocouple

A thermocouple (Figure 2.7) is an instrument that measures temperature. It is made up of two different metals that are attached at one end. A voltage is produced that is related to temperature when the junction of the two metals is heated or cooled. A thermocouple is a widely used temperature sensor that is straightforward, reliable, and reasonably priced. (Leonidas *et al.*, 2022). There are many different types of thermocouples that are produced, including thermocouple probes, thermocouple probes with connections, transition joint thermocouple probes, infrared thermocouples, bare wire thermocouples, and even plain thermocouple wire. There are numerous varieties of thermocouples that each have their unique temperature range and precision. The K-type thermocouple, which has a temperature range of -200 to 1350 °C, is the most popular form of thermocouple. The J-type (0 to 1200 °C), T-type (-200 to 350 °C), and E-type (-200 to 900 °C) are other thermocouple types. (Lian *et al.*, 2023).



Figure 2.7: The snapshot of 6802 Ii Durable Precision Dual Channel Digital Thermometer with 2 K-ty

Source: World of Electronics and Cyber Consultancy

2.5.3 An anemometer

An anemometer (Figure 2.16) is an instrument used to gauge the wind's speed. It is a typical tool used in weather stations, but it also has other uses, including sailing, windsurfing, and kite flying. (Zhang *et al.,* 2021). Anemometers are divided into two primary categories: cup anemometers and vane anemometers. Anemometers with cups have three or four cups that are fastened to horizontal arms. The cups are made to rotate when they encounter the wind. The speed at which the cups spin increases with the wind speed. A sensor detects how quickly the cups are moving and translates the speed into a usable value. A vertical vane that faces into the wind is included in vane anemometers. The vane is connected to a sensor that calculates the vane's angle with respect to the ground. The wind direction is determined using the vane's angle. The measurement of wind speed by an anemometer can be carried out using several of various units, such meters per second (m/s), kilometers per hour (km/h), and miles per hour (mph). The study of weather patterns and the prediction of future weather conditions are two essential tasks that meteorologists perform using anemometers. Engineers and scientists also use anemometers to investigate how wind affects solar radiation-generating machinery and structures. (Goldshmid *et al.,* 2022).



Figure 2.8: The snapshot diagram of digital an anemometer. (Zhang et al., 2022)

2.5.4 Digital multimeter

A multimeter is a versatile electronic measuring instrument used to assess various electrical parameters within a circuit. It combines several essential functions in a single device, including measuring voltage (both direct and alternating current), current, and resistance. Additionally, multimeters often feature functions such as continuity testing, diode testing, capacitance measurement, and frequency measurement, depending on their complexity. Equipped with a display screen and input jacks for test leads, users can select the desired measurement function on the multimeter's dial, connect it to the circuit of interest, and obtain accurate readings displayed digitally or via an analog needle. (Asadi & Eguchi, 2020).



Figure 2.9: The snapshot diagram of digital Multimeter (Asadi & Eguchi, 2020)

A multimeter is widely utilized by electricians, technicians, and hobbyists, multimeters play a crucial role in diagnosing electrical issues, troubleshooting circuits, and ensuring the proper functioning of electronic components.

Digital instruments such as a solar power meter, digital thermocouple, anemometer, and digital multimeter played crucial roles in the study of solar power generation. The digital solar power meter provides accurate measurements of solar irradiance, enabling researchers to assess sunlight intensity and optimize system design for maximum energy capture. A digital thermocouple monitors temperature variations in solar panels and components, aiding in thermal performance analysis and system optimization. By measuring wind direction and speed, an anemometer enables researchers to better understand how wind affects solar installations and to adjust maintenance procedures and system structure accordingly. To guarantee optimal performance and dependability, testing, troubleshooting, and verification of solar system components are made easier with the use of a digital multimeter, which provides accurate electrical measurements. When combined, these digital tools offer vital information and perspectives that further the development of effective and sustainable solar power producing systems.

CHAPTER THREE

METHODOLOGY

3.0 Introduction

This chapter presents materials and methods applied in actualize the objective of the study. It also highlights the study area, research philosophy, research methods, and sources of data, data collection instruments, and data collection procedures and data analysis.

3.1 Study area

The two transmission lines were considered; Bujagali – Kawanda (B-K) transmission line (220 kV) and the Masaka West - Mbarara North (MW-MN) transmission line (220 kV) as shown in Figure 3.1 and Figure 3.2 respectively. This study was conducted on Uganda Electricity Transmission Lines where the two transmission lines were selected. This study covered two transmission lines of 132 kV (Masaka West - Mbarara North) and 220 kV (Bujagali – Kawanda) as shown in Figure 3.1 and Figure 3.2 respectively. Masaka West - Mbarara North transmission lines cover a route length of 130.5 km, five districts of Masaka, Kiruhura, Lyantonde, Lwengo and Masaka with a line rating of 151.6 MVA per circuit. Bujagali – Kawanda North transmission lines cover a route length of 84km with a line rating of 205.8 MVA per circuit, which comprises four districts; Wakiso, Mukono, Buikwe and Jinja. Minimization of power losses in the transmission lines was carried out on both lines of Masaka West - Mbarara North which is located at 0°20'28.0"S, 31°44'10.0"E (Latitude:-0.341; Longitude:31.736) - 0° 36' 25.776" S and 30° 39' 16.211" E (Longitude: 30.655, Latitude: -0.607) respectively. Bujagali – Kawanda is located at 0.498° N, 33.139° E (Latitude: 0.495, Latitude 33.130°) - latitude 0.422 and the longitude is: 32.542 respectively. Solar power generation study was focused on the eastern region (1.2692° N, 33.4384° E) of Uganda. Due to the installation of the majority of the solar power plants, as shown in Figure 3.3, the central region was chosen.

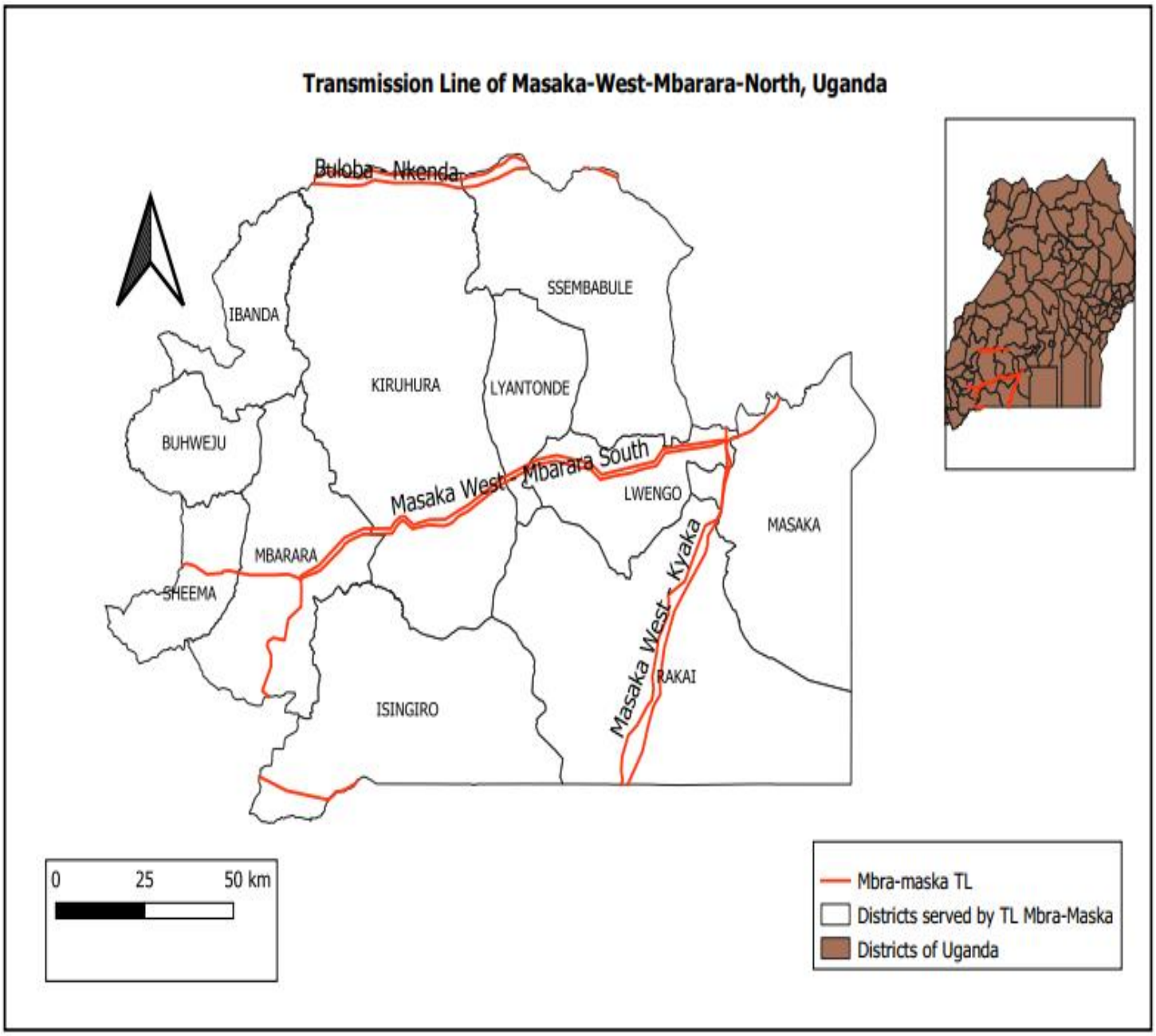

Figure 3.3: Map of the study area (Masaka West - Mbarara North) and the transmission lines

Source: Present study (2023)

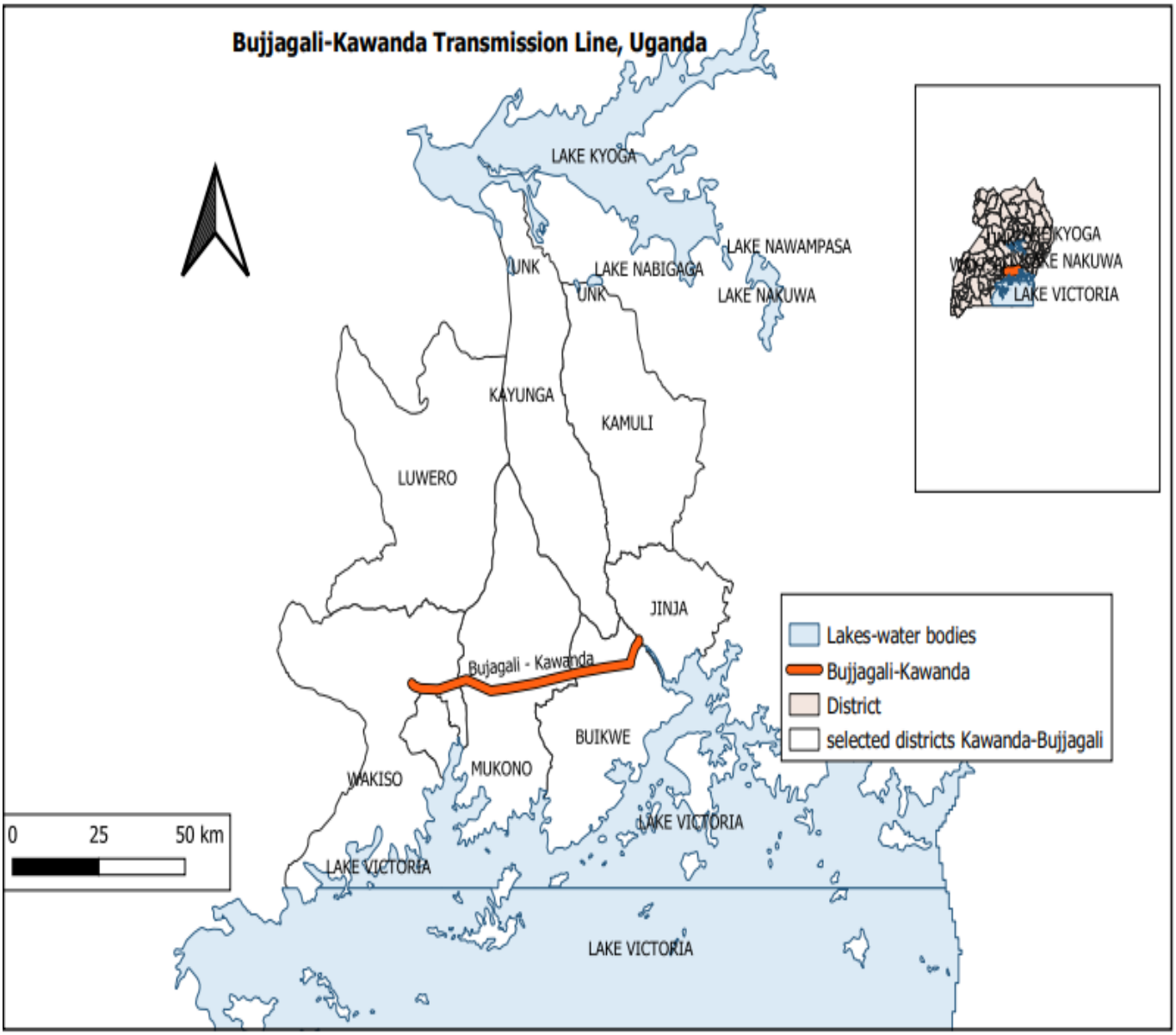

Figure 3.2: Map of the study area (Bujagali - Kawanda) and the transmission lines

Source: Present study (2023)

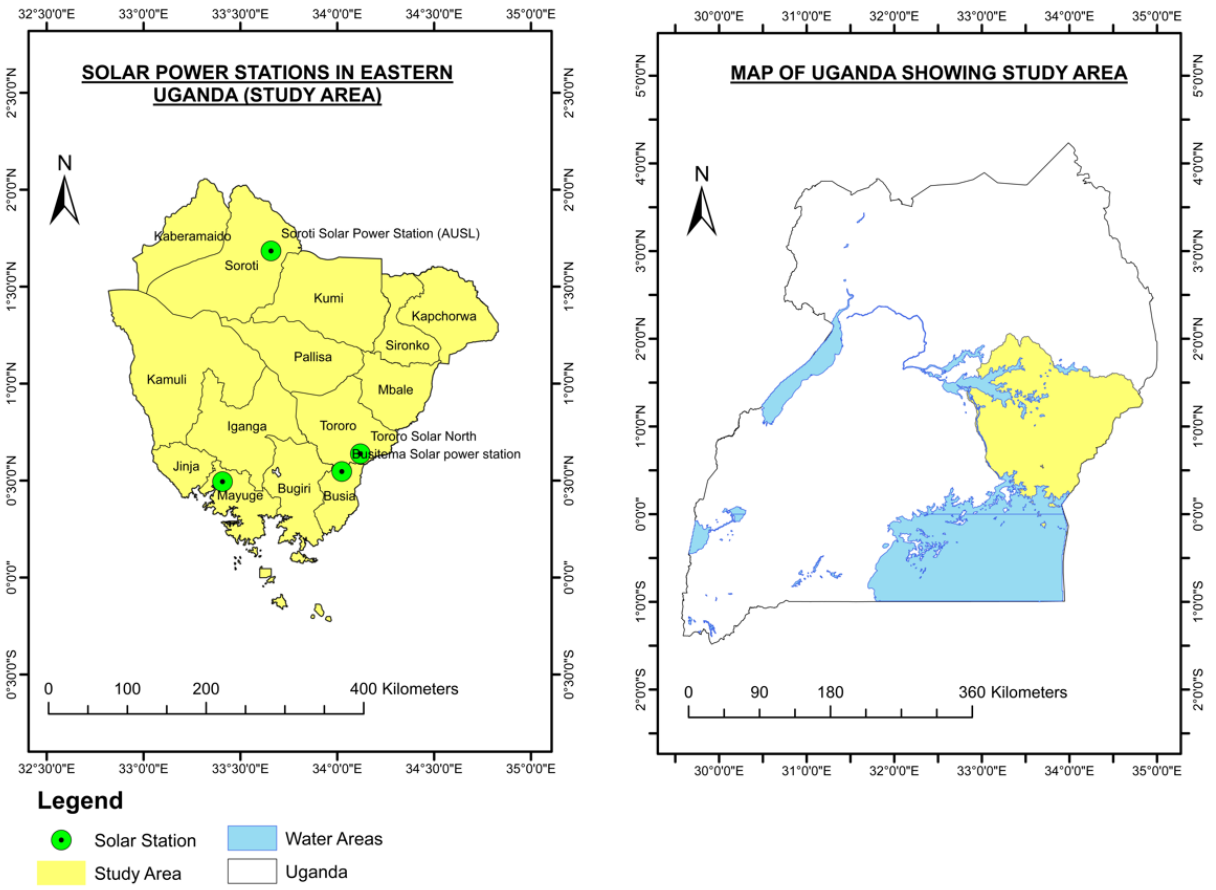

Figure 3.3: Solar power plants in eastern Region

Source: Present study (2023)

3.2 Research Philosophy

Research philosophy is the development of knowledge and its purpose, guiding the researcher in selecting appropriate methods for a study (Kankam, 2019). Three paradigms are postulated: epistemology (positivism, interpretivism, pragmatism), ontology (objectivism, subjectivism), and axiology (value-free, biased) (Rehman & Alharthi, 2016). Epistemology focuses on knowledge dissemination and human interaction with the environment, ontology explores reality, and axiology emphasizes the researcher's perception and ethics (Evans & Selgelid, 2015). In this study, the epistemological paradigm of pragmatism is combined with positivism and interpretivism, guiding the practical activities involved in the study.

3.3 Research Methods

3.3.1 Minimization of electric power losses in transmission lines

This subsection focuses on the methods used to develop and modify the traditional power loss objective model by integrating the third-dimensionally consistent factor of Corona and Ohms losses that validates the optimality of both unmodified and modified models on different power transmission lines in Uganda.

3.3.1.1 Description of the algorithm

In the flow chart (Figure 3.4), the input variables for the unmodified power loss model (current (I), cross-section area (A), thermal resistivity (ρ), phase voltage (V), disruptive voltage (V_0), frequency (f), air density (γ), length (l), radius (r), spacing between conductors (d), radios (r), spacing between transmission lines (d) were identified from the literature. The modified model is obtained by adding the third term to the unmodified model in Equation (3.1), which is a product of a loss reduction factor (0.25) in Equation (3.2) and the square root of Ohm and Corona losses. Maple software was used to obtain the optimum variables based on the first derivatives. The first derivative is further differentiated to obtain the second derivative, which forms the elements of the Hessian matrix. The determinant of the Hessian matrix is used to determine the optimality of power losses in the transmission lines. If the determinant is less than zero, implies minimization of power losses in the transmission lines, whereas a determinant greater than zero denotes maximization of power losses in the transmission lines. The optimum variables were used to calculate the optimum power losses in the transmission lines. The optimality test is implemented on the data acquired from the Uganda Electricity Transmission Company Limited UETCL, 2023. Verification of the unmodified and modified models for minimization of power losses in the transmission lines was carried out with the transmission data acquired from UETCL, 2023.

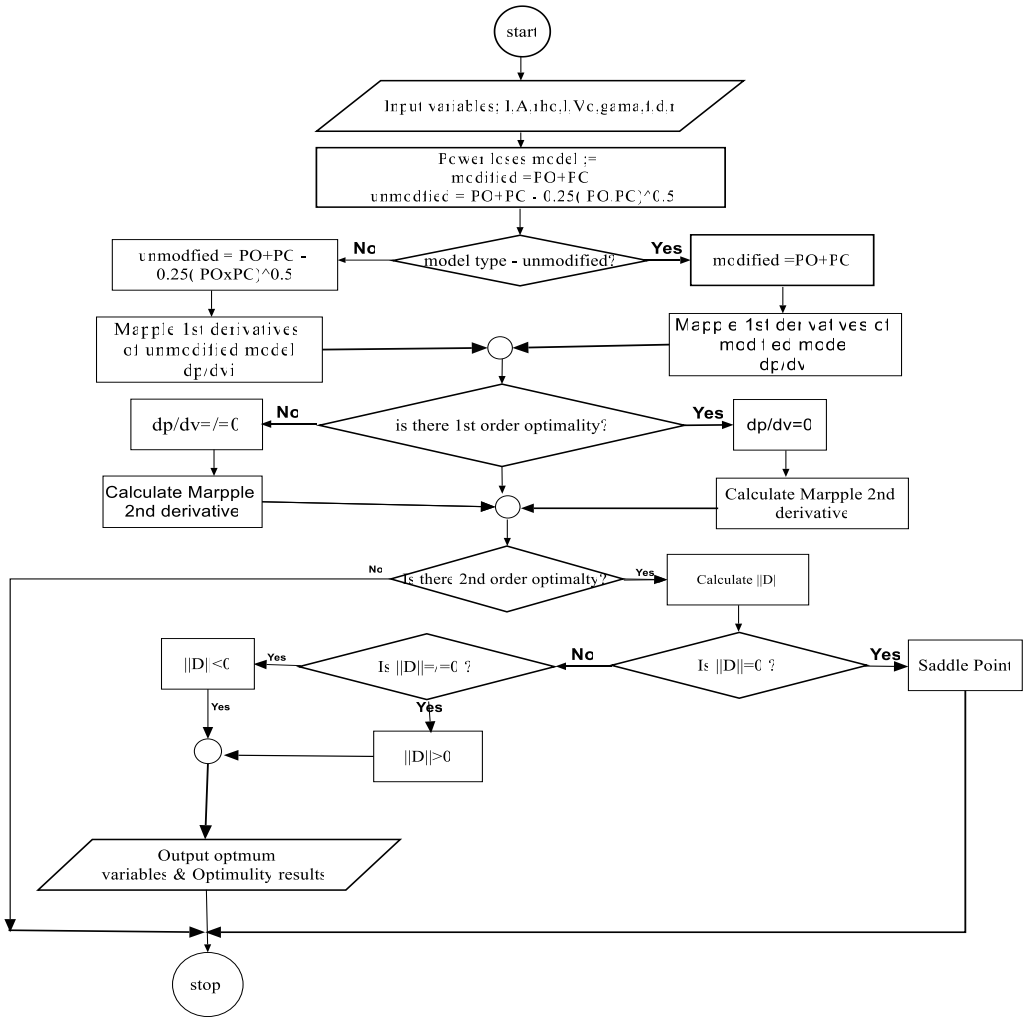

Figure 3.4: Flowchart for the minimization of power losses in the transmission lines Source: Present study (2023)

3.3.1.2 Formulation of power losses in transmission lines

Total transmission power losses are defined by Ohms and Corona losses Bamigbola, *et al.*, (2014) in Equation (3.1). Supposedly, Equation (3.1) minimizes total losses on the transmission lines via the Hessian matrix with a determinant above zero. Equation (3.1) serves an objective function for the minimization of power losses, p in the transmission line depends on the uncoupled (individual) losses in Equation (3.1).

$$\tilde{p} = p_O + p_C \tag{3.1}$$

where $p_O(\mathrm{W/km/Phase})$ is the Ohms loss and $p_C(\mathrm{W/km/Phase})$ is the Corona loss Equation (3.1) is fully defined in Equation (3.2)

$$\tilde{p} = \frac{I^2\rho}{A} + 242\times10^{-05}(V - V_O)^2\left(\frac{f+25}{\gamma l}\right)\left(\frac{r}{d}\right)^{0.5}\left(W/km/phase\right) \tag{3.2}$$

where $I(\text{A or C/s})$ is the transmission current, $\rho(\Omega\text{m})$ is the resistivity of the transmission cable, $l(\text{m})$ is the length of the transmission line, $A(\text{m}^2)$ is cross-section area, $V(\text{V})$ is the phase voltage, $V_0(\text{V})$ is the disruptive voltage, $f(\text{Hz})$ is the transmission frequency, $\gamma(\text{kg/m}^3)$ air density factor, $r(\text{m})$ is the radius of the transmission lines, $d(\text{m})$ is space between transmission lines.

Applying Equation (3.2) as an objective function for minimizing power losses on the transmission lines, the optimum variables (I^*, V^*, γ^*) cannot be established. Thus, the need to establish a modified objective function to obtain the optimum variables and to minimize transmission power losses in Equation (3.3). Equation (3.3) is made up of uncoupled (individual) and coupled (combined) losses

$$\tilde{p} = p_O + p_C - 0.25(p_O p_C)^{0.5} \tag{3.3}$$

Equation (3.3) can be presented in Equation (3.4), that is

$$\begin{aligned}\tilde{p} &= \frac{I^2\rho}{A} + 242\times10^{-5}(V - V_0)^2\left(\frac{f+25}{\gamma l}\right)\left(\frac{r}{d}\right)^{0.5} \\ &- 0.25\left[\left(\frac{I^2\rho}{A}\right)\left(242\times10^{-5}(V - V_0)^2\left(\frac{f+25}{\gamma l}\right)\left(\frac{r}{d}\right)^{0.5}\right)\right]^{0.5} \quad \left(kW/km/phase\right)\end{aligned} \tag{3.4}$$

The optimum transmission variables (I^*, V^*, γ^*) are obtained by differentiating Equation (3.4) with respect to these variables, equating the differential to zero and making the optimum variables the subject of the formula in Equations (3.5, 3.6, 3.7, 3.8). The differentiation was done using Maple 2021. Thus, differentiating Equation (3.4) with respect to (wrt) I gives optimum current, $I^*(\text{A})$ in Equation (3.5).

$$\frac{\partial\tilde{p}}{\partial I} = \frac{2I\rho}{A} - \frac{0.01229837388I\rho(V - V_0)^2(f+25)\sqrt{\frac{r}{d}}}{\sqrt{\frac{I^2\rho(V - V_0)^2(f+25)\sqrt{\frac{r}{d}}}{A\gamma l}A\gamma l}} \tag{3.5}$$

$$I^{*}=\frac{0.006149186940\sqrt{\sqrt{\frac{r}{d}}d\gamma l\rho Ar\left(f+25\right)\left(V-V_{0}\right)}}{\sqrt{\frac{r}{d}}d\gamma l\rho}$$

Differentiating Equation (3.4) with respect to transmission phase voltage gives optimum phase transmission voltage, $V^{*}(V)$ in Equation (3.6)

$$\frac{\partial\tilde{p}}{\partial V}=\frac{121(V-V_{0})\left(f+25\right)\sqrt{\frac{r}{d}}}{25000\gamma l}-\frac{0.01229837388\,I^{2}\rho(V-V_{0})\left(f+25\right)\sqrt{\frac{r}{d}}}{\sqrt{\frac{I^{2}\rho(V-V_{0})^{2}\left(f+25\right)\sqrt{\frac{r}{d}}}{A\gamma l}A\gamma l}}\;; \tag{3.6}$$

$$V^{*}=\frac{1}{\sqrt{\frac{r}{d}}A(f+25)}\left(8.264462810\times10^{-9}\left(\begin{array}{l}1.21\times10^{8}A\sqrt{\frac{r}{d}}fV+4.84\times10^{8}A\sqrt{\frac{r}{d}}V\\+3.025\times10^{9}\sqrt{\frac{r}{d}}AV-3.07459347\times10^{8}\sqrt{A\sqrt{\frac{r}{d}}f\gamma l\rho I^{2}+25A\sqrt{\frac{r}{d}}\gamma l\rho I^{2}}\end{array}\right)\right)$$

Differentiating Equation. (3.4) with respect to air density factor gives optimum air density factor, $\gamma^{*}(\mathrm{kg/m^{3}})$ in Equation. (3.7)

$$\frac{\partial\tilde{p}}{\partial\gamma}=-\frac{121(V-V_{0})^{2}\left(f+25\right)\sqrt{\frac{r}{d}}}{50000l\gamma^{2}}+\frac{0.00614940I^{2}\rho(V-V_{0})^{2}\left(f+25\right)\sqrt{\frac{r}{d}}}{\sqrt{\frac{I^{2}\rho(V-V_{0})^{2}\left(f+25\right)\sqrt{\frac{r}{d}}}{A\gamma l}A\gamma^{2}l}} \tag{3.7}$$

$$\gamma^{*}=\frac{0.000759215685\sqrt{\frac{r}{d}}A\left(V^{2}f-2VfV_{0}+fV_{0}^{2}+25V^{2}-50VV_{0}+25V_{0}^{2}\right)}{I^{2}\rho l}$$

3.3.1.3 Proof of optimality of the objective function-transmission losses

The objective function could be proved to be either maximum or minimum by obtaining the matrix of second order derivative of the objective function from Equation (3.4) in Equation (3.8) Hessian matrix, H

$$H = \begin{bmatrix} \frac{\partial^2(\tilde{p})}{\partial^2 I^2} & \frac{\partial^2(\tilde{p})}{\partial I \partial V} & \frac{\partial^2(\tilde{p})}{\partial I \partial \gamma} \\ \frac{\partial^2(\tilde{p})}{\partial V \partial I} & \frac{\partial^2(\tilde{p})}{\partial^2 V^2} & \frac{\partial^2(\tilde{p})}{\partial V \partial \gamma} \\ \frac{\partial^2(\tilde{p})}{\partial \gamma \partial I} & \frac{\partial^2(\tilde{p})}{\partial \gamma \partial V} & \frac{\partial^2(\tilde{p})}{\partial^2 \gamma^2} \end{bmatrix} \tag{3.8}$$

3.3.1.4 Derivatives of the Hessian matrix

The diagonal elements of the Hessian matrix in Equation (3.8) is given in Equations (3.9, 3.10, and 3.11). The second derivative of power losses, p with respect to I is given in Equation (3.8)

$$\frac{\partial^2 \tilde{p}}{\partial I^2} = \frac{2\rho}{A} + \frac{0.01229837388 I^2 \rho^2 (V - V_0)^4 (f + 25)^2 \left(\frac{r}{d}\right)}{\left(\frac{I^2 \rho (V - V_0)^2 (f + 25)\sqrt{\frac{r}{d}}}{A\gamma l}\right)^{3/2} A^2 \gamma^2 l^2} - \frac{0.01229837388 \rho (V - V_0)^2 (f + 25)\sqrt{\frac{r}{d}}}{\sqrt{\frac{I^2 \rho (V - V_0)^2 (f + 25)\sqrt{\frac{r}{d}}}{A\gamma l}} A\gamma l} \tag{3.9}$$

The second derivative of power losses, p with respect to V is given in Equation (3.10)

$$\frac{\partial^2 \tilde{p}}{\partial V^2} = \frac{121(f + 25)\sqrt{\frac{r}{d}}}{25000\gamma l} + \frac{0.0122983788 I^4 \rho^2 (V - V_0)^2 (f + 25)^2 \left(\frac{r}{d}\right)}{\left(\frac{I^2 \rho (V - V_0)^2 (f + 25)\sqrt{\frac{r}{d}}}{A\gamma l}\right)^{1.5} A^2 \gamma^2 l^2} - \frac{0.0122983788 I^2 \rho (f + 25)\sqrt{\frac{r}{d}}}{\sqrt{\frac{I^2 \rho (V - V_0)^2 (f + 25)\sqrt{\frac{r}{d}}}{A\gamma l}} A\gamma l} \tag{3.10}$$

The second derivative of power losses, p wrt γ is given in Equation (3.11)

$$\frac{\partial^2 \tilde{p}}{\partial \gamma^2} = \frac{121(V - V_0)^2 (f + 25)\sqrt{\frac{r}{d}}}{25000\gamma^3 l} + \frac{0.003074593470 I^4 \rho^2 (V - V_0)^4 (f + 25)^2 \left(\frac{r}{d}\right)}{\left(\frac{I^2 \rho (V - V_0)^2 (f + 25)\sqrt{\frac{r}{d}}}{A\gamma l}\right)^{3/2} A^2 \gamma^4 l^2} - \frac{0.0122983788 I^2 \rho (V - V_0)^2 (f + 25)\sqrt{\frac{r}{d}}}{\sqrt{\frac{I^2 \rho (V - V_0)^2 (f + 25)\sqrt{\frac{r}{d}}}{A\gamma l}} A\gamma^3 l} \tag{3.11}$$

3.3.1.5 Upper diagonal elements of Hessian matrix

Upper diagonal elements are derived in Equations (3.12-3.14). The second derivative of power losses with respect to I and V is given in Equation (12)

$$\frac{\partial^2 \tilde{p}}{\partial I \partial V} = \frac{0.01229837388 I^3 \rho^2 (V - V_0)^3 (f + 25)^2 \left(\frac{r}{d}\right)}{\left(\frac{I^2 \rho (V - V_0)^2 (f + 25)\sqrt{\frac{r}{d}}}{Al\gamma}\right)^{1.5} A^2 \gamma^2 l^2} - \frac{0.024596774776 I \rho (V - V_0)(f + 25)\sqrt{\frac{r}{d}}}{\sqrt{\frac{I^2 \rho (V - V_0)^2 (f + 25)\sqrt{\frac{r}{d}}}{Al\gamma}} A\gamma l} \quad (12)$$

The second derivative of power losses with respect to I and γ is given in Equation (3.13)

$$\frac{\partial^2 \tilde{p}}{\partial I \partial \gamma} = -\frac{0.00614918694 I^3 \rho^2 (V - V_0)^4 (f + 25)^2 \left(\frac{r}{d}\right)}{\left(\frac{I^2 \rho (V - V_0)^2 (f + 25)\sqrt{\frac{r}{d}}}{Al\gamma}\right)^{1.5} A^2 \gamma^3 l^2} + \frac{0.01229837388 \rho (V - V_0)^2 (f + 25)\sqrt{\frac{r}{d}}}{\sqrt{\frac{I^2 \rho (V - V_0)^2 (f + 25)\sqrt{\frac{r}{d}}}{A\gamma l}} A\gamma^2 l} \quad (3.13)$$

The second derivative of power losses with respect to V and γ is given in Equation (3.14)

$$\frac{\partial^2 \tilde{p}}{\partial V \partial \gamma} = -\frac{121(V - V_0)\sqrt{\frac{r}{d}}}{25000 l \gamma^2} - \frac{0.00614918694 I^4 \rho^2 (V - V_0)^3 (f + 25)^2 \left(\frac{r}{d}\right)}{\left(\frac{I^2 \rho (V - V_0)^2 (f + 25)\sqrt{\frac{r}{d}}}{Al\gamma}\right)^{1.5} A^2 \gamma^3 l^2} + \frac{0.01229837388 I^2 \rho (V - V_0)(f + 25)\sqrt{\frac{r}{d}}}{\sqrt{\frac{I^2 \rho (V - V_0)^2 (f + 25)\sqrt{\frac{r}{d}}}{A\gamma l}} A\gamma^2 l} \quad (3.14)$$

3.3.1.6 Lower diagonal elements of Hessian matrix

The lower diagonal elements of the Hessian matrix are obtained as the reciprocal of Equations (3.15, 3.16, and 3.17).

The second derivative of power losses with respect to V and I is given in Equation (3.15)

$$\frac{\partial^2 \tilde{p}}{\partial V \partial I} = \frac{0.01229837388 I^3 \rho^2 (V - V_0)^3 (f + 25)^2 \left(\frac{r}{d}\right)}{\left(\frac{I^2 \rho (V - V_0)^2 (f + 25)\sqrt{\frac{r}{d}}}{Al\gamma}\right)^{1.5} A^2 \gamma^2 l^2} - \frac{0.02459674776 I \rho (V - V_0)(f + 25)\sqrt{\frac{r}{d}}}{\sqrt{\frac{I^2 \rho (V - V_0)^2 (f + 25)\sqrt{\frac{r}{d}}}{Al\gamma}} A\gamma l} \quad (3.15)$$

The second derivative of power losses with respect to γ and I is given in Equation (3.16)

$$\frac{\partial^2 \tilde{p}}{\partial\gamma\partial I} = -\frac{0.00614918694 I^3\rho^2(V-V_0)^4\left(f+25\right)^2\left(\frac{r}{d}\right)}{\left(\frac{I^2\rho(V-V_0)^2\left(f+25\right)\sqrt{\frac{r}{d}}}{Al\gamma}\right)^{1.5} A^2\gamma^3 l^2} + \frac{0.01229837388 I\rho(V-V_0)^2\left(f+25\right)\sqrt{\frac{r}{d}}}{\sqrt{\frac{I^2\rho(V-V_0)^2\left(f+25\right)\sqrt{\frac{r}{d}}}{A\gamma l}} A\gamma^2 l} \tag{3.16}$$

The second derivative of power losses with respect to γ and V is given in Equation (3.17)

$$\frac{\partial^2 \tilde{p}}{\partial\gamma\partial V} = -\frac{121\left(V-V_0\right)\sqrt{\frac{r}{d}}}{25000 l\gamma^2} - \frac{0.006149186940 I^4\rho^2(V-V_0)^3\left(f+25\right)^2\left(\frac{r}{d}\right)}{\left(\frac{I^2\rho(V-V_0)^2\left(f+25\right)\sqrt{\frac{r}{d}}}{Al\gamma}\right)^{1.5} A^2\gamma^3 l^2} + \frac{0.01229837388 I^2\rho(V-V_0)\left(f+25\right)\sqrt{\frac{r}{d}}}{\sqrt{\frac{I^2\rho(V-V_0)^2\left(f+25\right)\sqrt{\frac{r}{d}}}{A\gamma l}} A\gamma^2 l} \tag{3.17}$$

where $I(\text{A or C/s})$ is the transmission current, $\rho(\Omega\text{m})$ is the resistivity of transmission cable, $l(\text{m})$ is the length of transmission line, $A(\text{m}^2)$ is cross-section area, $V(\text{V})$ is the phase voltage, $V_0(\text{V})$ is the disruptive voltage, $f(\text{Hz})$ is the transmission frequency, $\gamma(\text{kg/m}^3)$ air density factor, $r(\text{m})$ is the radius of transmission cable, $d(\text{m})$ is space between transmission cable.

Applying Equations (3.1 and 3.2) as an objective function for minimizing power losses on the transmission lines, the optimum variables (I^*, V^*, γ^*) cannot be established. Thus, the need to establish a modified objective function to obtain the optimum variables and to minimize transmission power losses in Equation (3.3). Equation (3.3) comprises of uncoupled (individual) and coupled (combined) losses

The determinant (D) of the unmodified Hessian matrix in Equation (3.8) is given in Equation (3.15) for 132 kV (Masaka West - Mbarara North)

$$D = \begin{bmatrix} 2\rho/\text{A} & 0 & 0 \\ 0 & \frac{\left(121\left(f+25\right)\sqrt{r/d}\right)}{25000\gamma l} & -\frac{\left(121\left(f+25\right)\left(V-V_0\right)\sqrt{r/d}\right)}{25000\gamma^2 l} \\ 0 & -\frac{\left(121\left(f+25\right)\left(V-V_0\right)\sqrt{r/d}\right)}{25000\gamma^2 l} & \frac{\left(121\left(f+25\right)\left(V-V_0\right)^2\sqrt{r/d}\right)}{25000\gamma^3 l} \end{bmatrix} = \tag{3.18}$$

$$\begin{bmatrix} 0.0001656250000 & 0 & 0 \\ 0 & 6.486280296\times10^{-8} & -0.0009321892659 \\ 0 & -0.0009321892659 & 13.39715194 \end{bmatrix}$$

The determinant (D) of modified Hessian matrix in Equation (3.8) is given in Equation (3.19) for 132 kV (Masaka West - Mbarara North)

$$D=\begin{bmatrix} \text{Eq.}(9) & \text{Eq.}(12) & \text{Eq.}(13) \\ \text{Eq.}(15) & \text{Eq.}(10) & \text{Eq.}(14) \\ \text{Eq.}(16) & \text{Eq.}(17) & \text{Eq.}(11) \end{bmatrix}=\begin{bmatrix} 0.000165625 & -4.09705\times10^{-7} & 0.002944 \\ -4.09705\times10^{-7} & 6.48628\times10^{-8} & -0.0009 \\ 0.002944077 & -0.000903709 & 12.78319 \end{bmatrix} \quad (3.19)$$

The determinant (D) of Unmodified Hessian matrix in Equation (3.8) is given in Equation (3.20) for 220 kV (Bujagali – Kawanda)

$$D=\begin{bmatrix} 2\rho/\text{A} & 0 & 0 \\ 0 & \dfrac{\left(121(f+25)\sqrt{r/d}\right)}{25000\gamma l} & -\dfrac{\left(121(f+25)(V-V_0)\sqrt{r/d}\right)}{25000\gamma^2 l} \\ 0 & -\dfrac{\left(121(f+25)(V-V_0)\sqrt{r/d}\right)}{25000\gamma^2 l} & \dfrac{\left(121(f+25)(V-V_0)^2\sqrt{r/d}\right)}{25000\gamma^3 l} \end{bmatrix} \quad (3.20)$$

$$=\begin{bmatrix} 0.0003386581470 & 0 & 0 \\ 0 & 4.770989518\times10^{-8} & -0.004323045167 \\ 0 & -0.004323045167 & 391.7157945 \end{bmatrix}$$

The determinant (D) of modified Hessian matrix in Equation (3.8) is given in Equation (3.21) for 220 kV (Bujagali – Kawanda)

$$D=\begin{bmatrix} \text{Eq.}(9) & \text{Eq.}(12) & \text{Eq.}(13) \\ \text{Eq.}(15) & \text{Eq.}(10) & \text{Eq.}(14) \\ \text{Eq.}(16) & \text{Eq.}(17) & \text{Eq.}(11) \end{bmatrix} \quad (3.21)$$

$$=\begin{bmatrix} 0.000338658 & -5.02452\text{E}\times10^{-7} & 0.022764 \\ -5.02452\times10^{-7} & 4.770989518\times10^{-8} & -0.004089287381 \\ 0.022763882 & 0.004264606 & 383.7729 \end{bmatrix}$$

3.3.2 Modeling of coupled and uncoupled transmission lines

This subsection focuses on the approaches used in developing the coupled and uncoupled transmission line models for estimating transmission losses

3.3.2.1 Introduction

The methods began with the acquisition of spot (historic) industrial data from the department of planning, design, operation, and maintenance at Uganda Electricity Transmission Company Limited (UETCL, 2023) for the development of power transmission models. The acquired data (measured or field) includes, transmission current (I_m), nominal voltage (V_m), power (P_m), circuit length (L_m) and temperature (T). The transmission model was developed based on; thermal (temperature) balance, power (voltage) balance, power (current) balance. Subsequently, thermal and power balance models were coupled to obtain a coupled system of differential equations (power transmission model) describing power transmission in the transmission line (Bujjagali-Kawanda). Additional losses or deteriorations in transmission line (equipment), with respect to transmission potentials were built into the transmission model. The deterioration constants were calculated as the coupling coefficient of the transmission potentials per unit time. The coupled system of differential equations is solved by using finite difference method based on the Crank Nicolson technique. The numerical model is used for the simulation of power transmission potentials (current, voltage, temperature and power) in Microsoft Excel**.** Power loss in the transmission line was estimated from the simulated results. In addition, the transmission models were statistically validated using Root Mean Square Error (RMSE) with respect to time.

3.3.2.2 Description of flow chart for analysis of Bujjagali-Kawanda transmission line.

The algorithm used in this work is illustrated in Figure 3.5. The input data consists of measured (or field) data for current (I_m), voltage (V_m), temperature (T_m), and power (P_m) obtained from (UETCL, 2023). A coupled model was subsequently developed according to the power potentials of current, voltage, and temperature, a tridiagonal matrix of current, voltage, and temperature was formulated to aid in the simulation of the model. The RMSE was then obtained which helped in model validation. Model simulation was facilitated through the construction of a tridiagonal matrix consisting of current, voltage and temperature. Subsequently, the RMSE was used in the model validation.

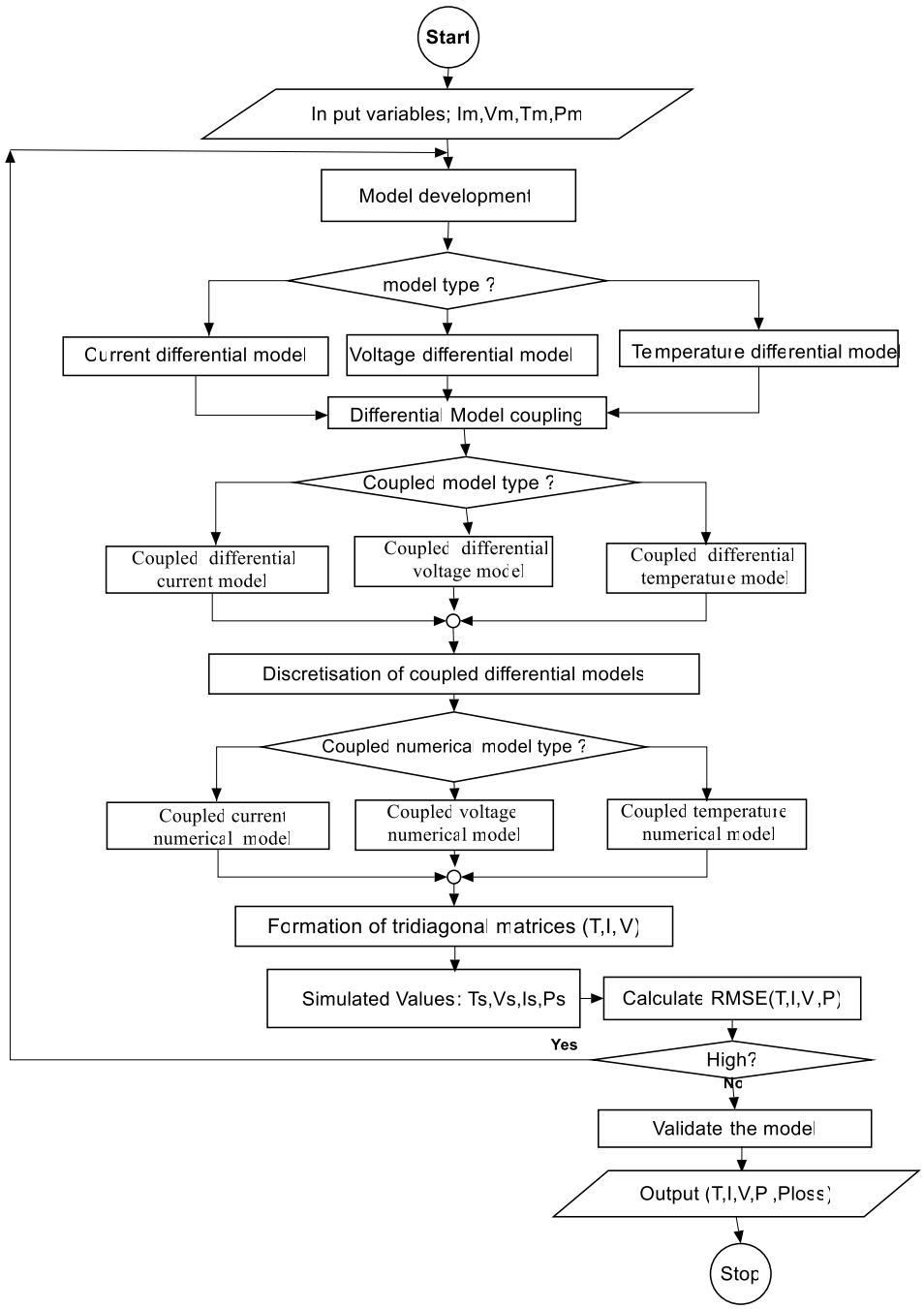

Figure 3.5: Flowchart for data acquisition and processing in coupled model.

Source: Present study (2023)

3.3.2.3 Model formulation

Considering that current has triple effects; thermal, electrical and electromagnetic. Hence, conducting thermal and electrical energy balance around the control volume in Figure 3.6 which represents a single phase. The energy accumulations formulation is obtained as presented in Equation (3.22).

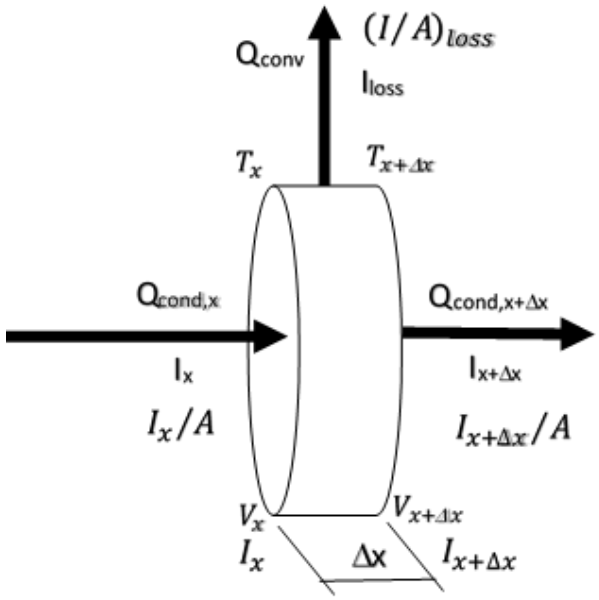

Figure 3.6: Transmission line control volume

Source: Present study (2023)

$$\text{Energy accumulation} = \text{Energy input} - \text{Energy output} \tag{3.22}$$

Fourier's thermal energy balance per unit volume of the control volume Filho, (2017) is given in Equation (3.23)

$$\begin{aligned} \rho cp\frac{\partial \mathrm{T}}{\partial \mathrm{t}} &= k\frac{\partial^2 T}{\partial \mathrm{x}^2} - \frac{\mathrm{hx}}{\mathrm{L}^2}\left(T - T_a\right) - \rho cpk_T\frac{x}{L}\left(T - T_a\right)^2 \\ \Rightarrow \frac{\partial \mathrm{T}}{\partial \mathrm{t}} &= \alpha\frac{\partial^2 T}{\partial \mathrm{x}^2} - \frac{\mathrm{hx}}{\mathrm{L}^2\rho cp}\left(T - T_a\right) - k_T\frac{x}{L}\left(T - T_a\right)^2 \end{aligned} \tag{3.23}$$

where $\alpha = \frac{k}{\rho cp}$, $\rho(\mathrm{kg/m^3})$ is the density of the transmission line (aluminum), $\mathrm{cp(J/kgK)}$ is the specific heat capacity of the transmission line, T(K) is the temperature of the transmission line, t(s) is time variable, $\mathrm{k(W/mK)}$ is the thermal conductivity of the transmission line, x(m) is the

transmission line space variable, $h(W/m^2K)$ is the heat transfer coefficient of the surrounding air, $L(m)$ is the transmission length, and k_T is thermal aging or second order deterioration constant. Ohm's electric energy balance around the control volume Ignjatovic and Cvetic, (2021) is given in Equation (3.24)

$$C\frac{\partial V}{\partial t} = D_e C\frac{\partial^2 V}{\partial x^2} - 242\times10^{-5}\frac{x}{L}(V-V_a)^2\frac{f+25}{\gamma}\sqrt{\frac{r}{d}} - \frac{x}{L}Ck_V(V-V_d)^2$$

Dividing through by C the equation becomes

$$\frac{\partial V}{\partial t} = D_e\frac{\partial^2 V}{\partial x^2} - 242\times10^{-5}\frac{x}{LC}(V-V_a)^2\frac{f+25}{\gamma}\sqrt{\frac{r}{d}} - \frac{x}{L}k_V(V-V_d)^2 \quad \exists \quad C = It; \tag{3.24}$$

$$V_d \approx V_a$$

where $\exists$ is there exist, C (Coulomb) is the product of current, $I(A)$ and time, $t(s)$, $D_e(m^2/s)$ is the electrical diffusivity, $V(V)$ is the phase voltage, $V_d(V)$ is the disruptive voltage, $H(Hz)$ is transmission frequency, $\gamma(kg/m^3)$ is the air density factor, $r(m)$ is the radius of transmission line, and $d(m)$ is the distance between the transmission line, and k_V is voltage aging or second order deterioration constant. The electromagnetic energy in the transmission line Ignjatovic and Cvetic, (2021) is further defined in Equation (3.25) as

$$RC\frac{\partial I}{\partial t} = D_e RC\frac{\partial^2 I}{\partial x^2} - \frac{I^2\sigma L}{A} - RC\frac{x}{L}k_I I^2 \qquad \exists \qquad C = It \quad \text{and} \quad R = \frac{V}{I}$$

Dividing RC the equation becomes (3.25)

$$\Rightarrow \frac{\partial I}{\partial t} = D_e\frac{\partial^2 I}{\partial x^2} - \frac{xI}{Lt} - \frac{x}{L}k_I I^2$$

where $I(A)$ is the current in the transmission line, $L(km)$ is the length of the transmission line, $A(m^2)$ is the cross-section area of the transmission line, and $\sigma(\Omega m)$ is the resistivity of the transmission line and k_I is current aging or second order deterioration constant.

.

The air density factor, $\gamma(kg/m^3)$ Tonmitr *et al.*, (2016) is defined in Equation (3.26) as

$$\gamma = \frac{3.94b}{273.15+temp} = \frac{3.94\times76}{273.15+temp} = \frac{299.44}{273.15+temp} \tag{3.26}$$

where b (cmHg) is the atmospheric pressure and $temp(\text{degree Celsius})$ is the atmospheric temperature.

The disruptive voltage, $V_d(V)$ Tonmitr *et al.*, (2016) is defined in Equation (3.27) as;

$$V_d = 121\mu \ln\left(1+\frac{0.3}{\sqrt{r\gamma}}\right) = 121\times 0.82\times \ln\left(1+\frac{0.3}{\sqrt{r\gamma}}\right) \tag{3.27}$$

where $\mu\ (-)$ is the roughness of stranded transmission lines.

3.3.2.4 Coupling of transmission models

Since the changes in the potentials (T, V and I) in Equation (3.23) in space and time are happening concurrently, thus, coupling them would help to explain the intricate physical phenomena among the potentials in space and time. The three coupling coefficients are the temperature, $\beta_T(1/\mathrm{K})$, phase voltage, $\beta_V(1/\mathrm{V})$ and current, $\beta_I(1/\mathrm{A})$ and their corresponding reciprocals; $1/\beta_T$ (K), $1/\beta_V$ (V) and $1/\beta_I$(A) result in diffusive coupling of Equations (3.23- 3.25) in Equations (3.28-3.30).

The coupled thermal model with Thermal aging/ deterioration term in transmission line is given in Equation (3.28) as

$$\Rightarrow \frac{\partial \mathrm{T}}{\partial \mathrm{t}} = \alpha\frac{\partial^2 T}{\partial \mathrm{x}^2} - \frac{\mathrm{hx}}{\mathrm{L}^2\rho cp}\left(T-T_a\right) + \alpha\frac{\beta_V}{\beta_T}\frac{\partial^2 V}{\partial \mathrm{x}^2} + \alpha\frac{\beta_I}{\beta_T}\frac{\partial^2 I}{\partial \mathrm{x}^2} - k_T\frac{x}{L}\left(T-T_a\right)^2 \tag{3.28}$$

The coupled electrical model with electrical (voltage and current) aging/ deterioration term are given in Equations (3.29) and (3.30) as

$$\Rightarrow \frac{\partial \mathrm{V}}{\partial \mathrm{t}} = D_e\frac{\partial^2 V}{\partial \mathrm{x}^2} - 242\times 10^{-5}\frac{x}{LIt}\left(V-V_a\right)^2\frac{f+25}{\gamma}\sqrt{\frac{r}{d}} - D_e\frac{\beta_T}{\beta_V}\frac{\partial^2 T}{\partial \mathrm{x}^2} - D_e\frac{\beta_I}{\beta_V}\frac{\partial^2 I}{\partial \mathrm{x}^2} - \frac{x}{L}k_V\left(V-V_d\right)^2 \tag{3.29}$$

and

$$\Rightarrow \frac{\partial \mathrm{I}}{\partial \mathrm{t}} = D_e\frac{\partial^2 I}{\partial \mathrm{x}^2} - \frac{Ix}{Lt} + D_e\frac{\beta_T}{\beta_I}\frac{\partial^2 T}{\partial \mathrm{x}^2} + D_e\frac{\beta_V}{\beta_I}\frac{\partial^2 V}{\partial \mathrm{x}^2} - \frac{x}{L}k_I I^2 \tag{3.30}$$

3.3.2.5 Boundary conditions

Simulation of transmission potentials was initiated by Dirichlet or first kind boundary conditions of transmission potentials (current, I(x), voltage V(x) temperature, T(x)); for the pairs $\mathrm{I}(\mathrm{x}=0\ \mathrm{m}), \mathrm{I}(\mathrm{l}=144000\ \mathrm{m});\ \mathrm{V}(\mathrm{x}=0\ \mathrm{m}), \mathrm{V}(\mathrm{l}=144000\ \mathrm{m});\ \mathrm{T}(\mathrm{x}=0\ \mathrm{m}), \mathrm{T}(\mathrm{l}=144000\ \mathrm{m});\ \mathrm{P}(\mathrm{x}=0\ \mathrm{m}), \mathrm{P}(\mathrm{l}=144000\ \mathrm{m})$.

3.3.2.6 Initial conditions

Similarly, simulation of transmission potentials was initiated by initial conditions of transmission potentials (current, I(x), voltage, V(x) temperature, T(x)) as follows; $\mathrm{I(t = 0\ s), V(t = 0\ s), T(t = 0\ s), P(t = 0\ s)}$. In complement to boundary conditions, the simulations were realized.

3.3.2.7 Numerical Solution of Dimension Equations

The numerical solutions of Equations (3.28 – 3.30) are obtained by the finite difference method (Crank Nicolson equal explicit and implicit techniques for uncoupled terms and pure explicit for coupled terms). The resulting algebraic equations are solved simultaneously to give the future values of the potentials.

Discretizing Equation (3.28) gives Equation (3.31). In the same way, discretizing Equations (3.29) and (3.30) gives Equations. (3.32) and (3.33) respectively.

$$\frac{T_i^{n+1}-T_i^n}{\Delta t}=\alpha\left(\psi\frac{T_{i-1}^{n+1}-2T_i^{n+1}+T_{i+1}^{n+1}}{(\Delta x)^2}+(1-\psi)\frac{T_{i-1}^{n}-2T_i^{n}+T_{i+1}^{n}}{(\Delta x)^2}\right)-\left(\frac{\mathrm{hx}}{\mathrm{L}^2\rho cp}\right)\left(T_i^n-T_a\right)$$
$$+\alpha\frac{\beta_V}{\beta_T}\left(\frac{V_{i-1}^{n}-2V_i^{n}+V_{i+1}^{n}}{(\Delta x)^2}\right)+\alpha\frac{\beta_I}{\beta_T}\left(\frac{I_{i-1}^{n}-2I_i^{n}+I_{i+1}^{n}}{(\Delta x)^2}\right)-k_T\frac{x_i^n}{L}\left(T_i^n-T_a\right)^2 \quad (3.31)$$

$$\frac{V_i^{n+1}-V_i^n}{\Delta t}=D_e\left(\psi\frac{V_{i-1}^{n+1}-2V_i^{n+1}+V_{i+1}^{n+1}}{(\Delta x)^2}+(1-\psi)\frac{V_{i-1}^{n}-2V_i^{n}+V_{i+1}^{n}}{(\Delta x)^2}\right)-\left(242\times10^{-5}\frac{x_i^n}{L}\frac{\left(V_i^n-V_d\right)^2}{I_i^n t_i^n}\frac{f+25}{\gamma}\left(\frac{r}{d}\right)^{0.5}\right) \quad (3.32)$$
$$-D_e\frac{\beta_T}{\beta_V}\left(\frac{T_{i-1}^{n}-2T_i^{n}+T_{i+1}^{n}}{(\Delta x)^2}\right)-D_e\frac{\beta_I}{\beta_V}\left(\frac{I_{i-1}^{n}-2I_i^{n}+I_{i+1}^{n}}{(\Delta x)^2}\right)-\frac{x_i^n}{L}k_V\left(V_i^n-V_d\right)^2$$

$$\frac{I_i^{n+1}-I_i^n}{\Delta t}=D_e\left(\psi\frac{I_{i-1}^{n+1}-2I_i^{n+1}+I_{i+1}^{n+1}}{(\Delta x)^2}+(1-\psi)\frac{I_{i-1}^{n}-2I_i^{n}+I_{i+1}^{n}}{(\Delta x)^2}\right)-\left(\frac{I_i^n x_i^n}{Lt_i^n}\right)$$
$$+D_e\frac{\beta_T}{\beta_I}\left(\frac{T_{i-1}^{n}-2T_i^{n}+T_{i+1}^{n}}{(\Delta x)^2}\right)+D_e\frac{\beta_V}{\beta_I}\left(\frac{V_{i-1}^{n}-2V_i^{n}+V_{i+1}^{n}}{(\Delta x)^2}\right)-\frac{x_i^n}{L}k_I\left(I_i^n\right)^2 \quad (3.33)$$

Rearranging Equation. (3.31) into $\mathrm{n+1}$ and n terms gives Equation (3.34)

(3.34)

$$\left(-\zeta_{T,i}^{n}\psi\right)T_{i-1}^{n+1}+\left(1+2\zeta_{T,i}^{n}\psi\right)T_{i}^{n+1}+\left(-\zeta_{T,i}^{n}\psi\right)T_{i+1}^{n+1}=T_{i}^{n}+\zeta_{T,i}^{n}\left(1-\psi\right)\left(T_{i-1}^{n}-2T_{i}^{n}+T_{i+1}^{n}\right)-\left(\frac{\mathrm{x_i^n h}\Delta t}{\mathrm{L}^2\rho cp}\right)\left(T_{i}^{n}-T_{a}\right)$$

$$+\zeta_{T,i}^{n}\frac{\beta_V}{\beta_T}\left(V_{i-1}^{n}-2V_{i}^{n}+V_{i+1}^{n}\right)+\zeta_{T,i}^{n}\frac{\beta_I}{\beta_T}\left(I_{i-1}^{n}-2I_{i}^{n}+I_{i+1}^{n}\right)-k_T\frac{x_i^n}{L}\left(T_{i}^{n}-T_{a}\right)^2=f_{T,i}^{n}\qquad\exists\qquad\zeta_{T,i}^{n}=\frac{\alpha\Delta t}{\left(\Delta x\right)^2}$$

For $\mathrm{n}=0$ and $1\le \mathrm{i}\le \mathrm{N}-1$ leads to a tridiagonal matrix in Equation (3.35)

$$\left(1+2\zeta_{T,1}^{0}\psi\right)T_{1}^{1}+\left(-\zeta_{T,1}^{0}\psi\right)T_{2}^{1}=\left(\zeta_{T,1}^{0}\psi\right)T_{0}^{1}+T_{1}^{0}+\zeta_{T,1}^{0}\left(1-\psi\right)\left(T_{0}^{0}-2T_{1}^{0}+T_{2}^{0}\right)-\left(\frac{\mathrm{x_i^n h}\Delta t}{\mathrm{L}^2\rho cp}\right)\left(T_{1}^{0}-T_{a}\right)$$

$$+\zeta_{T,1}^{0}\frac{\beta_V}{\beta_T}\left(V_{0}^{0}-2V_{1}^{0}+V_{2}^{0}\right)+\zeta_{T,1}^{0}\frac{\beta_I}{\beta_T}\left(I_{0}^{0}-2I_{1}^{0}+I_{2}^{0}\right)-k_T\frac{x_1^0}{L}\left(T_{1}^{0}-T_{a}\right)^2=f_{T,1}^{0}\qquad\exists\qquad\zeta_{T,1}^{0}=\frac{\alpha\Delta t}{\left(\Delta x\right)^2}$$

$$\left(-\zeta_{T,2}^{0}\psi\right)T_{1}^{1}+\left(1+2\zeta_{T,2}^{0}\psi\right)T_{2}^{1}+\left(-\zeta_{T,2}^{0}\psi\right)T_{3}^{1}=T_{2}^{0}+\zeta_{T,2}^{0}\left(1-\psi\right)\left(T_{1}^{0}-2T_{2}^{0}+T_{3}^{0}\right)-\left(\frac{\mathrm{x_i^n h}\Delta t}{\mathrm{L}^2\rho cp}\right)\left(T_{2}^{0}-T_{a}\right)$$

$$+\zeta_{T,2}^{0}\frac{\beta_V}{\beta_T}\left(V_{1}^{0}-2V_{2}^{0}+V_{3}^{0}\right)+\zeta_{T,2}^{0}\frac{\beta_I}{\beta_T}\left(I_{1}^{0}-2I_{2}^{0}+I_{3}^{0}\right)-k_T\frac{x_2^0}{L}\left(T_{2}^{0}-T_{a}\right)^2=f_{T,2}^{0}\qquad\exists\qquad\zeta_{T,2}^{0}=\frac{\alpha\Delta t}{\left(\Delta x\right)^2}$$

$$\left(-\zeta_{T,3}^{0}\psi\right)T_{2}^{1}+\left(1+2\zeta_{T,3}^{0}\psi\right)T_{3}^{1}+\left(-\zeta_{T,3}^{0}\psi\right)T_{4}^{1}=T_{3}^{0}+\zeta_{T,3}^{0}\left(1-\psi\right)\left(T_{2}^{0}-2T_{3}^{0}+T_{4}^{0}\right)-\left(\frac{\mathrm{x_i^n h}\Delta t}{\mathrm{L}^2\rho cp}\right)\left(T_{3}^{0}-T_{a}\right)$$

$$+\zeta_{T,3}^{0}\frac{\beta_V}{\beta_T}\left(V_{2}^{0}-2V_{3}^{0}+V_{4}^{0}\right)+\zeta_{T,3}^{0}\frac{\beta_I}{\beta_T}\left(I_{2}^{0}-2I_{3}^{0}+I_{4}^{0}\right)-k_T\frac{x_3^0}{L}\left(T_{3}^{0}-T_{a}\right)^2=f_{T,3}^{0}\qquad\exists\qquad\zeta_{T,3}^{0}=\frac{\alpha\Delta t}{\left(\Delta x\right)^2}$$

$$\vdots$$

$$\left(-\zeta_{T,N-3}^{0}\psi\right)T_{N-4}^{1}+\left(1+2\zeta_{T,N-3}^{0}\psi\right)T_{N-3}^{1}+\left(-\zeta_{T,N-3}^{0}\psi\right)T_{N-2}^{1}=T_{N-3}^{0}+\zeta_{T,N-3}^{0}\left(1-\psi\right)\left(T_{N-4}^{0}-2T_{N-3}^{0}+T_{N-2}^{0}\right)-\left(\frac{\mathrm{x_i^n h}\Delta t}{\mathrm{L}^2\rho cp}\right)\left(T_{N-3}^{0}-T_{a}\right)\qquad(3.35)$$

$$+\zeta_{T,N-3}^{0}\frac{\beta_V}{\beta_T}\left(V_{N-4}^{0}-2V_{N-3}^{0}+V_{N-2}^{0}\right)+\zeta_{T,N-3}^{0}\frac{\beta_I}{\beta_T}\left(I_{N-4}^{0}-2I_{N-3}^{0}+I_{N-2}^{0}\right)-k_I\frac{x_{N-3}^0}{L}\left(T_{N-3}^{0}-T_{a}\right)^2=f_{T,N-3}^{0}\qquad\exists\qquad\zeta_{T,N-3}^{0}=\frac{\alpha\Delta t}{\left(\Delta x\right)^2}$$

$$\left(-\zeta_{T,N-2}^{0}\psi\right)T_{N-3}^{1}+\left(1+2\zeta_{T,N-2}^{0}\psi\right)T_{N-2}^{1}+\left(-\zeta_{T,N-2}^{0}\psi\right)T_{N-1}^{1}=T_{N-2}^{0}+\zeta_{T,N-2}^{0}\left(1-\psi\right)\left(T_{N-3}^{0}-2T_{N-2}^{0}+T_{N-1}^{0}\right)-\left(\frac{\mathrm{x_i^n h}\Delta t}{\mathrm{L}^2\rho cp}\right)\left(T_{N-2}^{0}-T_{a}\right)$$

$$+\zeta_{T,N-2}^{0}\frac{\beta_V}{\beta_T}\left(V_{N-3}^{0}-2V_{N-2}^{0}+V_{N-1}^{0}\right)+\zeta_{T,N-2}^{0}\frac{\beta_I}{\beta_T}\left(I_{N-3}^{0}-2I_{N-2}^{0}+I_{N-1}^{0}\right)-k_T\frac{x_{N-2}^0}{L}\left(T_{N-2}^{0}-T_{a}\right)^2=f_{T,N-2}^{0}\qquad\exists\qquad\zeta_{T,N-2}^{0}=\frac{\alpha\Delta t}{\left(\Delta x\right)^2}$$

$$\left(-\zeta_{T,N-1}^{0}\psi\right)T_{N-2}^{1}+\left(1+2\zeta_{T,N-1}^{0}\psi\right)T_{N-1}^{1}=+\left(\zeta_{T,N-1}^{0}\psi\right)T_{N}^{1}+T_{N-1}^{0}+\zeta_{T,N-1}^{0}\left(1-\psi\right)\left(T_{N-2}^{0}-2T_{N-1}^{0}+T_{N}^{0}\right)-\left(\frac{\mathrm{x_i^n h}\Delta t}{\mathrm{L}^2\rho cp}\right)\left(T_{N-1}^{0}-T_{a}\right)$$

$$+\zeta_{T,N-1}^{0}\frac{\beta_V}{\beta_T}\left(V_{N-2}^{0}-2V_{N-1}^{0}+V_{N}^{0}\right)+\zeta_{T,N-1}^{0}\frac{\beta_I}{\beta_T}\left(I_{N-2}^{0}-2I_{N-1}^{0}+I_{N}^{0}\right)-k_T\frac{x_{N-1}^0}{L}\left(T_{N-1}^{0}-T_{a}\right)^2=f_{T,N-1}^{0}\qquad\exists\qquad\zeta_{T,N-1}^{0}=\frac{\alpha\Delta t}{\left(\Delta x\right)^2}$$

Arranging Equation (3.35) in matrix notation gives Equation (3.36), temperature distribution along the transmission line

$$\begin{bmatrix} \left(1+2\psi\zeta^{0}_{T,1}\right) & -\psi\zeta^{0}_{T,1} & 0 & 0 & 0 \\ -\psi\zeta^{0}_{T,2} & \left(1+2\psi\zeta^{0}_{T,2}\right) & \ddots & 0 & 0 \\ 0 & -\psi\zeta^{0}_{T,N-3} & \ddots & -\psi\zeta^{0}_{T,N-3} & 0 \\ 0 & 0 & \ddots & \left(1+2\psi\zeta^{0}_{T,N-2}\right) & -\psi\zeta^{0}_{T,N-2} \\ 0 & 0 & 0 & -\psi\zeta^{0}_{T,N-1} & \left(1+2\psi\zeta^{0}_{T,N-1}\right) \end{bmatrix} \begin{bmatrix} \theta^{1}_{T,1} \\ \theta^{1}_{T,2} \\ \vdots \\ \theta^{1}_{T,N-2} \\ \theta^{1}_{T,N-1} \end{bmatrix} = \begin{bmatrix} f^{1}_{T,1} \\ f^{1}_{T,2} \\ \vdots \\ f^{1}_{T,N-2} \\ f^{1}_{T,N-1} \end{bmatrix} \tag{3.36}$$

Similarly, Equation (3.37) gives phase voltage distribution along the transmission line

$$\begin{bmatrix} \left(1+2\psi\zeta^{0}_{V,1}\right) & -\psi\zeta^{0}_{V,1} & 0 & 0 & 0 \\ -\psi\zeta^{0}_{V,2} & \left(1+2\psi\zeta^{0}_{V,2}\right) & \ddots & 0 & 0 \\ 0 & -\psi\zeta^{0}_{V,N-3} & \ddots & -\psi\zeta^{0}_{V,N-3} & 0 \\ 0 & 0 & \ddots & \left(1+2\psi\zeta^{0}_{V,N-2}\right) & -\psi\zeta^{0}_{V,N-2} \\ 0 & 0 & 0 & -\psi\zeta^{0}_{V,N-1} & \left(1+2\psi\zeta^{0}_{V,N-1}\right) \end{bmatrix} \begin{bmatrix} \theta^{1}_{V,1} \\ \theta^{1}_{V,2} \\ \vdots \\ \theta^{1}_{V,N-2} \\ \theta^{1}_{V,N-1} \end{bmatrix} = \begin{bmatrix} f^{1}_{V,1} \\ f^{1}_{V,2} \\ \vdots \\ f^{1}_{V,N-2} \\ f^{1}_{V,N-1} \end{bmatrix} \tag{3.37}$$

Likewise, Equation (3.38) gives current distribution along the transmission line

$$\begin{bmatrix} \left(1+2\psi\zeta^{0}_{I,1}\right) & -\psi\zeta^{0}_{I,1} & 0 & 0 & 0 \\ -\psi\zeta^{0}_{I,2} & \left(1+2\psi\zeta^{0}_{I,2}\right) & \ddots & 0 & 0 \\ 0 & -\psi\zeta^{0}_{I,N-3} & \ddots & -\psi\zeta^{0}_{I,N-3} & 0 \\ 0 & 0 & \ddots & \left(1+2\psi\zeta^{0}_{I,N-2}\right) & -\psi\zeta^{0}_{I,N-2} \\ 0 & 0 & 0 & -\psi\zeta^{0}_{I,N-1} & \left(1+2\psi\zeta^{0}_{I,N-1}\right) \end{bmatrix} \begin{bmatrix} \theta^{1}_{I,1} \\ \theta^{1}_{I,2} \\ \vdots \\ \theta^{1}_{I,N-2} \\ \theta^{1}_{I,N-1} \end{bmatrix} = \begin{bmatrix} f^{1}_{I,1} \\ f^{1}_{I,2} \\ \vdots \\ f^{1}_{I,N-2} \\ f^{1}_{I,N-1} \end{bmatrix} \tag{3.38}$$

3.3.2.8 Thermal properties of Air

Air density, $\gamma(\mathrm{kg/m^3})$ in Equations (3.26 – 3.32) is defined as a function of temperature, $\mathrm{T(K)}$ in Equation (3.39) (Hussien, 2011; Nacho *et al.*, 2019)

$$\gamma = f(T)$$

$$\gamma = 2.1313 - 0.003T_{Air} \quad \exists \quad 293.15 \le T_{Air}(K) \le 363.15,\ R^2 = 0.99998743 \tag{3.39}$$

The convective heat transfer coefficient, $\mathrm{h(W/m^2K)}$ in Equations (3.23, 3.28, 3.31, and 3.35) is given as function of $\gamma(\mathrm{kg/m^3})$ or air temperature, $\mathrm{T(K)}$ in Equation (3.40) (Kosky, 2021).

$$h = f(\gamma), \tag{3.40}$$

$$h = -108.7643 + 317.8327\gamma - 202.0964\gamma^2 \quad \exists \quad 0.82456 \le \gamma\left(\frac{\text{kg}}{\text{m}^3}\right) \le 1.02146,\ \text{R}^2 = 0.9850;$$

or

$$h = f(T),$$

$$h = -267.1437 + 1.55467T - 0.00214\,T^2 \quad \exists \quad 293.15 \le T(\text{K}) \le 363.15,\ \text{R}^2 = 0.98938$$

or

h = 5.7 + 3.8 u according to (Tofighi, 2013).

3.3.2.9 Thermal properties of the transmission lines

The thermal conductivity, $k_{\text{Al}}(\text{W/mK})$ of the transmission line (aluminum) is given in Equation (3.41) (Ausloos, 2011)

$$k = 385.5 - 1.036T_{Al} + 0.0017\,T_{Al}^2 \quad \exists \quad 100 \le T_{Al}(\text{K}) \le 400,\ \text{R}^2 = 0.9376 \tag{3.41}$$

The density,$\gamma_{\text{Al}}(\text{kg/m}^3)$ of the transmission line (aluminum) is given in Equation (3.42) (Ujah, 2022)

$$\gamma = 2734.75 - 0.0845T_{Al} + 0.000125\,T_{Al}^2 \quad \exists \quad 100 \le T_{Al}(\text{K}) \le 400,\ \text{R}^2 = 0.999954 \tag{3.42}$$

The heat capacity, $\text{cp}_{\text{Al}}(\text{J/kgK})$ of the transmission line (aluminum) is given in Equation (3.43) (Moran *et al.*, 2002)

$$cp = 343.44\ln(\text{T}_{\text{Al}}) - 1071.4 \quad \exists \quad 100 \le T_{Al}(\text{K}) \le 400,\ \text{R}^2 = 0.9631 \tag{3.43}$$

The thermal diffusivity, $\alpha_{\text{Al}}(\text{m}^2/\text{s})$ of aluminum stranded transmission lines is given in equation (3.44) (ElSheikh, 2022)

$$\alpha_{Al} = \frac{k_{Al}}{\rho_{Al}\text{cp}_{\text{Al}}} \tag{3.44}$$

(Satpathy and Venkateswarlu, 2021; Ignjatovic and Cvetic, 2021) defined electrical diffusivity, $\text{D}_{\text{e}}(\text{m}^2/\text{s})$ is by of aluminum stranded transmission lines is given in Equation (3.45)

$$D_e \equiv 22.5\times10^{-4}\left(m^2/s\right) \tag{3.45}$$

The dynamic viscosity, $\mu(\text{kg/ms})$ is stated in Equation (3.45) (Nnamchi *et al.*, 2023)

$$\mu = 1.03\times10^{-6} + 7\times10^{-8}\overline{T} - 4\times10^{-11}\overline{T}^{2} \ni \overline{T}(K) \tag{3.47}$$

where $\overline{T}(K)$ is the average air temperature.

The RMSE of the input parameters is expressed in Equations. (3.46 – 3.49) for the transmission current, temperature, voltage and power, respectively.

$$RMSE_I = \sqrt{\frac{\sum_{i=1}^{n}\left(I_{Simulated} - \bar{I}_{Measured}\right)^2}{N}} \tag{3.46}$$

$$RMSE_T = \sqrt{\frac{\sum_{i=1}^{n}\left(T_{Simulated} - \overline{T}_{Measured}\right)^2}{N}} \tag{3.47}$$

$$RMSE_V = \sqrt{\frac{\sum_{i=1}^{n}\left(V_{Simulated} - \overline{V}_{Measured}\right)^2}{N}} \tag{3.48}$$

$$RMSE_P = \sqrt{\frac{\sum_{i=1}^{n}\left(P_{Simulated} - \overline{P}_{Measured}\right)^2}{N}} \tag{3.49}$$

3.3.3 Development of differential and empirical solar power generation models.

The method and material drawn in this sub-section takes attention of differential explicit model development in solar power generation

The methodology consists of developing a model for solar power generation and conducting experiments to develop an empirical model for solar power generation. Furthermore, gathering field data is essential to supplementing the outcomes of modeling and experiments.

3.3.3.1 Model formulation

Modelling and simulation, experimentation, and the acquisition/analysis of data are essential for the study of solar generation, as portrayed in Figure 3.7 process modelling and simulation of solar power generation. Based on simulations, solar power generation is influenced by the thermophysical characteristics of the ambient air, such as temperature and wind speed, as well as extraterrestrial parameters like solar irradiance. The temperature of the solar panel cells also has an impact on the empirical generation of solar power. The field data comes from the existing solar power plants within the study area. Where e is the error associated to the external variables, D/Dt is a substantial derivative, $H(W/m^2)$ is the solar irradiance, $U(m/s)$ is the wind speed, $P_{sim}(W)$ is the solar power simulated, $P_{gen}(W)$ is the solar power generated, $P_{stc}(W)$ is the solar power at standard test condition, $T_a(K)$ is the ambient temperature, $\beta_c(1/K)$ is the temperature coefficient of the solar cell, $\eta(\%)$ is the efficiency of solar cell, $N_p(-)$ is the number of solar panels and , $T_c(K)$ is the temperature of solar cell.

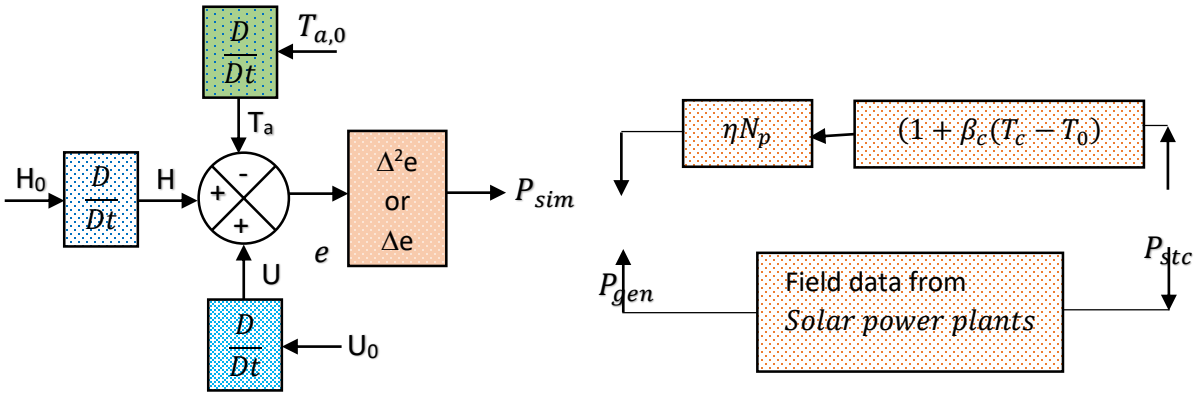

(a) Solar power simulated (b) Solar power generated

Fig. 3.7. Modelling of solar power generation in space and time.

Source: Present study 2023

3.3.3.2 The Navier Stokes Equation

Extrinsic variables such as wind speed (U), ambient temperature (T_a), and solar irradiation (H) have an impact on photovoltaic cell performance. The substantial derivatives of the Navier-Stokes equation are proposed for modeling solar power generation (Nnamchi *et al.*, 2023), as shown in Figure 3.7 The substantial derivative of the component and resultant wind speeds are defined in Equations (3.50a, 3.50b, 3.50c, 3.50d) as

$$\frac{DU_x}{Dt} = g_x - \frac{1}{\rho}\frac{\partial Patm}{\partial x} + \nu\left(\frac{\partial^2 U_x}{\partial x^2} + \frac{\partial^2 U_x}{\partial y^2} + \frac{\partial^2 U_x}{\partial z^2}\right);\ U_x = \frac{U}{\sqrt{3}};\ \nu = \mu_z/\rho \tag{3.50a}$$

$$\frac{DU_y}{Dt} = g_y - \frac{1}{\rho}\frac{\partial Patm}{\partial y} + \nu\left(\frac{\partial^2 U_y}{\partial x^2} + \frac{\partial^2 U_y}{\partial y^2} + \frac{\partial^2 U_y}{\partial z^2}\right);\ U_y = \frac{U}{\sqrt{3}};\ \nu = \mu_z/\rho \tag{3.50b}$$

$$\frac{DU_z}{Dt} = g_z - \frac{1}{\rho}\frac{\partial Patm}{\partial z} + \nu\left(\frac{\partial^2 U_z}{\partial x^2} + \frac{\partial^2 U_z}{\partial y^2} + \frac{\partial^2 U_z}{\partial z^2}\right);\ U_z = \frac{U}{\sqrt{3}};\ \nu = \mu_z/\rho \tag{3.50c}$$

$$\frac{DU}{Dt} = g - \frac{U\partial U}{\partial \chi} + \nu\left(\frac{\partial^2 U}{\partial x^2} + \frac{\partial^2 U}{\partial y^2} + \frac{\partial^2 U}{\partial z^2}\right);\qquad \nu = \mu_z/\rho;\qquad \chi = (xyz)^{1/3};$$
$$U = \sqrt{3}U_x = \sqrt{3}U_y = \sqrt{3}U_z;\ Patm = 0.5\rho U^2 \tag{3.50d}$$

Equations (3.50a, 3.50b, 3.50c, and 3.50d) are complemented with mass continuity equation in Equation (3.51)

$$\frac{\partial U_x}{\partial x} + \frac{\partial U_y}{\partial y} + \frac{\partial U_z}{\partial z} = 0;\ U_x = U_y = U_z = \frac{U}{\sqrt{3}} \tag{3.51}$$

Similarly, the substantial derivative of ambient temperature is formulated in Equation (3.53)

$$\frac{DT_a}{Dt} = \alpha\left(\frac{\partial^2 T_a}{\partial x^2} + \frac{\partial^2 T_a}{\partial y^2} + \frac{\partial^2 T_a}{\partial z^2}\right);\ \alpha = k/\rho cp \tag{3.52}$$

Likewise, the substantial derivative of solar irradiance is expressed in Equation (3.53) as

$$\frac{DH}{Dt} = \alpha\left(\frac{\partial^2 H}{\partial x^2} + \frac{\partial^2 H}{\partial y^2} + \frac{\partial^2 H}{\partial z^2}\right);\ \alpha = k/\rho cp \tag{3.53}$$

3.3.3.3 The Navier Stokes Equation for solar power generation

The Navier-Stokes equation is a first-order substantial derivative of solar power generation in three dimensions (3-D). It is adopted for modelling solar power generation and distribution due to its spatiality and chronological features. Integrally, solar power in Equation (3.54) is a function of U, T_a and H

$$\frac{DP}{Dt} = a_H \frac{DH}{Dt} - a_{T_a} \frac{DT_a}{Dt} + a_U \frac{DU}{Dt} \; ; \; \frac{DP}{Dt} = \frac{\beta_H}{\beta_P}\frac{DH}{Dt} - \frac{\beta_{T_a}}{\beta_P}\frac{DT_a}{Dt} + \frac{\beta_U}{\beta_P}\frac{DU}{Dt} \tag{3.54}$$

where $a_H(m^2)$, $a_{T_a}(W/K)$, $a_U(W/m/s)$ are power coupling coefficients of H, T_a and U respectively. The coupling coefficients in Equation (3.54) are defined Equation (3.55) as follows:

$$a_H = \frac{\beta_H}{\beta_P}; \quad a_{T_a} = \frac{\beta_{T_a}}{\beta_P}; \quad a_U = \frac{\beta_U}{\beta_P}; \; \beta_P = \frac{1}{P_{\max}} ; \quad \beta_H = \frac{1}{H_{\max}}; \; \beta_{T_a} = \frac{1}{T_{a,\max}} ; \; \beta_U = \frac{1}{U_{\max}} \tag{3.55}$$

Substituting substantial derivative of Equations. (3.50d, 3.51, 3.52, 3.53) into Equation (3.54) gives Equation (3.56) first order linear solar power generation model.

$$\begin{aligned} &\frac{\partial P}{\partial t} + U_x \frac{\partial P}{\partial x} + U_y \frac{\partial P}{\partial y} + U_z \frac{\partial P}{\partial z} = a_H \alpha \left(\frac{\partial^2 H}{\partial x^2} + \frac{\partial^2 H}{\partial y^2} + \frac{\partial^2 H}{\partial z^2} \right) - a_{T_a} \alpha \left(\frac{\partial^2 T_a}{\partial x^2} + \frac{\partial^2 T_a}{\partial y^2} + \frac{\partial^2 T_a}{\partial z^2} \right) \\ &+ a_U \left(g - \frac{U \partial U}{\partial \chi} + \nu \left(\frac{\partial^2 U}{\partial x^2} + \frac{\partial^2 U}{\partial y^2} + \frac{\partial^2 U}{\partial z^2} \right) \right) \end{aligned} \tag{3.56}$$

For dominant viscous force, Equation (3.56) reduces to Equation (3.57)

$$\begin{aligned} &\frac{\partial P}{\partial t} + U_x \frac{\partial P}{\partial x} + U_y \frac{\partial P}{\partial y} + U_z \frac{\partial P}{\partial z} = a_H \alpha \left(\frac{\partial^2 H}{\partial x^2} + \frac{\partial^2 H}{\partial y^2} + \frac{\partial^2 H}{\partial z^2} \right) - a_{T_a} \alpha \left(\frac{\partial^2 T_a}{\partial x^2} + \frac{\partial^2 T_a}{\partial y^2} + \frac{\partial^2 T_a}{\partial z^2} \right) \\ &+ a_U \nu \left(\frac{\partial^2 U}{\partial x^2} + \frac{\partial^2 U}{\partial y^2} + \frac{\partial^2 U}{\partial z^2} \right) \end{aligned} \tag{3.57}$$

3.3.3.4 The Modified Navier Stokes Equation for solar power generation

The modified Navier Stokes equation is a second-order substantial derivative of solar power generation in three dimensions (3-D), also, it is adopted for modelling solar power generation and distribution due to its spatial and chronological features. Essentially, solar power in Equation (3.54) is a function of U, T_a and H. Thus, an alternate power generation model (Modified Navier Stokes Equation, MNSE) is created by differentiating Equation (3.54) to a second-order in Equation (3.58)

$$\frac{D^2P}{Dt^2} = a_H \frac{D^2H}{Dt^2} - a_{T_a} \frac{D^2T_a}{Dt^2} + a_U \frac{D^2U}{Dt^2} \tag{3.58}$$

In addition, taking the second-order substantial derivative of equations (3.50d, 3.51, 3.52, 3.53) into Equation (3.56) gives Equation (3.59)

$$\begin{aligned}\frac{D^2P}{Dt^2} &= a_H \frac{D}{Dt}\left(\alpha\left(\frac{\partial^2 H}{\partial x^2}+\frac{\partial^2 H}{\partial y^2}+\frac{\partial^2 H}{\partial z^2}\right)\right) - a_{T_a}\frac{D}{Dt}\left(\alpha\left(\frac{\partial^2 T_a}{\partial x^2}+\frac{\partial^2 T_a}{\partial y^2}+\frac{\partial^2 T_a}{\partial z^2}\right)\right)\\ &+ a_U \frac{D}{Dt}\left(\sqrt{3}g_x - \frac{\sqrt{3}}{\rho}\frac{\partial Patm}{\partial \chi} + \nu\left(\frac{\partial^2 U}{\partial x^2}+\frac{\partial^2 U}{\partial y^2}+\frac{\partial^2 U}{\partial z^2}\right)\right)\end{aligned} \tag{3.59}$$

Substituting substantial derivative operators in Equation (3.59) yields Equation (3.60)

$$\begin{aligned}\frac{\partial^2 P}{\partial t^2} &= a_H\left(\alpha\left(\frac{\partial^2}{\partial x^2}+\frac{\partial^2}{\partial y^2}+\frac{\partial^2}{\partial z^2}\right)\right)\left(\alpha\left(\frac{\partial^2 H}{\partial x^2}+\frac{\partial^2 H}{\partial y^2}+\frac{\partial^2 H}{\partial z^2}\right)\right) - a_{T_a}\left(\alpha\left(\frac{\partial^2}{\partial x^2}+\frac{\partial^2}{\partial y^2}+\frac{\partial^2}{\partial z^2}\right)\right)\left(\alpha\left(\frac{\partial^2 T_a}{\partial x^2}+\frac{\partial^2 T_a}{\partial y^2}+\frac{\partial^2 T_a}{\partial z^2}\right)\right)\\ &+ a_U\left(\frac{g}{U} - \frac{U\partial}{\partial \chi} + \nu\left(\frac{\partial^2}{\partial x^2}+\frac{\partial^2}{\partial y^2}+\frac{\partial^2}{\partial z^2}\right)\right)\left(g - \frac{U\partial U}{\partial \chi} + \nu\left(\frac{\partial^2 U}{\partial x^2}+\frac{\partial^2 U}{\partial y^2}+\frac{\partial^2 U}{\partial z^2}\right)\right);\quad P_{atm} = 0.5\rho U^2\end{aligned} \tag{3.60}$$

The left hand side (LHS) of Equation (3.60) is defined in Equation (3.61)

$$\begin{aligned}\Delta^2 &= \frac{\partial^2 P}{\partial t^2} + 2U_x\frac{\partial^2 P}{\partial x\partial t} + 2U_y\frac{\partial^2 P}{\partial y\partial t} + 2U_z\frac{\partial^2 P}{\partial z\partial t} + U_x^2\frac{\partial^2 P}{\partial x^2} + U_y^2\frac{\partial^2 P}{\partial y^2} + U_z^2\frac{\partial^2 P}{\partial z^2} + 2U_xU_y\frac{\partial^2 P}{\partial x\partial y}\\ &+ 2U_xU_z\frac{\partial^2 P}{\partial x\partial z} + 2U_yU_z\frac{\partial^2 P}{\partial y\partial z}\end{aligned} \tag{3.61}$$

Combining Equations. (3.60, 3.61) gives Equation (3.62) solar power generation model

$$\begin{aligned}&\frac{\partial^2 P}{\partial t^2} + 2U_x\frac{\partial^2 P}{\partial x\partial t} + 2U_y\frac{\partial^2 P}{\partial y\partial t} + 2U_z\frac{\partial^2 P}{\partial z\partial t} + U_x^2\frac{\partial^2 P}{\partial x^2} + U_y^2\frac{\partial^2 P}{\partial y^2} + U_z^2\frac{\partial^2 P}{\partial z^2} + 2U_xU_y\frac{\partial^2 P}{\partial x\partial y} + 2U_xU_z\frac{\partial^2 P}{\partial x\partial z} + 2U_yU_z\frac{\partial^2 P}{\partial y\partial z}\\ &= a_H\alpha\left(\frac{\partial^4 H}{\partial x^4}+\frac{\partial^4 H}{\partial y^4}+\frac{\partial^4 H}{\partial z^4}+2\frac{\partial^4 H}{\partial x^2\partial y^2}+2\frac{\partial^4 H}{\partial x^2\partial z^2}+2\frac{\partial^4 H}{\partial y^2\partial z^2}\right) - a_{T_a}\alpha\left(\frac{\partial^4 T_a}{\partial x^4}+\frac{\partial^4 T_a}{\partial y^4}+\frac{\partial^4 T_a}{\partial z^4}+2\frac{\partial^4 T_a}{\partial x^2\partial y^2}+2\frac{\partial^4 T_a}{\partial x^2\partial z^2}+2\frac{\partial^4 T_a}{\partial y^2\partial z^2}\right)\\ &+ \nu a_U\left(\left(\frac{g^2}{U} - g\frac{\partial U}{\partial \chi} + \nu\frac{g}{U}\left(\frac{\partial^2 U}{\partial x^2}+\frac{\partial^2 U}{\partial y^2}+\frac{\partial^2 U}{\partial z^2}\right)\right) - \left(\frac{g\partial U}{\partial \chi} - \frac{U^2\partial^2 U}{\partial \chi^2} + \nu U\left(\frac{\partial^3 U}{\partial x^2\partial \chi}+\frac{\partial^3 U}{\partial y^2\partial \chi}+\frac{\partial^3 U}{\partial z^2\partial \chi}\right)\right)\right.\\ &\left. + \nu\left(\left(-\frac{U\partial^3 U}{\partial x^2\partial \chi} + \nu\left(\frac{\partial^4 U}{\partial x^4}+\frac{\partial^4 U}{\partial x^2\partial y^2}+\frac{\partial^4 U}{\partial x^2\partial z^2}\right)\right) + \left(-\frac{U\partial^3 U}{\partial y^2\partial \chi} + \nu\left(\frac{\partial^4 U}{\partial y^2\partial x^2}+\frac{\partial^4 U}{\partial y^4}+\frac{\partial^4 U}{\partial y^2\partial z^2}\right)\right) + \left(-\frac{U\partial^3 U}{\partial z^2\partial \chi} + \nu\left(\frac{\partial^4 U}{\partial x^2\partial z^2}+\frac{\partial^4 U}{\partial y^2\partial z^2}+\frac{\partial^4 U}{\partial z^4}\right)\right)\right)\right)\end{aligned} \tag{3.62}$$

Similarly, considering dominant viscous force, Equation (3.62) is simplified to Equation (3.63)

$$\begin{aligned}&\frac{\partial^2 P}{\partial t^2} + 2U_x\frac{\partial^2 P}{\partial x\partial t} + 2U_y\frac{\partial^2 P}{\partial y\partial t} + 2U_z\frac{\partial^2 P}{\partial z\partial t} + U_x^2\frac{\partial^2 P}{\partial x^2} + U_y^2\frac{\partial^2 P}{\partial y^2} + U_z^2\frac{\partial^2 P}{\partial z^2} + 2U_xU_y\frac{\partial^2 P}{\partial x\partial y} + 2U_xU_z\frac{\partial^2 P}{\partial x\partial z} + 2U_yU_z\frac{\partial^2 P}{\partial y\partial z}\\ &= a_H\alpha\left(\frac{\partial^4 H}{\partial x^4}+\frac{\partial^4 H}{\partial y^4}+\frac{\partial^4 H}{\partial z^4}+2\frac{\partial^4 H}{\partial x^2\partial y^2}+2\frac{\partial^4 H}{\partial x^2\partial z^2}+2\frac{\partial^4 H}{\partial y^2\partial z^2}\right) - a_{T_a}\alpha\left(\frac{\partial^4 T_a}{\partial x^4}+\frac{\partial^4 T_a}{\partial y^4}+\frac{\partial^4 T_a}{\partial z^4}+2\frac{\partial^4 T_a}{\partial x^2\partial y^2}+2\frac{\partial^4 T_a}{\partial x^2\partial z^2}+2\frac{\partial^4 T_a}{\partial y^2\partial z^2}\right)\\ &+ a_U\nu\left(\frac{\partial^4 U}{\partial x^4}+\frac{\partial^4 U}{\partial y^4}+\frac{\partial^4 U}{\partial z^4}+2\frac{\partial^4 U}{\partial x^2\partial y^2}+2\frac{\partial^4 U}{\partial x^2\partial z^2}+2\frac{\partial^4 U}{\partial y^2\partial z^2}\right)\end{aligned} \tag{3.63}$$

3.3.3.5 The numerical solution

Discretizing Equations (3.57, 3.63) by finite the difference method to discretize solar power generated and the influential factors (H, T_a, U), leads to numerical solutions of the first and second order solar power generation model in Equations (3.64a and 3.64b) and Equations (3.65a and 3.65b) respectively.

$$\begin{aligned}&\frac{P_i^{n+1}-P_i^n}{\Delta t}+U^n_{x,i}\left(\theta\frac{P_{i+1}^{n+1}-P_{i-1}^{n+1}}{2\Delta x}+(1-\theta)\frac{P_{i+1}^{n}-P_{i-1}^{n}}{2\Delta x}\right)+U^n_{y,i}\left(\theta\frac{P_{i+1}^{n+1}-P_{i-1}^{n+1}}{2\Delta y}+(1-\theta)\frac{P_{i+1}^{n}-P_{i-1}^{n}}{2\Delta y}\right)+U^n_{z,i}\left(\theta\frac{P_{i+1}^{n+1}-P_{i-1}^{n+1}}{2\Delta z}+(1-\theta)\frac{P_{i+1}^{n}-P_{i-1}^{n}}{2\Delta z}\right)\\&=a_H\alpha\left(\left(\frac{H_{i-1}^n-2H_i^n+H_{i+1}^n}{(\Delta x)^2}\right)+\left(\frac{H_{i-1}^n-2H_i^n+H_{i+1}^n}{(\Delta y)^2}\right)+\left(\frac{H_{i-1}^n-2H_i^n+H_{i+1}^n}{(\Delta z)^2}\right)\right)-a_{T_a}\alpha\left(\left(\frac{T_{a,i-1}^n-2T_{a,i}^n+T_{a,i+1}^n}{(\Delta x)^2}\right)+\left(\frac{T_{a,i-1}^n-2T_{a,i}^n+T_{a,i+1}^n}{(\Delta y)^2}\right)+\left(\frac{T_{a,i-1}^n-2T_{a,i}^n+T_{a,i+1}^n}{(\Delta z)^2}\right)\right)\\&+a_U\nu\left(\left(\frac{U_{i-1}^n-2U_i^n+U_{i+1}^n}{(\Delta x)^2}\right)+\left(\frac{U_{i-1}^n-2U_i^n+U_{i+1}^n}{(\Delta y)^2}\right)+\left(\frac{U_{i-1}^n-2U_i^n+U_{i+1}^n}{(\Delta z)^2}\right)\right)\end{aligned}\qquad(3.64a)$$

$$\begin{aligned}P_i^{n+1}=\Delta t\Bigg(&a_H\alpha\left(H_{i-1}^n-2H_i^n+H_{i+1}^n\right)\left(\left(\frac{1}{(\Delta x)^2}\right)+\left(\frac{1}{(\Delta y)^2}\right)+\left(\frac{1}{(\Delta z)^2}\right)\right)-a_{T_a}\alpha\left(T_{a,i-1}^n-2T_{a,i}^n+T_{a,i+1}^n\right)\left(\left(\frac{1}{(\Delta x)^2}\right)+\left(\frac{1}{(\Delta y)^2}\right)+\left(\frac{1}{(\Delta z)^2}\right)\right)\\&+a_U\nu\left(U_{i-1}^n-2U_i^n+U_{i+1}^n\right)\left(\left(\frac{1}{(\Delta x)^2}\right)+\left(\frac{1}{(\Delta y)^2}\right)+\left(\frac{1}{(\Delta z)^2}\right)\right)+\left(\frac{P_i^n}{\Delta t}\right)-\left(U^n_{x,i}\left(\frac{P_{i+1}^n-P_{i-1}^n}{2\Delta x}\right)+U^n_{y,i}\left(\frac{P_{i+1}^n-P_{i-1}^n}{2\Delta y}\right)+U^n_{z,i}\left(\frac{P_{i+1}^n-P_{i-1}^n}{2\Delta z}\right)\right)\Bigg)\end{aligned}\qquad(3.64b)$$

Similarly, Equation (3.63) is discretized in Equation (3.65) as

$$\frac{P_i^{n+2}-2P_i^{n+1}+P_i^n}{(\Delta t)^2}+2U^n_{x,i}\left(\theta\frac{P_{i+1}^{n+1}-2P_i^{n+1}+P_{i-1}^{n+1}}{(\Delta x)(\Delta t)}+(1-\theta)\frac{P_{i+1}^{n}-2P_i^{n}+P_{i-1}^{n}}{(\Delta x)(\Delta t)}\right)+2U^n_{y,i}\left(\theta\frac{P_{i+1}^{n+1}-2P_i^{n+1}+P_{i-1}^{n+1}}{(\Delta y)(\Delta t)}+(1-\theta)\frac{P_{i+1}^{n}-2P_i^{n}+P_{i-1}^{n}}{(\Delta y)(\Delta t)}\right)$$
$$+2U^n_{z,i}\left(\theta\frac{P_{i+1}^{n+1}-2P_i^{n+1}+P_{i-1}^{n+1}}{(\Delta z)(\Delta t)}+(1-\theta)\frac{P_{i+1}^{n}-2P_i^{n}+P_{i-1}^{n}}{(\Delta z)(\Delta t)}\right)+\left(U^n_{x,i}\right)^2\left(\theta\frac{P_{i+1}^{n+1}-2P_i^{n+1}+P_{i-1}^{n+1}}{(\Delta x)^2}+(1-\theta)\frac{P_{i+1}^{n}-2P_i^{n}+P_{i-1}^{n}}{(\Delta x)^2}\right)$$
$$+\left(U^n_{y,i}\right)^2\left(\theta\frac{P_{i+1}^{n+1}-2P_i^{n+1}+P_{i-1}^{n+1}}{(\Delta y)^2}+(1-\theta)\frac{P_{i+1}^{n}-2P_i^{n}+P_{i-1}^{n}}{(\Delta y)^2}\right)+\left(U^n_{z,i}\right)^2\left(\theta\frac{P_{i+1}^{n+1}-2P_i^{n+1}+P_{i-1}^{n+1}}{(\Delta z)^2}+(1-\theta)\frac{P_{i+1}^{n}-2P_i^{n}+P_{i-1}^{n}}{(\Delta z)^2}\right)$$
$$+2\left(U^n_{x,i}U^n_{y,i}\right)\left(\theta\frac{P_{i+1}^{n+1}-2P_i^{n+1}+P_{i-1}^{n+1}}{(\Delta x\Delta y)}+(1-\theta)\frac{P_{i+1}^{n}-2P_i^{n}+P_{i-1}^{n}}{(\Delta x\Delta y)}\right)+2\left(U^n_{x,i}U^n_{z,i}\right)\left(\theta\frac{P_{i+1}^{n+1}-2P_i^{n+1}+P_{i-1}^{n+1}}{(\Delta x\Delta z)}+(1-\theta)\frac{P_{i+1}^{n}-2P_i^{n}+P_{i-1}^{n}}{(\Delta x\Delta z)}\right)$$
$$+2\left(U^n_{y,i}U^n_{z,i}\right)\left(\theta\frac{P_{i+1}^{n+1}-2P_i^{n+1}+P_{i-1}^{n+1}}{(\Delta y\Delta z)}+(1-\theta)\frac{P_{i+1}^{n}-2P_i^{n}+P_{i-1}^{n}}{(\Delta y\Delta z)}\right)$$
$$=a_H\alpha\left(\begin{array}{l}\left(\frac{H_{i-2}^n-4H_{i-1}^n+6H_i^n-4H_{i+1}^n+H_{i+2}^n}{(\Delta x)^4}\right)+\left(\frac{H_{i-2}^n-4H_{i-1}^n+6H_i^n-4H_{i+1}^n+H_{i+2}^n}{(\Delta y)^4}\right)+\left(\frac{H_{i-2}^n-4H_{i-1}^n+6H_i^n-4H_{i+1}^n+H_{i+2}^n}{(\Delta z)^4}\right)\\+2\left(\frac{H_{i-2}^n-4H_{i-1}^n+6H_i^n-4H_{i+1}^n+H_{i+2}^n}{(\Delta x\Delta y)^2}\right)+2\left(\frac{H_{i-2}^n-4H_{i-1}^n+6H_i^n-4H_{i+1}^n+H_{i+2}^n}{(\Delta x\Delta z)^2}\right)+2\left(\frac{H_{i-2}^n-4H_{i-1}^n+6H_i^n-4H_{i+1}^n+H_{i+2}^n}{(\Delta y\Delta z)^2}\right)\end{array}\right) \quad (3.65a)$$
$$-a_{T_a}\alpha\left(\begin{array}{l}\left(\frac{T_{a,i-2}^n-4T_{a,i-1}^n+6T_{a,i}^n-4T_{a,i+1}^n+T_{a,i+2}^n}{(\Delta x)^4}\right)+\left(\frac{T_{a,i-2}^n-4T_{a,i-1}^n+6T_{a,i}^n-4T_{a,i+1}^n+T_{a,i+2}^n}{(\Delta y)^4}\right)+\left(\frac{T_{a,i-2}^n-4T_{a,i-1}^n+6T_{a,i}^n-4T_{a,i+1}^n+T_{a,i+2}^n}{(\Delta z)^4}\right)\\+2\left(\frac{T_{a,i-2}^n-4T_{a,i-1}^n+6T_{a,i}^n-4T_{a,i+1}^n+T_{a,i+2}^n}{(\Delta x\Delta y)^2}\right)+2\left(\frac{T_{a,i-2}^n-4T_{a,i-1}^n+6T_{a,i}^n-4T_{a,i+1}^n+T_{a,i+2}^n}{(\Delta x\Delta z)^2}\right)+2\left(\frac{T_{a,i-2}^n-4T_{a,i-1}^n+6T_{a,i}^n-4T_{a,i+1}^n+T_{a,i+2}^n}{(\Delta y\Delta z)^2}\right)\end{array}\right)$$
$$+a_U\nu\left(\begin{array}{l}\left(\frac{U_{i-2}^n-4U_{i-1}^n+6U_i^n-4U_{i+1}^n+U_{i+2}^n}{(\Delta x)^4}\right)+\left(\frac{U_{i-2}^n-4U_{i-1}^n+6U_i^n-4U_{i+1}^n+U_{i+2}^n}{(\Delta y)^4}\right)+\left(\frac{U_{i-2}^n-4U_{i-1}^n+6U_i^n-4U_{i+1}^n+U_{i+2}^n}{(\Delta z)^4}\right)\\+2\left(\frac{U_{i-2}^n-4U_{i-1}^n+6U_i^n-4U_{i+1}^n+U_{i+2}^n}{(\Delta x\Delta y)^2}\right)+2\left(\frac{U_{i-2}^n-4U_{i-1}^n+6U_i^n-4U_{i+1}^n+U_{i+2}^n}{(\Delta x\Delta z)^2}\right)+2\left(\frac{U_{i-2}^n-4U_{i-1}^n+6U_i^n-4U_{i+1}^n+U_{i+2}^n}{(\Delta y\Delta z)^2}\right)\end{array}\right)$$

$$P_i^{n+2}=(\Delta t)^2\left(\begin{array}{l}a_H\alpha\left(\left(H_{i-2}^n-4H_{i-1}^n+6H_i^n-4H_{i+1}^n+H_{i+2}^n\right)\left(\left(\frac{1}{(\Delta x)^4}\right)+\left(\frac{1}{(\Delta y)^4}\right)+\left(\frac{1}{(\Delta z)^4}\right)+2\left(\frac{1}{(\Delta x\Delta y)^2}\right)+2\left(\frac{1}{(\Delta x\Delta z)^2}\right)+2\left(\frac{1}{(\Delta y\Delta z)^2}\right)\right)\right)\\-a_{T_a}\alpha\left(\left(T_{a,i-2}^n-4T_{a,i-1}^n+6T_{a,i}^n-4T_{a,i+1}^n+T_{a,i+2}^n\right)\left(\left(\frac{1}{(\Delta x)^4}\right)+\left(\frac{1}{(\Delta y)^4}\right)+\left(\frac{1}{(\Delta z)^4}\right)+2\left(\frac{1}{(\Delta x\Delta y)^2}\right)+2\left(\frac{1}{(\Delta x\Delta z)^2}\right)+2\left(\frac{1}{(\Delta y\Delta z)^2}\right)\right)\right)\\+a_U\nu\left(\left(U_{i-2}^n-4U_{i-1}^n+6U_i^n-4U_{i+1}^n+U_{i+2}^n\right)\left(\left(\frac{1}{(\Delta x)^4}\right)+\left(\frac{1}{(\Delta y)^4}\right)+\left(\frac{1}{(\Delta z)^4}\right)+2\left(\frac{1}{(\Delta x\Delta y)^2}\right)+2\left(\frac{1}{(\Delta x\Delta z)^2}\right)+2\left(\frac{1}{(\Delta y\Delta z)^2}\right)\right)\right)-\\\left(\begin{array}{l}+\left(P_{i+1}^n-2P_i^n+P_{i-1}^n\right)\left(\left(\frac{2U^n_{x,i}}{(\Delta x)(\Delta t)}\right)+\left(\frac{2U^n_{y,i}}{(\Delta y)(\Delta t)}\right)+\left(\frac{2U^n_{z,i}}{(\Delta z)(\Delta t)}\right)+\left(\frac{\left(U^n_{x,i}\right)^2}{(\Delta x)^2}\right)\right)\\+\left(P_{i+1}^n-2P_i^n+P_{i-1}^n\right)\left(\left(\frac{U^n_{y,i}}{\Delta y}\right)^2+\left(\frac{U^n_{z,i}}{\Delta z}\right)^2+\left(\frac{2\left(U^n_{x,i}U^n_{y,i}\right)}{(\Delta x\Delta y)}\right)+\left(\frac{2\left(U^n_{x,i}U^n_{z,i}\right)}{(\Delta x\Delta z)}\right)+\left(\frac{2\left(U^n_{y,i}U^n_{z,i}\right)}{(\Delta y\Delta z)}\right)\right)\end{array}\right)-\left(\frac{P_i^n}{(\Delta t)^2}\right)\end{array}\right) \quad (3.65a)$$

3.3.3.6 The boundary conditions (BC)

The boundary conditions for solar power generation were derived from the field data obtained from the existing solar plants in Eastern Uganda (Figure 3.1 1 and **Table 2.1**) and the rest of the

boundary condition data were obtained from (Nnamchi *et al.*, 2023), (UNMA, 2023) and (UETCL, 2023) for Busitema (0.547°, 34.024°), Mayuge (0.495°, 0.495°), Soroti (1.685°, 33.658°) and Tororo (0.639°, 34.119°) study areas. These mercatorian coordinates were converted to space coordinates using Hervasine formula (Nnamchi *et al.*, 2019; Prasetya *et al.*, 2020) in Equation (3.66) as

$$d = 2r\sin^{-1}\left(\sqrt{\sin^2\left(\frac{\phi_2-\phi_1}{2}\right)+\cos(\phi_1)\cos(\phi_2)\sin^2\left(\frac{\lambda_2-\lambda_1}{2}\right)}\right) \quad \exists\ x_{i+1}=x_i+d \quad ; \quad y_{i+1}=y_i+d \tag{3.66}$$

where $d(m)$ is the distance between two coordinates, $r(m)$is the radius of the earth, $\phi_i, i=1,2$ is the latitude of the coordinates$\lambda_i, i=1,2$ is the longitude of the coordinates, x is the distance in x- direction and y is the distance in y-direction. The boundary conditions are function of x and y coordinate of their corresponding field data as presented in Equations (3.67a, 3.67b, 3.67c, 3.67d, 3.67e)

$$P_{i,j}^0 = f(x) = a_0 + a_1x + a_2x^2 \tag{3.67a}$$

$$H_{i,j}^0 = f(x) = b_0 + b_1x + b_2x^2 \tag{3.67b}$$

$$T_{i,j}^0 = f(x) = c_0 + c_1x + c_2x^2 \tag{3.67c}$$

$$U_{i,j}^0 = f(x) = d_0 + d_1x + d_2x^2 \tag{3.67d}$$

$$U_{x,i,j}^0 = U_{y,i,j}^0 = U_{z,i,j}^0 = f(x) = e_0 + e_1x + e_2x^2 \tag{3.67e}$$

where x and y are distance in x and y coordinates, $a_i, i=0,1,2$ are coefficients of solar power, $b_i, i=0,1,2$ are coefficients of solar irradiance, $c_i, i=0,1,2$ are coefficients of ambient temperature, $d_i, i=0,1,2$ are coefficients of resultant wind speed and $e_i, i=0,1,2$ are coefficients of component wind speed.

Alternatively, the present study defines $P_{i,j}^0$ in Equation (3.68a) as

$$P_{i,j}^0 = f(x,y) = \left[\frac{1+\left(\frac{x}{X}\right)\left(\frac{y}{Y}\right)}{\left(1+\left(\frac{x}{X}\right)^2+\left(\frac{y}{Y}\right)^2+\left(\frac{x}{X}\right)\left(\frac{y}{Y}\right)\right)^{1.2}}\right]^{\frac{1}{300}} \quad \exists \quad X = x_{max} = 187.62\,km; Y = y_{max} = 193.42\,km \tag{3.68a}$$

3.3.3.7 Initial condition

Initial conditions refer to the solar power generated in the reference year in Table 2.1 as stated in Equation (3.68b)

$$P_{i,j}^{0}(x,0) = \overline{P} = 7.5371 \ (MW) \quad \exists \quad t = 0 \,, \ 0 \le x \le 187.62 \ km \tag{3.68b}$$

3.3.3.8 Empirical Solar power generation

The empirical solar power model defined in Equation (3.69) were considered by the following literature (Al-Bashir *et al.,* 2020); (Scarabelot *et al.,* 2021) ; Skoplaki *et al.,* 2009) as

$$P_{gen,1} = P_{STC}\left(1 + \beta_c\left(T_c - T_0\right)\right)\eta \, N_p \quad \exists \quad \beta_c = \frac{\left(\frac{V_m - V_{oc}}{V_m}\right)}{T_m} \tag{3.69}$$

where $P_{gen}(W)$ is the solar power generated, $P_{stc}(W)$ is the solar power at the standard test condition, $T_a(K)$ is the ambient temperature, $T_0(K)$ is the reference temperature, $\beta_c(1/K)$ is the temperature coefficient of the solar cell, $\eta(\%)$ is the efficiency of solar cell, $N_p(-)$ is the number of solar panels and, $T_c(K)$ is the temperature of solar cell.

However, the present work considers an additional physical factor, wind speed, which enhances the cooling of the photovoltaic panel and constitute the second empirical solar power model in Equation (3.70) as

$$P_{gen,2} = P_{STC}\left(1 + \beta_c\left(T_c - T_0\right) + \beta_u U\right)\eta N_p \quad \exists \quad \beta_U = \frac{\left(\frac{P_{stc} - P_m}{P_m}\right)}{U_m} \tag{3.70}$$

Further modification is desired to improve the effectiveness of Equation (3.68) by considering the direct influence of insolation on the output power. Third empirical solar power model is developed in Equation (3.71)

$$P_{gen,3} = P_{STC}\left(1 + \beta_c\left(T_c - T_0\right) + \beta_u U + \beta_H H\right)\eta N_p \quad \exists \quad \beta_H = \frac{\left(\frac{I_{sc} - I_m}{I_m}\right)}{H_m} \tag{3.71}$$

where the coefficients in Equations (3.67, 3.68, 3.69) are similarly defined in Equation (3.55).

3.3.3.9 Thermophysical properties of air

The thermophysical properties of air are basically thermal and fluid diffusivity in Equations (3.72, 3.73, 3.74) and Equations (3.74, 3.75) respectively, which are employed in the simulations.

The thermal conductivity is defined in Equation (3.72) Nnamchi *et al.*, 2019.

$$k = 0.0121\exp\left(0.0025\overline{T}\right) \ \exists \ \overline{T}(K) \tag{3.72}$$

The density, $\rho(\mathrm{kg/m^3})$ is expressed in Equation (3.73) (Nnamchi *et al.*, 2019; Nnamchi *et al.*, 2023; Living *et al.*, 2023)

$$\rho_{Air} = 2.1313 - 0.003T_{Air} \quad \exists \quad 293.15 \le T_{Air}(K) \le 363.15, \ R^2 = 0.99998743 \tag{3.73}$$

The specific heat capacity, $\mathrm{cp(kJ/kgK)}$ is stated in Equation (3.73) (Nnamchi *et al.*, 2019; Nnamchi *et al.*, 2023)

$$cp = 2.1313 - 0.003\overline{T} \ \exists \ \overline{T}(K) \tag{3.74}$$

The dynamic viscosity, $\mu(\mathrm{kg/ms})$ is stated in Equation (3.73) (Nnamchi *et al.*, 2019; Nnamchi *et al.*, 2023)

$$\mu = 1.03\times10^{-6} + 7\times10^{-8}\overline{T} - 4\times10^{-11}\overline{T}^2 \ \exists \ \overline{T}(K) \tag{3.75}$$

where $\overline{\mathrm{T}}(\mathrm{K})$ is the average air temperature.

3.3.3.10 Error analysis and validation

Error analysis and validation of simulated and empirical, e solar power generation are presented in Equation (3.76)

$$RMSE = \sqrt{\frac{\left(P_{gen,sim} - P_{gen,e}\right)^2}{N}} \tag{3.76}$$

Whereas, the error analysis and validation of design capacity, dc and empirical solar power generation are given in Equation (3.77)

$$RMSE = \sqrt{\frac{\left(P_{gen,dc} - P_{gen,e}\right)^2}{N}} \tag{3.77}$$

where N is the number of observations (215 days), P is the solar power generated (gen) and subscript, e is the empirical power generation.

3.3.3.11 Description of the algorithm

The algorithm used in this work is illustrated in Figure 3.8. The input data of wind speed (U), irradiance (H), temperature (T), and power (P) were acquired from (Nnamchi *et al.*, 2019; Nnamchi *et al.*, 2023; UNMA, 2023; UETCL, 2023), respectively. Formulation of the first and second solar power generation models followed; the coefficients in the formulation are either extraterrestrial or thermophysical. Differential models of solar power generation were developed as a function of wind speed, temperature, and irradiance by coupling the aforementioned coefficients to wind speed, ambient temperature and solar irradiance. Further, explicit discretization of the differential models was carried out in order to obtain the numerical solutions of the first and second numerical models. Besides, empirical models were developed based on the experimental data and modified with the velocity; further modification with both wind speed and solar irradiance was considered. The solar power generation from simulated models was validated with empirical data. Similarly, the empirical solar generation models were validated with the design capacity of the solar power plants. Ultimately, the scheme outputted the essential results and stopped.

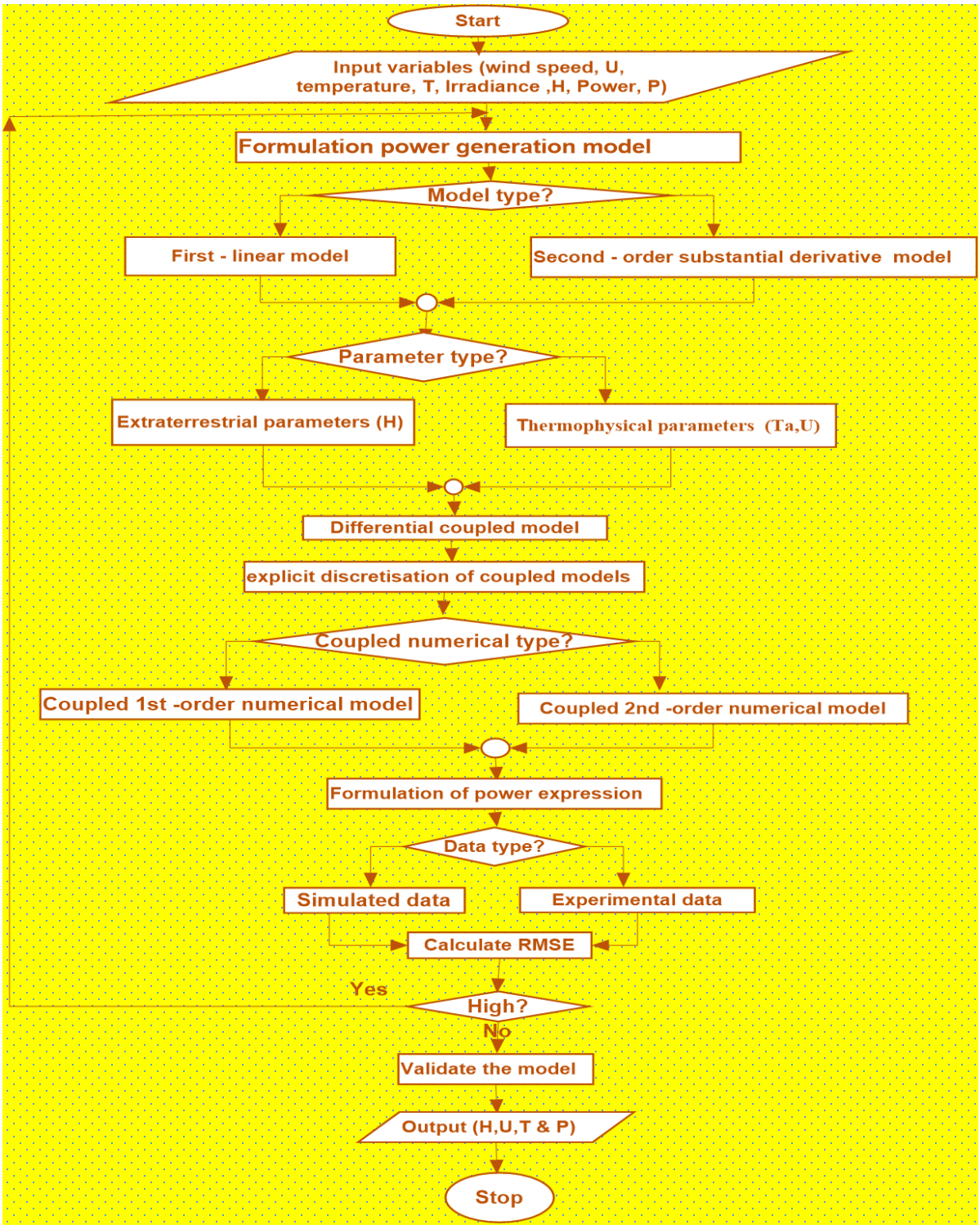

Fig. 4. Flowchart for data acquisition and power generation model

Source: Present study 2024

3.3.3.12 Experimentation

In the eastern part of Uganda, the experimental setup seen in Figure 3.9 was installed next to four solar power facilities (Busitema, Mayuge, Soroti and Tororo). The set-up consisted of two ADH solar PV modules (ASO 15W-18P), fixed on stand of 0.8m from the ground, two digital solar power meters (SM206), a digital multimeter (DT9205A C€), two digital thermocouples (DM6802B K-type) and a digital anemometer (UNI-T UT363S). The following data were recorded: ambient temperature, cell temperature, wind speed, irradiance, PV output voltage and electric current. Readings were recorded every 15 minutes from 09:00 a.m. to 17:00 p.m. on a daily basis. The experiment was conducted for 215 days in each study area. The algorithm in Figure 3.8, explains the aforementioned methodology. The coefficients of temperature, wind speed and irradiance in Equations (3.69, 3.70, and 3.71) and Table 4.6, they were determined as ratios of relative voltage to temperature, relative power to wind speed and relative current to irradiance, respectively. These coefficients were used to calculate empirical solar power generation.



Figure 3.9 Experimental set up

Source: Present study (2023)

3.4 Sources of data

In this study, two types of data were collected and used, primary and secondary data. The primary data collected in this study included; ambient temperature, cell temperature, wind speed, irradiance, PV output voltage and electric current. Daily readings were taken from 9:00 a.m. to

17:00 p.m. at intervals of fifteen minutes. In each study area, an experiment was conducted for 215 days. For the case of secondary data, it was obtained from UETCL, input data used in the analysis is courtesy of the planning, design, operations, and maintenance department of (UETCL, 2023). The following transmission data from (UETCL, 2023); voltage, current, frequency, conductor dimensions, spacing of conductors, thermal and electrical characteristics of the conductor for the transmission lines **(**132 kV (Masaka West - Mbarara North) and 220 kV (Bujagali - Kawanda) were used in the analysis**.**

3.5 Data Collection Instruments

The instruments used in data collection (primary data) consisted of the following; two ADH solar PV modules (ASO 15W-18P), two digital solar power meters (SM206), a digital multimeter (DT9205A C€), two digital thermocouples (DM6802B K-type) and a digital anemometer (UNI-T UT363S). For the secondary data the measured data was collected from UETCL and UNMA

3.7 Data Collection procedure

The procedures for primary data involved taking measurements on daily basis at an intervals of 15 minutes 09:00 a.m. to 17:00 p.m on a daily. The ambient temperature, cell temperature, wind speed, irradiance, PV output voltage and electric current of the two PV generators. An introduction letter from the University was collected by the researcher to introduce him in UETCL and UNMA for collecting secondary data, Secondary data included, transmission current (A), resistivity of transmission cable, length of transmission line (km), cross-section area, phase voltage, disruptive voltage, transmission frequency, air density factor, radius of transmission cable (30/3.71mm ≡ 30/0.00371 m), spacing between the transmission cables (m) for a period of three years.

3.8 Data Analysis Techniques

The data collected were analyzed using the following soft wares Microsoft Excel (programing and simulation), Maple 2021 (performing partial derivatives and simplification), OriginLab 8 (to obtain the coefficients of the models and the coefficient of determination, curve plotting), and ArcGIS (for contours and maps). The collected data was subjected to programming to achieve simulation of the developed models. The models developed were validated using Root-mean-square error also the secondary data obtained from UETCL, (2023) were imputed into Maple-derived models to calculate; the optimum values of the optimum variables, and second-order

derivatives of these variables. These results were exported to a Microsoft Excel spreadsheet to calculate the determinant of the Hessian matrix (matrix of second-order derivatives). The determinate of the Hessian matrix served as a criterion for the optimality test and decision. Also, a Spread sheet of power losses was developed in a Microsoft Excel spreadsheet as a function of current and voltages in the transmission lines. Furthermore, the spreadsheet power losses were exported to Origin (7.0) to obtain three dimensional (3D) plot of current, voltage and power losses in the transmission lines. The analysis was conducted for both unmodified and modified transmission power loss models to show the robustness of the modified model.

CHAPTER FOUR

RESULTS AND DISCUSSION

4.0 Introduction

This Chapter presents detailed results and analyses of the activities carried out as guided by the research objectives or questions outlined in Chapter One

4.1 Presentation of Results

The results from data analysis of the activities carried out as guided by the research objectives and methods are presented under this subsection.

4.1.1 Minimization of electric power losses in transmission lines.

Table 4.1 presents the Input data for the optimization of power losses on 132 kV (Masaka West - Mbarara North) and 220 kV (Bujagali – Kawanda) transmission lines. These parameters were used in obtaining optimum values for both modified and unmodified models as shown in Table 4.2. It was observed that for the unmodified model, there were no optimum variables nor values obtained for both transmission lines. However, the modified model on 132 kV (Masaka West - Mbarara North) transmission line optimum variables and values were obtained (Bamigbola et al., 2014); transmission current (33.99466040 A), Phase voltage (119.0972116 V), and air density (1.255443722 kg/m3); and on 220 kV (Bujagali – Kawanda) transmission line optimum variables and values were established, transmission current (132.7905080 A), Phase voltage (132.9176350 V) and air density (1.468830824 kg/m3). Table 4.3 presents optimality tests based on the Hessian matrix. It is observed that both 132 kV (Masaka West - Mbarara North) and 220 kV (Bujagali – Kawanda) transmission lines under an unmodified model maximized power losses as the determinant is less than zero (D < 0), and , respectively. It is also observed that 132 kV (Masaka West - Mbarara North) and 220 kV (Bujagali – Kawanda) transmission lines under the modified model supported minimization of power losses as the determinant is greater than zero ((D > 0), 1.53637 10-12 and 1.75675X10-11 respectively.

Figure 4.1 shows the power losses plotted against the phase voltage of the Bujagali – Kawanda transmission line plotted for both modified and unmodified models. The graphs show the voltage range: 66 to 402kV, the losses in unmodified and modified models ranged (0.408077441-0.406023685kW/km/phase) and (0.393143977-0.39112869 kW/km/phase) respectively. This shows that the modified model minimized power losses due to the implementation of optimum variables and values.

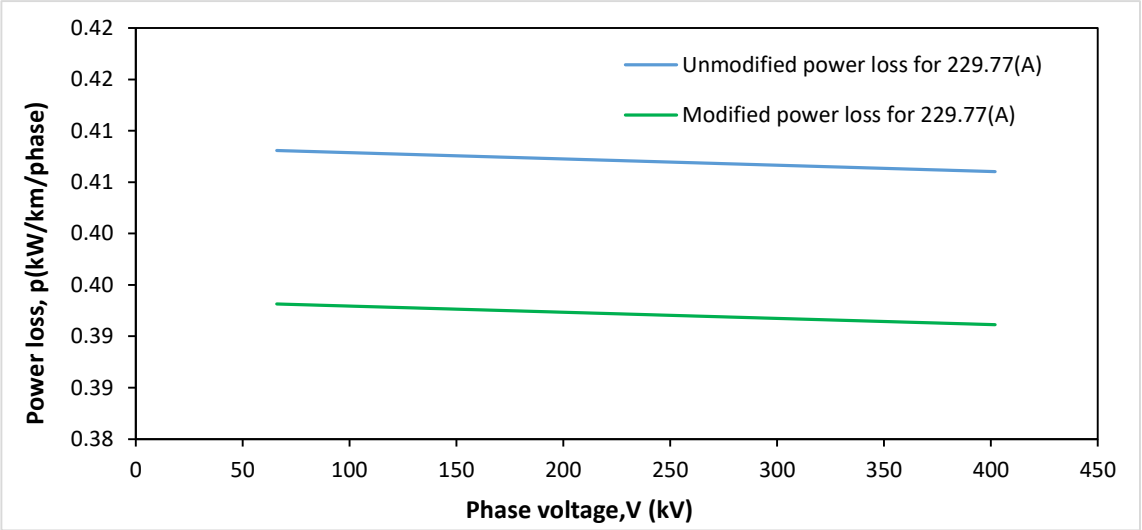

Figure. 4.1 Power losses in Bujagali – Kawanda transmission line.

Figure 4.2 presents the input data for power losses plotted against the phase voltage of the Masaka West - Mbarara North transmission line plotted for both modified and unmodified models. The graphs show the voltage range: 66 to 402kV, the losses in the unmodified and modified models ranged (0.454505268 - 0.451933075kW/km/phase) and (0.448067835-0.445513943 kW/km/phase) respectively. This shows that the modified model minimized power losses due to the implementation of optimum variables, values, and the virtue of the third term incorporated in the modified model.

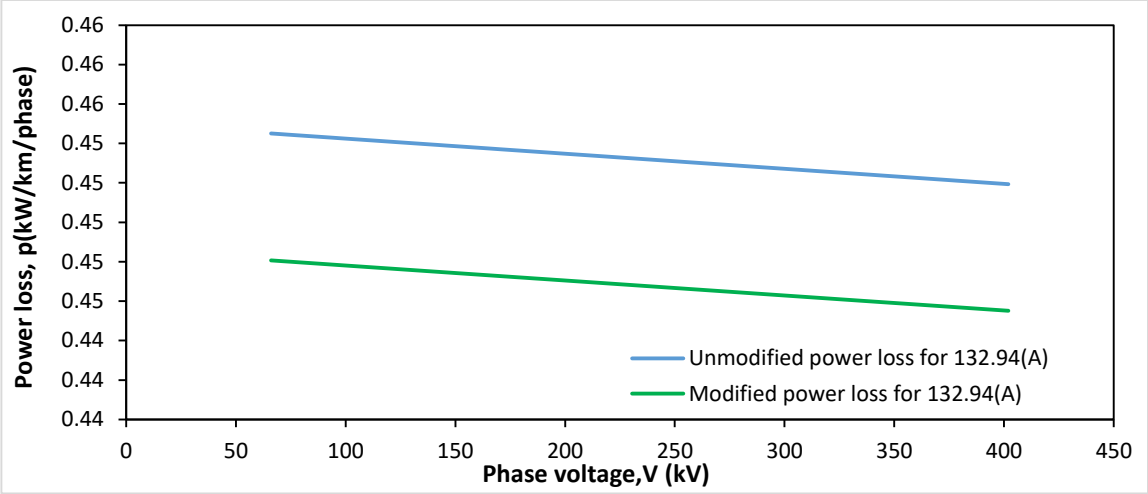

Figure 4.2 Power losses in Masaka West - Mbarara North transmission line.

Observation in Fig. 4.3 indicates that both models at low transmission current have no disparity but at high transmission current, there is a quite significant difference. This implies that the modified model has a high potential to minimize power loss relative to the unmodified model. The graphs show the transmission current ranged from 24 A to 238 A, and the losses in unmodified and modified models ranged (0.28420384-0.293697008 kW/km/phase) and (0.282898963-0.280648235 kW/km/phase) respectively.

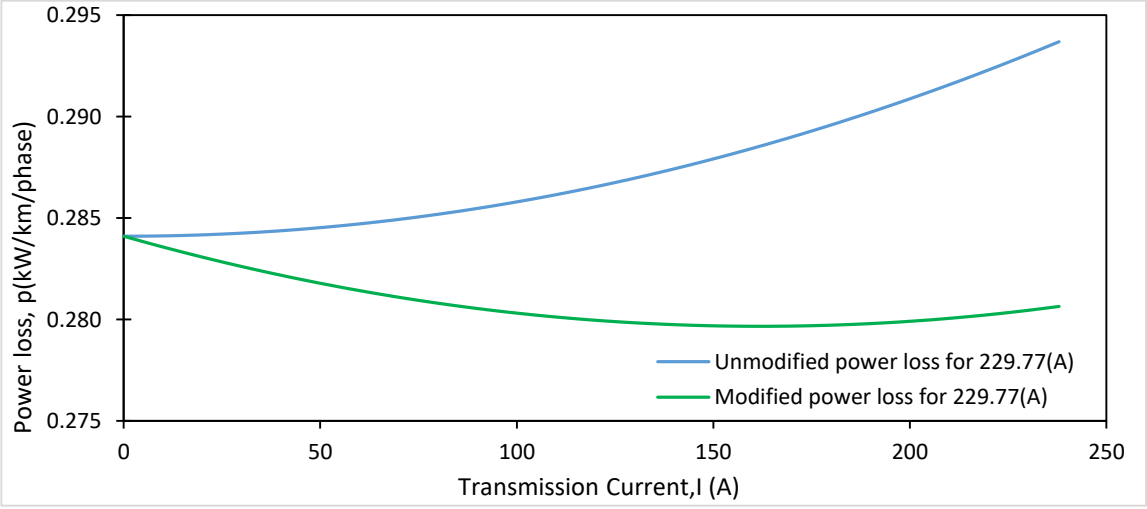

Figure 4.3 Power losses in Bujagali – Kawanda transmission line.

Figure 4.4 presents the input data for power losses plotted against the phase transmission current of the Masaka West - Mbarara North transmission lines plotted for both modified and unmodified models. The graphs show the transmission current range: 13 to 145A, the losses in unmodified and modified models ranged (0.344691715-0.346417624 kW/km/phase) and (0.344142083-0.34029535 kW/km/phase) respectively. This shows that the modified model minimized power losses when compared with the unmodified model (Bamigbola et al., 2014).

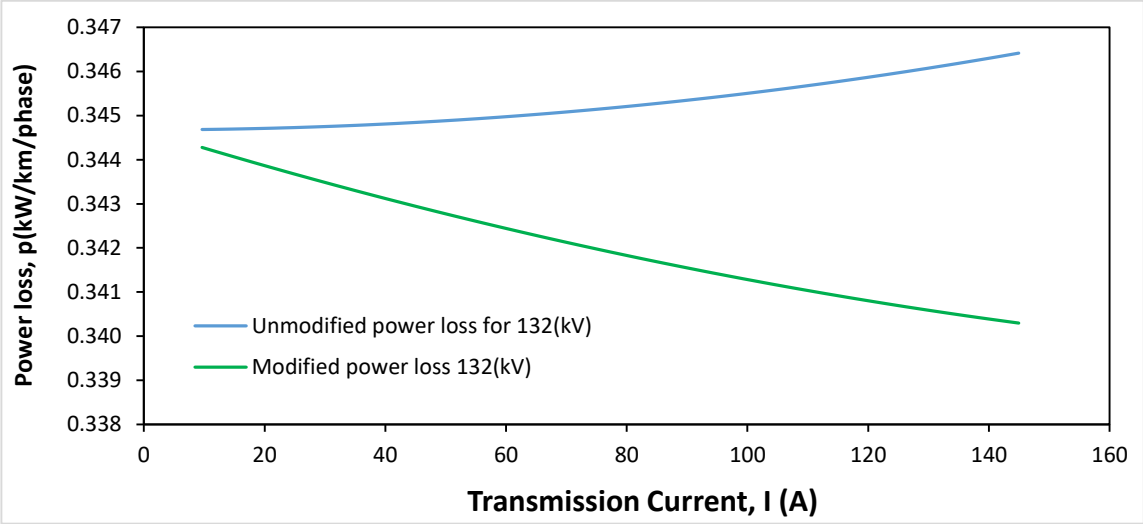

Figure 4.4 Power losses in Masaka West - Mbarara North transmission line.

Furthermore, Fig.4.5 presents the power losses plotted against the air density of the Bujagali – Kawanda transmission line plotted for both modified and unmodified models. The graph obtained shows that the results support or identify the modified model as an effective one in minimizing power losses and this means the power losses are attributed to both Corona and Ohms losses.

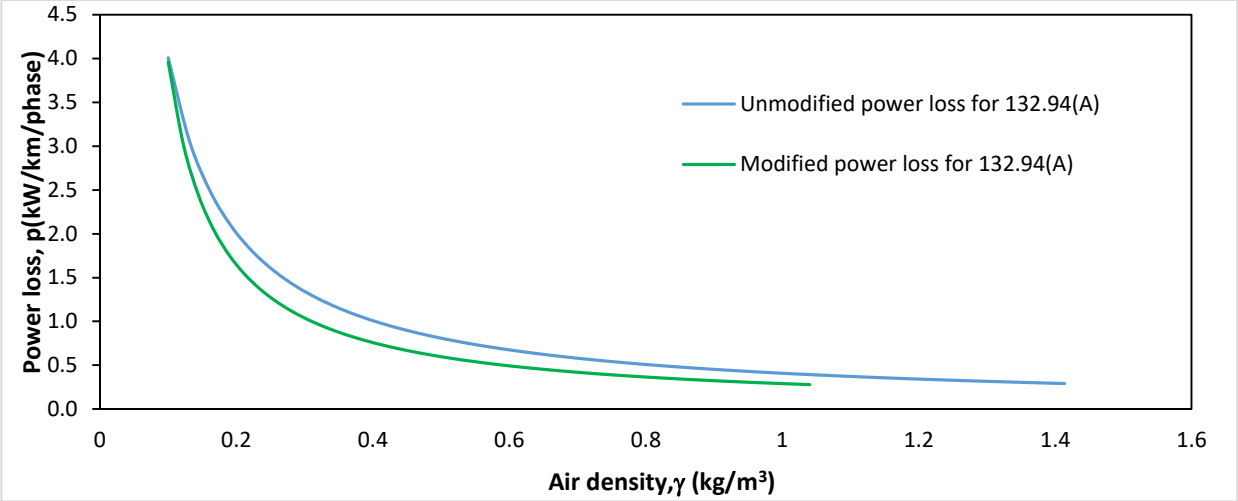

Figure 4.5 Power losses in Bujagali – Kawanda transmission line as a function of air density.

In addition, Fig. 4.6 shows an inappreciable discrepancy in the transmission power losses by unmodified and modified models, this means that the atmosphere in the transmission lines is uniform and could not support any meaningful difference in power losses for the unmodified and modified models.

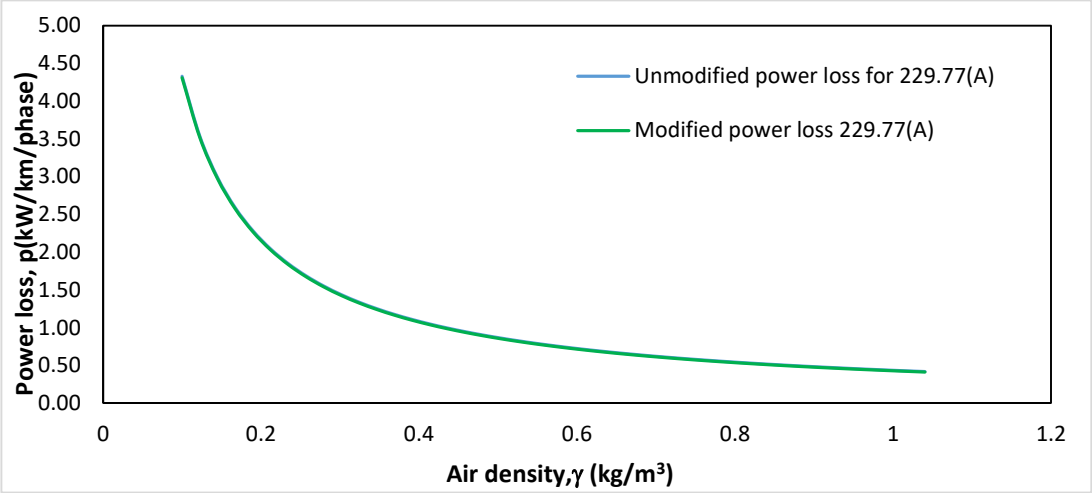

Figure 4.6 Power losses in Masaka West - Mbarara North transmission line as a function of air density.

Figures (4.7a and 4.7b) show the three-dimensional graph of power losses, phase voltage, and current for the 220 kV Bujagali-Kawana transmission lines. The power losses for both unmodified and modified are 0.304546 and 0.288325kV/km/phase respectively as shown in Figures (4.8a and 4.8b). For the 132 kV Masaka West-Mbarara North transmission lines. The power losses for both

unmodified and modified are 0.302389 and 0.28899kV/km/phase respectively as presented in Figures (4.8a and 4.8b) which implies that the modified has a high potential for power loss minimization in both transmission lines.

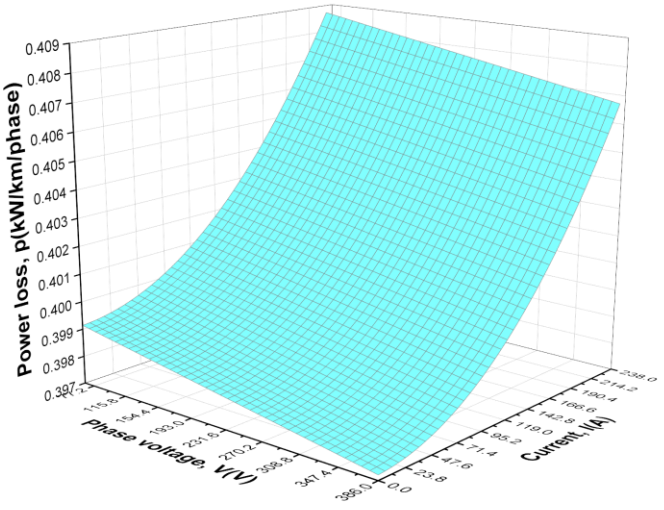

Figure 4.7a. Unmodified 3-D plot of power losses for 220 kV Bujagali-Kawana transmission line

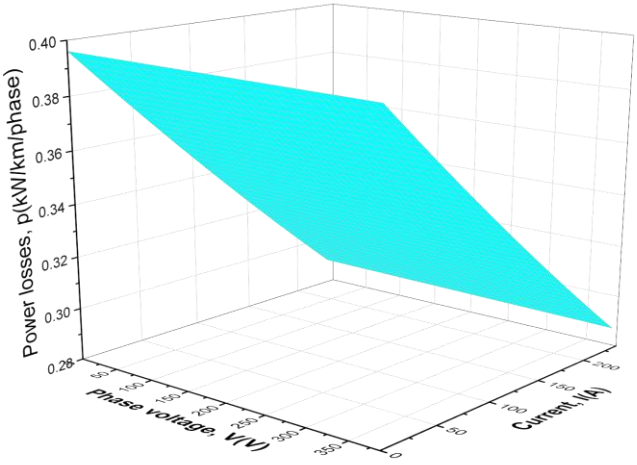

Figure 4.7b. Modified 3-D plot of power losses on 220 kV Bujagali-Kawana transmission line

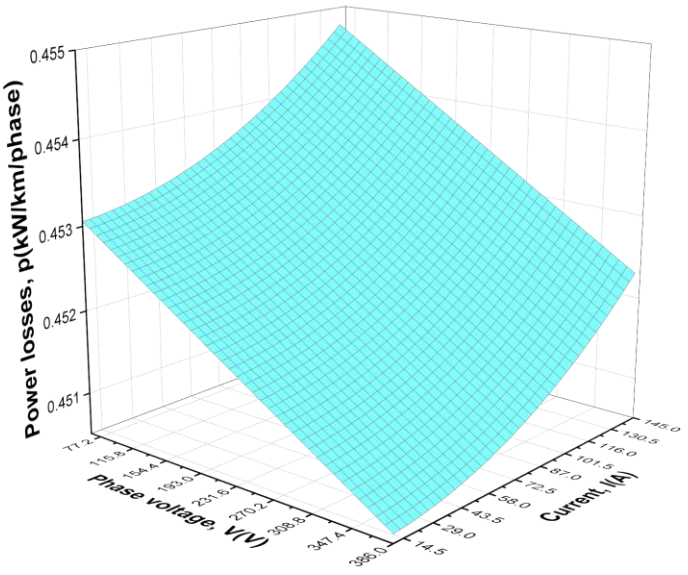

Figure 4.8a. Unmodified 3-D plot of power losses for 132 kV Masaka West-Mbarara North transmission line

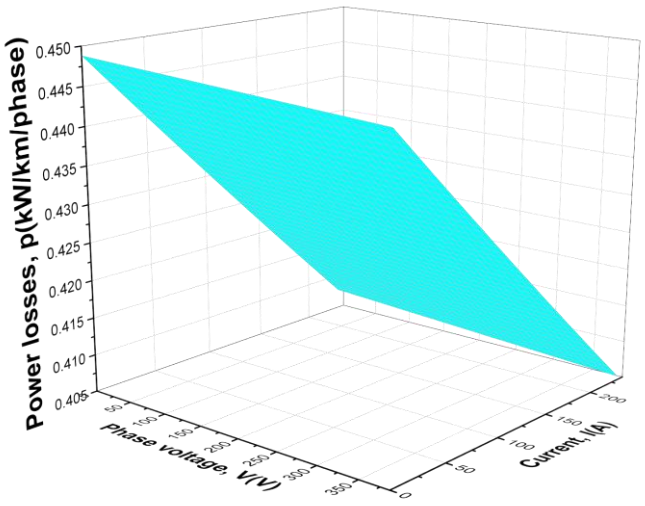

Figure 4.8b. Modified 3-D plot of power losses for 132 kV Masaka West-Mbarara North transmission line

Table 4.1 Input data for the optimization of power losses in the transmission lines (UETCL, 2022)

S #	Parameters	Symbol	132 kV (Masaka West - Mbarara North)	220 kV (Bujagali – Kawanda)
1.	Transmission current(A)	I	132.94	229.77
2.	Resistivity of transmission cable	ρ	2.65×10^{-8}	2.65×10^{-8}
3.	Length of transmission line(km)	l	130.5	130.5
4.	Cross-section area	A	0.00032	0.000157
5.	Phase voltage	V	132	220
6.	Disruptive voltage	V_0	88.409	94.555
7.	Transmission frequency	f	50.09	50.09
8.	Air density factor	γ	1.00433	1.00433
9.	Radius of transmission cable (30/3.71mm ≡ 30/0.00371 m)	r	0.00186	0.0013
10.	Spacing between the transmission cables(m)	d	3.740	4.540

Table 4.2 Optimization results of power losses in the transmission lines based on modified and unmodified models

			Unmodified model		Modified model	
S #	Parameters	Symbol	132 kV (Masaka West - Mbarara North)	220 kV (Bujagali – Kawanda)	132 kV (Masaka West - Mbarara North)	220 kV (Bujagali – Kawanda)

1.	Transmission current(A)	I^*	NA	NA	33.994	132.791
2.	Resistivity of transmission cable	ρ^*	NA	NA	NA	NA
3.	Length of transmission line(m)	l^*	NA	NA	NA	NA
4.	Cross-section area(m^2)	A^*	NA	NA	NA	NA
5.	Phase voltage(kV)	V^*	NA	NA	119.0972	132.918
6.	Disruptive voltage(kV)	V_0^*	NA	NA	NA	NA
7.	Transmission frequency	f^*	NA	NA	NA	NA
8.	Air density factor	γ^*	NA	NA	1.255	1.469
9.	Radius of transmission cable (30/3.71mm ≡ 30/0.00371 m)	r^*	NA	NA	NA	NA
10.	Space between transmission cable(m)	d^*	NA	NA	NA	NA

NA: Not Available

Table 4.3 Optimality tests based on the Hessian matrix in Equation (3.8)

S#	Transmission Line	Equation Number Hessian	Determinant	Value Determinant Hessian	Model type	Remarks
1.	132 kV (Masaka West - Mbarara North)	Eq.(3.8)	Eq.(3.18)	-1.573×10^{-19}	Unmodified	Maximization (D < 0)
2.	132 kV (Masaka West - Mbarara North)	Eq.(3.8)	Eq.(3.19)	1.536×10^{-12}	Modified	Minimization (D >0)

3.	220 kV (Bujagali – Kawanda)	Eq.(3.8)	Eq.(3.20)	$-6.765E\times10^{-18}$	Unmodified	Maximization (D < 0)
4.	220 kV (Bujagali – Kawanda)	Eq.(3.8)	Eq.(3.21)	$1.757X10^{-11}$	Modified	Minimization (D >0)

4.1.2 Modeling of coupled and uncoupled transmission lines

This sub-section presents the results of the numerical simulation obtained by the coupled power transmission model.

4.1.2.1 Simulation of transmission potentials

As mentioned earlier, the transmission potential could be space and time oriented. Implies that transmission potentials (temperature, current and voltage) are dependent on space and time according to Eqs. (3.28, 3.29, 3.30), respectively.

4.1.2.2 Space potentials

The space transmission potentials (current, voltage, temperature and power) are described in Figs. (4.19-4.12), respectively. A positive linear gradient was observed in behavior of current and temperature potentials which supports Joule-Thompson thermodynamic effects, thus, temperature and current have similar behavior due to linear relationship between them (Medved etal., 2022). Increment in temperature and current is supported by the coupled terms in Eqs. (3.28, 3.30), respectively, which implies that the coupling terms were well posed in the coupled model, hence, these models simulated the field potentials effectively. Furthermore, the positive linear behavior of temperature and current is supported by physical laws of Fourier's and Ohmic laws. Conversely, the space potential (voltage) exhibited reverse trend relative to current and temperature, which supports Ohm's law or inverse proportionality between current and voltage. This is further evidence that the coupled is well developed.

The transmission results comprise of variation of transmission potentials; current, voltage, temperature and power with space and time for Bujagali-Kawanda 220 kV as presented in Figures.

4.9, 4.10 ,4.11, 4.12 and Figs. 4.13, 4.14, 4.15, 4.16 respectively. Figure 4.17 portrays the power and power loss in the transmission line.

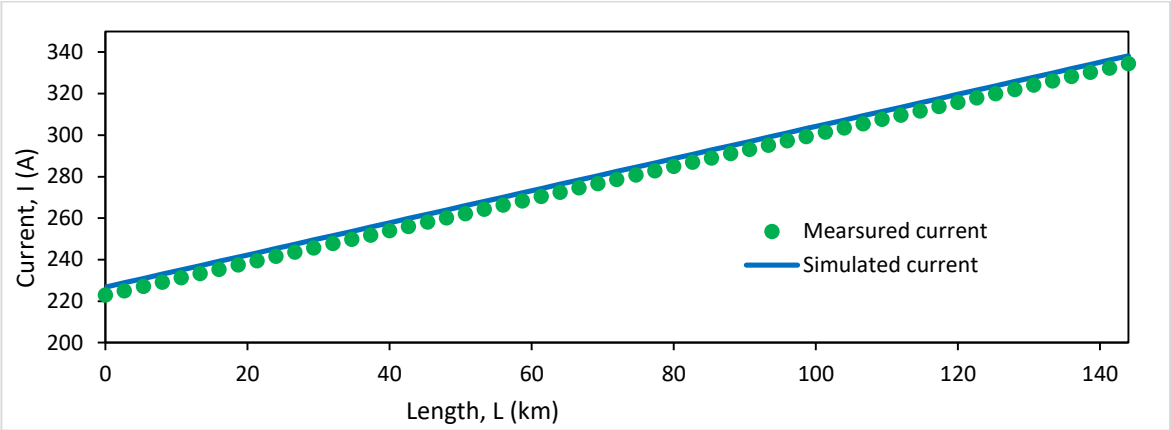

Figure 4.9 Current in the Bujjagali-Kawanda transmission line based on the coupled power model

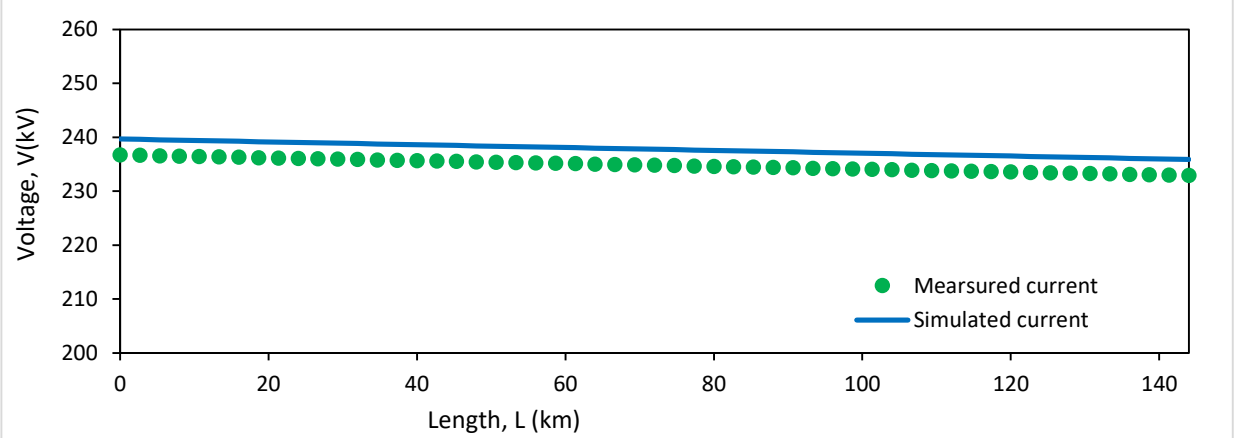

Figure 4.10 Voltage in the Bujjagali-Kawanda transmission line based on the coupled power model

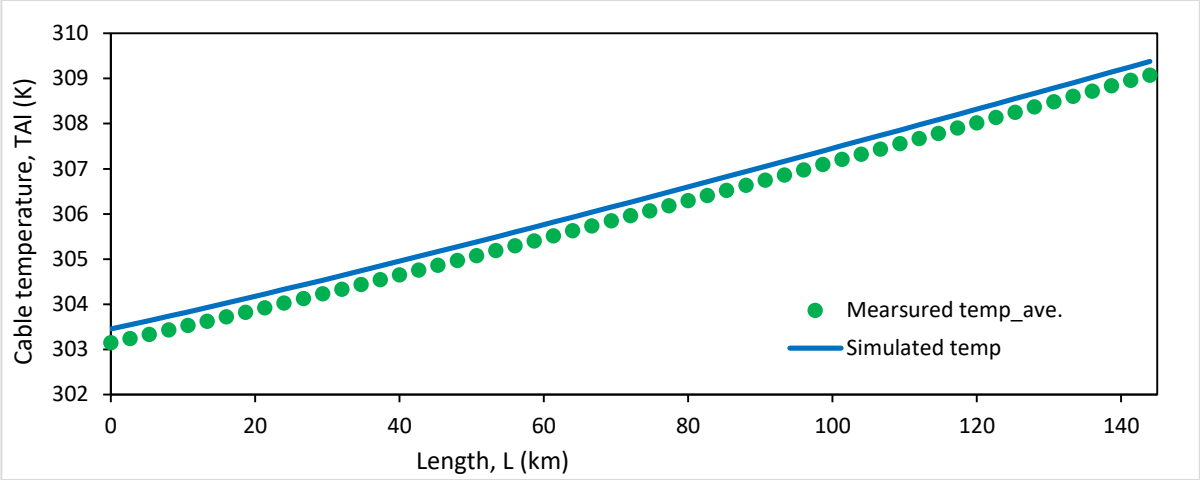

Figure 4.11 Temperature in the Bujjagali-Kawanda transmission line based on the coupled power model

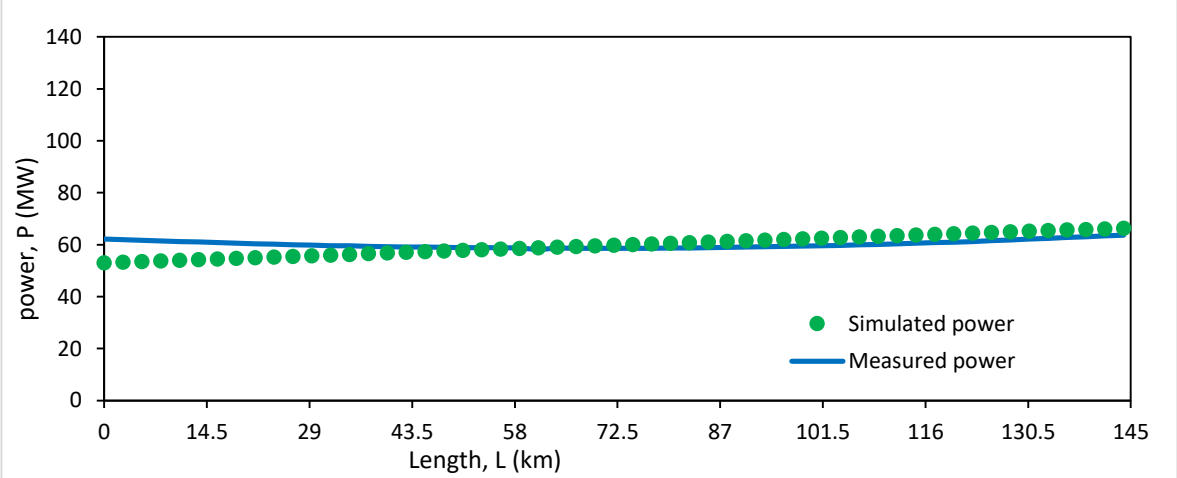

Figure 4.12. Power in the Bujjagali-Kawanda transmission line based on the coupled power model

4.1.2.3 Time potentials

The time dependent transmission potentials (current, voltage, temperature and power) are described in Figs. (4.9-4.16), respectively. Due to similarity of functions in Figs. 4.13 and 4.17, it can be inferred that current in the transmission line had more contribution in power transmission relative to voltage, which had different behavior or partner relative to power in Fig.4.14. Thus, deterioration in current (and Ohmic loss) is low compared to deterioration in voltage (and Corona loss) which is pronounced, hence, the difference in behavior of voltage relative to power. Also the

time dependence of temperature in Fig. 4.15 shows that the degree of temperature depends on the magnitude of current in the transmission cable. This portrays that thermal model could be considered or approximated with steady state model. Furthermore, apparent constant temperature implies that the transmission cable is made up of isotropic material (having uniform thermal conductivity), thus, thermal accumulation in the transmission cable was not observed as in current, voltage and power.

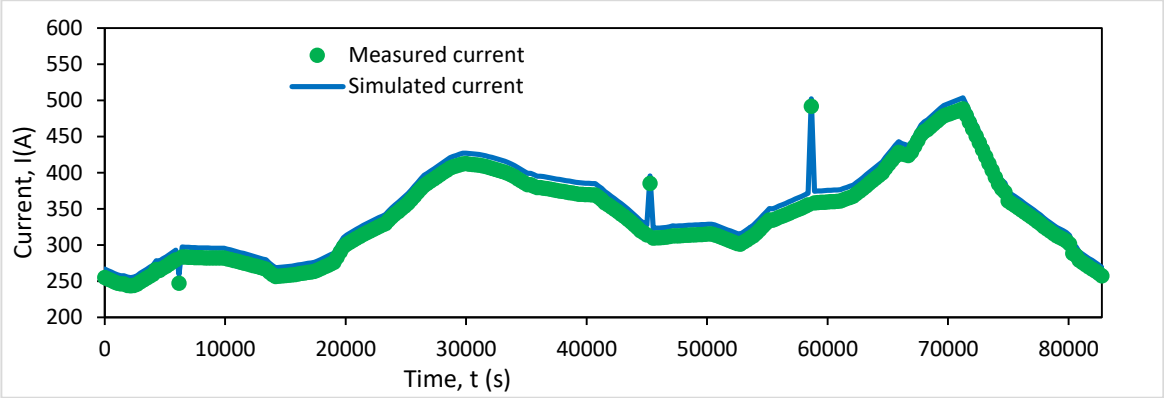

Figure 4.13. Historic current in the Bujjagali-Kawanda transmission line based on the coupled power model

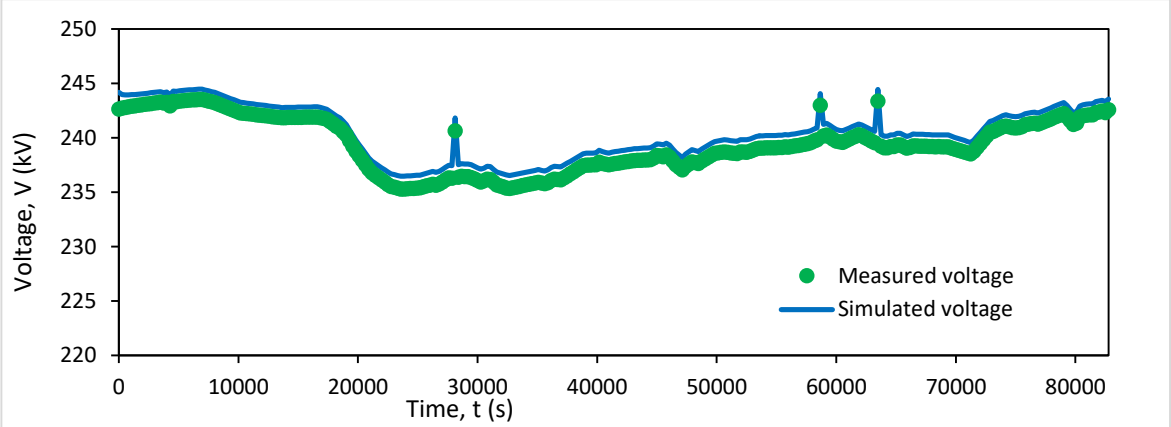

Figure 4.14. Historic voltage in the Bujjagali-Kawanda transmission line based on the coupled power model

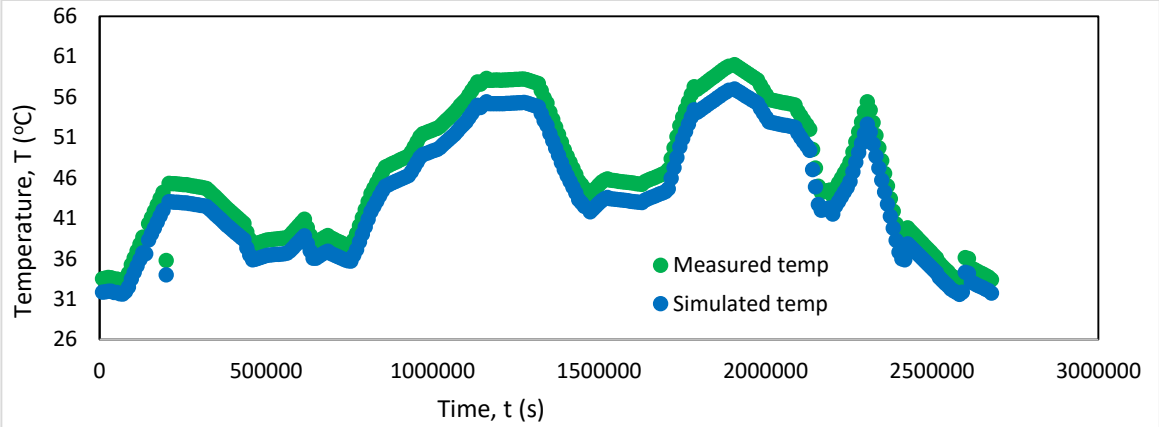

Figure 4.15. Historic temperature in the Bujjagali-Kawanda transmission line based on the coupled power model

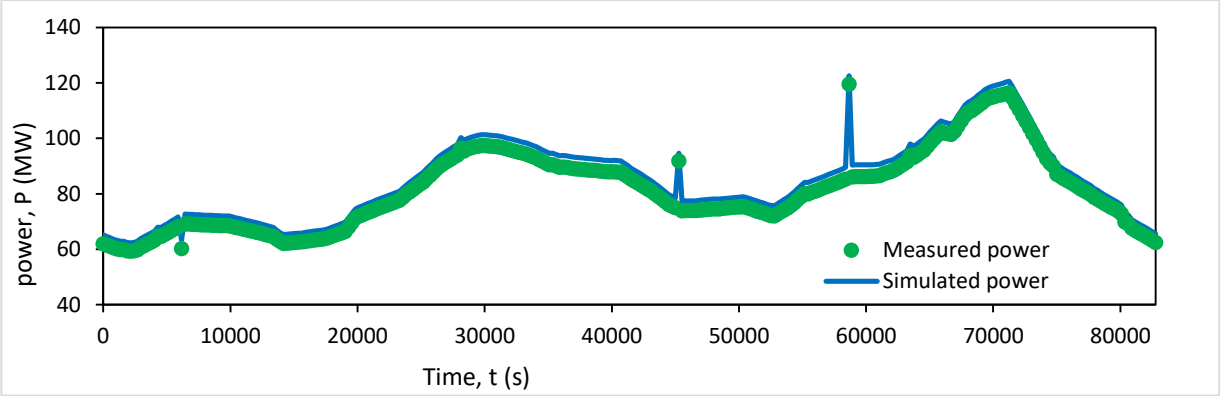

Figure 4.16. Historic power in the Bujjagali-Kawanda transmission line based on the coupled power model

4.1.2.4 Estimation of power and power losses in transmission line

Power and power losses are described in Fig. 4.17, positive linear gradient of power and power losses were observed, power losses are proportional to power in the transmission line. The apparent losses in the transmission line could be attributed to Ohmic loss due to resistivity of the transmission cable, to Corona loss due to decrease in disruptive voltage resulting from increase in pressure and the drop in temperature of the air, and possible deteriorations or aging of the transmission line. The deteriorations (temperature, current and voltage) emanate from the degradation of the transmission material and other transmission accessories (circuit breakers, magnetic starters, transformers). The power losses estimated in Fig. 4.17 ranges from 0.02 to

0.045, which is consistent with that recommended by Electricity Regulation Authority, ERA of Uganda (3.6 %) of total power transmitted.

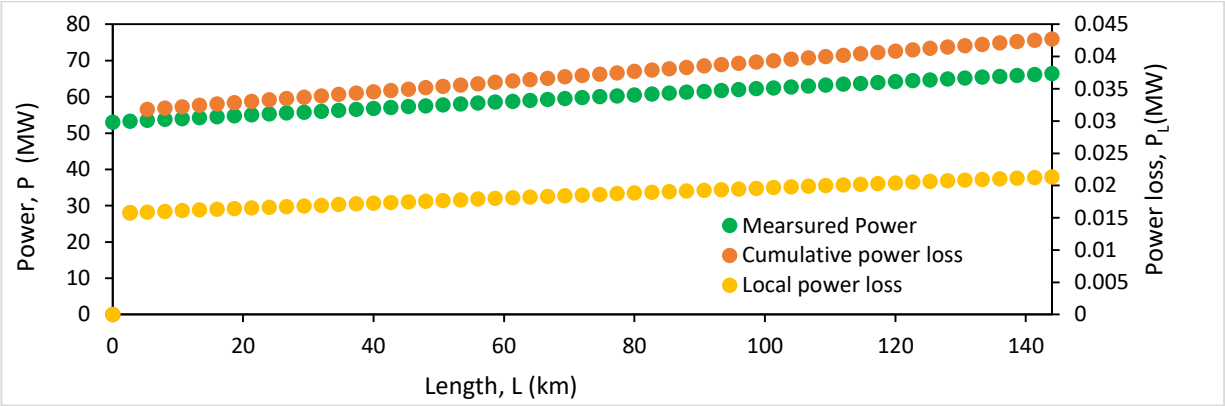

Figure 4.17. Power and power losses Bujjagali-Kawanda transmission line

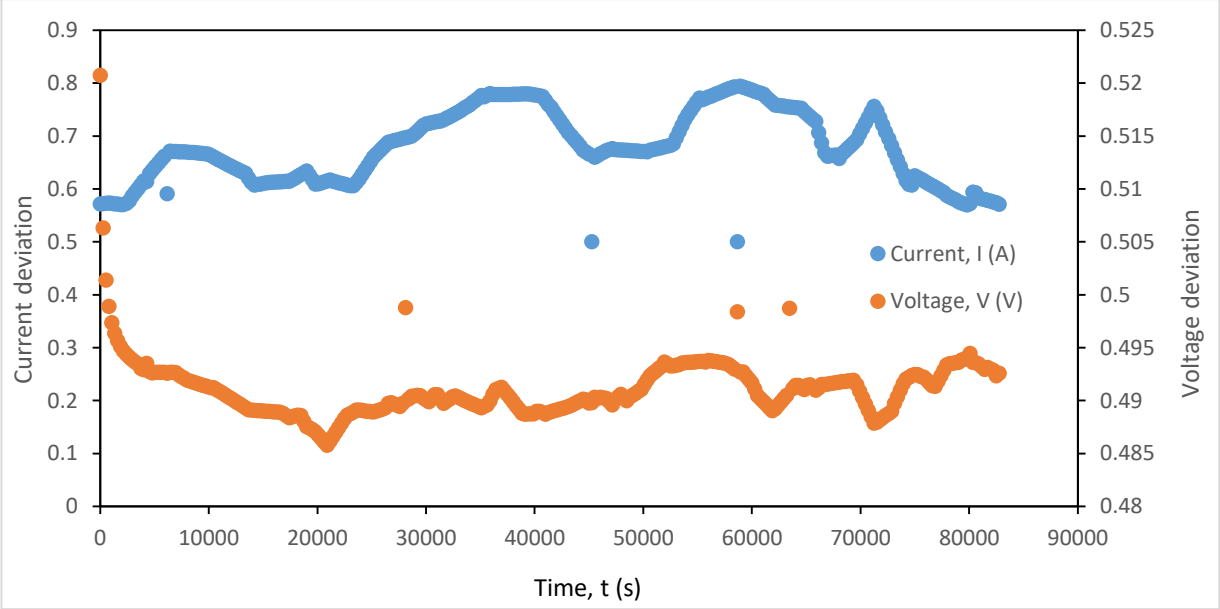

(a) Current and voltage deviation

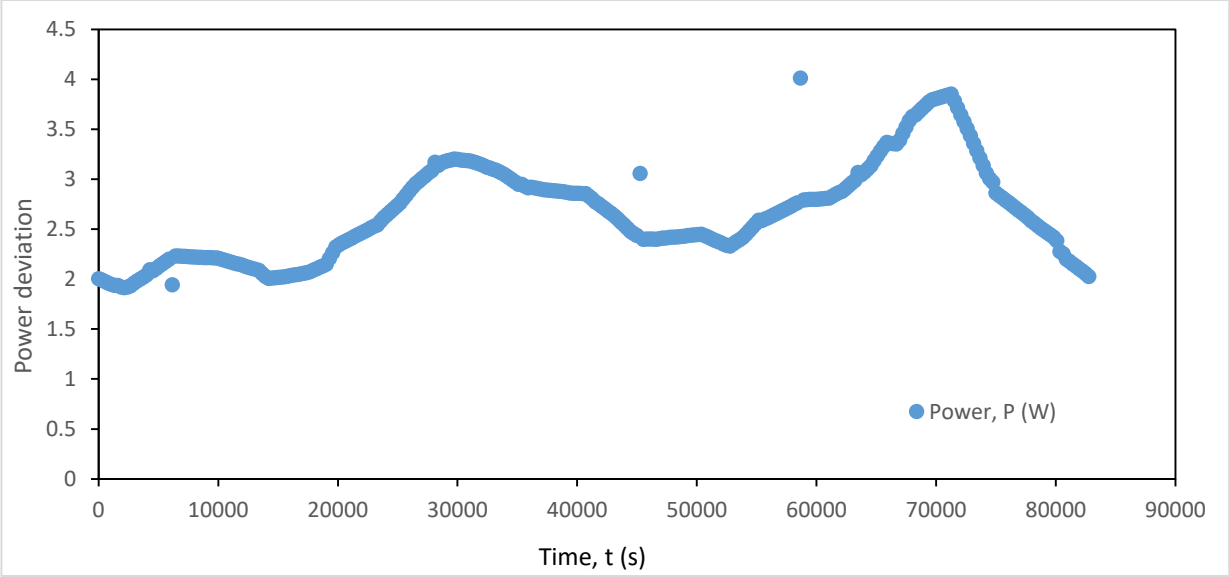

(b) Power deviation

Figure 4.18 Historic deviation or error in variables (current, voltage and power)

Table 4.4 Input data for system simulation

S#	Parameter	Symbol	Unit	Value		Source
				Lower limit	Upper limit	
1	Total iteration	N	-	1	310	Present study, 2023
2	Time division	n_t	-	100	100	Present study, 2023
3	Total time	t	s	267840	267840	UETCL, 2023
4	Space division	ns	_	55	55	Present study, 2023
5	Tlength	L	m	144000	144000	UETCL, 2023
6	Initial time	t_0	s	0	2678400	UETCL, 2023
7	Dspace	Δx	m	2.618181818	144	UETCL, 2023
8	Dtime	Δt	s	267.84	267.84	UETCL, 2023
9	Implicitness	θ	-	0.5	0.5	Present study, 2023

10	Max Aluminum temperature	$T_{Al,max}$	K	308.15	308.15	UETCL, 2023
11	Min Aluminum temperature	$T_{Al,min}$	K	303.15	303.15	UETCL, 2023
12	Initial max air temperature distribution	$T_{Air,max}$	K	299.15	299.15	UETCL, 2023
13	Initial min air temperature distribution	$T_{Air,min}$	K	296.15	296.15	UETCL, 2023
14	Initial air temperature distribution	T_{Air}	K	303.15	308.027110	UETCL, 2023
15	Initial max voltage	V_{max}	kV	236.6951348	236.5669387	UETCL, 2023
16	Initial min voltage	V_{min}	kV	230.8735807	230.8738865	UETCL, 2023
17	initial voltage distribution	V	kV	236.6951348	231.1055927	UETCL, 2023
18	Disruptive voltage	V_d	kV	228.836018	228.836018	Bamigbola *et al.*, 2014
19	Initial max current	I_{max}	A	287.8982562	289.6828392	UETCL, 2023
20	Initial min Current	I_{min}	A	223.0452015	225.3469998	UETCL, 2023
21	Convective heat transfer coefficient of air	h	W/m^2K	5.58350035	7.22934835	Kosky, 2023
22	Density of Aluminum	ρ	Kgm^{-3}	2720.621315	2720.621315	UETCL, 2023
23	Specific heat capacity of Aluminum	cp	J/kgK	891.0943725	891.0943725	Moran *et al.*, 2002
24	Thermal conductivity of Aluminum	k	$Wm^{-1}K^{-1}$	227.6664683	227.6664683	Ausloos, 2011
24	Thermal diffusivity of Aluminum	α	M^2s^{-1}	9.39090E-05	9.39090E-05	ElSheikh, 2022

26	Electron diffusivity	D_e	M^2s^{-1}	2.22726E-03	2.25E-03	Satpathy and Venkateswarlu, 2021 and Ignjatovic and Cvetic, 2021
27	Temperature Stability	ζ_T	-	0.003669299	0.003669299	Present study, 2023
28	Voltage Stability	ζ_V	-	0.087025634	0.087025634	Present study, 2023
29	Current Stability	ζ_I	-	0.087025634	0.087025634	Present study, 2023
30	Radius of transmission wire	r	m	0.0013	0.0013	UETCL, 2023
31	Perimeter of transmission wire	p	m	0.008171429	0.008171429	UETCL, 2023
32	Air pressure	P_{Air}	cmHg	76	76	
33	Air density	γ	kg/m^3	1.011109235	0.991030945	UETCL, 2023
34	Temperature coefficient	k_T	K^{-1}	0.003271716	0.003271716	Moran *et al.*, 2002
35	Voltage coefficient	k_V	V^{-1}	0.004277446	0.004277446	Moran *et al.*, 2002
36	Current coefficient	k_I	A^{-1}	0.003914327	0.003914327	Moran *et al.*, 2002
37	Frequency	f	Hz	50.09	50.09	UETCL, 2023
38	Space	h	m	4.54	4.54	UETCL, 2023
39	Cross section Area	A	m^2	5.31143E-06	5.31143E-06	UETCL, 2023
40	Resistivity of transmission line	s	Ω m	2.65E-08	2.65E-08	Living *et al* ., 2024

Table 4.5 Statistical validation of coupled transmission model

#	Parameter	Symbol	Equation number	RMSE value

1	Current	I	(25)	0.68
2	Voltage	V	(27)	0.70
3	Power	P	(28)	1.63

4.1.3 Development of differential and empirical solar power generation models.

This subsection presents the findings on; development of differential solar power generation model for simulation and multiple empirical models for improving PV system design and operation, ensuring infinitesimal discrepancies.

The results are made up of tables and figures substantiating the objectives of this study. Table 4.6 contains the empirical power generation coefficients; Table 4.7 describes the coefficients of boundary conditions; and Table 4.8 gives the statistical description of the experimental data. Table 4.9 presents the validation of simulated solar power with empirical solar power generation and Table 4.10 comprises the validation of solar power design capacity with empirical solar power generation.

The figures are as follows: Figure 4.19 portrays the solar power generation based on the first order generation model; Figure 4.20 proffers the solar power generation based on the second order model, Figure 4.21 holds the empirical solar power generation at the Busitema study area and Figure 4.22 depicts the empirical solar power generation at Tororo study area, Figure 4.23 describes the empirical solar power generation at Soroti study area, Figure 4.24 gives the empirical solar power generation at Mayuge study area, Figure 4.25 shows the empirical solar power generation based on the first model for the Eastern region of Uganda; Figure 4.26 illustrates the empirical solar power generation based on the second model for the Eastern region of Uganda; Figure 4.27 demonstrates the empirical solar power generation based on the third model for the Eastern region of Uganda.

Table 4.6 Empirical power generation coefficients.

S#		Coefficient	Busitema	Mayuge	Soroti	Tororo	Source
1.	Cell temperature	$\beta_c(\%°C^{-1})$	-0.000142	-0.000157	-0.000132	-0.000351	Present study, 2023
2.	Wind speed	$\beta_u(\%sm^{-1})$	0.112316	0.135124	0.129189	0.091326	Present study, 2023
3.	Irradiance	$\beta_H\ (\%m^2W^{-1})$	0.000104	0.000112	0.000067	0.000164	Present study, 2023

Table 4.7 Coefficients of boundary conditions.

S#	Variable	Symbol/Unit	Coefficient, k = 0,1,2			R^2	Source
			0	1	2		
1.	Solar power	$P_{i,j}^0(MW)$	7.5200	-4×10^{-5}	-4.0×10^{-7}	0.9985	UETCL, 2023
2.	Irradiance	$H_{i,j}^0(Wm^{-2})$	684.7600	1.232	0.0035	1.0000	Nnamchi *et al.*, 2019
3.	Ambient temperature	$T_{i,j}^0(K)$	268.9400	0.0058	3.0×10^{-5}	1.0000	UNMA, 2023
4.	Resultant wind speed	$U_{i,j}^0(ms^{-1})$	0.5195	-0.0026	2.0×10^{-5}	0.9984	Nnamchi *et al.*, 2019
5.	Component wind speed	$U_{x,i,j}^0 = U_{y,i,j}^0 = U_{z,i,j}^0(ms^{-1})$	0.2999	-0.0015	1.0×10^{-5}	0.9984	Nnamchi *et al.*, 2019

These coefficients were obtained by correlating field data from UETCL, 2023 and Nnamchi *et al.*, 2019

Table 4.8 Statistical description of the experimental data.

S #	Study area	Statistics	Ambient temperature (℃)	Cell temperature (℃)	Wind speed (m/s)	Irradiance (W/m^2)	Voltage (V)	Current (A)
1.	Busitema	Lower limit	21.20	26.50	0.00	76.40	37.60	0.12
		Mean	31.71	42.11	1.12	617.57	41.33	0.85
		Upper limit	46.70	63.80	4.14	1249.50	43.10	1.94
		SD	4.14	7.65	0.75	335.48	0.80	0.44
		MAD	3.32	6.22	0.57	302.23	0.59	0.38
2.	Mayuge	Lower limit	23.90	25.70	0.10	32.40	36.80	0.05
		Mean	32.02	41.65	0.97	588.26	41.13	0.82
		Upper limit	44.90	63.10	3.43	1382.50	43.40	1.94
		SD	3.70	9.15	0.57	353.13	0.87	0.48
		MAD	2.67	7.91	0.42	308.10	0.62	0.43
3.	Soroti	Lower limit	21.00	32.00	0.02	207.60	38.70	0.31
		Mean	28.55	44.46	0.99	717.74	41.47	1.01
		Upper limit	43.70	65.60	3.09	1331.90	44.90	2.19
		SD	3.10	6.52	0.53	348.15	1.06	0.49
		MAD	2.38	4.99	0.39	313.91	0.83	0.43
4.	Tororo	Lower limit	22.51	22.90	0.14	32.60	38.00	0.08
		Mean	29.24	44.91	1.56	682.16	41.27	1.05
		Upper limit	40.30	64.90	5.50	1314.00	43.40	2.29
		SD	3.24	10.28	0.98	343.08	1.06	0.49
		MAD	2.42	8.32	0.81	297.61	0.83	0.42

where MAD implies mean absolute deviation and SD designates standard deviation. The detailed experimental data is found in the supplementary file.

Table 4.9 Validation of simulated with the empirical solar power generation.

S#	Study area	Mercator coordinates	Solar power generation, P_{gen} (MW)	Root mean square error, RMSE

				Simulated		Empirical		
		Lat.	Long.	First order $P_{gen,sim1}$	Second order $P_{gen,sim2}$	$\overline{P}_{gen,emp1}$	$RSME_1$	$RSME_2$
1.	Busitema	0.547	34.023	5.6078	7.1512	7.7818	2.1778	0.6437
2.	Mayuge	0.495	33.408	5.6075	7.1484	7.8014	2.1987	0.6692
3.	Soroti	1.685	33.658	5.6072	7.1462	7.2698	1.6701	0.2008
4.	Tororo	0.639	34.112	5.6078	7.1516	7.2190	1.6288	0.1804

Table 4.10 Validation of solar power design capacity with the empirical solar power generation.

S#	Study area	Mercator coordinates		Solar power generation, P_{gen} (MW)				Root mean square error, RSME		
		Lat.	Long.	Design capacity, dc	Empirical, e			$RSME_1$	$RSME_2$	$RSME_3$
				$P_{gen,dc}$	Implicit	Explicit				
					$\overline{P}_{gen,e1}$	$\overline{P}_{gen,e2}$	$\overline{P}_{gen,e3}$			
1.	Busitema	0.547	34.023	10	7.782	8.367	8.622	2.222	1.645	1.419
2.	Mayuge	0.495	33.408	10	7.801	8.419	9.028	2.199	1.587	1.023
3.	Soroti	1.685	33.658	10	7.270	7.790	8.901	2.735	2.217	1.151
4.	Tororo	0.639	34.112	10	7.232	7.780	8.345	2.772	2.227	1.683

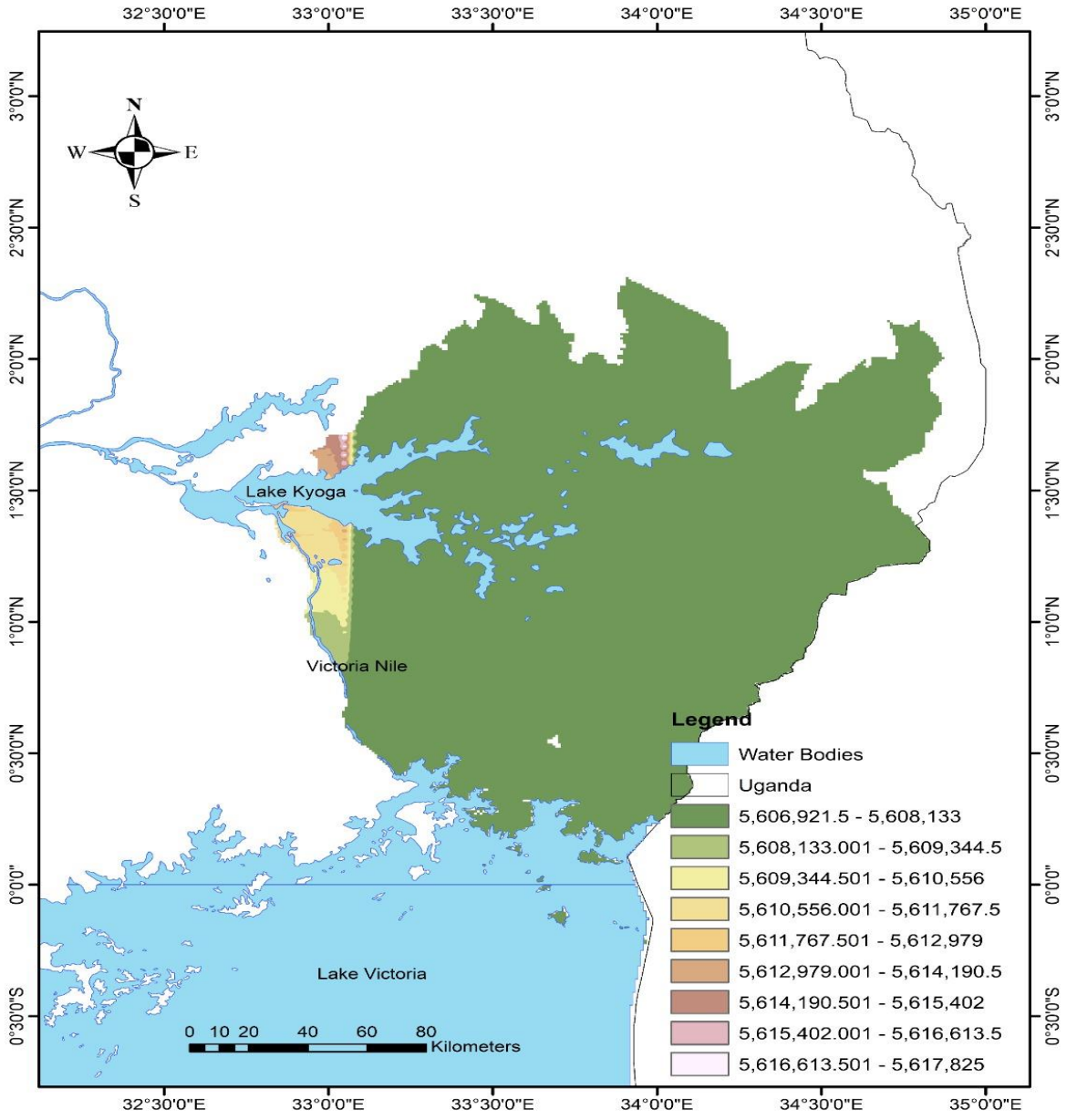

Figure 4.19 Solar power generation (W) based on the first order generation model

Source: Present study (2023)

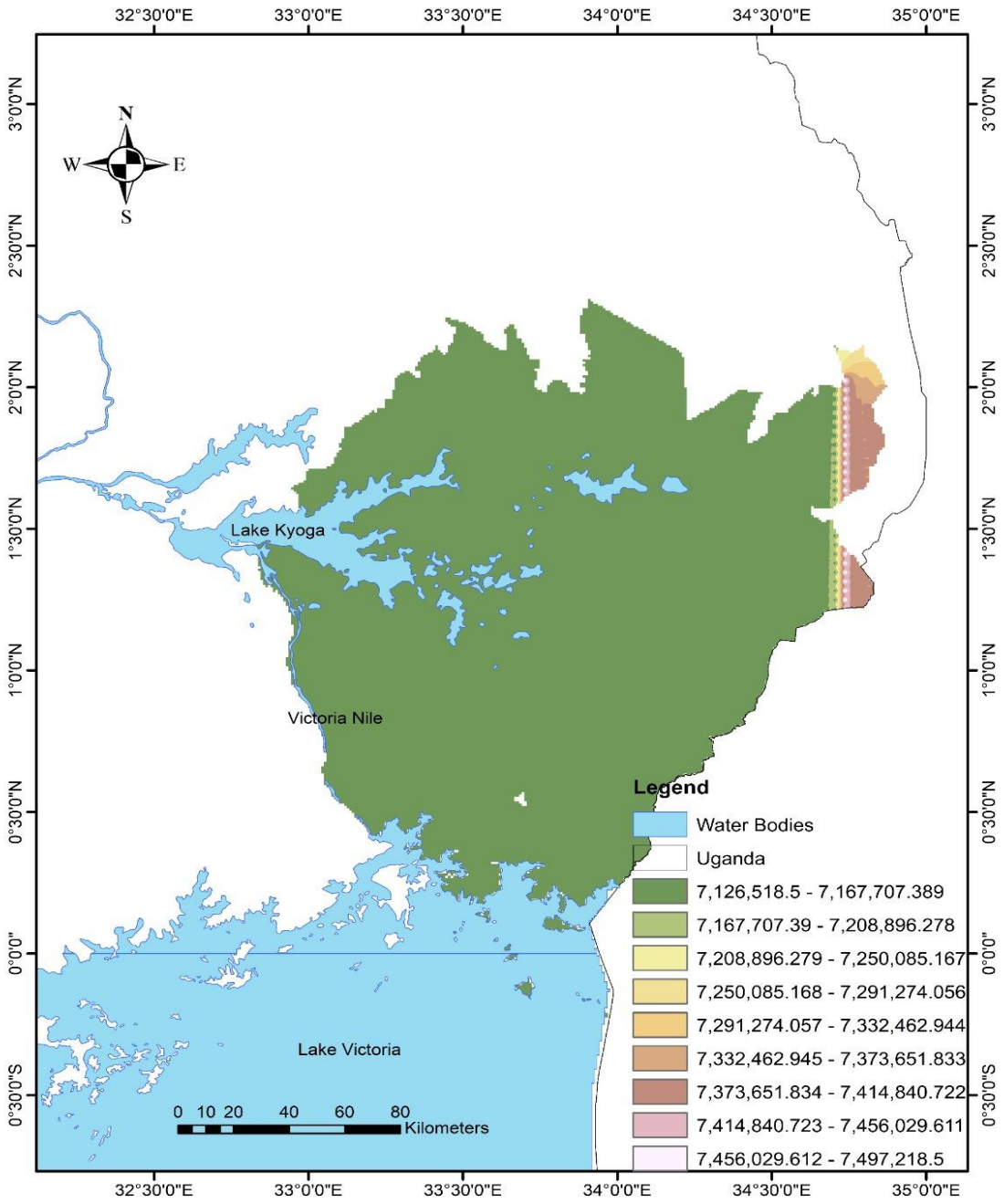

Figure 4.20 Solar power generation (W) based on the second order generation model **Source: Present study (2023)**

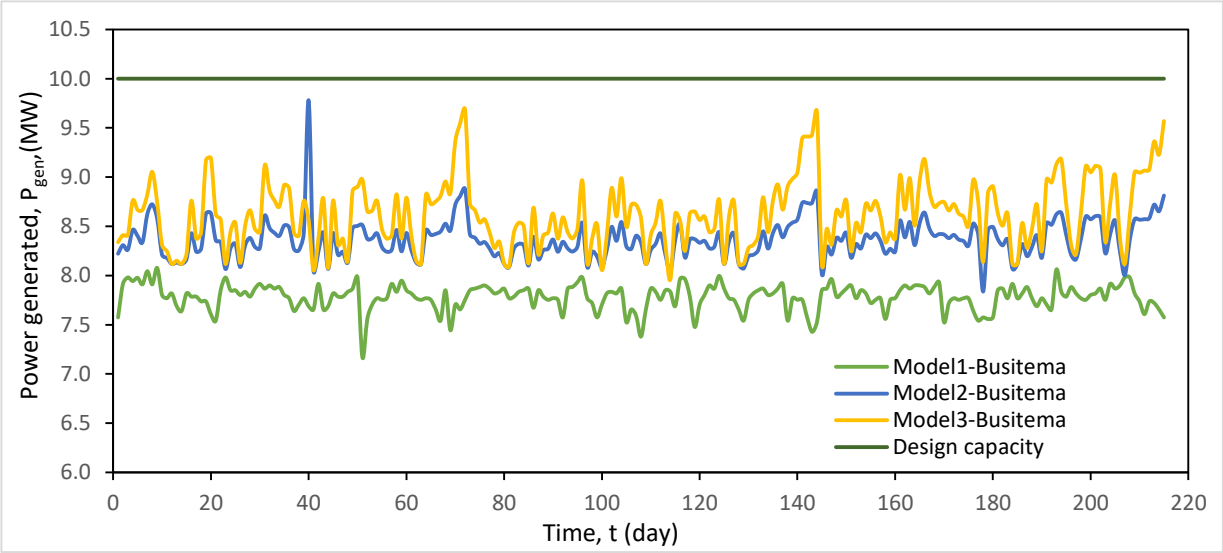

Figure 4.21 Empirical solar power generation at Busitema study area

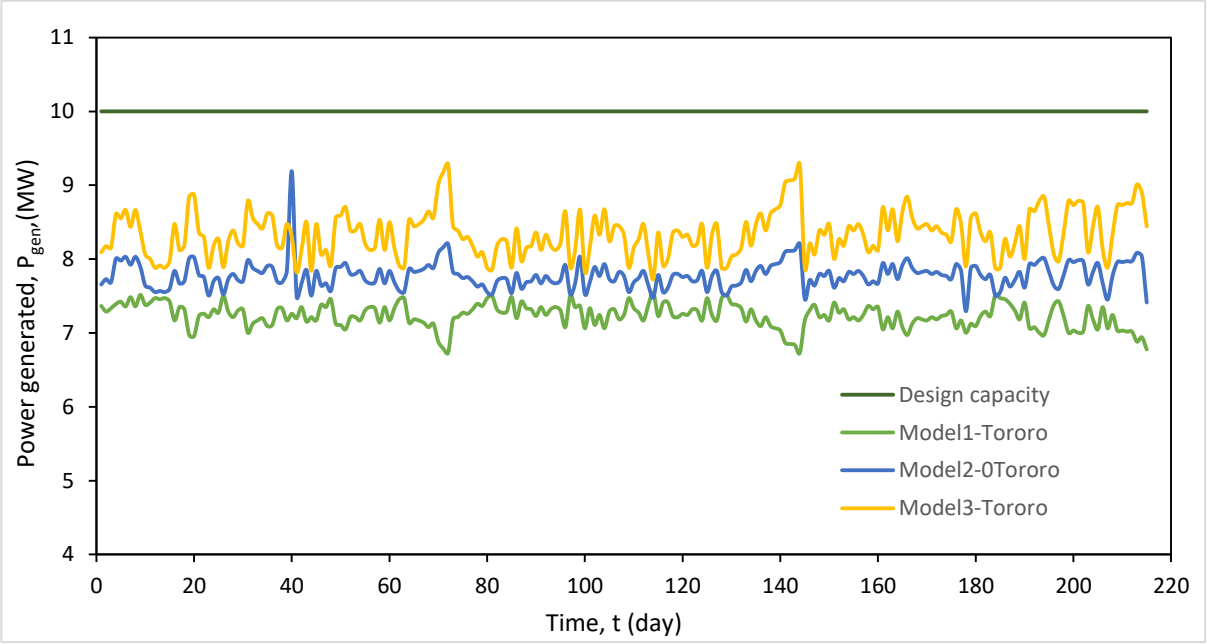

Figure 4.22 Empirical solar power generation at Tororo study area

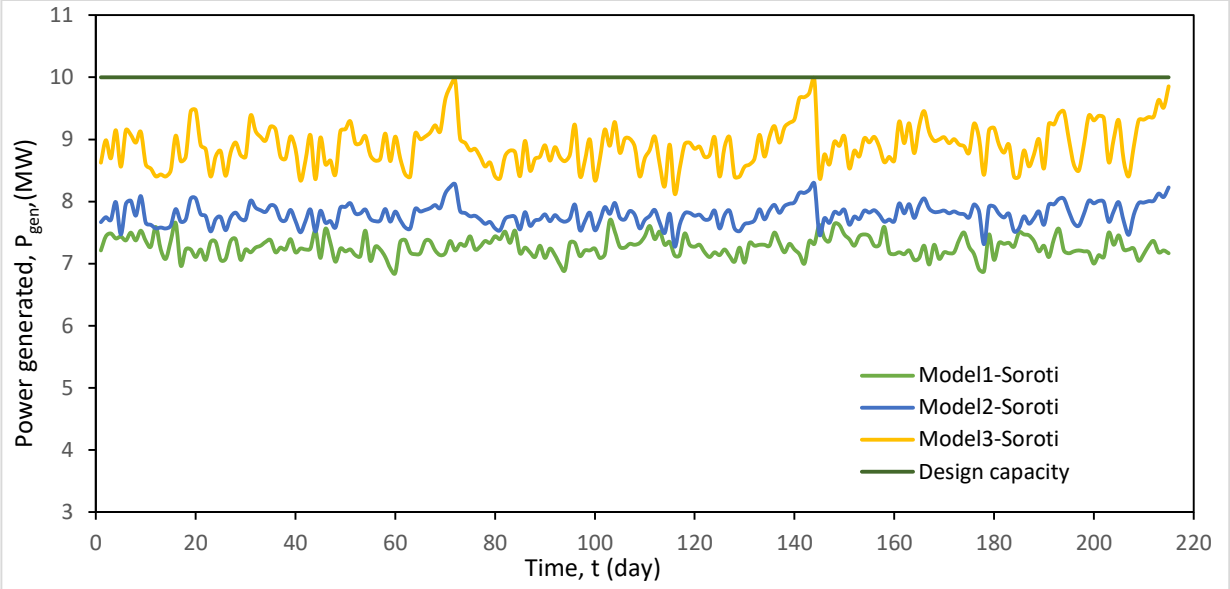

Figure 4.23 Empirical solar power generation at Soroti study area

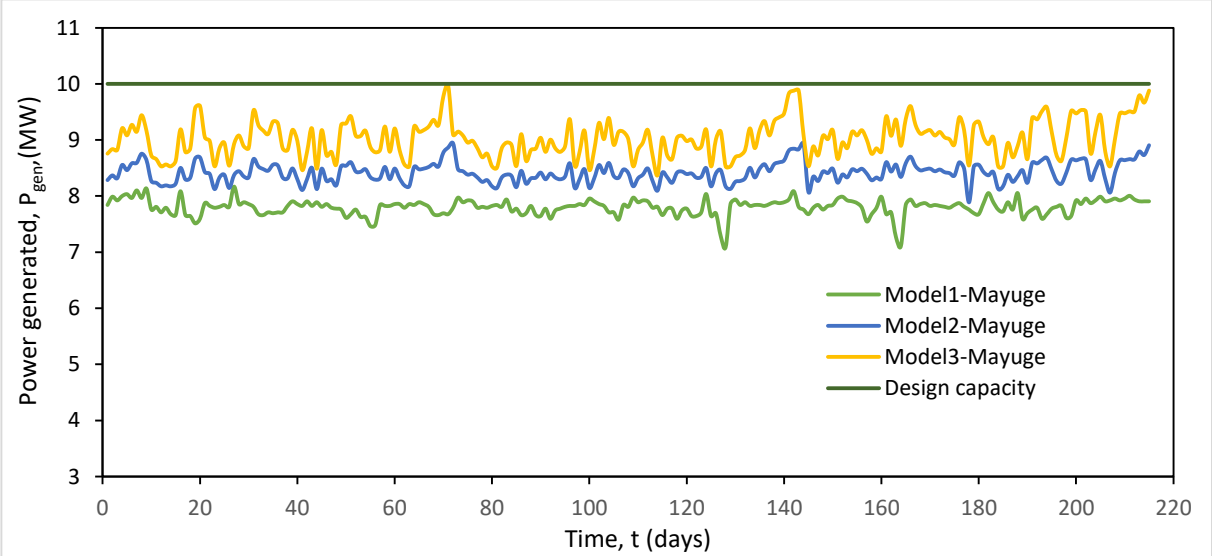

Figure 4.24 Empirical solar power generation at Mayuge study area

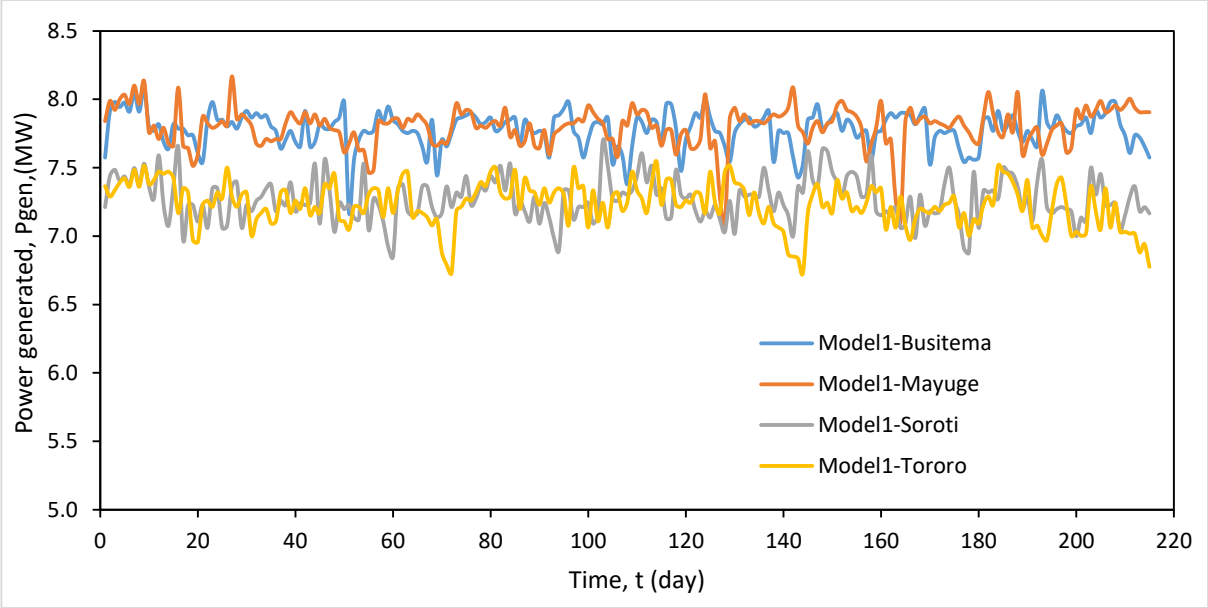

Figure 4.25 Empirical solar power generation based on first model for Eastern region of Uganda

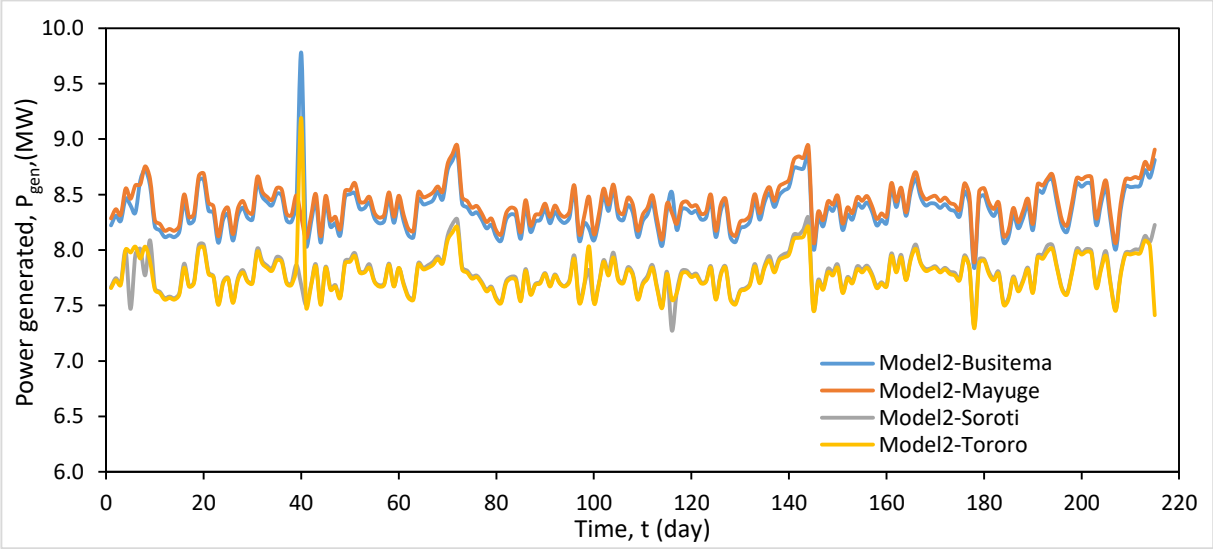

Figure 4.26 Empirical solar power generation based on second model for Eastern region of Uganda

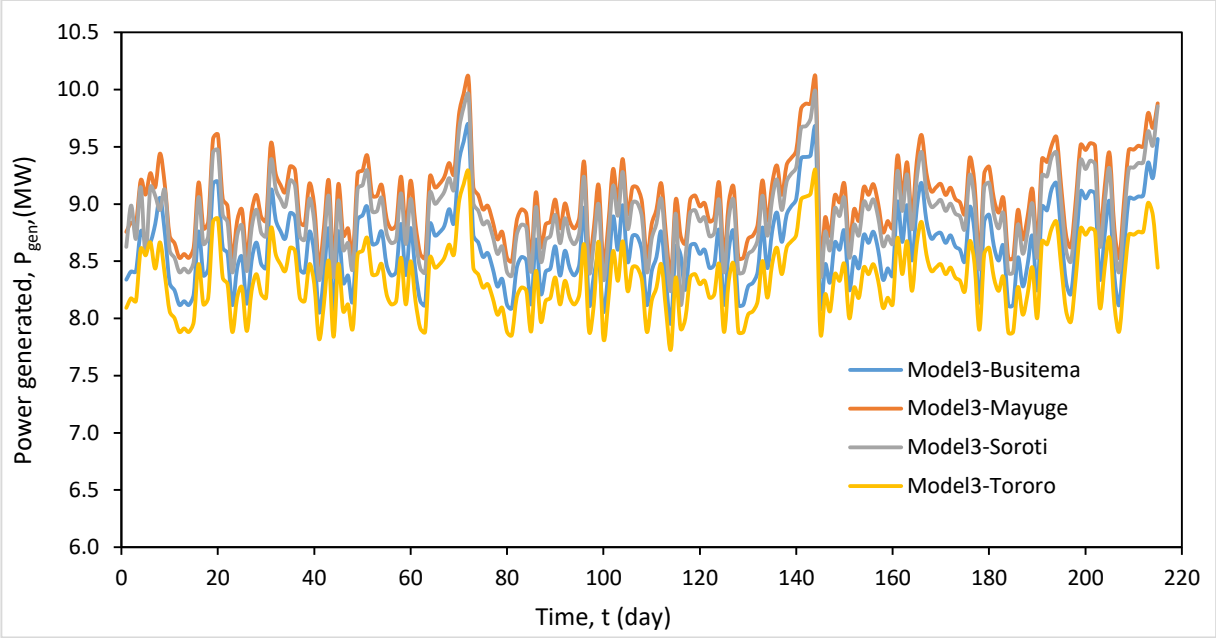

Figure 4.27 Empirical solar power generation based on third model for Eastern region of Uganda

4.2 Discussion of results basing on the specific objectives

4.2.1 Minimization of electric power losses in transmission lines

The discussion presented under this subsection is on the results of modification of the traditional power loss objective function by integrating the third-dimensionally consistent factor of Corona and Ohms losses that validates the optimality of both unmodified and modified models on different power transmission lines in Uganda.

4.2.1.1 Unmodified and modified power transmission models

Table 4.1 presents the Input data for the optimization of power losses on 132 kV (Masaka West - Mbarara North) and 220 kV (Bujagali – Kawanda) transmission lines. These parameters were used to obtain optimum values for both modified and unmodified models as shown in Table 4.2. It was observed that for the unmodified model, there were no optimum variables nor values obtained for both transmission lines because the model could not yield optimal variables. However, the modified model on 132 kV (Masaka West - Mbarara North) transmission line optimum variables and values were obtained UETCL (2023) as a result of power loss penalty function introduced in the traditional power loss model; the optimum transmission current (33.995 A), Phase voltage

(119.0972 V), and air density (1.255 kg/m^3) minimized power loss in the transmission line; and on 220 kV (Bujagali – Kawanda) transmission line optimum variables and values were established, transmission current (132.7905080 A), Phase voltage (132.918 V) and air density (1.469 kg/m^3), which minimize power losses. Table 4.3 presents optimality tests based on the Hessian matrix. It is observed that both 132 kV (Masaka West - Mbarara North) and 220 kV (Bujagali – Kawanda) transmission lines under an unmodified model maximized power losses as the determinant is less than zero (D < 0), -1.573×10^{-19} and $-6.765\text{E}\times10^{-18}$, respectively. It is also observed that 132 kV (Masaka West - Mbarara North) and 220 kV (Bujagali – Kawanda) transmission lines under the modified model supported minimization of power losses as the determinant of Hessian matrix is greater than zero (D > 0), 1.536×10^{-12} and $1.757\text{X}10^{-11}$ respectively.

4.2.1.2 Discussion of power losses in the transmission lines

Figure 4.1 shows the power losses plotted against the phase voltage of the Bujagali – Kawanda transmission line plotted for both modified and unmodified models. The graphs show the voltage range: 66 to 402kV, the losses in unmodified and modified models ranged (0.408-0.406kW/km/phase) and (0.393-0.391 kW/km/phase) respectively. This shows that the modified model minimized power losses due to the implementation of optimum variables and values.

Figure 4.2 presents the input data for power losses plotted against the phase voltage of the Masaka West - Mbarara North transmission line plotted for both modified and unmodified models. The graphs show the voltage range: 66 to 402kV, the losses in the unmodified and modified models ranged (0.455 - 0.452kW/km/phase) and (0.448-0.446 kW/km/phase) respectively. This shows that the modified model minimized power losses due to the implementation of optimum variables, values, and the virtue of the third term (presence of power loss penalty function) incorporated in the modified model.

Observation in Figure 4.3 indicates that both models at low transmission current have no disparity but at high transmission current because ohmic losses is weak, there is a quite appreciable difference because ohmic effect is strong. This implies that the modified model has a high potential to minimize power loss relative to the unmodified model. The graphs show the transmission current ranged from 24 A to 238 A, and the losses in unmodified and modified models ranged (0.284-0.294 kW/km/phase) and (0.283-0.281 kW/km/phase) respectively.

Figure 4.4 presents the input data for power losses plotted against the phase transmission current of the Masaka West - Mbarara North transmission lines plotted for both modified and unmodified models. The graph shows the transmission current range: 13 to 145A, the losses in unmodified and modified models ranged (0.345-0.347 kW/km/phase) and (0.344-0.340 kW/km/phase) respectively. This shows that the modified model minimized power losses when compared with the unmodified model due to presence of power loss penalty function (Bamigbola *et al.*, 2014).

Furthermore, Figure 4.4 presents the power losses plotted against the air density of the Bujagali – Kawanda transmission line plotted for both modified and unmodified models. The graph obtained shows that the results support or identify the modified model as an effective one in minimizing power losses and this means the power losses are attributed to both Corona and Ohms losses are effectively minimized.

In addition, Figure 4. 6 shows an inappreciable discrepancy in the transmission power losses by unmodified and modified models, this means that the atmosphere in the transmission lines is uniform and could not support any meaningful difference in power losses for the unmodified and modified models because air factor contribution to power losses is minimal relative to other transmission variables.

Figures (4.7a and 4.7b) show the three-dimensional graph of power losses, phase voltage, and current for the 220 kV Bujagali-Kawana transmission lines. The power losses for both unmodified and modified are 0.305 and 0.288kV/km/phase respectively as shown in Figures (4.8a and 4.8b). For the 132 kV Masaka West-Mbarara North transmission lines. The power losses for both unmodified and modified are 0.302 and 0.289kV/km/phase respectively as presented in Figures (4.8a and 4.8b) which implies that the modified has a high potential for power loss minimization in both transmission lines engendered by the power loss penalty function or power loss modification term.

4.2.1.3 Optimality test

The Hessian matrix was used to carry out optimality test for both modified and unmodified models. It is observed that both 132 kV (Masaka West - Mbarara North) and 220 kV (Bujagali – Kawanda) transmission lines under an unmodified model maximized power losses as $D < 0$, -1.573×10^{-19} and -6.765×10^{-18} respectively, as it lacks optimum variables and values. It is also observed that for both 132 kV (Masaka West - Mbarara North) and 220 kV (Bujagali – Kawanda) transmission

lines under the modified model minimized power losses as D > 0, 1.536×10^{-12} and $1.757X10^{-11}$ respectively, since it has both optimum variables and values.

4.2.2 Modeling of coupled and uncoupled transmission lines

The discussion of the results in sub section focuses on the simulation and prediction of power potentials and power losses in the transmission line.

4.2.2.1 Simulation of transmission potentials

As mentioned earlier, the transmission potential could be space and time oriented. Implies that transmission potentials (temperature, current and voltage) are dependent on space and time according to Equations (3.28, 3.29, 3.30), respectively.

4.2.2.2 Space potentials

The space transmission potentials (current, voltage, temperature and power) are described in Figures. (4.9, 4.10, 4.11, 4.12), respectively. A positive linear gradient was observed in behavior of current and temperature potentials which supports Joule-Thompson thermodynamic effects, thus, temperature and current have similar behavior due to linear relationship between them (Medved *et al.,* 2022). Increment in temperature and current is supported by the coupled terms in Equations (3.28, 3.30), respectively, which implies that the coupling terms were well posed in the coupled model, hence, these models simulated the field potentials effectively. Furthermore, the positive linear behavior of temperature and current is supported by physical laws of Fourier's and Ohmic laws. Conversely, the space potential (voltage) exhibited reverse trend relative to current and temperature, which supports Ohm's law or inverse proportionality between current and voltage. This is further evidence that the coupled is well developed.

4.2.2.3 Time potentials

The time dependent transmission potentials (current, voltage, temperature and power) are described in Figs. (4.13, 4.14, 4.15, 4.16), respectively. Due to similarity of functions in Figures. 4.13 and 4.16, it can be inferred that current in the transmission line had more contribution in power transmission relative to voltage, which had different behavior or partner relative to power in Figure. 4.14. Thus, deterioration in current (and Ohmic loss) is low compared to deterioration in voltage (and Corona loss) which is pronounced, hence, the difference in behavior of voltage

relative to power. Also the time dependence of temperature in Figure. 4.15 shows that the degree of temperature depends on the magnitude of current in the transmission cable. This portrays that thermal model could be considered or approximated with steady state model. Furthermore, apparent constant temperature implies that the transmission cable is made up of isotropic material (having uniform thermal conductivity), thus, thermal accumulation in the transmission cable was not observed as in current, voltage and power.

4.2.2.4 Estimation of power and power losses in transmission line

Power and power losses are described in Figure 4.17, positive linear gradient of power and power losses were observed, power losses are proportional to power in the transmission line. The apparent losses in the transmission line could be attributed to Ohmic loss due to resistivity of the transmission cable, to Corona loss due to decrease in disruptive voltage resulting from increase in pressure and the drop in temperature of the air, and possible deteriorations or aging of the transmission line. The deteriorations (temperature, current and voltage) emanate from the degradation of the transmission material and other transmission accessories (circuit breakers, magnetic starters, transformers). The power losses estimated in Figure 4.17 ranges from 0.02 to 0.045, which is consistent with that recommended by Electricity Regulation Authority, ERA of Uganda (3.6 %) of total power transmitted.

4.2.2.5 Validation of transmission potentials

The validity of the coupled models developed in this work cannot be attested without statistical error analysis or assessment of deviation between measured (field data) a Bujjagali-Kawanda transmission line and simulated transmission potentials as in Equations (3.46, 3.48, 3.49) for temperature, voltage, power and current respectively. Root mean square error analysis from Bujjagali-Kawanda transmission line reviewed for the aforementioned power transmission variables in Table 4.4 are 0.68, 0.70, and 1.63 respectively. High RMSE of power could be attributed to its high value relative to that of current and voltage. The RMSE and deviations in the transmission variables (Figure 4.18) are minimal, which supports the fact that the coupled model effectively defined the transmission data. Thus, the result signifies that power transmission in Bujjagali-Kawanda transmission line is justified. Therefore, the coupled model developed is valid for prediction and estimation of power and power losses respectively.

4.2.2.6 Application of results

From the ongoing results and discussion, it is justifiable to implement the coupled model developed in this work for the effective operations and monitoring of transmission lines in Uganda and elsewhere. Contrary to the lumped models, which cannot offer information on the transmission losses due to absence of diffusion or space terms, coupled model can excellently define transmission losses.

4.2.3 Development of differential and empirical solar power generation models.

This subsection discussion is composed according to the concepts of modeling of differential and empirical for solar power generation models and its applications.

4.2.3.1 Development differential models for solar power generation

Solar power generation models could be intrinsic or extrinsic models. The intrinsic model considers the generation, mobility (diffusion) and recombination of charge carriers, thus neglecting the influence of external factors (cell/ambient temperatures, wind speed and irradiance). Obviously, the impact of these factors cannot be undermined, so there is a silent need to develop a differential model that develops solar power generation as a substantial derivative of the aforementioned factors. The results in Figure 4.19 and Figure 4.20 present the first and second-order differential models. Validation of these results in Table 4.9 shows that the second order differential model validated experimental data better than the first order differential model as the RMSEs of the second order model for the study areas (Busitema, Mayuge, Soroti and Tororo) are much lower than those of the first order model. The observation could be attributed to the extended multiple spatial terms in both convective and diffusive components of the second differential model. The validation results also portrays that the boundary conditions in Equations (3.67a, 3.67b, 3.67c, 3.67d, 3.67e) and the initial condition in Equation (3.68b) are precise. Consequently, the second order differential model is applicable to the global development and prediction of solar power generation in space and time (Nnamchi *et al.*, 2019).

4.2.3.2 Development of empirical models for solar power generation

Empirical models are vital for ascertaining the reason behind the wide discrepancies between the design and field (operational) solar power plant capacities shown in Table 2.1 for the study area. The empirical model is categorized into two categories: implicit Equation (3.69) and explicit Equations (3.70, 3.71) models. Implicit mode refers to a model with ambient /cell temperature as the only variable; hence, wind speed and irradiance have an indirect impact on solar power generation, whereas the explicit model does not encapsulate wind speed or irradiance, thus having a direct impact on solar power generation. Observing Figures. (4.21, 4.22, 4.23, 4.24), the operational solar power generated for the implicit empirical model is far from reaching the design capacity in Table 2.1, and the operational solar generation data for the explicit (double), minimize the gap between the design and operational solar power capacities and operational solar power generation data for explicit (triple) much closer the gap between the design and operational solar power plant capacities. The phenomena observed in these Figures. (4.21, 4.22, 4.23, 4.24), show that the implicit model is far insufficient for predicting the solar power generated as it does not have a direct impact of both wind speed and solar irradiance in its formulation

(Chung, 2020; Sun, 2020; Sarniak, 2020; Al-Amri & Abdelmagid, 2021; Atia *et al.,* 2023; El Hammoumi *et al.,* 2022;Alhmoud, 2023). Conversely, the explicit (double) in Equation (3.70) has both cell temperature and wind speed directly built into the formulation, thus, it has the ability to bridge the gap between the design and operational capacities relative to the implicit model. Moreover, the explicit (triple) model in Equation (3.71) is built on the three extrinsic factors (ambient/cell temperature, wind speed and irradiance) to further bridge the gap or discrepancy between the design and operational capacities (Nguyen *et al.,* 2021; Kichou *et al.,* 2022; Toreti Scarabelot *et al.,* 2021; Muneeshwaran *et al.,* 2020; Dong *et al.,* 2021; Al-Dahidi, 2020; Ndegwa *et al.,* 2020); However, explicit (triple) draws the operational to design capacity only when the combination of the extrinsic factors is favorable and vice versa. Observing Figures. (4.25, 4.26, 4.27), Mayuge recorded the highest solar power generation based on model 1, model 2 and model 3 compared to other study areas. This result is supported by the RMSE analysis in Table 4.10, which recorded the lowest values compared to other study areas. Future solar plants should be sited at Mayuge as the leading site.

4.2.3.3 Applications of the developed models

An explicit (triple) model should be implemented in the design of solar power plants, as its sensitivity to solar power generation is very high. Both empirical (explicit-triple) and second order differential models are useful for the effective operation of solar power plants. The second differential model could compliment the empirical model in providing detailed and accurate design information in space and time.

CHAPTER FIVE

SUMMARY, CONCLUSIONS AND RECOMMENDATIONS

5.0 Summary

This is the concluding chapter of this study. This chapter sums up the conclusions and recommendations arising from this study, it is based on the objectives and the significant findings of this study. Moreover, the presentation of the recommendations is based on the conclusions of this study.

5.1 Conclusions

The conclusions drawn from this study has been cataloged rendering to the objectives outlined in chapter one as follows.

5.1.1 Minimization of electric power losses in transmission lines

A modified model for power loss minimization in the transmission lines of Bujagali – Kawanda and Masaka West - Mbarara North in Uganda has been developed. The optimum variables and values of transmission current, phase voltage and air density were determined using the gradient optimization technique that is the first derivative of the modified model is feasible with the modified model. An optimality test was also carried out using Hessian matrix both on the unmodified and modified models. The optimal results for both modified and unmodified established that the modified model has a high potential to minimize power losses in the transmission lines. Consequently, this paper recommends that a modified model should be implemented in the transmission line in the design and operation of transmission lines, due to its ability to minimize power losses in the transmission lines. The results of this study are not limited nor peculiar to Uganda Electricity Transmission Lines, they could be implemented by other transmission lines outside Uganda.

5.1.2 Modeling of coupled and uncoupled transmission lines

This study has developed a coupled power transmission model for Bujjagali-Kawanda transmission line in Uganda; the models were developed on local or spot terms, diffusion terms and loss terms for the transmission potentials (current, voltage and temperature) by observing thermal and electrical balances around the transmission line. Secondly, the numerical solutions of

the coupled model were used to simulate the transmission potentials. The simulated results strongly validated with the measured (field) results, as RMSE results are very low (ranged from 0.68 to 1.63). The model developed is quite robust or efficient in describing the transmission line. Also, the power loss estimated (ranged from 0.03 to 0.06 %) from the transmission line is strongly in agreement with that of Electricity Regulatory Authority, Uganda (≤ 3.6 %) (https://www.era.go.ug/index.php/stats/transmission-stats/energy-purchases-sales-and-losses), this signifies that the transmission line losses is within the standard or threshold limit. Thus, the coupled model developed in this work would be useful for the effective operation of transmission lines in space and time. Therefore, it is recommended for other transmission line within and outside Uganda.

5.1.3 Development of differential and empirical solar power generation models.

This study has carried out modeling and simulation of solar power generation with the aim to develop a realistic design and operational models, which minims the gap between their capacities. The modeling encompasses differential modeling and empirical models. The differential model covers first and second order models for simulation of solar power generation, whereas the empirical model comprises explicit and implicit models. The explicit models could be double or triple depending on direct impacts number extrinsic factors. Based on the differential modeling, simulation and validation, the second order differential model (7.1484 MW) showed good agreement with experimental (7.8014 MW) results relative to first order differential model (5.6075 MW) due to the extended space terms in its formulation.

Explicit models bridged the gap between the design and operational solar power generation capacities. However, explicit triple model performed better than explicit double model due to more extrinsic factors directly impacting the solar power generation. It was observed that both implicit (7.801 MW) and explicit (8.419 – 9.028 MW) model worked well for Mayuge compared to other study areas (Busitema, Soroti and Tororo) this results signifies that solar power generation in Mayuge is favored by the extrinsic factors (ambient/cell temperature, wind speed and irradiance). If the extrinsic factors are not favorable, the discrepancy between the design and operational solar power generation remains imminent.

5.2. Recommendations

The current work provides the following recommendations in accordance with the results listed in sub-section 5.1 after taking care of the all requirements listed in chapter one of the study using the right methods and tools (as specified in chapter three).

5.2.1 Minimization of electric power losses in transmission lines

The recommendations presented below is in accordance with objective one.

1. Implementation of Modified Model: this study strongly recommends the use of the modified model in the design and operation of transmission lines due to its effectiveness in minimizing power losses. This recommendation suggests that using this model could enhance the efficiency of the transmission lines mentioned in Uganda.
2. Global applicability: this study accentuates that the findings and benefits of the modified model are not limited to the specific transmission lines in Uganda. The study suggests that these results could potentially be applied to other transmission lines globally, indicating the broader relevance and transferability of the proposed model to different contexts.

5.2.2 Modeling of coupled and uncoupled transmission lines

The recommendations in this section therefore support the second objectives of the research.

1. Effective Operation of Transmission Lines: The coupled model demonstrated its capability to improve the effectiveness of transmission line operations by considering both spatial and temporal factors. Its implementation can aid in better management, monitoring, and control of transmission lines, leading to increased reliability and reduced downtime.
2. Applicability beyond Uganda: While initially developed and validated within the context of Ugandan transmission lines, the recommended model's effectiveness extends beyond national borders. Its adaptability and relevance to different geographical locations and diverse transmission line configurations make it a valuable asset for optimizing transmission networks globally.
3. Enhanced Efficiency and Reliability: By utilizing this coupled model, transmission line operators and engineers can expect enhancements in efficiency and reliability. The model's ability to account for spatial and temporal dynamics allows for more accurate predictions and proactive measures, ultimately leading to improved system performance.

4. Cross-Industry Adoption: The recommendation extends to both existing and upcoming transmission line projects. Incorporating this coupled model into the planning, design, and operational phases of transmission lines can greatly benefit the energy sector by optimizing resource utilization and minimizing disruptions.

5.2.3 Development of differential and empirical solar power generation models.

Additionally, this section's recommendations align with the third objective of the study.

1. Adoption of second order differential model: This model offers a more refined and comprehensive approach to predicting solar power generation. By considering not just first-order differentials but second-order differentials as well, it takes into account more nuanced variations in environmental parameters, leading to more accurate predictions of solar power output. Its adoption is encouraged due to its ability to provide more detailed and precise estimations.
2. Utilization of explicit triple model: The explicit triple model, incorporating three key factors or variables relevant to solar power generation, presents a comprehensive framework. By explicitly considering and integrating these factors into the model, it provides a more holistic understanding of the system, thus contributing to more accurate predictions of solar power output. Its inclusion is recommended for its ability to encompass multiple relevant aspects affecting solar energy generation.
3. Implementation in solar power plant design: These recommended models should be integrated into the design phase of solar power plants. By incorporating these predictive models into the planning and development of solar energy systems, engineers and designers can optimize the plant's layout, component selection, and overall configuration to maximize performance under various ambient conditions. This integration ensures the design of solar power plants that can adapt and perform efficiently across diverse environmental scenarios.
4. Focus on high performance: The emphasis is placed on utilizing these models specifically for designing high-performance solar power plants. By leveraging the predictive capabilities of these models, engineers can strive for superior efficiency and output from solar installations, leading to more reliable and productive renewable energy sources

5.2 Contributions to Knowledge

1. This study introduces a gradient optimization technique that enhances power transmission line design and operation, outperforming traditional artificial intelligence methods, providing valuable insights.
2. This study developed a distributed model of thermal and power equations for simulating transmission losses, demonstrating accuracy using a Finite Difference Method and validating its effectiveness using field data.
3. The study addresses a significant 35% underperformance in solar power generation in eastern Uganda by developing empirical explicit and second-order differential models, incorporating extrinsic factors like wind speed and irradiance, ultimately validating their efficacy in predicting solar power generation and narrowing the gap between designed and operational capacities.

5.5 Prospects for Future Research

The results of this study could be useful for modeling the parameters of power transmission lines, differential, and experimental or empirical solar power generation. to boost the nation's solar energy production and lower power transmission line losses. Nonetheless, the locations listed below have been determined to require additional investigations.

1. This study examined the performance of the updated power loss model on Ugandan electrical transmission lines operating at 132 kV and 220 kV. Future research should take this into consideration and be extended to higher voltage levels more than 132 and 220kV. Given the particular difficulties and traits of ultra-high voltage transmission networks, research could examine its suitability and effectiveness in reducing power losses in these systems.

2. Further studies in modeling power transmission lines could investigate into optimizing additional variables beyond current, voltage, and air density, such as exploring the impact of resistivity of the transmission cable, radiation, transmission frequency, radius of the transmission lines,

3. Cost-Benefit Evaluation in Various Situations: To ascertain the economic viability and possible savings associated with applying the updated model in various power grid infrastructures, conduct thorough cost-benefit studies in various areas or nations.

4. Environmental and Economic Impact Assessment: Conduct an in-depth analysis of the environmental and economic impacts of reducing transmission losses using the developed model. This could involve cost-benefit analyses and environmental assessments to guide decision-making and policy formulation.

5. Impact of Faults and Contingencies: Investigate the model's response to faults or contingencies in the transmission line network. Developing scenarios and simulations to understand how the coupled model behaves under fault conditions would be beneficial for assessing reliability and proposing mitigation strategies.

6. Analysis of Long-Term Performance and Degradation: Using the created models, examine the performance and degradation of solar panels during an approximate ten-year test period. Planning maintenance and making investment decisions would be aided by predictive models that calculate degradation rates and efficiency losses during the lifecycle of solar installations.

7. Hybrid Renewable Energy Systems: Look into combining solar energy with hydroelectric or wind power, among other renewable energy sources. It may be possible to improve the integration of renewable energy sources for increased efficiency and dependability by modeling hybrid systems.

References

Aarakit, S. M., Ssennono, V. F., & Adaramola, M. S. (2021). Estimating market potential for solar photovoltaic systems in Uganda. Frontiers in Energy Research, 9, 602468.

Abadi, A. K. A., Mehrabi-Kooshki, M., & Jamali, S. (2020). A Differential Protection Scheme based on Pi-Model for Bipolar HVDC Transmission Lines. In 2020 15th International Conference on Protection and Automation of Power Systems (IPAPS) (pp. 140-148). IEEE.

Agyekum, E. B., PraveenKumar, S., Alwan, N. T., Velkin, V. I., Shcheklein, S. E., & Yaqoob, S. J. (2021). Experimental investigation of the effect of a combination of active and passive cooling mechanism on the thermal characteristics and efficiency of solar PV module. Inventions, 6(4), 63.

Akhsassi, M., El Fathi, A., Erraissi, N., Aarich, N., Bennouna, A., Raoufi, M., & Outzourhit, A. (2016). Confrontation à l'expérience de divers modèles du comportement thermique de modules solaires photovoltaïques. 4ème Congr. l'Association Marocaine Therm, 1-7.

Al-Amri, F. G., & Abdelmagid, T. I. M. (2021). Analytical model for the prediction of solar cell temperature for a high-concentration photovoltaic system. Case Studies in Thermal Engineering, 25, 100890.

Al-Bashir, A. (2020). Analysis of effects of solar irradiance, cell temperature and wind speed on photovoltaic systems performance. International Journal of Energy Economics and Policy.

Al-Dahidi, S., Al-Nazer, S., Ayadi, O., Shawish, S., & Omran, N. (2020). Analysis of the effects of cell temperature on the predictability of the solar photovoltaic power production. International Journal of Energy Economics and Policy, 10(5), 208.

Alhmoud, L. (2023). Why Does the PV Solar Power Plant Operate Ineffectively?. Energies, 16(10), 4074.

Alibakhshikenari, M., Virdee, B. S., Azpilicueta, L., Naser-Moghadasi, M., Akinsolu, M. O., See, C. H., & Limiti, E. (2020). A comprehensive survey of "metamaterial transmission-line based antennas: Design, challenges, and applications". Ieee Access, 8, 144778-144808.

Anumaka, M. C. (2012). Analysis of technical losses in electrical power system (Nigerian 330kV network as a case study). Int. J. Res. Rev. Appl. Sci, 12(2), 320-327.

Araneo, R., Grasselli, U., & Celozzi, S. (2014). Assessment of a practical model to estimate the cell temperature of a photovoltaic module. International Journal of Energy and Environmental Engineering, 5, 1-16.

Asadi, F., & Eguchi, K. (2020). Fundamental concepts of power electronic circuits. In Simulation of Power Electronics Converters Using PLECS (pp. 421-526). Academic.

Atia, D. M., Hassan, A. A., El-Madany, H. T., Eliwa, A. Y., & Zahran, M. B. (2023). Degradation and energy performance evaluation of mono-crystalline photovoltaic modules in Egypt. Scientific Reports, 13(1), 13066.

Ausloos, M. (2001). Thermal conductivity. Encyclopedia of Materials: Science and Technology, 9151-9155.

Ayaz, R., Nakir, I., & Tanrioven, M. (2014). An improved Matlab-Simulink model of PV module considering ambient conditions. International Journal of Photoenergy, 2014.

Baharozu, E., Soykan, G., Altay, O., & Kalenderli, O. (2015, November). An improved particle swarm optimization method to optimal reactive power flow problems. In *2015 9th International Conference on Electrical and Electronics Engineering (ELECO)* (pp. 991-995). IEEE.

Bamigbola, O. M., Ali, M. M., & Awodele, K. O. (2014). Predictive models of current, voltage, and power losses on electric transmission lines. Journal of Applied Mathematics, 2014.

Bamigbola, O. M., Ali, M. M., & Oke, M. O. (2014). Mathematical modeling of electric power flow and the minimization of power losses on transmission lines. Applied Mathematics and Computation, 241, 214-221.

Barrera, J. M., Reina, A., Maté, A., & Trujillo, J. C. (2020). Solar energy prediction model based on artificial neural networks and open data. Sustainability, 12(17), 6915.

Barykina, E., & Hammer, A. (2017). Modeling of photovoltaic module temperature using Faiman model: Sensitivity analysis for different climates. Solar Energy, 146, 401-416.

Belhocine, M., & Marinescu, B. (2017). A systemic viewpoint on the approximation of a power transmission line model. IFAC-PapersOnLine, 50(1), 14818-14823.

Belyaev, V. A., & Shapeev, V. P. (2018, November). Solving the biharmonic equation in irregular domains by the least squares collocation method. In AIP conference proceedings (Vol. 2027, No. 1, p. 030094). AIP Publishing LLC.

Besedin, I., & Menushenkov, A. P. (2018). Quality factor of a transmission line coupled coplanar waveguide resonator. EPJ Quantum Technology, 5(1), 1-16.

Bin Hussien, I. Z. F., Rahim, A. A., & Abdullah, N. (2011). Electric power transmission. In Alternative Energy in Power Electronics (pp. 317-347). Butterworth-Heinemann.

Bisiriyu, A. O., Ajetunmobi, E. O., Omotayo, M. E., & Adeshola, M. (2017). Analysis of Corona Loss on the Nigerian 28-Bus, 330 kV Transmission Grid. International Journal of Science and Research (IJSR), 6, 2009-2011.

Brito Filho, J. P. (2017). Heat transfer in bare and insulated electrical wires with linear temperature-dependent resistivity. Applied Thermal Engineering, 112, 881-887.

Brito, E. M., Cupertino, A. F., Reigosa, P. D., Yang, Y., Mendes, V. F., & Pereira, H. A. (2018). Impact of meteorological variations on the lifetime of grid-connected PV inverters. Microelectronics Reliability, 88, 1019-1024.

Brusso, B. C. (2019). A brief history of the energy conversion of light [history]. IEEE Industry Applications Magazine, 25(4), 8-13.

Caballero, P. T., Costa, E. C. M., & Kurokawa, S. (2015). Frequency-dependent multiconductor line model based on the Bergeron method. Electric Power Systems Research, 127, 314-322.

Cheldavi, A., & Ansari, D. (2004). Spice Compatible Model for Multiple Coupled Nonuniform Transmission Lines: Application in Transient Analysis of VLSI Circuits.

Chu, X. (2019). Transient numerical calculation and differential protection algorithm for HVDC transmission lines based on a frequency-dependent parameter model. International Journal of Electrical Power & Energy Systems, 108, 107-116.

Chung, M. H. (2020). Estimating solar insolation and power generation of photovoltaic systems using previous day weather data. Advances in Civil Engineering, 2020, 1-13.

Colqui, J. S., de Araújo, A. R., Kurokawa, S., & Filho, J. P. (2021). Optimization of lumped parameter models to mitigate numerical oscillations in the transient responses of short transmission lines. Energies, 14(20), 6534.

Corkish, R., Green, M. A., Watt, M. E., & Wenham, S. R. (2013). Applied photovoltaics. Routledge.

Corkish, R., Green, M. A., Watt, M. E., & Wenham, S. R. (2013). Applied photovoltaics. Routledge.

Costa De Miranda, Antonio Emilio, Angueth De Araujo, Rodney Rezende Saldanha, Jose Pissolato Filho, G. (1999). Finite element method for transmission line corona effect simulation using the EMTP. Electric Machines &Power Systems, 27(7), 781-794.

Czarnecki, L. S. (2013). Meta-theory of electric powers and present state of power theory of circuits with periodic voltages and currents. Przegląd Elektrotechniczny, 89(6), 26-31.

Da Costa, E. C. M., Kurokawa, S., Gomes Pinto, A. J., Kordi, B., & Pissolato, J. (2013). Simplified computational routine to correct the modal decoupling in transmission lines and power systems modelling. IET Science, Measurement & Technology, 7(1), 7-15.

da Silva, R. C., & Kurokawa, S. (2013). Model of three-phase transmission line with the theory of modal decomposition implied. Energy and Power Engineering, 5(04), 1139.

Daafouz, J., Tucsnak, M., & Valein, J. (2014). Nonlinear control of a coupled PDE/ODE system modeling a switched power converter with a transmission line. Systems & Control Letters, 70, 92-99.

Dambhare, S., Soman, S. A., & Chandorkar, M. C. (2009). Adaptive current differential protection schemes for transmission-line protection. IEEE Transactions on Power Delivery, 24(4), 1832-1841.

Diaz, A., Vorobiev, D., Indahl, B., Chafetz, D., Snyder, W., Williams, J., ... & Fleming, B. (2023, October). Fabrication and testing of high fill-factor solar panels for SPRITE CubeSat. In

UV, X-Ray, and Gamma-Ray Space Instrumentation for Astronomy XXIII (Vol. 12678, pp. 443-453). SPIE.

DoE, U. S. (2017). Energy Literacy: Essential Principles and Fundamental Concepts for Energy Education. US Department of Energy.

Dong, X. J., Shen, J. N., He, G. X., Ma, Z. F., & He, Y. J. (2021). A general radial basis function neural network assisted hybrid modeling method for photovoltaic cell operating temperature prediction. Energy, 234, 121212.

Doukas, H., Karakosta, C., Flamos, A., & Psarras, J. (2011). Electric power transmission: An overview of associated burdens. International journal of energy research, 35(11), 979-988.

du Can, S. D. L. R., Pudleiner, D., & Pielli, K. (2018). Energy efficiency as a means to expand energy access: A Uganda roadmap. Energy Policy, 120, 354-364.

El Hammoumi, A., Chtita, S., Motahhir, S., & El Ghzizal, A. (2022). Solar PV energy: From material to use, and the most commonly used techniques to maximize the power output of PV systems: A focus on solar trackers and floating solar panels. Energy Reports, 8, 11992-12010.

ElSheikh, A., Barakat, N., Abu-Nabah, B. A., & Hamdan, M. O. (2022). Thermal diffusivity estimation in metallic alloys using a one-dimensional flux-based thermography. Infrared Physics & Technology, 127, 104411.

Evans, N., & Selgelid, M. J. (2015). Censorship in Research and Scholarship. In International Encyclopedia of the Social & Behavioural Sciences (pp. 279-283). Elsevier.

Fashina, A., Mundu, M., Akiyode, O., Abdullah, L., Sanni, D., & Ounyesiga, L. (2018). The drivers and barriers of renewable energy applications and development in Uganda: a review. Clean Technologies, 1(1), 9-39.

Garcia-Sanchez, J. L., Moreno, P., Gutierrez-Robles, J. A., Loo-Yau, J. R., Sotelo, J., Bañuelos, E. S., & Galván, V. A. (2016). Aerial line model for power system electromagnetic transients simulation. IET Generation, Transmission & Distribution, 10(7), 1597-1604.

Ghazizadeh-Ahsaee, M., & Sadeh, J. (2012). Accurate fault location algorithm for transmission lines in the presence of shunt-connected flexible AC transmission system devices. IET generation, transmission & distribution, 6(3), 247-255.

Goldshmid, R. H., Winiarska, E., & Liberzon, D. (2022). Next generation combined sonic-hotfilm anemometer: wind alignment and automated calibration procedure using deep learning. Experiments in Fluids, 63(1), 30.

González-García, A., Ciller, P., Lee, S., Palacios, R., de Cuadra García, F., & Pérez-Arriaga, J. I. (2022). A Rising Role for Decentralized Solar Minigrids in Integrated Rural Electrification Planning? Large-Scale, Least-Cost, and Customer-Wise Design of Grid and Off-Grid Supply Systems in Uganda. Energies, 15(13), 4517.

Heilmann, A., Odake Junior, E. M., Dartora, C. A., & Adams, A. M. (2022). Local Atmospheric Electric Circuit Model Using Electrostatic Pickups on a 375kV Transmission Line. Brazilian Archives of Biology and Technology, 65, e22210630.

Hu, J., Xiong, X., & Wang, J. (2018). Current tolerance capability calculation model of transmission lines and its application in overload protection. Electric Power Components and Systems, 46(14-15), 1509-1521.

Hussein, I. A., & Mahmoud, M. (Eds.). (2023). Fluid–Solid Interactions in Upstream Oil and Gas Applications. Elsevier.

Ignjatovic, M., & Cvetic, J. (2021). Drift-diffusion model of corona discharge in coaxial geometry due to negative lightning impulse voltage. International Journal of Electrical Power & Energy Systems, 129, 106815.

Ikwaba Paul, D., & Uhomoibhi, J. (2013). Solar electricity generation: issues of development and impact on ICT implementation in Africa. Campus-Wide Information Systems, 31(1), 46-62.

Iranmehr, H., Aazami, R., Tavoosi, J., Shirkhani, M., Azizi, A. R., Mohammadzadeh, A., ... & Guo, W. (2022). Modeling the price of emergency power transmission lines in the reserve market due to the influence of renewable energies. Frontiers in Energy Research, 9, 792418.

Jenkins, N., & Thornycroft, J. (2018). Grid connection of photovoltaic systems: technical and regulatory issues. In McEvoy's Handbook of Photovoltaics (pp. 847-876). Academic Press.

Kaldellis, J. K., Kapsali, M., & Kavadias, K. A. (2014). Temperature and wind speed impact on the efficiency of PV installations. Experience obtained from outdoor measurements in Greece. Renewable energy, 66, 612-624.

Kamkird, P., Ketjoy, N., Rakwichian, W., & Sukchai, S. (2012). Investigation on temperature coefficients of three types photovoltaic module technologies under Thailand operating condition. Procedia Engineering, 32, 376-383.

Kankam, P. K. (2019). The use of paradigms in information research. Library & Information Science Research, 41(2), 85-92.

Kavuma, C., Sandoval, D., & de Dieu, H. K. J. (2022). Analysis of solar photo-voltaic for grid integration viability in Uganda. Energy Science & Engineering, 10(3), 694-706.

Kengne, E., Liu, W. M., English, L. Q., & Malomed, B. A. (2022). Ginzburg–Landau models of nonlinear electric transmission networks. Physics Reports, 982, 1-124.

Kersting, W. H. (2018). Distribution system modeling and analysis. In Electric power generation, transmission, and distribution (pp. 26-1). CRC press.

Kichou, S., Skandalos, N., & Wolf, P. (2022). Floating photovoltaics performance simulation approach. Heliyon, 8(12).

Kitunzi Mutunzi, A., & Vyakarnam, S. (2019). Cooperatives' Potential to Diffuse Appropriate Solar Technologies in Uganda. Energy in Africa: Policy, Management and Sustainability, 99-116.

Koehl, M., Heck, M., Wiesmeier, S., & Wirth, J. (2011). Modeling of the nominal operating cell temperature based on outdoor weathering. Solar Energy Materials and Solar Cells, 95(7), 1638-1646.

Kosky, P. Balmer, R. Keat, W. Wise, G. (2021) Chapter 12 - Manufacturing Engineering, Explor. Eng. Fifth Ed. 259–291. https://sciencedirect.com/science/article/pii/B9780128150733000120.

Kuchanskyy, V., & Zaitsev, I. O. (2020, May). Corona discharge power losses measurement systems in extra high voltage transmissions lines. In 2020 IEEE 7th International Conference on Energy Smart Systems (ESS) (pp. 48-53). IEEE.

Kumar, A. S. H. O. K. (2013). Corona Effect on Transmission Lines. International Journal of Electrical and Electronics Engineering Research (IJEEER), 3(5), 133-136.

Kurokawa, S., Yamanaka, F. N., Prado, A. J., & Pissolato, J. (2009). Inclusion of the frequency effect in the lumped parameters transmission line model: State space formulation. Electric power systems research, 79(7), 1155-1163.

Lalbakhsh, A., Simorangkir, R. B., Bayat-Makou, N., Kishk, A. A., & Esselle, K. P. (2022). Advancements and artificial intelligence approaches in antennas for environmental sensing. Artificial Intelligence and Data Science in Environmental Sensing, 19-38.

Lee, K., Miguel, E., & Wolfram, C. (2020). Experimental evidence on the economics of rural electrification. Journal of Political Economy, 128(4), 1523-1565.

Leonidas, E., Ayvar-Soberanis, S., Laalej, H., Fitzpatrick, S., & Willmott, J. R. (2022). A comparative review of thermocouple and infrared radiation temperature measurement methods during the machining of metals. Sensors, 22(13), 4693.

Lian, Y., Chen, X., Zhang, T., Liu, C., Lin, L., Lin, F., ... & Zhou, W. (2023). Temperature measurement performance of thin-film thermocouple cutting tool in turning titanium alloy. Ceramics International, 49(2), 2250-2261.

Liu, H., Li, B., Wen, W., Green, T. C., Zhang, J., Zhang, N., & Chen, L. (2021). Ultra-fast current differential protection with high-sensitivity for HVDC transmission lines. International Journal of Electrical Power & Energy Systems, 126, 106580.

Living, O., Nnamchi, S. N., Mundu, M. M., Ukagwu, K. J., & Abdulkarim, A. (2024). Coupled modelling and simulation of power transmission lines: A systematic analysis of line losses. Electric Power Systems Research, 226, 109954.

Maffucci, A., & Miano, G. (2013). A general transmission line model for conventional metallic nanowires and innovative carbon nano-interconnects. In 2013 17th IEEE Workshop on Signal and Power Integrity (pp. 1-4). IEEE.

Mahdy, A. M. S., Lotfy, K., Ahmed, M. H., El-Bary, A., & Ismail, E. A. (2020). Electromagnetic Hall current effect and fractional heat order for microtemperature photo-excited semiconductor medium with laser pulses. *Results in Physics*, *17*, 103161.

Mamis, M. S., & Koksal, M. (2000). Remark on the lumped parameter modeling of transmission lines. Electric machines and power systems, 28(6), 565-576.

Mattei, M., Notton, G., Cristofari, C., Muselli, M., & Poggi, P. (2006). Calculation of the polycrystalline PV module temperature using a simple method of energy balance. Renewable energy, 31(4), 553-567.

Medveď, D., Beňa, Ľ., Kolcun, M., & Pavlík, M. (2022). Influence of Impurities in Electrical Contacts on Increasing the Efficiency of Energy Transmission. Energies, 15(7), 2339.

Mestriner, D., & Brignone, M. (2020). Corona effect influence on the lightning performance of overhead distribution lines. Applied Sciences, 10(14), 4902.

Moran, M. J., Shapiro, H. N., Munson, B. R., & DeWitt, D. P. (2002). Introduction to thermal systems engineering: thermodynamics, fluid mechanics, and heat transfer. John Wiley & Sons.

Mugisa, S. (2013). Transmission grid expansion constraints in Uganda: going beyond the standard solution (Master's thesis, University of Cape Town).

Mukisa, P. J., Ketuama, C. T., & Roubík, H. (2022). Biogas in Uganda and the Sustainable Development Goals: A Comparative Cross-Sectional Fuel Analysis of Biogas and Firewood. Agriculture, 12(9), 1482.

Muneeshwaran, M., Sajjad, U., Ahmed, T., Amer, M., Ali, H. M., & Wang, C. C. (2020). Performance improvement of photovoltaic modules via temperature homogeneity improvement. Energy, 203, 117816.

Naima, K., Fadela, B., Imene, C., & Abdelkader, C. (2015). Use of genitic algorithm and particle swarm optimisation methods for the optimal control of the reactive power in Western Algerian power system. Energy Procedia, 74, 265-272.

Ndegwa, R., Ayieta, E., Simiyu, J., & Odero, N. (2020). A simplified simulation procedure and analysis of a photovoltaic solar system using a single diode model.

Nguyen, D. P. N., Neyts, K., & Lauwaert, J. (2021). Proposed Models to Improve Predicting the Operating Temperature of Different Photovoltaic Module Technologies under Various Climatic Conditions. Applied Sciences, 11(15), 7064.

Ni, H., Zhang, W., & Dong, Z. (2023, June). The Validation of The Weak Coupling Assumption in Transmission Line Equations of Coaxial Cables. In Journal of Physics: Conference Series (Vol. 2530, No. 1, p. 012027). IOP Publishing.

Nnamchi, S. N., & Mundu, M. M. (2022). Development of solar isodose lines: Mercatorian and spatial guides for mapping solar installation areas. Heliyon, 8(10).

Nnamchi, S. N., Jagun, Z. O., Nnamchi, O. A., Mundu, M. M., & Onochie, U. (2023). Modelling and simulation of wind flow: A gradient method of identifying windy region. Wind Engineering, 0309524X231178793.

Nnamchi, S. N., Mundu, M. M., Nnamchi, O. A., Onochie, U., & Jagun, Z. O. (2021). Differential modelling and simulation of solar power potential: a helio-application of biharmonic model. Modeling Earth Systems and Environment, 0123456789. https://doi.org/10.1007/s40808-021-01232-2

Nnamchi, S. N., Nnamchi, O. A., Martins Onyekwelu Onuorah, E. O., & Sangotayo, V. G. (2019). Modelling and simulation of heat transfer through the finned hollow cylindrical surfaces of an insulation testing rig. World Journal of Modelling and Simulation, 15(3), 243-261.

Ogar, V. N., Bendor, S. A., & James, A. E. (2017). Analysis of corona effect on transmission line. Am. J. Eng. Res, 6, 75-87.

Okba, M. H., Saied, M. H., Mostafa, M. Z., & Abdel-Moneim, T. M. (2012). High voltage direct current transmission-A review, part I. 2012 IEEE energytech, 1-7.

Oku, T. (2016). Solar cells and energy materials. Walter de Gruyter GmbH & Co KG.

Olukan, T. A., & Emziane, M. (2014). A comparative analysis of PV module temperature models. Energy Procedia, 62, 694-703.

Othieno, H., Awange, J., Othieno, H., & Awange, J. (2016). Energy Resources in Northern Africa. Energy resources in Africa: Distribution, opportunities and challenges, 193-222.

Patil N, Vijay KE, and Kulkarni GA. Power losses Minimization in Transmission System using Particle Swarm Optimization and Salp Swarm Algorithm, European Journal of Molecular and Clinical Medicine 2020;7(4):2020. https://ejmcm.com/article_1818.html.

Pelay, U., Lingai, L. U. O., Yilin, F. A. N., & Stitou, D. (2020). Dynamic modeling and simulation of a concentrating solar power plant integrated with a thermochemical energy storage system. Journal of energy storage, 28, 101164.

Pengyuan, Z. H. A. O., Chenchen, W. U., & Yangmin, L. I. (2022). Design and application of solar sailing: A review on key technologies. Chinese Journal of Aeronautics.

Petrovic, S., & Williams, N. (2023). Uganda. In World Energy Handbook (pp. 117-122). Cham: Springer International Publishing.

Pourakbari-Kasmaei, M., & Lehtonen, M. (2020). Enhancing the protective performance of surge arresters against indirect lightning strikes via an inductor-based filter. Energies, 13(18), 4754.

Prasetya, D. A., Nguyen, P. T., Faizullin, R., Iswanto, I., & Armay, E. F. (2020). Resolving the shortest path problem using the haversine algorithm. Journal of critical reviews, 7(1), 62-64.

Pretl, H., & Eberlein, M. (2021). Fifty nifty variations of two-transistor circuits: A tribute to the versatility of MOSFETs. IEEE Solid-State Circuits Magazine, 13(3), 38-46.

Razzaghi, R., Lugrin, G., Paolone, M., & Rachidi, F. (2013, June). On the use of electromagnetic time reversal to locate faults in series-compensated transmission lines. In 2013 IEEE Grenoble Conference (pp. 1-5). IEEE.

Rehman, A. A., & Alharthi, K. (2016). An introduction to research paradigms. International Journal of Educational Investigations, 3(8), 51-59.

Renner, J., & Steeb, H. (2015). Modeling of fluid transport in geothermal research. Handbook of geomathematics, 1443-1505.

Riba, J. R., Larzelere, W., & Rickmann, J. (2018). Voltage correction factors for air-insulated transmission lines operating in high-altitude regions to limit corona activity: A review. Energies, 11(7), 1908.

Rivera, N., & Kaminer, I. (2020). Light–matter interactions with photonic quasiparticles. Nature Reviews Physics, 2(10), 538-561.

Rozegnał, B., Albrechtowicz, P., Mamcarz, D., Rerak, M., & Skaza, M. (2021). The power losses in cable lines supplying nonlinear loads. Energies, 14(5), 1374.

Rühle, S. (2016). Tabulated values of the Shockley–Queisser limit for single junction solar cells. Solar energy, 130, 139-147.

Salilih, E. M., & Birhane, Y. T. (2019). Modeling and analysis of photo-voltaic solar panel under constant electric load. Journal of Renewable Energy, 2019.

Sarniak, M. T. (2020). Modeling the functioning of the half-cells photovoltaic module under partial shading in the matlab package. Applied Sciences, 10(7), 2575.

Satpathy, R., & Pamuru, V. (2021). Chapter 5-Manufacturing of crystalline silicon solar PV modules. Solar PV Power, 135-241.

Scarabelot, L.T. Rampinelli, G.A. Rambo, C.R. (2021). Overirradiance effect on the electrical performance of photovoltaic systems of different inverter sizing factors, J. Sol. Energy 225561-568, https://doi.org/10.3390/app13053155

Schwingshackl, C., Petitta, M., Wagner, J. E., Belluardo, G., Moser, D., Castelli, M., ... & Tetzlaff, A. (2013). Wind effect on PV module temperature: Analysis of different techniques for an accurate estimation. Energy Procedia, 40, 77-86.

Sharma, S., Goel, K., Gupta, A., & Kumar, H. (2012). Corona effects on eHv AC transmission lines. International Journal of Scientific Research Engineering & Technology, 1(5), 160-164.

Shockley, W., & Queisser, H. (2018). Detailed balance limit of efficiency of p–n junction solar cells. In *Renewable Energy* (pp. Vol2_35-Vol2_54). Routledge.

Skoplaki, E. P. J. A., & Palyvos, J. A. (2009). Operating temperature of photovoltaic modules: A survey of pertinent correlations. Renewable energy, 34(1), 23-29.

Sun, V., Asanakham, A., Deethayat, T., & Kiatsiriroat, T. (2020). A new method for evaluating nominal operating cell temperature (NOCT) of unglazed photovoltaic thermal module. Energy reports, 6, 1029-1042.

Suntola, T. (2017). Photon—The Minimum Dose of Electromagnetic Radiation. In The Nature of Light (pp. 259-272). CRC Press.

Tofighi, A. (2013). Performance evaluation of pv module by dynamic thermal model. Journal of Power Technologies, 93(2), 111.

Tonmitr, K., Ratanabuntha, T., Tonmitr, N., & Kaneko, E. (2016). Reduction of power loss from corona phenomena in high voltage transmission line 115 and 230 kV. Procedia Computer Science, 86, 381-384.

Tonmitr, K., Ratanabuntha, T., Tonmitr, N., & Kaneko, E. (2016). Reduction of power loss from corona phenomena in high voltage transmission line 115 and 230 kV. Procedia Computer Science, 86, 381-384.

Toreti Scarabelot, L., Arns Rampinelli, G., & Rambo, C. R. (2021). Overirradiance effect on the electrical performance of photovoltaic systems of different inverter sizing factors. Solar Energy, 225, 561-568.

Tozzi Jr, P., & Jo, J. H. (2017). A comparative analysis of renewable energy simulation tools: Performance simulation model vs. system optimization. Renewable and Sustainable Energy Reviews, 80, 390-398.

Twaha, S., Ramli, M. A., Murphy, P. M., Mukhtiar, M. U., & Nsamba, H. K. (2016). Renewable based distributed generation in Uganda: Resource potential and status of exploitation. Renewable and Sustainable Energy Reviews, 57, 786-798.

UETCL Electricity transmission for sustainable regional development, 2023. (accessed: 29 August 2022). https://uetcl.go.ug/.

Ujah, C. O., Kallon, D. V. V., Aikhuele, D. O., & Aigbodion, V. S. (2022). Advanced Composite Materials: A Panacea for Improved Electricity Transmission. Applied Sciences, 12(16), 8291.

UNMA (2023) Uganda National Meteorological Authority UNMA, weather-ambient temperature https://www.unma.go.ug/. Accessed on 14 July 2022.

van der Ven, M. J. (2020). An overview of recent developments and the current state of the Ugandan energy sector. International Growth Centre.

Velásquez, R. M. A., & Lara, J. V. M. (2023). The problem of the actual insulation coordination for 500 kV with overvoltage in substations and the needed for more surge arresters in high voltage grid. Ain Shams Engineering Journal, 14(9), 102130.

Wain-Martin, A., Campana, R., Morán-Ruiz, A., Larrañaga, A., & Arriortua, M. I. (2022). Synthesis and processing of SOFC components for the fabrication and characterization of anode supported cells. Boletín de la Sociedad Española de Cerámica y Vidrio, 61(4), 264-274.

Wang, D., Meng, Y., Chen, S., Xie, C., & Liu, Z. (2021). A hybrid model for vessel traffic flow prediction based on wavelet and prophet. Journal of Marine Science and Engineering, 9(11), 1231.

Wang, H., Yang, G., Li, E., Tian, Y., Zhao, M., & Liang, Z. (2019, July). High-voltage power transmission tower detection based on faster R-CNN and YOLO-V3. In 2019 Chinese Control Conference (CCC) (pp. 8750-8755). IEEE.

Weedy, B. M., Cory, B. J., Jenkins, N., Ekanayake, J. B., & Strbac, G. (2012). Electric power systems. John Wiley & Sons.

Xu, Q., Zhang, H., Cao, Y., Qin, H., & Gao, Z. (2022). Power System State Estimation Approach Considering Transmission Line Temperature. Applied Sciences, 12(19), 10171.

Yahaya, E. A., Jacob, T., Nwohu, M. N., & Sadiq, A. A. (2013). Power loss due to corona on High Voltage Transmission lines.

Yamaguchi, M., Suezawa, K., Takahashi, Y., Arai, K. I., Kikuchi, S., Shimada, Y., ... & Ito, K. (2000). Magnetic thin-film inductors for RF-integrated circuits. Journal of magnetism and magnetic materials, 215, 807-810.

Zhang, C. Q., Gao, Z. Y., Chen, Y. Y., Dai, Y. J., Wang, J. W., & Zhang, P. W. (2021). Experimental determination of the dominant noise mechanism of rotating rotors using hot-wire anemometer. Applied Acoustics, 173, 107703.

Zhou, H., Lu, T., Zhang, S., & Zhang, X. (2021). Lumped-Circuits Model of Lossless Transmission Lines and Its Numerical Characteristics. Frontiers in Energy Research, 9, 809434.

APPENDICES

APPENDIX I: INTRODUCTION LETTER FROM DIRECTOR HIGHER DEGREES AND RESEARCH FOR FIELD DATA COLLECTION AT UGANDA ELECTRICITY TRANSMISSION COMPANY LIMITED

KAMPALA INTERNATIONAL UNIVERSITY
EXPLORING THE HEIGHTS

WESTERN CAMPUS
PO BOX 71, Ishaka, Bushenyi, Uganda
pgr.wc@kiu.ac.ug
Website: http://www.kiu.ac.ug
773501693/+256761222772

8th August 2022

The **Manager,**
Uganda Electricity Transmission Company Limited (UETCL)
Through:
The Minister of Energy Uganda.

Sir/Ma,

LETTER OF INTRODUCTION OF OUNYESIGA LIVING (2021-08-01254)

I am happy to introduce to you one of our postgraduate students by the name Ounyesiga Living, a second year PhD student at the Department of Electrical and Telecommunication Engineering, School of Engineering and Applied Sciences, Kampala International University Ishaka, Bushenyi, Uganda.

Ounyesiga Living is undertaking a research project titled; **"Modeling, simulation and optimization of solar power generation and transmission in Uganda".** He has chosen your organization for his study and for his data collection. This study will require that he interacts with some of the staff on ground and to also collect data from documents that are related to his study area only.

I shall be very grateful for any assistance render to him to enable him collect all the necessary data towards the completion of this field work within the shortest possible time.

Thank you and please accept my highest esteem regards.

Yours sincerely,

KIU WESTERN CAMPUS * Directorate Of Postgraduate Studies And Research * 08 AUG 2022 P O BOX 71 BUSHENYI

Engr. Dr. Abubakar Abdulkarim
Deputy Director-DHDR KIU-WC

"Exploring the Heights"

APPENDIX II: ACKNOWLEDGMENT OF RECIEPT OF ALLOWANCE LETTER BY UGANDA ELECTRICITY TRANSMISSION COMPANY LIMITED

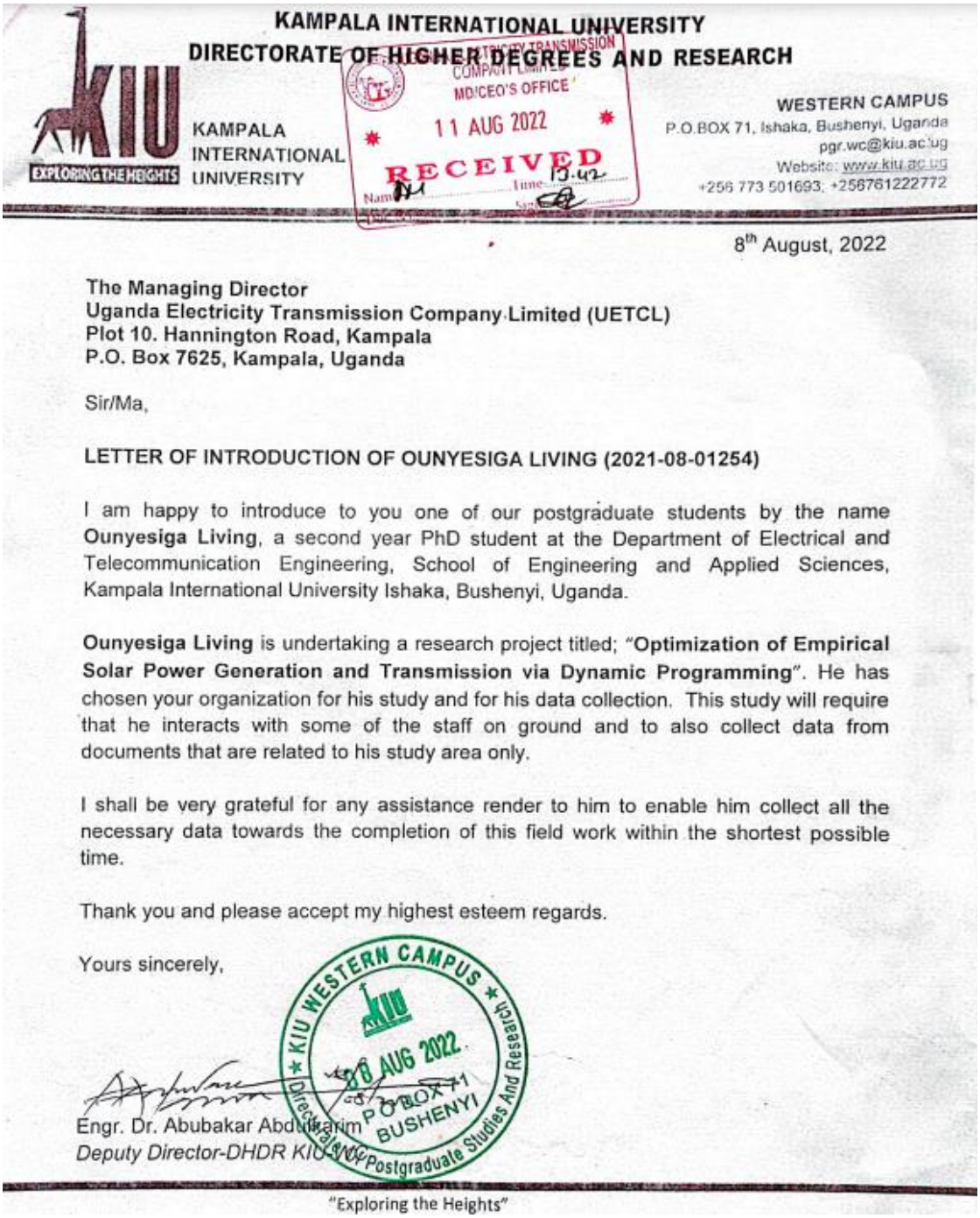

KAMPALA INTERNATIONAL UNIVERSITY
DIRECTORATE OF HIGHER DEGREES AND RESEARCH

KAMPALA INTERNATIONAL UNIVERSITY
EXPLORING THE HEIGHTS

UGANDA ELECTRICITY TRANSMISSION COMPANY LIMITED
MD/CEO'S OFFICE
11 AUG 2022
RECEIVED
Time 13.42

WESTERN CAMPUS
P.O.BOX 71, Ishaka, Bushenyi, Uganda
pgr.wc@kiu.ac.ug
Website: www.kiu.ac.ug
+256 773 501693; +256761222772

8th August, 2022

The Managing Director
Uganda Electricity Transmission Company Limited (UETCL)
Plot 10. Hannington Road, Kampala
P.O. Box 7625, Kampala, Uganda

Sir/Ma,

LETTER OF INTRODUCTION OF OUNYESIGA LIVING (2021-08-01254)

I am happy to introduce to you one of our postgraduate students by the name **Ounyesiga Living**, a second year PhD student at the Department of Electrical and Telecommunication Engineering, School of Engineering and Applied Sciences, Kampala International University Ishaka, Bushenyi, Uganda.

Ounyesiga Living is undertaking a research project titled; "**Optimization of Empirical Solar Power Generation and Transmission via Dynamic Programming**". He has chosen your organization for his study and for his data collection. This study will require that he interacts with some of the staff on ground and to also collect data from documents that are related to his study area only.

I shall be very grateful for any assistance render to him to enable him collect all the necessary data towards the completion of this field work within the shortest possible time.

Thank you and please accept my highest esteem regards.

Yours sincerely,

KIU WESTERN CAMPUS
30 AUG 2022
P O BOX 71
BUSHENYI
Director/Deputy Director Postgraduate Studies And Research

Engr. Dr. Abubakar Abdulkarim
Deputy Director-DHDR KIU-WC

"Exploring the Heights"

APPENDIX III: PERMISSION LETTER BY TO COLLECT DATA FROM UGANDA ELECTRICITY TRANSMISSION COMPANY LIMITED

P.O. Box 7625
Kampala, Uganda
Plot 10, Hannington Rd

Phone: +256 41 233433/4
Fax: +256 41 341789
Email: transco@uetcl.com

UGANDA ELECTRICITY TRANSMISSION COMPANY LTD

RM/DN/KIU/24.08.2022

24th August, 2022

Mr. Ounyesiga Living
Kampala International University
Department of Electrical and Telecommunication Engineering
Tel: +256-706412575

Dear Mr. Ounyesiga

SUBJECT: REQUETS FOR PERMISSION TO COLLECT DATA AT UETCL

Reference is made to your letter dated 8th August, 2022, and received on 11th August ,2022, requesting for permission to collect data to carry out a Research study in Uganda Electricity Transmission Company Limited (UETCL) on the topic "**Optimization of Empirical Solar Power Generation and Transmission via Dynamic Programming**.

I write to inform you that your request is granted, you are free to come at any time of your choice.

You will report to Mr. Denis Okot the Principal Control Engineer who will accord you necessary assistance. Also, you will avail a copy of the research report to the undersigned for reference purposes in the Company.

UETCL will not be liable for any accident occurring to you while undergoing research.

You will not be paid any salary/wage or access any facilities enjoyed by staff of UETCL.

Yours Sincerely,

Masiko

Richard Matsiko
AG. DEPUTY CHIEF EXECUTIVE OFFICER

c.c Eng. Abubakar Abdul Karim
Deputy Director –DHDR KIU-WC

Principal Control Engineer, UETCL

APPENDIX IV: INTRODUCTION LETTER FROM DIRECTOR HIGHER DEGREES AND RESEARCH FOR EXPERIMENTAL SET UP AND DATA COLLECTION AT BUSITEMA SOLAR POWER STATION

DIRECTORATE OF HIGHER DEGREES AND RESEARCH

KAMPALA INTERNATIONAL UNIVERSITY

WESTERN CAMPUS
PO BOX 71, Ishaka, Bushenyi, Uganda
pgr.wc@kiu.ac.ug
Website: http://www.kiu.ac.ug
773501693/+256761222772

8th August 2022

The **Manager,**
Busitema Solar Power Plant Station
Through:
The Minister of Energy Uganda.

Sir/Ma,

LETTER OF INTRODUCTION OF OUNYESIGA LIVING (2021-08-01254)

I am happy to introduce to you one of our postgraduate students by the name Ounyesiga Living, a second year PhD student at the Department of Electrical and Telecommunication Engineering, School of Engineering and Applied Sciences, Kampala International University Ishaka, Bushenyi, Uganda.

Ounyesiga Living is undertaking a research project titled; **"Modeling, simulation and optimization of solar power generation and transmission in Uganda".** He has chosen your organization for his study and for his data collection. This study will require that he interacts with some of the staff on ground and to also collect data from documents that are related to his study area only.

I shall be very grateful for any assistance render to him to enable him collect all the necessary data towards the completion of this field work within the shortest possible time.

Thank you and please accept my highest esteem regards.

Yours sincerely,

KIU WESTERN CAMPUS * Directorate Of Postgraduate Studies And Research * 08 AUG 2022 P O BOX 71 BUSHENYI

Engr. Dr. Abubakar Abdulkarim
Deputy Director-DHDR KIU-WC

"Exploring the Heights"

APPENDIX V: INTRODUCTION LETTER FROM DIRECTOR HIGHER DEGREES AND RESEARCH FOR EXPERIMENTAL SET UP AND DATA COLLECTION AT MAYUGE SOLAR POWER STATION

KAMPALA INTERNATIONAL UNIVERSITY
DIRECTORATE OF HIGHER DEGREES AND RESEARCH

KAMPALA INTERNATIONAL UNIVERSITY

WESTERN CAMPUS
PO BOX 71, Ishaka, Bushenyi, Uganda
pgr.wc@kiu.ac.ug
Website: http://www.kiu.ac.ug
773501693/+256761222772

8th August 2022

The **Manager,**
Mayuge Solar Power Plant Station
Through:
The Minister of Energy Uganda.

Sir/Ma,

LETTER OF INTRODUCTION OF OUNYESIGA LIVING (2021-08-01254)

I am happy to introduce to you one of our postgraduate students by the name Ounyesiga Living, a second year PhD student at the Department of Electrical and Telecommunication Engineering, School of Engineering and Applied Sciences, Kampala International University Ishaka, Bushenyi, Uganda.

Ounyesiga Living is undertaking a research project titled; **"Modeling, simulation and optimization of solar power generation and transmission in Uganda"**. He has chosen your organization for his study and for his data collection. This study will require that he interacts with some of the staff on ground and to also collect data from documents that are related to his study area only.

I shall be very grateful for any assistance render to him to enable him collect all the necessary data towards the completion of this field work within the shortest possible time.

Thank you and please accept my highest esteem regards.

Yours sincerely,

KIU WESTERN CAMPUS * Directorate Of Postgraduate Studies And Research * "Exploring The Heights"
04 AUG 2022
P O BOX 71 BUSHENYI

Engr. Dr. Abubakar Abdulkarim
Deputy Director-DHDR KIU-WC

APPENDIX VI: INTRODUCTION LETTER FROM DIRECTOR HIGHER DEGREES AND RESEARCH FOR EXPERIMENTAL SET UP AND DATA COLLECTION AT SROTI SOLAR POWER STATION

KAMPALA INTERNATIONAL UNIVERSITY
DIRECTORATE OF HIGHER DEGREES AND RESEARCH

KAMPALA INTERNATIONAL UNIVERSITY

WESTERN CAMPUS
PO BOX 71, Ishaka, Bushenyi, Uganda
pgr.wc@kiu.ac.ug
Website: http://www.kiu.ac.ug
773501693/+256761222772

8th August 2022

The **Manager,**
Soroti Solar Power Plant Station
Through:
The Minister of Energy Uganda.

Sir/Ma,

LETTER OF INTRODUCTION OF OUNYESIGA LIVING (2021-08-01254)

I am happy to introduce to you one of our postgraduate students by the name Ounyesiga Living, a second year PhD student at the Department of Electrical and Telecommunication Engineering, School of Engineering and Applied Sciences, Kampala International University Ishaka, Bushenyi, Uganda.

Ounyesiga Living is undertaking a research project titled; **"Modeling, simulation and optimization of solar power generation and transmission in Uganda".** He has chosen your organization for his study and for his data collection. This study will require that he interacts with some of the staff on ground and to also collect data from documents that are related to his study area only.

I shall be very grateful for any assistance render to him to enable him collect all the necessary data towards the completion of this field work within the shortest possible time.

Thank you and please accept my highest esteem regards.

Yours sincerely,

KIU WESTERN CAMPUS * P O BOX 71 BUSHENYI * Directorate Of Postgraduate Studies And Research

03 AUG 2022

Engr. Dr. Abubakar Abdulkarim
Deputy Director-DHDR KIU-WC

"Exploring the Heights"

APPENDIX VII: INTRODUCTION LETTER FROM DIRECTOR HIGHER DEGREES AND RESEARCH FOR EXPERIMENTAL SET UP AND DATA COLLECTION AT TORORO SOLAR POWER STATION

KAMPALA INTERNATIONAL UNIVERSITY
EXPLORING THE HEIGHTS

WESTERN CAMPUS
PO BOX 71, Ishaka, Bushenyi, Uganda
pgr.wc@kiu.ac.ug
Website: http://www.kiu.ac.ug
773501693/+256761222772

8th August 2022

The **Manager,**
Tororo Solar Power Plant Station
Through:
The Minister of Energy Uganda.

Sir/Ma,

LETTER OF INTRODUCTION OF OUNYESIGA LIVING (2021-08-01254)

I am happy to introduce to you one of our postgraduate students by the name Ounyesiga Living, a second year PhD student at the Department of Electrical and Telecommunication Engineering, School of Engineering and Applied Sciences, Kampala International University Ishaka, Bushenyi, Uganda.

Ounyesiga Living is undertaking a research project titled; **"Modeling, simulation and optimization of solar power generation and transmission in Uganda".** He has chosen your organization for his study and for his data collection. This study will require that he interacts with some of the staff on ground and to also collect data from documents that are related to his study area only.

I shall be very grateful for any assistance render to him to enable him collect all the necessary data towards the completion of this field work within the shortest possible time.

Thank you and please accept my highest esteem regards.

Yours sincerely,

KIU WESTERN CAMPUS ★ Office Of Postgraduate Studies And Research ★ P O BOX 71 BUSHENYI
08 AUG 2022

Engr. Dr. Abubakar Abdulkarim
Deputy Director-DHDR KIU-WC

"Exploring the Heights"

APPENDIX VIII: AVERAGE DAILY EXPERIMENTAL VALUES (215 DAYS)

Busitema

S#	Temperature		Wind speed, U(m/s)	Irradiance, H(W/m^2)	Electrical parameters		
	Ambient, T_{amb} (K)	Cell, T_c (K)			Voltage, V(V)	Current, I (A)	Power, P(w)
1	21.2	26.5	0.821	355.8	40.1	0.39	15.64
2	21.6	26.8	1.316	311.8	42.2	0.41	17.30
3	24.5	37	0.891	674.1	42.6	0.98	41.75
4	36.5	49.3	0.891	1008.6	42	1.43	60.06
5	39	45.5	0.709	1067.8	42.4	1.4	59.36
6	34.4	42.7	0.685	941.1	42.8	1.2	51.36
7	38.3	54.2	0.406	764.2	41	0.92	37.72
8	37.5	50.5	1.69	1072.6	40.3	0.69	27.81
9	34.7	38.2	1.116	334.3	41.3	0.49	20.24
10	35.1	40.1	1.709	414.8	41.5	0.61	25.32
11	34.9	37.4	0.633	358.2	41.3	0.49	20.24
12	35.3	39.4	1.608	436.2	41.6	0.63	26.21
13	37.5	44.8	2.208	469.3	40.8	0.8	32.64
14	36.9	43.2	0.021	608.5	40.5	0.47	19.04
15	28.2	31.6	0.032	242.3	41.6	0.37	15.39
16	28.2	32.1	0.012	263.4	41.4	0.35	14.49
17	28.9	32.9	0.016	278.4	41.4	0.41	16.97
18	31.9	37	0.984	359.5	41.1	0.46	18.91
19	31.4	38.8	0.72	414.2	41.1	0.52	21.37
20	34	38.7	0.16	321.6	40.3	0.4	16.12
21	31.2	33.5	0.14	167.4	39.9	0.21	8.38
22	27	28.1	3.209	167.2	41.8	0.28	11.70
23	34.5	43.8	0.514	527.1	42.6	0.78	33.23
24	37.8	44.1	0.423	603.6	41.8	0.79	33.02

25	38.4	42.6	0.677	894.6	41.8	1.26	52.67
26	36.2	54.4	1.538	1021.7	41.5	1.38	57.27
27	35.9	48.1	0.606	1082.7	41.7	1.42	59.21
28	38.6	52	1.225	847	41.4	1.34	55.48
29	35.5	44.3	2.198	923.8	41.9	1.16	48.60
30	34.3	42.7	2.515	798.8	42.2	0.98	41.36
31	31.4	38.9	2.049	668.9	41.9	0.78	32.68
32	29.7	38.2	3.292	614.1	42.1	0.63	26.52
33	28.2	33.9	1.123	598.2	41.9	0.61	25.56
34	27.9	37.2	1.544	651.1	42	0.56	23.52
35	27.2	33.9	1.193	539.8	41.5	0.53	22.00
36	25.7	31.2	1.998	409.1	41.3	0.49	20.24
37	28.1	36.9	0.274	409.9	40.5	0.65	26.33
38	27.4	35.7	1.343	432.1	40.9	0.44	18.00
39	24.6	42.2	0.426	403.8	41.3	0.74	30.56
40	26.9	44.4	0.419	569.3	40.8	0.8	32.64
41	34.8	47.6	1.363	1112.4	40.6	0.79	32.07
42	35.4	45.7	0.997	1002.4	42.2	1.59	67.10
43	37.6	51.9	0.899	303.3	40.6	0.56	22.74
44	36.4	48.7	1.381	488.5	40.8	0.73	29.78
45	34	37.2	0.906	350.8	41.6	0.54	22.46
46	35.5	39.2	0.989	418.1	41.4	0.58	24.01
47	34.5	37.8	0.582	378.5	41.4	0.57	23.60
48	34.7	38.5	1.708	426.1	41.7	0.6	25.02
49	31.6	48.4	0.709	920.5	41.9	1.29	54.05
50	33	44	0.613	518.8	42.6	0.89	37.91
51	33.4	63.8	0.712	552.6	37.6	0.99	37.22
52	32.6	62.6	0.613	1030.7	40	1.43	57.20
53	40	59.4	2.461	951.8	40.9	1.46	59.71
54	26.9	54.6	1.265	1139.2	41.3	1.59	65.67

55	28.4	54.5	0.761	1133.2	41.2	1.62	66.74
56	31	54.7	0.721	1117.3	41.3	1.63	67.32
57	27.2	43	1.028	805.8	42.2	1.29	54.44
58	29.6	47.9	0.49	872.8	41.7	1.49	62.13
59	35.8	38.2	0.592	579.6	42.4	0.85	36.04
60	36.6	42.8	0.831	482.8	41.8	0.86	35.95
61	29.2	32.4	0.932	242.1	41.6	0.35	14.56
62	28.8	33.1	0.842	277	41.3	0.41	16.93
63	29.1	33.2	0.67	280.1	41.2	0.4	16.48
64	30.8	37.1	0.164	360.5	41.3	0.49	20.24
65	31.8	39.7	1.83	440.7	41.2	0.52	21.42
66	31.7	38.3	0.81	268.6	40.6	0.37	15.02
67	31.4	33.6	1.45	166.7	39.9	0.21	8.38
68	26.9	28.2	3.481	198.7	41.8	0.28	11.70
69	31.3	52.7	0.181	366.8	39.3	0.77	30.26
70	30.4	45.3	0.591	400.9	40.9	1.27	51.94
71	27.6	42.6	0.819	396.9	40.6	0.58	23.55
72	32.2	40.4	1.267	421.9	41.2	0.56	23.07
73	28.1	47.1	1.590	946.8	41.8	1.3	54.34
74	29.3	48.2	0.770	983	41.9	1.31	54.89
75	29.7	50.4	1.310	1000.3	42	1.33	55.86
76	30.7	51.7	2.180	1034.1	42.1	0.98	41.26
77	35.4	44.7	1.643	1248.3	41.9	1.09	45.67
78	38.2	50.0	1.207	1041.6	41.6	1.01	42.02
79	36.6	45.3	0.906	614.7	41.7	0.63	26.27
80	36.1	44.8	2.604	613.8	41.9	0.89	37.29
81	34.4	37.1	1.618	436.6	41.3	0.59	24.37
82	35.0	38.8	1.768	414.1	41.4	0.57	23.60
83	34.4	38.0	0.466	430.4	41.7	0.6	25.02
84	35.2	38.3	1.064	435.3	41.8	0.61	25.50

85	35.3	38.8	0.563	423.1	41.9	0.71	29.75
86	37.0	42.9	0.086	309.9	40.7	0.53	21.57
87	28.9	30.8	0.312	234.5	41.8	0.32	13.38
88	29.4	32.6	1.331	254.2	41.4	0.36	14.90
89	29.8	33.3	0.782	284.9	41.2	0.41	16.89
90	31.1	37.2	0.091	328.6	41.3	0.49	20.24
91	32.3	40.0	1.334	412.6	41.2	0.52	21.42
92	31.4	38.2	0.322	263.5	40.1	0.97	38.90
93	31.3	44.5	0.748	989.8	41.9	1.09	45.67
94	26.8	49.7	0.443	998.7	42	1.21	50.82
95	31.3	52.4	4.140	1010.4	42.3	1.41	59.64
96	32.1	53.7	2.340	1065.1	42.6	1.49	63.47
97	31.0	45.7	2.230	781	41.3	0.93	38.41
98	31.3	44.9	3.560	324.4	41	0.47	19.27
99	31.1	40.8	0.420	320.6	41.4	0.47	19.46
100	31.1	40.4	1.080	651.1	40.9	0.51	20.86
101	29.7	35.9	0.890	313.7	41.6	0.55	22.88
102	30.5	36.5	0.970	260.5	41.7	0.38	15.85
103	29.8	35	1.050	217.3	41.6	0.36	14.98
104	30.0	35.7	1.760	454.2	41.9	0.81	33.94
105	29.6	33.9	1.450	148	39.8	0.21	8.36
106	29.0	30.8	1.561	237.9	40.6	0.39	15.83
107	29.1	31.2	1.489	201.7	40.2	0.43	17.29
108	28.8	30.6	0.982	96.8	38.9	0.33	12.84
109	25.7	38.7	1.363	314.4	40.6	0.63	25.58
110	24.8	49.4	1.482	997.8	41.9	1.19	49.86
111	26.9	40	0.756	931.3	41.7	1.12	46.70
112	27.9	40.3	2.061	909.2	41.2	1.09	44.91
113	27.4	47.4	1.538	1198.4	41.8	1.66	69.39
114	26.7	43.4	1.444	1053.9	41.7	1.53	63.80

115	31	51.1	1.075	1091.8	40.8	1.64	66.91
116	27.2	41.9	0.683	341.4	40.2	1.04	41.81
117	29.1	45.6	0.966	1138.2	42.5	1.75	74.38
118	28.3	37.1	0.755	332.3	41.4	1.06	43.88
119	30.5	40.8	0.728	401	39.5	0.52	20.54
120	30	47.8	0.36	969.8	40.9	1.47	60.12
121	30.4	47.4	0.739	1169.6	41.5	1.64	68.06
122	30	41.4	0.659	924.6	42.1	1.29	54.31
123	30.7	46.8	1.743	1037.6	41.9	1.36	56.98
124	28.3	36.9	1.927	600.4	42.7	0.83	35.44
125	29.8	41.4	2.087	599.7	41.9	0.75	31.43
126	30.6	37.2	0.002	358.7	41.3	0.49	20.24
127	32.7	39.9	1.291	411.9	41.2	0.51	21.01
128	31.3	38.1	1.733	277.9	40.6	0.32	12.99
129	31.1	33.5	2.648	164.4	39.9	0.21	8.38
130	28.2	41.2	0.827	487.3	41.2	0.43	17.72
131	35.6	45.1	0.56	604.7	41.6	0.94	39.10
132	36.1	43	2.174	602.4	41.8	0.8	33.44
133	34.8	38.3	0.983	467.6	41.9	0.66	27.65
134	34.9	38.2	0.894	403.4	41.5	0.55	22.83
135	35.3	38	0.909	468.4	41.6	0.66	27.46
136	35	38	0.829	456.8	41.9	0.62	25.98
137	35.7	40	0.706	644.7	42.2	0.82	34.60
138	35.6	42.7	0.041	249.9	39.9	0.37	14.76
139	29	31.6	0.662	113.2	41.3	0.32	13.22
140	29	33.1	0.963	286.2	41.2	0.42	17.30
141	29.2	33.2	3.304	290.6	41.2	0.41	16.89
142	26.3	27.9	2.01	98.7	40.1	0.17	6.82
143	25.5	27.9	0.462	76.4	39.2	0.12	4.70
144	24.9	27	1.315	97.9	39.8	0.14	5.57

145	28.3	40.2	0.734	312.1	41.8	0.56	23.41
146	28.8	44.6	1.095	367.8	41.9	0.63	26.40
147	30.1	47.3	1.152	573.2	42.5	1.02	43.35
148	31.5	47.9	0.556	1115.3	41.4	1.24	51.34
149	30.4	48	0.634	984.7	41.6	1.09	45.34
150	41	50	0.899	928.1	41.9	1.34	56.15
151	38.1	45.7	0.504	749.3	42.1	0.94	39.57
152	35.5	41.7	0.909	429.3	41.3	0.64	26.43
153	35.6	38.8	1.012	481.5	41.8	0.67	28.01
154	34.5	37.6	1.408	389.1	41.6	0.54	22.46
155	30.6	56.2	1.021	1160.5	41	1.64	67.24
156	30.9	56.1	1.597	1162.3	41.2	1.65	67.98
157	30.5	56.2	1.482	1162.7	41.3	1.63	67.32
158	28.7	47.8	1.309	1123.7	40	1.05	42.00
159	31.7	46.1	1.049	708.9	41.2	0.98	40.38
160	32.7	52.5	0.614	507.3	41.3	1.19	49.15
161	31.8	53.1	0.258	1008.4	41.8	1.59	66.46
162	33.4	56.5	0.57	1249.5	42.1	1.94	81.67
163	35.7	59.1	0.439	1073.4	41.9	1.66	69.55
164	46.7	60.4	0.892	1012.3	42.1	1.46	61.47
165	44.8	50.3	1.342	1085.9	42.1	1.36	57.26
166	40.7	47.8	2.134	1039.2	42	1.37	57.54
167	35.5	39	0.619	468.6	41.6	0.63	26.21
168	35	37.5	0.9	470	42	0.62	26.04
169	36.6	40.9	0.908	990	42.3	0.96	40.61
170	36.4	41.5	0.909	224	39.8	0.31	12.34
171	28.3	31.9	0.489	179.2	41	0.32	13.12
172	29.3	33.1	2.896	280.2	41.3	0.37	15.28
173	29.6	33	2.641	290.5	41.2	0.42	17.30
174	32.4	37.7	0.012	370.4	41.3	0.48	19.82

175	32.9	40	1.474	408.5	41.3	0.51	21.06
176	31.5	38.1	2.296	286.9	40.5	0.37	14.99
177	31	33.6	2.582	163.9	39.9	0.21	8.38
178	26.7	31.2	0.981	104.7	40.1	0.2	8.02
179	26.3	29.8	0.406	100.7	40	0.16	6.40
180	26	28.1	0.854	89.8	40.1	0.13	5.21
181	28.2	43.2	0.986	315.6	41.8	0.59	24.66
182	28.3	49.6	1.096	365.8	41.9	0.61	25.56
183	33.7	42.3	0.671	1115.3	41.3	1.21	49.97
184	35.8	57.3	1.615	994.5	42.2	1.36	57.39
185	30.7	52.5	1.398	1014.1	41.3	1.41	58.23
186	41.6	49.7	1.006	926.8	41.6	1.41	58.66
187	40.5	47.3	1.062	851.9	42	1.26	52.92
188	30.7	50.4	1.482	1063.9	41.3	1.41	58.23
189	32.3	52.6	0.518	1014.4	40.8	1.29	52.63
190	30.7	52.5	0.637	1063.9	41.3	1.41	58.23
191	32.4	55.2	1.312	836.7	40.9	1.23	50.31
192	32.7	52.5	1.408	1014.4	40.6	1.28	51.97
193	38.6	43.5	0.676	838.4	43.1	1.43	61.63
194	28.9	41.9	0.543	880.1	41.7	0.86	35.86
195	26.1	39.6	0.799	872.3	41.4	0.89	36.85
196	24.8	40.3	2.061	909.1	42	0.99	41.58
197	26.5	40	0.749	931.3	41.6	1.12	46.59
198	25.9	45.1	0.352	965.2	41.3	1.18	48.73
199	24.2	41.6	0.824	1006.9	41.2	1.27	52.32
200	28	45.6	0.668	1003.3	41.5	1.31	54.37
201	25	44.4	0.6	1015.4	41.6	1.4	58.24
202	24.8	49.4	1.482	997.7	41.9	1.68	70.39
203	30.8	47.6	0.9887	1112.4	41.2	1.09	44.91
204	35.4	45.7	1.342	1003.8	42.2	1.59	67.10

205	35.5	48.6	0.899	928.1	41.9	1.34	56.15
206	36.6	40.9	0.918	980.8	42.1	0.98	41.26
207	34.6	48.8	1.679	1009.2	42.6	1.32	56.23
208	36.2	49.5	0.638	997.4	42.6	1.28	54.53
209	32.4	43.4	0.301	466.9	41.6	1.03	42.85
210	30	33.3	0.031	396.2	41.1	0.96	39.46
211	30.3	33.5	0.022	296.1	40.3	0.42	16.93
212	31.9	37.7	0.01	367.8	41.1	0.48	19.73
213	33.2	39.9	0.462	407.2	41	0.51	20.91
214	31.8	38.2	0.319	257.8	40.6	0.39	15.83
215	31.1	33.7	2.614	162.6	40.1	0.25	10.03
216	26.7	28.3	3.401	172.7	38.6	0.31	11.97

Mayuge

S#	Temperature		Wind speed, U(m/s)	Irradiance, $H(W/m^2)$	Electrical parameters		
	Ambient, T_{amb} (K)	Cell, T_c (K)			Voltage, V(V)	Current, I (A)	Power, P(w)
1	30.3	39.6	1.411	590	41.4	1.08	44.71
2	32.4	37.8	1.3	579.2	42.3	0.96	40.61
3	31.6	40	0.769	672.3	41.9	0.96	40.22
4	32	40.2	1.931	700.1	41.8	1.08	45.14
5	31.4	43	0.589	709.1	42.4	1.09	46.22
6	34.4	49.8	0.614	771.6	41.6	1.17	48.67
7	38.4	47.5	0.894	647.6	41.6	1.24	51.58
8	44.9	48.1	0.947	798.7	40.5	0.7	28.35
9	40.2	54.3	1.501	1035	41.3	1.58	65.25
10	36.9	57.4	0.67	1023.4	40.9	1.5	61.35

11	35	51	0.746	964.6	41.2	1.42	58.50
12	35.6	55	0.86	1030.7	40.6	1.47	59.68
13	35.4	49.9	0.906	920.4	41.1	1.28	52.61
14	36.6	53	2.203	863.9	40.4	0.98	39.59
15	32.5	39.8	0.809	267.6	40.3	0.39	15.72
16	32.6	36.9	0.772	750.7	42.9	1.07	45.90
17	33	39.8	1.038	288.7	40.3	0.38	15.31
18	31.4	34.2	1.621	193	40.2	0.25	10.05
19	29.6	30.9	0.974	114.5	39.4	0.15	5.91
20	27.3	26.3	1.436	131.2	39.9	0.19	7.58
21	26.6	27.3	0.768	127.5	41.6	0.25	10.40
22	27.1	30.1	0.781	113.8	41.3	0.3	12.39
23	30.2	36.1	1.345	170.1	41.1	0.42	17.26
24	30.3	37	1.116	165.7	41.2	0.41	16.89
25	30.6	37.7	0.666	365.5	41.4	0.51	21.11
26	30.4	37.2	1.077	311.7	41.2	0.44	18.13
27	30.7	34.4	1.517	317.9	43.4	0.38	16.49
28	30	34.2	1.089	418.6	41.5	0.4	16.60
29	31.1	33.3	0.899	400.8	41.7	0.66	27.52
30	30.9	32.7	2.419	379.4	41.5	0.58	24.07
31	31.1	33	0.519	357.6	41.2	0.37	15.24
32	30.7	32.9	0.2	222.1	40.4	0.31	12.52
33	30.8	32.6	0.96	173.9	40.3	0.27	10.88
34	30.5	31.6	0.403	179.6	40.6	0.27	10.96
35	30.6	31.9	0.151	180.2	40.5	0.27	10.94
36	30.4	31.5	0.344	181.5	40.6	0.24	9.74
37	29.7	37	1.342	480.4	40.6	0.41	16.65
38	30.5	40	0.539	560.3	41.3	1.07	44.19
39	33	36.9	0.415	680.5	41.8	0.99	41.38
40	39.4	48.8	0.62	1001.2	41.5	1.56	64.74

41	34.5	47.9	0.508	1106.5	41.3	1.48	61.12
42	30.8	49.9	0.831	1204.7	41.8	1.49	62.28
43	31.8	50.2	1.291	1210.1	41.3	1.53	63.19
44	32.2	55	1.05	986.9	41.7	1.49	62.13
45	37.9	50.2	2.798	1209.7	41.2	1.44	59.33
46	40.1	51	1.006	998.9	41.5	1.46	60.59
47	35.9	51.4	1.706	1006.7	41.1	1.48	60.83
48	37.9	53	1.963	1049.2	41	1.5	61.50
49	34.7	51.1	1.2	870.9	40.9	1.25	51.13
50	34.7	49.8	0.845	535.3	40	0.76	30.40
51	33.4	38.9	1.199	256.3	40.4	0.39	15.76
52	32.8	38.6	1.45	353.2	40.9	0.55	22.50
53	32.9	39	0.383	228.4	40.1	0.35	14.04
54	30.8	33.1	0.903	154.3	40.1	0.23	9.22
55	30.1	32.5	2.327	96.4	39.1	0.15	5.87
56	29.5	30.5	2.101	32.4	39.2	0.15	5.88
57	26.7	26.1	0.79	192.7	41.4	0.26	10.76
58	27.4	30.6	0.55	259.3	41.3	0.31	12.80
59	30.3	34.6	0.615	350.4	41.3	0.41	16.93
60	30	34.5	1.101	346.9	41.5	0.42	17.43
61	30.2	37.8	1.314	373.4	41.5	0.49	20.34
62	30.7	36.6	0.766	200.9	41.1	0.5	20.55
63	31.2	34	0.532	332.5	41.5	0.41	17.02
64	31.3	34.3	0.675	341.6	41.4	0.45	18.63
65	31.2	33.4	0.691	397.8	41.7	0.65	27.11
66	31.1	32.7	0.309	391.7	41.5	0.57	23.66
67	30.9	33.5	1.037	310.8	41.2	0.37	15.24
68	30.6	33	0.492	213.4	40.4	0.43	17.37
69	30.7	32.5	0.856	205	40.3	0.27	10.88
70	30.5	32.4	1.341	185.6	40.5	0.26	10.53

71	30.3	32.2	1.689	167.6	40.4	0.27	10.91
72	30.4	32.3	0.523	168.9	41.1	0.3	12.33
73	25.8	41.4	0.582	536.9	42.2	1.04	43.89
74	29.6	45.4	0.479	674.2	41.7	1.27	52.96
75	30.0	48.8	0.598	1133.3	41.9	1.59	66.62
76	25.8	44.0	0.891	722.9	41.8	1.03	43.05
77	30.5	42.3	0.102	457	41.1	0.63	25.89
78	32.5	41.8	0.617	415.9	41.2	0.6	24.72
79	31.4	42.6	0.404	509.4	41.1	0.56	23.02
80	38.4	51.2	1.093	809.6	41.3	1.08	44.60
81	39.6	54.9	1.498	981.9	41.4	1.09	45.13
82	35.4	49.1	1.117	690	41.2	1.34	55.21
83	38.0	54.9	0.569	1037.2	42	1.49	62.58
84	36.4	54.2	0.408	1044	40.7	1.44	58.61
85	34.4	51.4	0.890	857.2	41	1.2	49.20
86	35.1	48.9	0.968	457.6	40.3	0.62	24.99
87	32.4	37.6	1.055	240.9	40.5	0.37	14.99
88	33.6	38.2	1.246	433.1	41.3	0.79	32.63
89	31.7	49.5	0.614	507.3	40.3	0.79	31.84
90	32.8	63.1	0.258	1208.4	40.2	1.59	63.92
91	32.4	62.5	0.570	1349.5	41	1.94	79.54
92	34.7	61.1	0.439	1072.4	39.9	1.66	66.23
93	44.7	59.4	0.892	1002.3	40.8	1.46	59.57
94	30.6	56.2	1.021	1160.5	41	1.64	67.24
95	30.9	56.1	1.597	1162.3	41.2	1.65	67.98
96	30.5	56.2	1.482	1162.7	41.3	1.63	67.32
97	30.4	37.4	1.982	348.9	41.3	0.48	19.82
98	31.4	34.2	0.354	271.4	41.5	0.43	17.85
99	31.1	33.5	0.660	351.4	41.5	0.52	21.58
100	31.4	34.3	0.150	339	42.1	0.46	19.37

101	31.0	33.3	1.071	390.3	41.8	0.63	26.33
102	31.2	32.6	0.734	442	41.5	0.49	20.34
103	30.7	32.5	1.389	312.2	41.3	0.5	20.65
104	30.3	31.4	0.309	206.9	40.6	0.49	19.89
105	31.7	38.3	0.891	217.1	40.6	0.37	15.02
106	30.2	35	0.613	199.3	39.8	0.22	8.76
107	28.0	33.4	0.390	200.3	41.4	0.37	15.32
108	27.2	28.9	0.315	199.8	41.2	0.24	9.89
109	25.8	41.4	0.582	536.9	42.2	1.04	43.89
110	29.6	45.4	0.479	674.2	41.7	1.27	52.96
111	30	48.8	0.598	1133.3	41.9	1.59	66.62
112	25.8	44	0.891	722.9	41.8	1.03	43.05
113	30.5	42.3	0.102	457	41.1	0.63	25.89
114	32.5	41.8	0.617	415.9	41.2	0.6	24.72
115	31.7	49.5	0.614	507.3	40.3	0.79	31.84
116	32.8	63.1	0.258	1203.4	40.2	1.59	63.92
117	32.4	62.5	0.57	1349.5	41	1.94	79.54
118	34.7	61.1	0.439	1072.4	39.9	1.66	66.23
119	44.7	59.4	0.892	1002.3	40.8	1.46	59.57
120	33.9	50.7	0.209	889.3	41	1.27	52.07
121	35.2	54.5	0.103	951.9	40.2	0.37	14.87
122	35.7	45.9	1.452	407.7	40.2	0.59	23.72
123	33.1	37.3	0.849	250.4	40.6	0.38	15.43
124	31.9	38.8	2.365	739.4	42.6	0.76	32.38
125	32.2	37.2	1.692	202.7	40.2	0.3	12.06
126	30.1	32.1	1.302	172.5	40.5	0.25	10.13
127	29	29.8	0.756	67.4	38	0.1	3.80
128	26.2	25.9	0.423	38.4	36.8	0.06	2.21
129	26	28.3	0.968	209.1	41.5	0.28	11.62
130	29	32.5	1.111	349.2	42	0.5	21.00

131	31.2	34	1.106	336.5	41.4	0.54	22.36
132	31	33.5	1.312	344.3	41.7	0.5	20.85
133	30.6	37.2	0.971	344.7	41.3	0.45	18.59
134	29.8	35	0.793	324.6	41.4	0.43	17.80
135	31.3	34.2	0.409	228.5	41.4	0.44	18.22
136	31.4	34.1	0.578	335.9	41.3	0.47	19.41
137	31.2	33.3	0.998	372.6	41.5	0.58	24.07
138	30.8	47.9	0.541	883.9	41.7	1.38	57.55
139	31	48.8	0.561	1053.4	41.6	1.39	57.82
140	31.9	49.8	0.513	875.6	41.7	1.36	56.71
141	30	47	2.314	963.9	42	1.32	55.44
142	31	47.1	3.431	986.2	42.9	1.36	58.34
143	31.6	49	2.09	867	41.2	1.09	44.91
144	30	42.5	1.718	347.6	40.9	0.98	40.08
145	29.8	31.4	1.329	445.9	40.4	0.63	25.45
146	31.4	36.2	0.9	305.6	41.1	0.51	20.96
147	31.8	39.3	0.76	483.9	41.4	0.59	24.43
148	34.8	49.8	0.699	782.1	40.9	0.98	40.08
149	34.9	48.3	1.004	980	41.3	1.39	57.41
150	35.7	49.3	1.591	978.9	41.4	1.4	57.96
151	38.9	49.9	0.692	1002.2	42.1	1.42	59.78
152	40.1	50	1.014	1204.5	42.3	1.47	62.18
153	43.6	50.2	0.95	1220.6	41.9	0.99	41.48
154	44	50.3	0.789	999.7	41.8	1.32	55.18
155	42.9	49.6	0.998	897.9	41.6	1.4	58.24
156	34.2	50.4	0.206	906.8	41.1	1.34	55.07
157	36	52.7	0.455	1082.1	39.6	1.02	40.39
158	34.7	43.1	1.181	386.6	40.4	0.53	21.41
159	32.6	37.4	1.307	267	41.1	0.43	17.67
160	34.3	39.9	0.91	741.9	42.3	1.08	45.68

161	32.4	36.7	1.095	188.7	40.4	0.32	12.93
162	30.4	31.8	1.68	176.4	40.6	0.26	10.56
163	28	29.3	2.714	58.2	37.9	0.09	3.41
164	26.5	25.7	1.38	38.6	36.9	0.05	1.85
165	27	28.8	1.031	244.8	41.4	0.28	11.59
166	29.4	34	0.852	393.2	42	0.53	22.26
167	31.1	34.1	0.814	331	41.3	0.51	21.06
168	30.9	33.7	1.862	346.2	41.5	0.52	21.58
169	31.1	33.8	1.504	349.8	41.6	0.6	24.96
170	30.4	35.4	2.118	319	41.3	0.44	18.17
171	31.4	34.2	0.343	359.4	41.4	0.53	21.94
172	31.1	33.3	1.004	361.1	41.3	0.58	23.95
173	31	32.6	1.15	421.2	41.2	0.47	19.36
174	30.9	38.3	1.089	618	41.1	0.98	40.28
175	31.2	39.4	0.524	564.9	41.4	1.15	47.61
176	32.5	37.4	0.29	403.2	41.6	0.49	20.38
177	31.1	33.7	0.47	394.9	41.2	0.37	15.24
178	30.8	33.5	0.24	203.6	40.9	0.41	16.77
179	30.5	32.9	0.289	200.6	40.5	0.29	11.75
180	30	32.4	0.389	198.9	40.4	0.23	9.29
181	23.9	41.3	0.598	458.9	41.6	0.84	34.94
182	26.4	43.8	1.062	956.8	42.7	1.64	70.03
183	28.2	48.4	0.747	1161.8	41.7	1.44	60.05
184	28.6	44.4	0.179	535.8	40.9	0.77	31.49
185	29.3	42.5	0.649	390.4	40.7	0.57	23.20
186	32.4	40.8	0.897	514.6	41.7	0.85	35.45
187	31.8	49	1.284	830.8	40.9	0.95	38.86
188	34.7	45.1	0.964	1368.5	42.7	1.23	52.52
189	28.7	62.3	0.821	1382.5	39.9	1.76	70.22
190	31.4	62.7	0.613	1234.5	40.5	1.79	72.50

191	41.6	59.3	0.431	1007.6	40.9	1.45	59.31
192	35.1	51	0.332	955.4	41.1	1.38	56.72
193	33.7	48.5	0.417	672.4	39.9	0.62	24.74
194	34.1	39.2	0.887	318.7	40.4	0.51	20.60
195	30.6	56.2	1.021	1160.5	41	1.64	67.24
196	30.9	56.1	1.597	1162.3	41.2	1.65	67.98
197	30.5	56.2	1.482	1162.7	41.3	1.63	67.32
198	28.7	47.8	1.309	403.7	40	0.5	20.00
199	31.7	46.1	1.049	708.9	40.2	0.59	23.72
200	32.5	34.6	2.9716	318.4	41.9	0.43	18.02
201	36.4	53.9	2.098	1020.8	41.5	1.39	57.69
202	36.8	48.2	0.79	1082.5	42.1	1.42	59.78
203	39.9	50.1	0.9	847.6	41.6	1.31	54.50
204	34.9	44.2	1.339	923.8	41.9	1.18	49.44
205	34.8	47.7	1.49	798.8	42.3	0.89	37.65
206	31.8	38.6	1.285	668.9	41.8	0.78	32.60
207	32.1	38.3	0.893	679.8	41.9	0.91	38.13
208	29.9	37.7	1.036	614.1	42.1	0.62	26.10
209	28.9	35.8	0.809	601.9	41.9	0.59	24.72
210	29.7	37.8	2.42	600.1	42.1	0.46	19.37
211	27.9	33.8	0.857	596.8	42.4	0.64	27.14
212	27.4	37.6	0.893	653.1	42	0.61	25.62
213	27.2	33.5	1.064	651.2	41.8	0.58	24.24
214	28	34	0.912	552.7	41.8	0.56	23.41
215	25.7	33.2	0.684	499	41.8	0.47	19.65
216	25.9	33	0.392	407.9	41.5	0.45	18.68

Soroti

S#	Temperature		Wind speed, U(m/s)	Irradiance, $H(W/m^2)$	Electrical parameters		
	Ambient, T_{amb} (K)	Cell, T_c (K)			Voltage, V(V)	Current, I (A)	Power, P(w)
1	31.2	33.5	0.461	207.6	41.1	0.32	13.15
2	24.1	36.7	0.641	703.6	42.6	0.53	22.58
3	25.3	36.8	0.701	706.9	42.9	0.48	20.59
4	25.8	37.8	1.068	331.4	41.3	0.46	19.00
5	25.7	32.9	0.589	764	44.9	1.16	52.08
6	25	39.4	0.849	372.1	41.5	0.54	22.41
7	23.6	37.4	1.264	277.9	41.2	0.41	16.89
8	24.9	40.2	0.962	590	42.8	1.35	57.78
9	26.1	40.4	0.394	359.7	40.7	0.55	22.39
10	27.3	46.2	0.642	1058.2	42.1	1.42	59.78
11	27.5	49.4	1.934	1034.5	41.5	1.43	59.35
12	27.6	37.7	1.106	1152.2	43.6	1.63	71.07
13	27.2	40.9	0.643	347	41.2	0.53	21.84
14	27	44.9	0.718	407.2	40.2	0.61	24.52
15	29.3	43.6	0.619	713.9	42.1	1.29	54.31
16	29	37.9	0.461	1329.1	44	1.91	84.04
17	28.1	46.2	0.441	309.1	39.5	0.46	18.17
18	29.9	52.4	1.603	1291.4	41.2	1.89	77.87
19	21	53.2	0.962	1221.5	41.2	1.8	74.16
20	30.9	55.8	0.969	1315.7	40.4	1.93	77.97
21	30.8	51.1	1.134	871.7	41.2	1.32	54.38
22	30.9	47.9	1.691	659.2	40.1	1.01	40.50
23	30.4	47.1	2.451	973.8	42	1.32	55.44
24	30.2	45.5	1.094	1049.3	42	1.33	55.86
25	30.4	46.5	1.691	931.6	40.1	1.02	40.90
26	28.9	44.3	0.981	952.6	40.2	1.04	41.81

27	29.7	44.2	0.731	963	42.1	1.13	47.57
28	29.2	44	1.642	835.8	42.3	1.11	46.95
29	28.4	43	1.341	836.2	40.1	1.13	45.31
30	29	43.9	0.946	837.3	41.2	1.01	41.61
31	27.6	44.1	0.781	838	40.9	1.12	45.81
32	26.3	43.5	0.932	839	41.4	1.21	50.09
33	30.6	48.1	0.931	999.8	41.6	1.35	56.16
34	28.8	41	3.09	946.2	42	1.3	54.60
35	30	46	2.13	963	42.2	1.32	55.70
36	29.8	38.9	1.719	347.5	40.9	1.09	44.58
37	28.6	32.5	0.349	216.7	41.4	0.33	13.66
38	24.4	36.5	0.981	246.9	41.2	0.37	15.24
39	24.2	36.1	0.604	420.9	42.3	0.38	16.07
40	24.3	36	1.086	240.9	40.9	0.36	14.72
41	24.4	35.8	0.934	270.5	41.3	0.39	16.11
42	23.9	38.1	1.07	271.6	41.2	0.41	16.89
43	38.4	38	1.007	280.6	41.3	0.43	17.76
44	25.6	41.1	0.596	870.6	43.2	1.33	57.46
45	25.8	40.8	0.916	350.5	40.3	0.49	19.75
46	26.9	45.1	1.094	1003.5	43.4	1.51	65.53
47	27.4	47.1	0.894	1039.2	41.9	1.42	59.50
48	26.7	49.2	1.184	291.7	39.9	0.44	17.56
49	29	39.7	0.492	1184.5	41.3	1.46	60.30
50	28.9	45.1	1.061	562.2	41	0.83	34.03
51	27.5	40.5	1.462	368.8	41.2	0.55	22.66
52	28.4	43.9	1.131	416.5	40.6	0.62	25.17
53	26.5	44.5	0.919	425.3	40.5	0.59	23.90
54	30	42.2	0.656	1093.6	43.2	1.96	84.67
55	27.5	45.1	0.734	302.4	40	0.46	18.40
56	30.1	52.4	0.891	1293	41.5	1.88	78.02

57	31.7	54.2	1.094	1225.6	41.2	1.81	74.57
58	31.3	56.2	0.643	1317.7	40.4	1.94	78.38
59	30.4	49.5	0.684	346.3	39.2	0.5	19.60
60	28.4	45.9	0.946	219.4	38.7	0.31	12.00
61	29.7	46.9	3.012	950.4	42	1.3	54.60
62	34.9	65.6	0.815	1331.9	42.2	2.19	92.42
63	34.9	63	0.351	1256.9	40.9	1.43	58.49
64	41.3	59.2	2.218	923.7	40.7	1.34	54.54
65	24.7	43.6	0.668	474.8	40.8	0.65	26.52
66	28.3	43.1	0.178	632.4	42.1	1.12	47.15
67	30.2	46.6	0.983	968.4	42.1	1.59	66.94
68	30.1	44.2	0.6	645.8	41.1	0.97	39.87
69	29	43.3	0.569	456.9	40.6	0.59	23.95
70	31.9	40.3	0.619	377.3	40.8	0.54	22.03
71	32.1	47.5	0.641	694.5	42.1	1.2	50.52
72	34.3	43.6	0.713	510.6	41.1	0.71	29.18
73	26.4	32.0	2.406	246.6	41.8	0.42	17.56
74	24.2	35.8	0.764	781.9	41.6	0.79	32.86
75	25.1	36.0	0.296	438.1	42.6	0.39	16.61
76	24.5	35.3	1.089	240.1	41.2	0.36	14.83
77	25.4	35.1	0.296	299.3	41.5	0.4	16.60
78	24.2	36.5	0.946	323.1	42.1	0.57	24.00
79	24.0	36.5	0.931	352.9	41.9	0.58	24.30
80	24.5	42.4	0.996	1021.9	42.6	1.19	50.69
81	25.3	39.9	1.306	509.7	42.3	0.59	24.96
82	26.9	44.5	1.964	1118.5	43.1	1.39	59.91
83	27.5	46.5	0.694	1046.7	41.9	1.43	59.92
84	26.7	41.3	0.931	1134	43.2	1.73	74.74
85	26.5	44.8	0.694	433.5	40.8	0.67	27.34
86	26.7	39.9	0.166	369.7	41.4	0.56	23.18

87	27.3	43.0	0.891	420.4	40.9	0.62	25.36
88	26.9	44.0	1.314	596.2	40.4	0.49	19.80
89	32.5	42.6	0.700	591.6	41.6	0.71	29.54
90	27.4	43.7	0.428	311.3	40.3	0.48	19.34
91	29.8	53.0	0.931	1292.7	41.3	1.89	78.06
92	30.5	56.7	1.061	1239.9	40.6	1.82	73.89
93	29.1	48.1	1.436	330.1	39.6	0.5	19.80
94	27.9	43.6	0.276	215.5	39	0.31	12.09
95	29.5	46.9	1.464	954.3	41.9	1.3	54.47
96	29.3	45.7	1.891	1074.8	41.9	1.28	53.63
97	27.2	44.9	2.061	488.6	40.5	0.5	20.25
98	29.3	54.3	1.152	1145.2	41.1	1.67	68.64
99	30.3	54.4	1.161	1154.3	41.2	1.68	69.22
100	28.9	54.5	0.761	1160.2	41.3	1.64	67.73
101	33.0	51	0.916	421.7	40.3	0.64	25.79
102	33.6	45.5	0.691	1120.7	40.7	0.62	25.23
103	31.2	45.9	0.548	1082.2	44.3	1.48	65.56
104	33.0	46.6	0.639	983.5	43.1	1.38	59.48
105	34.5	48.9	0.576	924.3	41.5	1.09	45.24
106	30.3	49.2	0.572	909.8	41.4	1.12	46.37
107	28.2	49.8	1.096	367.9	41.8	0.56	23.41
108	28.1	40.8	0.738	312.1	41.7	0.49	20.43
109	24.1	35.2	0.629	327.9	41.9	1.22	51.12
110	24.3	35.1	0.569	346.4	42.6	1.13	48.14
111	24.4	35.1	0.54	706.9	43.7	1.1	48.07
112	25	34.7	0.332	270.6	42.3	1.13	47.80
113	25.1	35.1	0.694	354.6	43.1	1.04	44.82
114	24.4	36.1	1.541	338.9	41.7	0.52	21.68
115	25.7	36.3	1.009	396.1	42	0.57	23.94
116	24.8	43.2	1.039	1038	42.7	1.4	59.78

117	24.9	39	0.997	292.5	40.6	0.44	17.86
118	26.4	44.1	1.164	1143.5	42.9	1.51	64.78
119	27.4	46.3	0.692	1024.6	41.7	1.4	58.38
120	30.1	43.1	1.291	675.9	41.5	0.82	34.03
121	27.4	39.3	0.894	399.8	41.7	0.65	27.11
122	28.4	43.5	0.443	416.5	40.9	0.62	25.36
123	27	42.8	1.18	299.6	40.4	0.44	17.78
124	28.9	42.8	0.021	436.5	40.9	0.66	26.99
125	27.2	42.9	0.794	323.7	40.6	0.5	20.30
126	31.9	53	1.491	1293	41.2	2.07	85.28
127	32.8	56.8	0.568	1247.9	40.5	1.84	74.52
128	29.3	46.4	1.562	331.3	39.9	0.53	21.15
129	30.5	50.9	0.334	859.2	41.4	1.31	54.23
130	27.3	41.8	1.561	225.5	39.8	0.32	12.74
131	30	47.1	0.997	1067	41.9	1.37	57.40
132	30	45.7	1.391	1045.3	41.6	1.25	52.00
133	31.3	52	1.318	1078	41.7	1.61	67.14
134	31.3	51.8	0.832	1107.7	41.7	1.66	69.22
135	31	49.6	0.799	857.6	41.6	1.29	53.66
136	28.5	42.4	1.569	1073.9	43	1.46	62.78
137	29.1	45.5	1.612	891	41.9	1.24	51.96
138	30	42.5	1.719	347.5	40.9	0.98	40.08
139	27.2	43.5	1.996	345.7	41.8	0.58	24.24
140	30.1	47.1	0.987	356.3	41.2	0.56	23.07
141	30.7	44.9	1.678	341.4	40.7	0.91	37.04
142	29.4	49	1.309	400.5	39.7	0.52	20.64
143	28.9	33.8	1.126	579.8	42.1	0.98	41.26
144	27	34.4	1.89	549.1	41.8	1.04	43.47
145	25.2	36.6	1.092	921.6	43.8	0.65	28.47
146	25.3	37	1.172	365.9	42.4	0.66	27.98

147	24.8	37.1	0.433	406.9	42.1	0.64	26.94
148	25.6	36.8	2.391	849.6	43.9	1.06	46.53
149	27.4	36.7	0.394	841.9	43.8	1.21	53.00
150	26.7	40.8	0.762	729.3	42.8	1.02	43.66
151	26.4	42.2	1.089	731.8	42.3	0.61	25.80
152	24.2	39.5	0.192	400.7	41.6	0.62	25.79
153	23.9	36.5	0.743	449.6	42.6	0.66	28.12
154	27.5	44.3	0.846	1002.4	42.8	1.33	56.92
155	26.3	45.1	1.069	1146.8	42.6	1.49	63.47
156	28.9	47.5	0.773	1027.5	41.6	1.4	58.24
157	29.9	43.9	0.608	674.7	41.7	0.84	35.03
158	27.7	39.2	0.231	1131.9	43.6	1.75	76.30
159	28	42.3	0.931	407.6	40.9	0.61	24.95
160	26.4	41.6	1.291	292.1	40.7	0.44	17.91
161	28.3	43	1.349	423.9	40.9	0.64	26.18
162	27.9	42.3	0.962	340.7	40.7	0.54	21.98
163	32.4	54.5	0.551	1297.2	41.1	1.9	78.09
164	30.2	56.5	1.077	1264.4	40.1	1.86	74.59
165	30.2	45.7	1.706	345.2	40.3	0.54	21.76
166	27.3	40.5	0.719	469.5	41.6	1.26	52.42
167	30.2	47.5	1.531	1104.7	39.6	1.05	41.58
168	29.9	46.4	1.312	919.8	41.7	1.17	48.79
169	29.8	43.1	1.776	619.1	40.2	0.44	17.69
170	29.9	55.5	0.718	1186.9	40.9	1.6	65.44
171	30	55.2	0.816	1182.7	40.8	1.67	68.14
172	30.1	55.3	0.917	1185.8	40.9	1.68	68.71
173	33.5	45.6	1.273	1156.4	42.2	1.52	64.14
174	33.6	45.1	0.569	1129.4	43	1.55	66.65
175	32.2	49	0.816	727.8	41.5	1.35	56.03
176	38.2	46.1	0.129	482.4	40.7	0.78	31.75

177	33.4	65.5	0.312	569.8	39.1	0.83	32.45
178	33.2	62.5	0.671	574.8	38.9	0.87	33.84
179	32.6	50.4	1.115	572.9	42.8	1.02	43.66
180	30.1	41.9	1.89	398.9	40.1	0.91	36.49
181	26	37.5	0.557	510.6	41.9	0.4	16.76
182	25.7	37.6	0.723	594.4	41.8	0.42	17.56
183	26	37.9	1.006	435	41.9	0.43	18.02
184	25.3	36.6	1.094	862.4	41.5	0.69	28.64
185	25.3	39.2	0.759	759.8	43	1.02	43.86
186	26.8	41.9	0.694	717.4	42.8	1.02	43.66
187	25.1	37.1	0.269	544.7	42.7	0.8	34.16
188	26.6	45.4	0.989	1126	42.1	1.53	64.41
189	24.9	38.3	1.469	274.8	41	0.41	16.81
190	30.4	48.1	0.561	1034.8	41.6	1.42	59.07
191	25.5	41.6	0.896	294.4	40.4	0.43	17.37
192	26.7	44.5	0.981	656.4	42.3	0.83	35.11
193	30	41.6	0.342	1262.2	43.4	1.53	66.40
194	27.1	42.1	0.916	423.1	41.1	0.62	25.48
195	26.3	40.7	0.716	289.7	40.8	0.44	17.95
196	28.9	43	1.189	430.7	41	0.66	27.06
197	30.1	42.1	0.998	355.1	41.1	0.56	23.02
198	31.8	55.3	0.306	1301.2	41	1.91	78.31
199	29.6	55.8	0.971	1315.7	40.9	1.92	78.53
200	30.5	55.3	0.643	811.3	39.7	1.37	54.39
201	30.4	56.2	0.342	1296.8	40.6	1.92	77.95
202	30.5	44.8	1.59	341.9	40.4	0.51	20.60
203	28.9	40.8	1.692	1082.9	43	1.44	61.92
204	29.8	45	2.491	992.9	41.7	0.95	39.62
205	28.5	42.2	2.961	914.4	42.7	1.26	53.80
206	30.1	54.2	0.816	1183.2	41.2	1.69	69.63

207	30.7	54.3	1.089	1186.7	41.2	1.68	69.22
208	31.4	54.4	0.475	1187.6	41.3	1.69	69.80
209	31.2	51	0.608	1052.3	40	0.53	21.20
210	43.7	59.5	0.706	957.9	40.7	1.38	56.17
211	25.7	41.2	0.673	446.6	41.6	0.8	33.28
212	26.5	44.2	1.08	859.9	42.1	1.45	61.05
213	28.8	49	0.982	769.8	40.9	1.4	57.26
214	26.7	44.2	0.594	584	41.1	0.8	32.88
215	28.4	42.5	0.431	393.9	40.8	0.57	23.26
216	32.6	41.4	0.549	426.9	40.9	0.63	25.77

Tororo

S#	Temperature		Wind speed, U(m/s)	Irradiance, $H(W/m^2)$	Electrical parameters		
	Ambient, T_{amb} (K)	Cell, T_c (K)			Voltage, V(V)	Current, I (A)	Power, P(w)
1	26.8	41.5	1.37	609.4	42.2	1.12	47.26
2	27.1	42.5	2.83	677.3	41.7	1.21	50.46
3	27.6	41.9	1.75	738.1	42	1.23	51.66
4	27.5	40.7	1.4	570.1	41.1	0.97	39.87
5	27	34.4	1.92	388.5	41.3	1.4	57.82
6	27.5	37	2.46	537.1	40.9	0.77	31.49
7	27.9	41.4	2.41	819	41.7	1.49	62.13
8	29	45.2	3.71	986.5	40.9	1.46	54.05
9	30	47.3	0.41	978	41.9	1.29	54.05
10	30.4	51.9	1.34	1010.7	42.3	1.47	62.18
11	30.5	51.5	2.3	1028.8	42.5	1.45	61.63
12	30.8	53	0.53	1029.5	42.9	1.47	63.06
13	30.7	56.5	1.66	1038.5	42.8	1.64	70.19
14	31.1	55.7	0.74	1039.1	42.9	1.69	72.50

15	32	57.1	1.76	1045.8	42.6	1.39	59.21
16	31.9	59.3	1.59	1039.3	40.9	1.44	58.90
17	31.26	60.9	0.86	1027.8	42.1	1.39	58.52
18	31.96	60.4	3.18	1014.6	41.9	1.43	59.92
19	32.12	55.9	1.4	998.9	39.6	1.47	58.21
20	31.58	59.4	2.66	976.3	39.5	1.42	56.09
21	32.44	58.5	0.2	926	41.3	1.3	53.69
22	32.7	55.2	2.61	914.1	41.5	1.29	53.54
23	32.76	56.2	0.94	877.4	41.2	1.4	57.68
24	32.76	56.2	2.13	830	41.9	1.13	47.35
25	32.86	54.9	1.27	784.7	41.6	1.43	59.49
26	33.02	54.4	0.9	708.5	43.1	0.99	42.67
27	32.76	51.2	2.3	661.8	41.7	1.56	65.05
28	32.7	49.3	0.48	605.8	41.2	0.98	40.38
29	32.44	46.5	1.29	707.6	41.8	1.03	43.05
30	32.76	46.5	1.95	627.2	41.9	1.29	54.05
31	31.53	39.6	1.45	239.9	39.8	0.29	11.54
32	30.03	36.5	2.08	492.5	40.6	0.59	23.95
33	30.03	35.8	1.82	390.5	40.9	0.66	26.99
34	29.9	34.4	3.02	253.4	41.1	0.27	11.10
35	27.9	31	1.48	230.6	40.4	0.43	17.37
36	27.3	28.8	0.61	122.5	40.5	0.26	10.53
37	25.9	40.3	0.39	619.5	41.9	1.09	45.67
38	27.1	44.5	0.84	681.2	42	1.2	50.40
39	27.9	47.5	1.99	723.4	40.9	1.4	57.26
40	28.2	47.6	0.6	737.2	41.5	1.35	56.03
41	28.5	49.2	2.33	806	41.1	1.43	58.77
42	28.8	50.9	2.38	878.7	42.1	1.45	61.05
43	29.3	51.8	2.21	913.4	40.8	1.38	56.30
44	30.3	51.2	0.37	953.4	41.2	1.39	57.27

45	30.3	55.8	2.02	986	40.9	1.41	57.67
46	31	56.7	1.9	1011	42.3	1.46	61.76
47	30.5	58.3	1.86	1032	42.1	1.52	63.99
48	31.2	57.1	0.93	1029.4	42.8	1.41	60.35
49	31.3	59	0.61	1038.9	40.6	1.45	58.87
50	31.42	59.2	0.74	1040.9	40.5	1.47	59.54
51	31.74	60.1	0.77	1033.2	40.1	1.48	59.35
52	30.99	52.1	1.48	1054.8	41.2	1.44	59.33
53	30.99	55.5	2.87	1060.1	41.2	1.54	63.45
54	31.1	55.7	1.72	1006.2	40.9	1.43	58.49
55	31.31	54.7	1.49	979.5	41.8	1.32	55.18
56	31.15	54.1	1.4	991.2	42.1	1.49	62.73
57	31.26	54	1.17	968.6	42	1.26	52.92
58	31.42	51.3	0.88	930.6	40.7	1.38	56.17
59	31.15	49.9	2.43	876.8	42.1	1.43	60.20
60	31.8	49.7	0.32	833.3	40.9	1.24	50.72
61	31.53	47.8	1.15	796.1	42	1.23	51.66
62	31.58	47.2	1.56	718	42.8	1.02	43.66
63	31.85	46.7	1.59	693.8	42.9	0.99	42.47
64	32.01	46.7	0.88	650.1	40.7	0.59	24.01
65	31.8	46.5	2.73	676.9	41	0.92	37.72
66	30.94	39.8	3.01	530.4	40.9	0.74	30.27
67	30.3	36.6	1.34	459.9	40.7	0.68	27.68
68	31.05	38.3	0.75	418.5	40.3	0.64	25.79
69	29.98	34.6	1.52	165.7	40.6	0.25	10.15
70	30.14	34.7	0.63	114.3	39	0.28	10.92
71	28.81	29.3	0.24	50.4	38.4	0.09	3.46
72	27.95	27.4	0.54	32.6	38	0.08	3.04
73	22.6	29.6	0.320	259.2	41	0.39	15.99
74	23.0	30.6	0.420	323.6	41.2	0.44	18.13

75	23.7	33.8	0.660	380.4	41.6	0.59	24.54
76	24.1	36.3	0.230	413.1	41.5	0.71	29.47
77	25.0	38.4	0.830	483.7	41.9	0.78	32.68
78	25.4	40.5	0.600	561.7	42.4	0.84	35.62
79	25.5	40.5	1.260	736.9	42.2	1.21	51.06
80	26.2	45.0	2.690	864	42.9	1.42	60.92
81	27.4	48.2	0.240	885	43.1	1.43	61.63
82	27.4	49.3	1.230	931.3	41.9	1.34	56.15
83	27.8	48.4	1.380	853	41.6	1.27	52.83
84	28.1	45.8	2.290	856.6	41.7	1.29	53.79
85	28.4	53.0	0.770	1224.9	43	1.53	65.79
86	27.6	44.6	2.220	504.6	41.1	1.22	50.14
87	28.3	49.8	3.110	564.7	42.6	1.35	57.51
88	28.7	52.7	0.960	1049	42	1.33	55.86
89	29.1	52.9	1.360	994.1	41.9	1.31	54.89
90	29.2	54.0	1.720	1064	41.3	1.42	58.65
91	29.1	54.2	1.410	306.4	42.1	0.43	18.10
92	28.8	44.4	1.250	1084.5	41.4	1.04	43.06
93	29.0	46.9	1.060	240.8	41.9	0.34	14.25
94	29.7	48.8	2.570	994.9	42.1	1.56	65.68
95	31.1	55.3	1.960	970.5	41.8	1.46	61.03
96	30.1	51.8	1.590	912.9	40.3	1.49	60.05
97	30.6	52.2	0.750	836.9	43.1	1.26	54.31
98	31.0	52.2	0.740	759.7	42.1	1.23	51.78
99	30.3	47.5	1.810	677.3	40.9	0.98	40.08
100	29.2	39.7	2.410	469.6	40.2	0.69	27.74
101	29.3	38.2	1.660	494.1	42	0.85	35.70
102	29.1	37.5	1.600	444.1	40.5	0.59	23.90
103	29.0	36.9	2.430	274.7	41.4	0.39	16.15
104	27.6	31.6	1.440	162.2	40.2	0.19	7.64

105	27.5	30.4	0.760	197	41.7	0.88	36.70
106	28.8	33.5	0.590	281.9	41.9	0.39	16.34
107	28.8	32.9	1.130	300.8	41	0.46	18.86
108	27.6	30.9	1.440	239.8	41.4	0.35	14.49
109	25.98	36.3	3.72	540.5	42.9	0.87	37.32
110	26.46	38.4	2.6	625.2	42	1.13	47.46
111	27.2	40.9	2.54	689.7	41.6	1.4	58.24
112	27.74	44.2	3.24	777.6	40.9	1.4	57.26
113	28.11	46.7	4.74	828.8	42.3	1.09	46.11
114	28.75	48.8	4.1	889.3	43.4	1.21	52.51
115	28.59	50.9	3.21	939.1	41.3	1.5	61.95
116	29.02	50.3	3.47	1014.9	42.7	1.58	67.47
117	29.18	50.6	3.83	907.6	42.5	1.51	64.18
118	29.45	52.5	5.5	474.4	41.3	0.74	30.56
119	28.97	43.5	2.37	460.3	41.2	0.69	28.43
120	28.22	40.4	2.41	457.7	41.5	0.65	26.98
121	28.65	40.3	2.54	475.6	41.4	0.78	32.29
122	28.38	40.1	2.47	650.9	41.9	1.5	62.85
123	28.86	45.2	2.19	570.3	41.8	1.28	53.50
124	28.86	43.9	3.91	508.5	40.9	1.24	50.72
125	29.23	45.1	2.06	1022.9	42.9	1.42	60.92
126	29.71	46.5	2.67	760.1	41.4	1.43	59.20
127	29.18	43.4	3.71	448	40.9	0.93	38.04
128	29.29	43.7	3.48	1193.9	42.9	1.56	66.92
129	30.57	51.7	1.94	1156.1	43.2	1.62	69.98
130	31.1	55.9	2.15	1039.9	42.4	1.43	60.63
131	30.73	53	2.35	1064.7	42.3	1.46	61.76
132	31.58	53.2	0.68	960.2	42	1.39	58.38
133	31.26	46.4	0.58	452	40.8	0.89	36.31
134	31.1	44.1	0.26	940.8	41.9	1.42	59.50

135	30.41	41.7	2.19	399.3	40.9	0.49	20.04
136	25.82	30.3	3.1	304.9	40.4	0.59	23.84
137	25.5	32.7	2.34	570.9	41.2	0.92	37.90
138	23.15	26.9	3.18	187.7	40.4	0.35	14.14
139	23.15	25.6	3.07	178.1	40.2	0.33	13.27
140	23.41	25.8	1.3	170.5	40	0.32	12.80
141	23.04	24.8	3	98.8	38.9	0.16	6.22
142	23.09	24.1	0.75	76.7	38.8	0.12	4.66
143	22.99	23.3	1.07	51	38.7	0.11	4.26
144	22.99	22.9	0.56	36.8	38	0.08	3.04
145	25.44	41.1	0.71	576	40.9	1.01	41.31
146	26.14	43.8	1.02	695.5	41.8	1.22	51.00
147	26.78	47.7	0.93	771.6	42.3	1.18	49.91
148	26.62	46.3	0.43	559.4	41.2	1.1	45.32
149	27.26	46.1	0.8	586.9	41.4	1.2	49.68
150	27.2	45.5	0.92	715.8	40.9	1.09	44.58
151	28.06	48.5	0.26	1081.2	42.5	1.46	62.05
152	28.16	46.6	1.93	555.6	41.6	1.12	46.59
153	28.91	49	0.81	1284.5	41.9	1.64	68.72
154	29.5	55.7	1.57	802.2	41	1.17	47.97
155	29.45	49.4	0.43	881.4	41.2	1.14	46.97
156	30.03	52.5	0.33	598.8	40.9	0.79	32.31
157	29.61	52.2	2.31	818.2	41.4	1.12	46.37
158	30.83	55.2	1.56	1314	42.2	2.29	96.64
159	30.73	55.9	1.03	1240	41.9	1.45	60.76
160	30.09	54.9	1.2	999.6	42.1	1.59	66.94
161	32.01	57.9	1.05	297.5	40.1	0.95	38.10
162	30.62	48	1.59	1102.4	41.2	1.64	67.57
163	30.51	55.2	2.37	299	40.2	0.46	18.49
164	31.58	55.3	1.14	958.5	41.7	1.3	54.21

165	32.97	59.9	2.65	1133	40.3	1.73	69.72
166	32.06	54.1	1.18	1039.9	39.6	1.51	59.80
167	32.76	58.4	2.47	870	40.6	1.09	44.25
168	30.83	46.8	2.68	377.6	41.1	0.48	19.73
169	30.14	40.5	1.75	219.2	41	0.31	12.71
170	31.21	45.4	1.97	755	40.9	1.19	48.67
171	31.64	49.5	2.49	792.4	41.2	1.52	62.62
172	31.05	46.9	2.23	243.7	41	0.4	16.40
173	26.24	30.7	1.26	255.4	41.3	0.46	19.00
174	24.48	28	1.53	257.9	41.4	0.51	21.11
175	25.76	30.6	2.02	302.4	41.7	0.64	26.69
176	25.6	30.5	2.76	198.1	40.2	0.49	19.70
177	23.68	25.3	2.15	86.6	40.9	0.17	6.95
178	23.15	24.1	2.02	92.9	39.8	0.18	7.16
179	23.57	25	2.28	146	40.6	0.34	13.80
180	23.95	24.9	2.52	110.2	40.4	0.32	12.93
181	25.3	29.9	0.35	187.9	41.3	0.31	12.80
182	28.6	36.8	0.275	512.4	41.7	0.88	36.70
183	26.1	31.5	0.842	270.4	41.3	0.39	16.11
184	30.6	39.2	0.289	1078.9	43.2	1.65	71.28
185	28.9	46.2	0.712	1031	42.9	1.64	70.36
186	28	41.7	0.532	1022.2	42.8	1.41	60.35
187	29.7	45	0.431	1071.6	42.4	1.45	61.48
188	30.7	49.3	0.892	1206.9	41.8	1.66	69.39
189	32.7	41.4	0.609	352.3	41	0.98	40.18
190	32	42	0.8	761.6	42.5	1.22	51.85
191	36.5	60.6	0.413	1200.6	40.2	1.84	73.97
192	36.4	64.2	0.433	1134.5	40.3	1.73	69.72
193	40	64.7	0.361	1220.6	39.8	1.76	70.05
194	37.7	64.9	0.439	1071.3	39.6	1.51	59.80

195	30.1	43.6	0.739	1120.5	41	1.82	74.62
196	31.1	43.5	0.716	1146.5	42.3	1.39	58.80
197	30.8	43.5	0.406	1147.1	42.6	1.39	59.21
198	31.3	43.6	0.493	998.9	41.3	1.32	54.52
199	38.5	61.2	1.41	1068.9	39.8	1.53	60.89
200	39.3	61.3	0.51	1067.8	40	1.55	62.00
201	40.3	61.4	0.7	1066.7	39.8	1.59	63.28
202	39.8	61	2.01	1069.7	39.9	1.51	60.25
203	26.4	32.2	1.89	410.2	42.2	0.51	21.52
204	25.8	40.8	1.71	410.6	41	0.63	25.83
205	27.8	42.2	1.93	319.9	40.1	0.44	17.64
206	28.9	45.2	0.84	1034.7	42.1	1.53	64.41
207	27.9	49.8	0.942	549.2	40.2	0.81	32.56
208	32.9	45.9	0.831	680.1	41.4	0.88	36.43
209	30	48.1	0.468	370.4	40	0.55	22.00
210	29.8	47.6	0.45	355.5	40	0.54	21.60
211	22.83	24.4	1.05	81.2	39.9	0.19	7.58
212	23.25	23.9	2.27	92.6	39.9	0.23	9.18
213	23.31	24.9	1.04	88.7	39	0.12	4.68
214	23.04	23.6	0.51	71.6	39.4	0.12	4.73
215	22.67	23	0.14	47.1	38.3	0.09	3.45
216	22.51	23.2	0.21	69.7	38.8	0.1	3.88

APPENDIX IX: TRANSMISSION LINE DATA FOR KAWANDA – BUJAGALI AND MBARARA NORTH-MASAKA WEST

Kawanda - Bujagali					
Date	Time	Time	KWAD 220 kV Bujagali 1 MW	KWAD 220 kV Bus Bar kV	System frequency
2022-07-01	0:00	1:00	-63.34	232.30	50.18
	1:00	2:00	-56.57	233.23	50.09
	2:00	3:00	-55.40	233.56	50.22
	3:00	4:00	-55.68	232.13	50.12
	4:00	5:00	-56.31	231.99	50.09
	5:00	6:00	-60.43	230.84	50.05
	6:00	7:00	-65.08	228.00	50.05
	7:00	8:00	-64.69	226.93	49.99
	8:00	9:00	-71.61	225.92	50.05
	9:00	10:00	-68.50	226.72	50.09
	10:00	11:00	-57.36	225.92	50.08
	11:00	12:00	0.00	0.00	0.00
	12:00	13:00	0.00	0.00	0.00
	13:00	14:00	-53.85	231.87	50.18
	14:00	15:00	-54.94	230.84	50.14
	15:00	16:00	-48.16	232.70	50.17
	16:00	17:00	-50.63	231.44	50.14

Mbarara North-Masaka West					
Date	Time	Time	MSKW 132kV Mbarara North MW	MSKW 132 kV Bus Bar Voltage	System frequency
2022-07-01	0:00	1:00	4.85	134.03	50.01
	1:00	2:00	-0.26	134.64	50.13
	2:00	3:00	-0.29	135.05	50.04
	3:00	4:00	2.30	133.98	50.17
	4:00	5:00	2.26	133.96	50.07
	5:00	6:00	2.73	133.55	50.04
	6:00	7:00	-0.97	131.86	50.00
	7:00	8:00	-0.26	130.96	49.99
	8:00	9:00	1.35	129.80	49.94
	9:00	10:00	2.74	130.67	50.00
	10:00	11:00	4.98	129.98	50.04
	11:00	12:00	0.00	0.00	50.03
	12:00	13:00	0.00	0.00	50.65
	13:00	14:00	2.02	134.12	50.55
	14:00	15:00	4.40	133.62	50.13
	15:00	16:00	3.44	134.60	50.09
	16:00	17:00	4.74	133.13	50.12

	17:00	18:00	-54.24	231.20	50.13
	18:00	19:00	-67.17	234.19	50.13
	19:00	20:00	-90.87	233.76	50.11
	20:00	21:00	-95.10	233.48	50.07
	21:00	22:00	-91.56	234.55	50.17
	22:00	23:00	-80.80	235.76	50.22
	23:00	0:00	-67.49	230.33	50.12
2022-07-02	0:00	1:00	-63.44	232.09	50.15
	1:00	2:00	-58.69	233.54	50.14
	2:00	3:00	-57.63	234.35	50.19
	3:00	4:00	-56.41	234.26	50.04
	4:00	5:00	-55.58	234.70	50.07
	5:00	6:00	-55.36	234.63	49.99
	6:00	7:00	-60.41	232.72	50.08
	7:00	8:00	-68.88	230.69	50.09
	8:00	9:00	-75.78	231.18	49.97
	9:00	10:00	-83.08	230.96	50.00
	10:00	11:00	-86.71	230.10	50.25
	11:00	12:00	-83.47	227.73	49.95
	12:00	13:00	-82.39	231.03	49.95
	13:00	14:00	-62.55	232.85	50.13
	14:00	15:00	-58.02	231.54	50.04
	15:00	16:00	-55.71	230.87	50.05
	16:00	17:00	-54.84	230.67	49.96
	17:00	18:00	-54.37	233.47	50.09
	18:00	19:00	-71.21	233.32	50.05
	19:00	20:00	-87.86	229.83	50.14
	20:00	21:00	-93.22	230.51	50.21
	21:00	22:00	-89.21	231.48	50.17

	17:00	18:00	6.53	132.43	50.09
	18:00	19:00	5.16	134.54	50.08
	19:00	20:00	12.93	136.15	50.08
	20:00	21:00	15.60	136.02	50.06
	21:00	22:00	13.21	135.50	50.02
	22:00	23:00	5.33	136.46	50.12
	23:00	0:00	0.86	133.59	50.17
2022-07-02	0:00	1:00	3.86	134.38	50.07
	1:00	2:00	1.80	134.96	50.10
	2:00	3:00	2.51	135.62	50.09
	3:00	4:00	3.04	135.46	50.14
	4:00	5:00	2.01	135.72	49.99
	5:00	6:00	0.56	135.69	50.02
	6:00	7:00	0.34	134.59	49.94
	7:00	8:00	5.76	133.47	50.03
	8:00	9:00	5.20	133.34	50.04
	9:00	10:00	7.64	132.86	49.92
	10:00	11:00	11.73	131.97	49.95
	11:00	12:00	10.42	130.68	50.20
	12:00	13:00	8.30	134.77	49.90
	13:00	14:00	7.45	135.16	49.90
	14:00	15:00	8.91	134.26	50.08
	15:00	16:00	3.54	133.11	49.99
	16:00	17:00	4.55	132.38	50.00
	17:00	18:00	6.14	134.04	49.91
	18:00	19:00	3.88	134.01	50.04
	19:00	20:00	9.13	132.36	50.00
	20:00	21:00	12.46	132.82	50.09
	21:00	22:00	9.46	133.57	50.16

	22:00	23:00	-81.02	234.22	50.16
	23:00	0:00	-68.98	234.48	50.25
2022-07-03	0:00	1:00	-62.59	235.69	50.15
	1:00	2:00	-58.11	235.36	50.15
	2:00	3:00	-53.32	236.27	50.01
	3:00	4:00	-50.95	237.21	50.12
	4:00	5:00	-50.93	237.77	50.18
	5:00	6:00	-52.52	237.92	50.21
	6:00	7:00	-65.81	234.63	50.06
	7:00	8:00	-86.79	229.10	49.94
	8:00	9:00	-84.97	231.95	50.14
	9:00	10:00	-83.72	231.43	50.24
	10:00	11:00	-86.04	228.98	50.09
	11:00	12:00	-85.15	230.22	50.16
	12:00	13:00	-85.45	230.80	50.11
	13:00	14:00	-85.57	232.50	50.12
	14:00	15:00	-80.20	233.47	50.03
	15:00	16:00	-81.38	231.46	49.94
	16:00	17:00	-82.87	232.43	50.04
	17:00	18:00	-87.87	230.93	50.09
	18:00	19:00	-93.53	227.34	49.91
	19:00	20:00	-119.93	229.53	50.01
	20:00	21:00	-136.32	224.40	50.16
	21:00	22:00	-92.00	230.38	50.17
	22:00	23:00	-74.82	231.62	50.25
	23:00	0:00	-61.93	232.74	50.13

	22:00	23:00	7.16	135.66	50.12
	23:00	0:00	0.98	135.89	50.11
2022-07-03	0:00	1:00	3.91	136.60	50.20
	1:00	2:00	3.52	136.50	50.10
	2:00	3:00	0.89	136.95	50.10
	3:00	4:00	-1.49	137.57	49.96
	4:00	5:00	-0.98	138.02	50.07
	5:00	6:00	0.17	138.03	50.13
	6:00	7:00	-2.95	136.04	50.16
	7:00	8:00	-4.19	132.57	50.01
	8:00	9:00	-0.34	133.74	49.89
	9:00	10:00	1.35	133.46	50.09
	10:00	11:00	2.96	131.90	50.19
	11:00	12:00	2.07	132.50	50.04
	12:00	13:00	2.89	132.69	50.11
	13:00	14:00	2.75	133.44	50.06
	14:00	15:00	2.56	134.09	50.07
	15:00	16:00	1.63	132.85	49.98
	16:00	17:00	5.36	133.31	49.89
	17:00	18:00	6.38	132.40	49.99
	18:00	19:00	2.36	130.28	50.04
	19:00	20:00	9.52	133.80	49.86
	20:00	21:00	12.11	131.60	49.96
	21:00	22:00	9.41	134.04	50.11
	22:00	23:00	5.47	134.46	50.12
	23:00	0:00	1.19	134.62	50.20

2022-07-04	0:00	1:00	-54.38	234.62	50.08
	1:00	2:00	-66.74	235.99	50.16
	2:00	3:00	-84.99	234.85	50.06
	3:00	4:00	-83.96	234.57	49.97
	4:00	5:00	-76.40	235.32	50.04
	5:00	6:00	-54.13	235.18	50.00
	6:00	7:00	-60.91	233.35	50.03
	7:00	8:00	-66.44	230.18	50.18
	8:00	9:00	-74.32	229.67	50.01
	9:00	10:00	-74.94	230.17	50.17
	10:00	11:00	-60.35	231.84	50.14
	11:00	12:00	-60.03	230.50	50.02
	12:00	13:00	-59.13	230.94	50.04
	13:00	14:00	-56.50	233.90	50.21
	14:00	15:00	-56.39	229.42	49.97
	15:00	16:00	-55.75	230.23	50.01
	16:00	17:00	-57.96	229.92	50.03
	17:00	18:00	-61.89	230.37	49.95
	18:00	19:00	-77.04	233.17	50.24
	19:00	20:00	-91.26	228.83	49.99
	20:00	21:00	-99.74	228.85	50.13
	21:00	22:00	-95.05	231.19	50.15
	22:00	23:00	-82.91	231.15	50.19
	23:00	0:00	-68.75	231.37	50.24
2022-07-05	0:00	1:00	-63.01	232.98	50.14
	1:00	2:00	-60.30	233.58	50.19
	2:00	3:00	-59.15	232.50	50.13
	3:00	4:00	-57.95	232.31	50.02

2022-07-04	0:00	1:00	1.92	135.72	50.08
	1:00	2:00	2.63	136.62	50.03
	2:00	3:00	0.64	135.90	50.11
	3:00	4:00	0.34	135.69	50.01
	4:00	5:00	1.28	136.25	49.92
	5:00	6:00	4.15	136.25	49.99
	6:00	7:00	6.56	134.84	49.95
	7:00	8:00	9.44	133.29	49.98
	8:00	9:00	7.14	132.96	50.13
	9:00	10:00	10.65	133.04	49.96
	10:00	11:00	12.28	134.78	50.12
	11:00	12:00	10.30	133.90	50.09
	12:00	13:00	9.81	134.14	49.97
	13:00	14:00	8.81	135.62	49.99
	14:00	15:00	9.26	132.39	50.16
	15:00	16:00	8.26	132.98	49.92
	16:00	17:00	10.42	132.36	49.96
	17:00	18:00	11.95	132.36	49.98
	18:00	19:00	8.56	133.94	49.90
	19:00	20:00	11.23	132.05	50.19
	20:00	21:00	16.01	132.17	49.94
	21:00	22:00	12.27	133.72	50.08
	22:00	23:00	7.09	133.83	50.10
	23:00	0:00	1.73	134.08	50.14
2022-07-05	0:00	1:00	4.52	134.82	50.19
	1:00	2:00	4.00	135.14	50.09
	2:00	3:00	5.88	134.64	50.14
	3:00	4:00	5.38	134.37	50.08

	4:00	5:00	-59.52	232.39	50.12
	5:00	6:00	-66.69	230.90	50.09
	6:00	7:00	-71.90	228.44	49.93
	7:00	8:00	-75.65	229.08	50.03
	8:00	9:00	-78.85	232.31	50.04
	9:00	10:00	-79.57	228.75	50.19
	10:00	11:00	-60.79	226.90	50.11
	11:00	12:00	-60.17	228.43	50.10
	12:00	13:00	-59.61	228.08	49.92
	13:00	14:00	-65.83	232.57	50.00
	14:00	15:00	-69.51	230.90	50.00
	15:00	16:00	-61.41	229.89	49.91
	16:00	17:00	-62.12	230.89	50.17
	17:00	18:00	-59.56	231.39	50.09
	18:00	19:00	-79.22	232.03	50.09
	19:00	20:00	-94.56	228.71	49.81
	20:00	21:00	-100.24	229.59	50.15
	21:00	22:00	-97.21	232.32	50.18
	22:00	23:00	-82.31	232.05	50.10
	23:00	0:00	-69.27	230.54	50.10
2022-07-06	0:00	1:00	-65.32	231.56	50.13
	1:00	2:00	-60.23	231.63	50.16
	2:00	3:00	-57.66	232.63	50.14
	3:00	4:00	-58.84	232.13	50.07
	4:00	5:00	-61.22	231.92	50.08
	5:00	6:00	-65.83	230.58	50.08
	6:00	7:00	-72.65	228.75	50.10
	7:00	8:00	-75.67	228.36	50.06

	4:00	5:00	7.60	134.52	49.97
	5:00	6:00	10.00	133.75	50.07
	6:00	7:00	10.42	131.86	50.04
	7:00	8:00	13.78	132.47	49.88
	8:00	9:00	12.91	133.91	49.98
	9:00	10:00	13.53	131.40	49.99
	10:00	11:00	14.30	130.27	50.14
	11:00	12:00	11.37	131.72	50.06
	12:00	13:00	10.52	131.54	50.05
	13:00	14:00	12.51	134.73	49.87
	14:00	15:00	11.36	133.76	49.95
	15:00	16:00	15.99	133.20	49.95
	16:00	17:00	18.52	133.23	49.86
	17:00	18:00	11.42	132.38	50.12
	18:00	19:00	9.44	133.24	50.04
	19:00	20:00	15.50	132.00	50.04
	20:00	21:00	17.58	133.08	49.76
	21:00	22:00	16.43	135.26	50.10
	22:00	23:00	5.73	135.19	50.13
	23:00	0:00	0.31	133.78	50.05
2022-07-06	0:00	1:00	4.96	134.05	50.05
	1:00	2:00	4.62	134.33	50.08
	2:00	3:00	2.26	135.12	50.11
	3:00	4:00	4.14	134.67	50.09
	4:00	5:00	7.61	134.62	50.02
	5:00	6:00	8.39	133.88	50.03
	6:00	7:00	10.85	132.57	50.03
	7:00	8:00	12.16	132.24	50.05

	8:00	9:00	-80.62	226.52	49.99
	9:00	10:00	-70.75	226.74	50.15
	10:00	11:00	-62.64	226.59	50.16
	11:00	12:00	-60.39	226.85	50.00
	12:00	13:00	-61.24	229.14	49.94
	13:00	14:00	-56.67	231.23	49.81
	14:00	15:00	-59.03	228.77	49.99
	15:00	16:00	-59.37	227.30	49.93
	16:00	17:00	-65.76	229.14	49.99
	17:00	18:00	-84.08	232.10	50.27
	18:00	19:00	-83.58	233.97	50.10
	19:00	20:00	-95.84	229.11	49.81
	20:00	21:00	-102.98	229.85	50.07
	21:00	22:00	-100.34	232.50	50.24
	22:00	23:00	-86.39	233.26	50.06
	23:00	0:00	-72.44	234.59	50.19
2022-07-07	0:00	1:00	-67.76	231.23	50.10
	1:00	2:00	-63.90	232.09	50.06
	2:00	3:00	-62.01	232.12	50.03
	3:00	4:00	-61.08	233.18	50.14
	4:00	5:00	-61.31	233.49	50.10
	5:00	6:00	-65.62	232.34	50.07
	6:00	7:00	-71.08	229.52	50.06
	7:00	8:00	-74.13	227.24	50.09
	8:00	9:00	-80.92	226.76	50.05
	9:00	10:00	-85.60	229.00	50.05
	10:00	11:00	-72.18	227.88	49.98

	8:00	9:00	13.71	131.54	50.01
	9:00	10:00	17.83	131.47	49.94
	10:00	11:00	19.71	131.01	50.10
	11:00	12:00	15.10	131.24	50.11
	12:00	13:00	15.72	133.55	49.95
	13:00	14:00	11.78	133.77	49.89
	14:00	15:00	13.61	131.66	49.76
	15:00	16:00	13.26	130.50	49.94
	16:00	17:00	14.79	131.68	49.88
	17:00	18:00	14.35	133.08	49.94
	18:00	19:00	12.07	134.06	50.22
	19:00	20:00	16.25	131.42	50.05
	20:00	21:00	20.62	132.00	49.76
	21:00	22:00	20.40	133.84	50.02
	22:00	23:00	14.61	134.92	50.19
	23:00	0:00	6.71	135.92	50.01
2022-07-07	0:00	1:00	9.65	132.83	50.13
	1:00	2:00	9.06	133.47	50.05
	2:00	3:00	7.17	133.64	50.01
	3:00	4:00	6.40	134.37	49.98
	4:00	5:00	8.34	134.55	50.09
	5:00	6:00	9.15	133.93	50.05
	6:00	7:00	8.85	132.01	50.02
	7:00	8:00	11.60	130.15	50.01
	8:00	9:00	13.26	128.96	50.04
	9:00	10:00	16.43	131.25	50.00
	10:00	11:00	16.93	130.67	50.00

	11:00	12:00	-61.87	229.72	50.25
	12:00	13:00	-55.93	229.31	49.98
	13:00	14:00	-58.23	234.12	50.18
	14:00	15:00	-57.03	229.92	49.95
	15:00	16:00	-60.11	229.08	50.15
	16:00	17:00	-60.79	229.35	49.99
	17:00	18:00	-65.67	233.60	50.24
	18:00	19:00	-81.56	233.98	50.27
	19:00	20:00	-96.13	229.90	50.18
	20:00	21:00	-98.12	232.13	50.07
	21:00	22:00	-94.79	232.05	50.15
	22:00	23:00	-83.15	233.07	50.20
	23:00	0:00	-73.85	234.22	50.18
2022-07-08	0:00	1:00	-66.37	234.64	50.09
	1:00	2:00	-61.89	233.57	50.00
	2:00	3:00	-60.84	234.79	50.11
	3:00	4:00	-58.16	236.10	50.09
	4:00	5:00	-57.07	236.38	50.03
	5:00	6:00	-63.99	235.02	50.10
	6:00	7:00	-68.82	231.86	49.96
	7:00	8:00	-72.67	230.20	50.08
	8:00	9:00	-80.17	225.94	50.06
	9:00	10:00	-83.31	222.90	50.00
	10:00	11:00	-72.10	227.42	50.06
	11:00	12:00	-61.41	225.37	49.98
	12:00	13:00	-62.08	227.78	50.13
	13:00	14:00	-59.59	227.78	49.92
	14:00	15:00	-61.19	224.89	49.97
	15:00	16:00	-62.16	228.38	50.19

	11:00	12:00	16.49	131.92	49.93
	12:00	13:00	16.12	131.50	50.20
	13:00	14:00	15.09	134.65	49.93
	14:00	15:00	11.54	132.57	50.13
	15:00	16:00	12.87	131.93	49.90
	16:00	17:00	14.60	131.66	50.10
	17:00	18:00	15.74	134.27	49.94
	18:00	19:00	10.77	134.08	50.19
	19:00	20:00	18.82	133.37	50.22
	20:00	21:00	17.96	136.05	50.13
	21:00	22:00	17.31	135.07	50.02
	22:00	23:00	11.32	134.45	50.10
	23:00	0:00	7.05	135.31	50.15
2022-07-08	0:00	1:00	10.90	135.16	50.13
	1:00	2:00	8.27	134.28	50.04
	2:00	3:00	8.94	135.12	49.95
	3:00	4:00	8.25	136.22	50.06
	4:00	5:00	7.59	136.41	50.04
	5:00	6:00	10.75	135.67	49.98
	6:00	7:00	9.77	133.46	50.05
	7:00	8:00	11.85	132.23	49.91
	8:00	9:00	16.02	129.22	50.03
	9:00	10:00	16.53	127.55	50.01
	10:00	11:00	17.51	132.63	49.95
	11:00	12:00	16.50	130.95	50.01
	12:00	13:00	18.19	132.20	49.93
	13:00	14:00	16.33	131.83	50.08
	14:00	15:00	15.97	130.10	49.87
	15:00	16:00	18.23	132.82	49.92

	16:00	17:00	-62.41	232.72	50.13
	17:00	18:00	-79.51	233.73	50.03
	18:00	19:00	-82.68	234.78	50.17
	19:00	20:00	-95.49	232.12	50.28
	20:00	21:00	-99.08	230.74	50.14
	21:00	22:00	-96.70	233.02	50.05
	22:00	23:00	-86.27	233.46	50.24
	23:00	0:00	-76.19	233.20	50.15
2022-07-09	0:00	1:00	-69.76	230.88	50.24
	1:00	2:00	-64.23	230.87	50.15
	2:00	3:00	-61.66	231.15	50.10
	3:00	4:00	-59.84	231.75	50.15
	4:00	5:00	-55.09	232.78	50.04
	5:00	6:00	-56.35	233.20	50.13
	6:00	7:00	-58.16	232.46	50.03
	7:00	8:00	-65.26	229.00	50.03
	8:00	9:00	-73.04	226.67	50.01
	9:00	10:00	-80.66	225.19	50.04
	10:00	11:00	-79.19	223.70	50.00
	11:00	12:00	-64.73	225.62	50.14
	12:00	13:00	-58.10	224.02	49.94
	13:00	14:00	-56.42	225.20	50.08
	14:00	15:00	-56.39	226.30	50.24
	15:00	16:00	-53.83	227.25	49.96
	16:00	17:00	-54.93	231.28	50.08
	17:00	18:00	-54.14	234.44	50.02
	18:00	19:00	-69.09	234.22	50.14
	19:00	20:00	-86.67	227.07	50.13
	20:00	21:00	-90.88	227.21	50.15

	16:00	17:00	19.66	135.52	50.14
	17:00	18:00	16.13	135.95	50.08
	18:00	19:00	13.45	134.45	49.98
	19:00	20:00	19.15	133.12	50.12
	20:00	21:00	19.03	132.41	50.23
	21:00	22:00	18.68	133.84	50.09
	22:00	23:00	13.75	135.09	50.00
	23:00	0:00	8.19	134.96	50.19
2022-07-09	0:00	1:00	11.90	133.27	50.10
	1:00	2:00	10.23	133.34	50.19
	2:00	3:00	8.71	133.56	50.10
	3:00	4:00	8.18	134.02	50.05
	4:00	5:00	4.54	134.67	50.10
	5:00	6:00	6.30	135.18	49.99
	6:00	7:00	3.58	134.84	50.08
	7:00	8:00	8.91	132.15	49.98
	8:00	9:00	11.08	130.60	49.98
	9:00	10:00	13.92	129.61	49.96
	10:00	11:00	14.24	128.62	49.99
	11:00	12:00	15.97	129.42	49.95
	12:00	13:00	16.73	128.58	50.09
	13:00	14:00	13.38	129.23	49.89
	14:00	15:00	13.06	129.88	50.03
	15:00	16:00	11.60	130.37	50.19
	16:00	17:00	13.73	134.75	49.91
	17:00	18:00	14.02	137.50	50.03
	18:00	19:00	9.52	136.33	49.97
	19:00	20:00	12.36	131.22	50.09
	20:00	21:00	11.51	131.26	50.07

	21:00	22:00	-86.89	230.27	50.13
	22:00	23:00	-76.01	228.95	50.17
	23:00	0:00	-61.17	233.91	50.25
2022-07-10	0:00	1:00	-59.25	232.57	50.19
	1:00	2:00	-55.25	233.19	50.21
	2:00	3:00	-51.95	234.80	50.01
	3:00	4:00	-49.47	235.90	50.11
	4:00	5:00	-49.33	236.71	50.16
	5:00	6:00	-49.35	237.50	50.16
	6:00	7:00	-51.07	236.93	50.17
	7:00	8:00	-83.92	231.21	49.96
	8:00	9:00	-107.62	231.73	50.17
	9:00	10:00	-116.94	227.53	50.09
	10:00	11:00	-116.40	226.61	50.32
	11:00	12:00	-113.40	225.09	49.91
	12:00	13:00	-112.06	226.43	50.09
	13:00	14:00	-92.50	229.30	50.21
	14:00	15:00	-77.94	227.29	49.92
	15:00	16:00	-78.67	227.72	50.05
	16:00	17:00	-103.48	227.91	50.20
	17:00	18:00	-112.60	228.30	50.17

	21:00	22:00	10.62	133.18	50.10
	22:00	23:00	5.71	132.86	50.08
	23:00	0:00	0.00	144.95	50.12
2022-07-10	0:00	1:00	0.00	135.75	50.20
	1:00	2:00	0.00	135.12	50.14
	2:00	3:00	0.00	135.73	50.16
	3:00	4:00	0.00	135.70	49.96
	4:00	5:00	0.00	136.04	50.06
	5:00	6:00	0.00	136.66	50.11
	6:00	7:00	0.00	136.65	50.11
	7:00	8:00	0.00	133.39	50.12
	8:00	9:00	0.00	134.04	49.91
	9:00	10:00	0.00	132.15	50.12
	10:00	11:00	0.00	130.96	50.04
	11:00	12:00	0.00	129.97	50.27
	12:00	13:00	0.00	130.81	49.86
	13:00	14:00	0.00	133.12	50.04
	14:00	15:00	0.00	131.88	50.16
	15:00	16:00	0.00	132.31	49.87
	16:00	17:00	0.00	132.20	50.00
	17:00	18:00	0.00	132.29	50.15

	18:00	19:00	-111.73	230.33	49.95
	19:00	20:00	-120.13	226.73	49.98
	20:00	21:00	-92.61	232.63	50.05
	21:00	22:00	-88.99	233.60	50.17
	22:00	23:00	-77.86	236.06	50.12
	23:00	0:00	-63.00	234.18	50.11
2022-07-11	0:00	1:00	-57.93	235.41	50.22
	1:00	2:00	-51.01	237.14	50.19
	2:00	3:00	-49.18	237.95	50.23
	3:00	4:00	-48.90	237.96	50.24
	4:00	5:00	-49.28	236.85	50.00
	5:00	6:00	-54.02	236.14	50.08
	6:00	7:00	-61.74	232.50	50.04
	7:00	8:00	-66.52	229.04	50.06
	8:00	9:00	-75.31	226.77	49.94
	9:00	10:00	-78.34	229.34	50.11
	10:00	11:00	-75.02	229.44	50.08
	11:00	12:00	-78.11	226.29	49.97
	12:00	13:00	-79.17	229.54	49.98
	13:00	14:00	-76.27	232.86	50.13
	14:00	15:00	-76.01	230.95	49.98
	15:00	16:00	-77.07	229.67	49.93
	16:00	17:00	-79.19	229.83	49.95
	17:00	18:00	-82.06	232.73	50.11
	18:00	19:00	-81.60	236.31	50.11
	19:00	20:00	-95.56	232.19	49.94
	20:00	21:00	-99.86	233.19	50.10

	18:00	19:00	0.16	132.36	50.12
	19:00	20:00	0.00	130.86	49.90
	20:00	21:00	11.03	133.53	49.93
	21:00	22:00	15.80	134.63	50.00
	22:00	23:00	11.20	136.61	50.12
	23:00	0:00	5.89	135.69	50.06
2022-07-11	0:00	1:00	9.69	137.43	50.06
	1:00	2:00	5.47	138.51	50.17
	2:00	3:00	5.61	139.13	50.14
	3:00	4:00	6.68	139.26	50.18
	4:00	5:00	6.63	138.44	50.19
	5:00	6:00	7.70	138.28	49.95
	6:00	7:00	7.77	136.24	50.03
	7:00	8:00	8.38	134.19	49.99
	8:00	9:00	8.39	131.20	50.01
	9:00	10:00	6.31	131.52	49.89
	10:00	11:00	7.56	132.56	50.06
	11:00	12:00	10.29	131.15	50.03
	12:00	13:00	11.47	132.58	49.92
	13:00	14:00	8.52	134.77	49.93
	14:00	15:00	8.10	133.64	50.08
	15:00	16:00	10.75	132.83	49.93
	16:00	17:00	13.04	132.85	49.88
	17:00	18:00	15.35	134.13	49.90
	18:00	19:00	13.01	135.56	50.06
	19:00	20:00	16.74	133.66	50.06
	20:00	21:00	17.41	134.49	49.89

	21:00	22:00	-96.22	236.25	50.14
	22:00	23:00	-85.14	234.03	50.18
	23:00	0:00	-73.42	230.15	50.10
2022-07-12	0:00	1:00	-69.32	230.60	50.11
	1:00	2:00	-64.79	231.96	50.15
	2:00	3:00	-61.62	231.80	50.15
	3:00	4:00	-60.05	232.55	50.25
	4:00	5:00	-60.45	232.34	50.15
	5:00	6:00	-64.59	230.65	50.02
	6:00	7:00	-73.60	228.95	50.04
	7:00	8:00	-75.97	228.50	50.09
	8:00	9:00	-81.62	228.67	50.06
	9:00	10:00	-83.49	225.98	50.16
	10:00	11:00	-82.77	226.19	50.00
	11:00	12:00	-81.37	226.90	50.21
	12:00	13:00	-74.53	233.55	50.18
	13:00	14:00	-79.27	231.59	50.04
	14:00	15:00	-82.58	229.80	50.03
	15:00	16:00	-82.60	230.01	50.00
	16:00	17:00	-84.58	229.88	50.07
	17:00	18:00	-85.06	230.90	50.02
	18:00	19:00	-82.34	232.79	50.14
	19:00	20:00	-95.52	228.61	50.10
	20:00	21:00	-100.53	229.04	50.15
	21:00	22:00	-94.87	230.29	50.09
	22:00	23:00	-86.18	231.41	50.24
	23:00	0:00	-75.27	231.38	50.20

	21:00	22:00	15.32	136.64	50.05
	22:00	23:00	11.83	135.93	50.09
	23:00	0:00	4.08	133.02	50.13
2022-07-12	0:00	1:00	10.57	133.25	50.04
	1:00	2:00	8.52	133.85	50.06
	2:00	3:00	6.83	134.54	50.10
	3:00	4:00	7.60	135.15	50.10
	4:00	5:00	9.61	135.03	50.20
	5:00	6:00	11.01	134.50	50.10
	6:00	7:00	12.68	133.33	49.97
	7:00	8:00	13.71	132.63	49.99
	8:00	9:00	15.66	132.24	50.04
	9:00	10:00	14.94	129.86	50.01
	10:00	11:00	13.39	130.68	50.11
	11:00	12:00	15.09	131.20	49.95
	12:00	13:00	14.41	135.58	50.16
	13:00	14:00	13.99	134.58	50.13
	14:00	15:00	13.54	133.19	49.99
	15:00	16:00	11.99	133.62	49.98
	16:00	17:00	15.13	133.08	49.95
	17:00	18:00	16.62	133.13	50.02
	18:00	19:00	15.00	133.61	49.97
	19:00	20:00	18.93	132.76	50.09
	20:00	21:00	18.62	133.18	50.05
	21:00	22:00	14.43	133.28	50.10
	22:00	23:00	11.46	134.20	50.04
	23:00	0:00	8.41	134.68	50.19

2022-07-13	0:00	1:00	-70.50	231.80	50.01
	1:00	2:00	-66.26	233.45	50.19
	2:00	3:00	-62.54	234.16	50.05
	3:00	4:00	-60.09	234.21	50.05
	4:00	5:00	-61.74	234.44	50.09
	5:00	6:00	-65.75	229.45	49.91
	6:00	7:00	-74.15	227.24	50.06
	7:00	8:00	-76.02	226.19	50.33
	8:00	9:00	-82.15	223.92	50.09
	9:00	10:00	-87.27	223.73	50.03
	10:00	11:00	-89.07	224.24	50.18
	11:00	12:00	-89.12	223.80	50.17
	12:00	13:00	-89.10	223.96	50.12
	13:00	14:00	-84.42	229.19	50.12
	14:00	15:00	-87.92	224.22	49.91
	15:00	16:00	-89.93	228.75	50.13
	16:00	17:00	-86.89	229.98	49.88
	17:00	18:00	-86.64	232.34	50.04
	18:00	19:00	-84.66	233.10	50.06
	19:00	20:00	-97.51	229.02	49.59
	20:00	21:00	-103.36	232.44	50.14
	21:00	22:00	-98.23	231.73	50.21
	22:00	23:00	-86.96	231.09	50.23
	23:00	0:00	-75.69	231.24	50.12
2022-07-14	0:00	1:00	-70.92	233.15	50.03
	1:00	2:00	-66.48	233.67	50.16
	2:00	3:00	-60.37	230.76	50.15

2022-07-13	0:00	1:00	13.14	134.72	50.15
	1:00	2:00	12.98	135.95	49.96
	2:00	3:00	9.08	136.28	50.14
	3:00	4:00	6.63	136.59	50.00
	4:00	5:00	10.21	136.48	50.00
	5:00	6:00	10.92	133.81	50.04
	6:00	7:00	13.08	132.26	49.86
	7:00	8:00	12.89	131.40	50.01
	8:00	9:00	14.52	128.74	50.28
	9:00	10:00	15.82	128.16	50.04
	10:00	11:00	18.12	128.56	49.98
	11:00	12:00	16.79	128.03	50.13
	12:00	13:00	16.79	128.26	50.12
	13:00	14:00	13.73	131.41	50.07
	14:00	15:00	16.62	128.28	50.07
	15:00	16:00	17.58	134.38	49.86
	16:00	17:00	15.64	134.47	50.08
	17:00	18:00	16.67	135.72	49.83
	18:00	19:00	11.55	135.56	49.99
	19:00	20:00	15.43	133.15	50.01
	20:00	21:00	17.90	135.22	49.54
	21:00	22:00	13.90	132.96	50.09
	22:00	23:00	9.57	133.26	50.16
	23:00	0:00	5.44	133.53	50.18
2022-07-14	0:00	1:00	9.74	134.74	50.07
	1:00	2:00	9.04	135.15	49.98
	2:00	3:00	8.33	133.79	50.11

	3:00	4:00	-58.89	231.37	50.15
	4:00	5:00	-60.90	230.33	50.11
	5:00	6:00	-64.17	230.41	50.01
	6:00	7:00	-69.45	231.04	49.98
	7:00	8:00	-73.96	230.68	50.15
	8:00	9:00	-79.31	226.74	50.14
	9:00	10:00	-81.29	226.91	50.14
	10:00	11:00	-82.70	226.61	50.17
	11:00	12:00	-79.53	228.99	50.24
	12:00	13:00	-80.14	227.55	50.09
	13:00	14:00	-76.10	231.00	50.16
	14:00	15:00	-76.23	228.24	50.11
	15:00	16:00	-60.04	226.98	50.18
	16:00	17:00	-70.55	228.70	50.26
	17:00	18:00	-83.70	231.23	49.99
	18:00	19:00	-78.64	232.86	50.08
	19:00	20:00	-93.15	226.99	50.03
	20:00	21:00	-99.36	228.38	50.19
	21:00	22:00	-95.14	229.04	50.14
	22:00	23:00	-85.76	229.20	50.15
	23:00	0:00	-73.75	231.10	50.24
2022-07-15	0:00	1:00	-69.91	233.34	50.17
	1:00	2:00	-63.86	234.45	50.17
	2:00	3:00	-60.75	234.31	50.11
	3:00	4:00	-57.99	233.90	50.11
	4:00	5:00	-58.08	231.58	50.01
	5:00	6:00	-62.48	229.67	49.85
	6:00	7:00	-69.33	228.21	49.87
	7:00	8:00	-72.33	229.31	50.16

	3:00	4:00	8.61	134.75	50.10
	4:00	5:00	10.84	134.04	50.10
	5:00	6:00	11.10	134.23	50.06
	6:00	7:00	10.46	134.61	49.96
	7:00	8:00	13.86	134.33	49.93
	8:00	9:00	22.45	130.60	50.10
	9:00	10:00	25.29	128.83	50.09
	10:00	11:00	25.95	128.68	50.09
	11:00	12:00	16.53	132.01	50.12
	12:00	13:00	15.73	131.19	50.19
	13:00	14:00	13.30	133.12	50.04
	14:00	15:00	14.07	130.37	50.11
	15:00	16:00	17.27	128.93	50.06
	16:00	17:00	18.50	130.90	50.13
	17:00	18:00	18.37	132.67	50.21
	18:00	19:00	7.39	134.16	49.94
	19:00	20:00	13.40	131.99	50.03
	20:00	21:00	16.26	133.07	49.98
	21:00	22:00	15.47	133.89	50.14
	22:00	23:00	12.30	133.48	50.09
	23:00	0:00	8.15	134.19	50.10
2022-07-15	0:00	1:00	13.82	135.57	50.19
	1:00	2:00	10.15	136.12	50.12
	2:00	3:00	7.48	136.13	50.12
	3:00	4:00	5.79	135.71	50.06
	4:00	5:00	7.20	133.64	50.06
	5:00	6:00	8.56	132.46	49.96
	6:00	7:00	10.68	131.04	49.80
	7:00	8:00	12.09	133.27	49.82

	8:00	9:00	-80.66	221.91	50.04
	9:00	10:00	-86.02	223.59	50.14
	10:00	11:00	-84.81	228.35	50.25
	11:00	12:00	-88.43	222.49	49.97
	12:00	13:00	-89.55	229.06	50.15
	13:00	14:00	-83.87	233.77	50.14
	14:00	15:00	-81.69	232.98	49.97
	15:00	16:00	-83.53	231.63	50.07
	16:00	17:00	-86.42	231.72	50.15
	17:00	18:00	-88.10	232.85	50.21
	18:00	19:00	-81.89	231.64	50.09
	19:00	20:00	-95.40	227.01	50.14
	20:00	21:00	-98.59	227.69	50.04
	21:00	22:00	-95.94	232.29	50.16
	22:00	23:00	-87.09	235.15	50.11
	23:00	0:00	-74.94	231.76	50.10
2022-07-16	0:00	1:00	-70.71	232.26	50.13
	1:00	2:00	-66.04	234.54	50.15
	2:00	3:00	-61.00	232.33	50.14
	3:00	4:00	-59.42	232.04	49.94
	4:00	5:00	-60.59	231.50	49.85
	5:00	6:00	-62.12	231.65	49.90
	6:00	7:00	-64.90	230.91	49.98
	7:00	8:00	-72.40	226.98	49.99
	8:00	9:00	-82.53	225.69	49.77
	9:00	10:00	-88.95	226.97	50.05
	10:00	11:00	-87.67	228.15	50.09
	11:00	12:00	-88.31	229.79	50.12
	12:00	13:00	-87.68	231.15	50.06

	8:00	9:00	23.78	127.80	50.11
	9:00	10:00	21.16	130.12	49.99
	10:00	11:00	21.94	133.81	50.09
	11:00	12:00	22.06	127.54	50.20
	12:00	13:00	28.50	134.13	49.92
	13:00	14:00	24.89	138.00	50.10
	14:00	15:00	21.34	137.81	50.09
	15:00	16:00	22.22	137.04	49.92
	16:00	17:00	22.05	137.03	50.02
	17:00	18:00	19.88	137.77	50.10
	18:00	19:00	12.60	133.94	50.16
	19:00	20:00	15.51	131.39	50.04
	20:00	21:00	16.29	131.88	50.09
	21:00	22:00	17.37	134.89	49.99
	22:00	23:00	14.74	137.00	50.11
	23:00	0:00	8.34	135.37	50.06
2022-07-16	0:00	1:00	12.07	135.56	50.05
	1:00	2:00	10.86	136.88	50.08
	2:00	3:00	8.72	135.21	50.10
	3:00	4:00	8.36	135.04	50.09
	4:00	5:00	10.26	134.69	49.89
	5:00	6:00	12.19	134.67	49.80
	6:00	7:00	10.47	134.29	49.85
	7:00	8:00	12.68	131.43	49.93
	8:00	9:00	18.36	129.67	49.94
	9:00	10:00	20.01	130.93	49.72
	10:00	11:00	19.69	131.72	50.00
	11:00	12:00	21.10	133.65	50.04
	12:00	13:00	19.03	134.86	50.07

	13:00	14:00	-84.09	233.58	50.14
	14:00	15:00	-85.16	230.46	49.99
	15:00	16:00	-84.36	231.78	50.06
	16:00	17:00	-86.10	229.74	49.97
	17:00	18:00	-85.00	231.97	50.11
	18:00	19:00	-82.21	236.00	50.09
	19:00	20:00	-94.03	231.25	50.02
	20:00	21:00	-99.16	231.08	50.08
	21:00	22:00	-93.40	233.64	50.13
	22:00	23:00	-82.57	232.65	50.14
	23:00	0:00	-70.49	230.47	50.14
2022-07-17	0:00	1:00	-67.32	230.89	50.09
	1:00	2:00	-62.62	232.54	50.05
	2:00	3:00	-59.26	233.79	50.05
	3:00	4:00	-57.80	233.98	49.95
	4:00	5:00	-57.58	234.15	49.98
	5:00	6:00	-58.27	234.31	50.07
	6:00	7:00	-59.93	232.36	50.05
	7:00	8:00	-65.22	229.72	49.97
	8:00	9:00	-68.72	226.36	49.87
	9:00	10:00	-72.38	224.15	50.17
	10:00	11:00	-62.22	228.21	50.17
	11:00	12:00	-55.76	227.67	50.08
	12:00	13:00	-69.03	227.93	50.08
	13:00	14:00	-60.61	229.38	50.02
	14:00	15:00	-53.75	228.33	49.84
	15:00	16:00	-53.90	229.59	50.04
	16:00	17:00	-53.64	231.08	50.20
	17:00	18:00	-71.18	229.87	50.05

	13:00	14:00	17.59	135.77	50.01
	14:00	15:00	18.56	133.34	50.09
	15:00	16:00	17.17	134.23	49.94
	16:00	17:00	18.65	132.74	50.01
	17:00	18:00	16.54	133.98	49.92
	18:00	19:00	12.26	136.92	50.06
	19:00	20:00	14.71	134.72	50.04
	20:00	21:00	17.93	135.05	49.97
	21:00	22:00	15.81	136.59	50.03
	22:00	23:00	12.03	135.65	50.07
	23:00	0:00	6.20	134.50	50.09
2022-07-17	0:00	1:00	11.17	134.57	50.09
	1:00	2:00	9.53	135.50	50.04
	2:00	3:00	8.41	136.25	50.00
	3:00	4:00	8.45	136.39	50.00
	4:00	5:00	10.16	136.44	49.90
	5:00	6:00	10.62	136.60	49.93
	6:00	7:00	9.83	135.58	50.02
	7:00	8:00	11.71	133.57	50.00
	8:00	9:00	12.49	130.89	49.92
	9:00	10:00	14.69	129.73	49.82
	10:00	11:00	18.27	133.15	50.12
	11:00	12:00	16.57	131.96	50.12
	12:00	13:00	16.59	131.98	50.03
	13:00	14:00	14.26	133.11	50.03
	14:00	15:00	13.40	132.41	49.97
	15:00	16:00	14.89	133.40	49.79
	16:00	17:00	17.64	134.28	49.99
	17:00	18:00	14.97	132.87	50.15

	18:00	19:00	-74.03	230.17	49.94
	19:00	20:00	-90.48	224.45	50.04
	20:00	21:00	-96.61	223.50	50.09
	21:00	22:00	-92.08	227.49	50.17
	22:00	23:00	-78.93	233.71	50.25
	23:00	0:00	-65.82	234.03	50.15
2022-07-18	0:00	1:00	-59.88	234.38	50.08
	1:00	2:00	-55.18	235.42	50.06
	2:00	3:00	-51.56	236.10	49.92
	3:00	4:00	-51.56	236.16	50.00
	4:00	5:00	-52.51	236.62	50.11
	5:00	6:00	-56.73	234.12	49.88
	6:00	7:00	-65.68	233.15	49.94
	7:00	8:00	-69.98	231.27	50.14
	8:00	9:00	-77.13	230.39	50.08
	9:00	10:00	-83.42	230.13	50.06
	10:00	11:00	-86.13	230.82	50.02
	11:00	12:00	-88.61	229.58	49.99
	12:00	13:00	-86.69	232.13	50.13
	13:00	14:00	-81.71	235.78	50.10
	14:00	15:00	-85.10	232.47	49.95
	15:00	16:00	-86.78	231.90	50.08
	16:00	17:00	-86.68	231.96	50.13
	17:00	18:00	-87.68	232.70	50.08
	18:00	19:00	-82.69	232.71	50.17
	19:00	20:00	-95.51	226.24	50.17
	20:00	21:00	-99.87	226.82	50.20
	21:00	22:00	-94.03	230.27	50.17
	22:00	23:00	-83.36	232.33	50.24

	18:00	19:00	7.62	133.41	50.00
	19:00	20:00	14.23	130.29	49.89
	20:00	21:00	16.69	129.79	49.99
	21:00	22:00	15.11	132.80	50.04
	22:00	23:00	13.04	136.33	50.12
	23:00	0:00	7.28	136.11	50.20
2022-07-18	0:00	1:00	8.74	135.82	50.10
	1:00	2:00	7.57	136.36	50.03
	2:00	3:00	6.60	136.78	50.01
	3:00	4:00	5.93	136.66	49.87
	4:00	5:00	6.35	136.81	49.95
	5:00	6:00	7.34	135.72	50.06
	6:00	7:00	10.44	134.83	49.83
	7:00	8:00	10.66	133.53	49.89
	8:00	9:00	10.72	132.58	50.09
	9:00	10:00	13.33	133.28	50.03
	10:00	11:00	16.68	133.79	50.01
	11:00	12:00	18.75	133.24	49.97
	12:00	13:00	17.13	135.46	49.94
	13:00	14:00	14.24	136.57	50.08
	14:00	15:00	14.91	134.12	50.05
	15:00	16:00	11.93	134.96	49.90
	16:00	17:00	13.57	134.48	50.03
	17:00	18:00	15.40	134.49	50.08
	18:00	19:00	9.27	133.87	50.03
	19:00	20:00	14.92	129.34	50.12
	20:00	21:00	17.01	129.58	50.12
	21:00	22:00	13.99	132.04	50.15
	22:00	23:00	10.68	134.03	50.12

	23:00	0:00	-72.08	231.83	50.15
2022-07-19	0:00	1:00	-65.93	229.48	50.17
	1:00	2:00	-61.34	230.06	50.09
	2:00	3:00	-59.21	230.77	50.06
	3:00	4:00	-58.19	231.27	50.02
	4:00	5:00	-58.19	231.42	50.10
	5:00	6:00	-63.37	229.44	50.08
	6:00	7:00	-69.93	228.11	50.16
	7:00	8:00	-73.45	227.83	50.09
	8:00	9:00	-78.67	230.64	50.12
	9:00	10:00	-80.73	227.18	50.06
	10:00	11:00	-85.67	224.98	50.07
	11:00	12:00	-79.74	228.13	50.09
	12:00	13:00	-81.78	230.02	50.11
	13:00	14:00	-74.84	232.53	50.23
	14:00	15:00	-73.82	229.09	50.03
	15:00	16:00	-76.99	227.63	50.06
	16:00	17:00	-80.50	233.13	50.07
	17:00	18:00	-83.83	230.98	50.06
	18:00	19:00	-80.95	232.99	50.13
	19:00	20:00	-92.31	227.39	50.11
	20:00	21:00	-98.86	226.87	50.08
	21:00	22:00	-95.55	229.19	50.07
	22:00	23:00	-83.84	230.91	50.18
	23:00	0:00	-72.24	234.05	50.18
2022-07-20	0:00	1:00	-65.83	233.72	50.09
	1:00	2:00	-61.35	233.65	50.17
	2:00	3:00	-59.97	234.72	50.10

	23:00	0:00	6.75	133.94	50.19
2022-07-19	0:00	1:00	10.22	132.26	50.10
	1:00	2:00	8.12	132.63	50.12
	2:00	3:00	6.87	133.12	50.04
	3:00	4:00	7.88	133.43	50.01
	4:00	5:00	8.53	133.56	49.97
	5:00	6:00	9.84	132.49	50.05
	6:00	7:00	9.33	131.66	50.03
	7:00	8:00	12.24	131.02	50.10
	8:00	9:00	13.21	132.02	50.04
	9:00	10:00	15.31	129.33	50.07
	10:00	11:00	17.55	127.11	50.01
	11:00	12:00	18.08	128.13	50.02
	12:00	13:00	18.22	129.83	50.04
	13:00	14:00	14.54	132.08	50.06
	14:00	15:00	13.17	130.32	50.18
	15:00	16:00	15.09	129.48	49.98
	16:00	17:00	18.81	137.47	50.01
	17:00	18:00	25.69	134.29	50.02
	18:00	19:00	13.16	134.57	50.01
	19:00	20:00	14.34	130.60	50.08
	20:00	21:00	16.84	130.50	50.06
	21:00	22:00	16.08	132.85	50.03
	22:00	23:00	12.51	133.32	50.01
	23:00	0:00	7.68	135.49	50.13
2022-07-20	0:00	1:00	10.08	135.22	50.13
	1:00	2:00	7.09	135.33	50.04
	2:00	3:00	7.03	135.82	50.12

	3:00	4:00	-60.55	233.89	50.16
	4:00	5:00	-61.55	230.38	49.92
	5:00	6:00	-66.64	229.07	49.91
	6:00	7:00	-74.76	227.28	49.96
	7:00	8:00	-76.45	226.81	50.16
	8:00	9:00	-82.71	228.96	50.03
	9:00	10:00	-87.29	226.31	50.09
	10:00	11:00	-91.36	225.91	50.22
	11:00	12:00	-90.57	226.26	50.14
	12:00	13:00	-91.76	225.07	50.15
	13:00	14:00	-88.32	227.51	50.14
	14:00	15:00	-86.63	225.05	50.03
	15:00	16:00	-75.68	224.21	49.92
	16:00	17:00	-61.89	230.69	50.09
	17:00	18:00	-61.23	230.46	50.13
	18:00	19:00	-70.57	228.46	50.05
	19:00	20:00	-94.85	225.14	50.07
	20:00	21:00	-98.69	226.45	50.19
	21:00	22:00	-92.89	225.68	50.19
	22:00	23:00	-80.61	229.62	50.19
	23:00	0:00	-68.81	228.16	50.09
2022-07-21	0:00	1:00	-61.78	231.50	50.08
	1:00	2:00	-58.07	234.30	50.12
	2:00	3:00	-59.91	230.66	50.04
	3:00	4:00	-58.52	231.68	49.99
	4:00	5:00	-55.55	232.02	50.11
	5:00	6:00	-60.79	227.32	49.88
	6:00	7:00	-68.97	225.25	50.00
	7:00	8:00	-75.68	227.44	50.30

	3:00	4:00	10.51	135.30	50.05
	4:00	5:00	12.56	132.60	50.11
	5:00	6:00	14.30	131.97	49.87
	6:00	7:00	15.80	130.67	49.86
	7:00	8:00	17.12	130.15	49.91
	8:00	9:00	17.63	130.83	50.11
	9:00	10:00	16.45	128.78	49.98
	10:00	11:00	19.86	130.48	50.04
	11:00	12:00	17.97	131.80	50.17
	12:00	13:00	16.60	131.02	50.09
	13:00	14:00	18.24	132.57	50.10
	14:00	15:00	12.60	131.47	50.09
	15:00	16:00	15.58	130.06	49.98
	16:00	17:00	15.10	134.73	49.87
	17:00	18:00	15.03	133.37	50.04
	18:00	19:00	15.18	131.14	50.08
	19:00	20:00	22.31	130.53	50.00
	20:00	21:00	23.44	131.69	50.02
	21:00	22:00	17.32	129.07	50.14
	22:00	23:00	10.67	131.95	50.14
	23:00	0:00	7.35	131.45	50.14
2022-07-21	0:00	1:00	10.44	133.29	50.04
	1:00	2:00	10.49	135.32	50.03
	2:00	3:00	9.04	133.43	50.07
	3:00	4:00	8.98	133.92	49.99
	4:00	5:00	10.39	134.15	49.94
	5:00	6:00	11.58	131.36	50.06
	6:00	7:00	10.97	129.66	49.83
	7:00	8:00	13.18	130.71	49.95

	8:00	9:00	-82.25	228.36	50.02
	9:00	10:00	-87.71	226.80	50.16
	10:00	11:00	-72.82	228.56	50.05
	11:00	12:00	-66.24	229.17	50.00
	12:00	13:00	-82.17	230.17	50.06
	13:00	14:00	-70.83	234.21	50.03
	14:00	15:00	-66.91	231.21	49.92
	15:00	16:00	-77.96	232.79	50.06
	16:00	17:00	-76.93	234.71	50.11
	17:00	18:00	-61.53	234.93	50.08
	18:00	19:00	-59.34	233.85	50.17
	19:00	20:00	-83.25	227.82	50.05
	20:00	21:00	-97.99	230.25	50.18
	21:00	22:00	-96.34	232.29	50.18
	22:00	23:00	-86.28	232.20	50.15
	23:00	0:00	-73.48	227.68	50.07
2022-07-22	0:00	1:00	-68.85	229.86	50.13
	1:00	2:00	-64.13	231.02	50.10
	2:00	3:00	-57.62	232.86	50.04
	3:00	4:00	-56.48	233.41	50.01
	4:00	5:00	-59.69	232.10	49.98
	5:00	6:00	-66.51	229.27	49.96
	6:00	7:00	-71.84	228.30	50.04
	7:00	8:00	-76.05	226.07	50.17
	8:00	9:00	-83.59	225.87	50.05
	9:00	10:00	-86.23	228.98	50.23
	10:00	11:00	-87.74	227.28	50.02
	11:00	12:00	-88.37	226.26	50.06
	12:00	13:00	-86.91	227.28	50.17

	8:00	9:00	17.91	131.22	50.25
	9:00	10:00	19.53	131.23	49.97
	10:00	11:00	17.91	132.52	50.11
	11:00	12:00	18.89	132.70	50.00
	12:00	13:00	20.18	132.86	49.95
	13:00	14:00	16.81	134.55	50.01
	14:00	15:00	17.24	132.29	49.98
	15:00	16:00	21.46	132.74	49.87
	16:00	17:00	22.05	134.02	50.01
	17:00	18:00	23.03	134.11	50.06
	18:00	19:00	19.75	134.38	50.03
	19:00	20:00	20.22	131.13	50.12
	20:00	21:00	17.96	132.76	50.00
	21:00	22:00	18.91	134.74	50.13
	22:00	23:00	13.22	134.83	50.13
	23:00	0:00	5.08	131.38	50.10
2022-07-22	0:00	1:00	11.41	132.66	50.02
	1:00	2:00	11.74	133.23	50.08
	2:00	3:00	8.62	134.50	50.05
	3:00	4:00	8.45	135.06	49.99
	4:00	5:00	10.70	134.43	49.96
	5:00	6:00	11.76	133.03	49.93
	6:00	7:00	10.41	132.23	49.91
	7:00	8:00	14.26	130.57	49.99
	8:00	9:00	17.36	129.26	50.12
	9:00	10:00	16.97	132.28	50.00
	10:00	11:00	18.63	132.23	50.18
	11:00	12:00	20.77	131.44	49.97
	12:00	13:00	19.67	131.83	50.01

	13:00	14:00	-79.95	233.04	50.08
	14:00	15:00	-84.01	227.95	50.14
	15:00	16:00	-82.16	227.21	49.86
	16:00	17:00	-83.46	230.60	50.06
	17:00	18:00	-82.52	232.63	50.19
	18:00	19:00	-81.04	233.94	0.00
	19:00	20:00	-93.86	229.60	50.07
	20:00	21:00	-99.83	231.35	50.24
	21:00	22:00	-95.05	232.43	50.19
	22:00	23:00	-83.96	230.98	50.19
	23:00	0:00	-75.77	230.43	50.20
2022-07-23	0:00	1:00	-69.41	229.71	50.07
	1:00	2:00	-64.31	231.21	50.11
	2:00	3:00	-58.89	233.21	50.08
	3:00	4:00	-58.73	233.07	50.08
	4:00	5:00	-55.98	234.77	50.13
	5:00	6:00	-58.25	232.46	50.05
	6:00	7:00	-64.00	229.27	50.08
	7:00	8:00	-72.20	224.28	50.02
	8:00	9:00	-77.30	228.15	50.12
	9:00	10:00	-76.41	231.97	50.04
	10:00	11:00	-76.60	230.32	49.99
	11:00	12:00	-68.63	230.95	50.15
	12:00	13:00	-53.82	233.68	50.19
	13:00	14:00	-52.11	233.75	50.21
	14:00	15:00	-54.47	229.92	50.01
	15:00	16:00	-55.71	230.26	49.98
	16:00	17:00	-55.52	233.31	50.12
	17:00	18:00	-53.07	231.68	49.98

	13:00	14:00	18.07	62.44	50.12
	14:00	15:00	17.33	63.66	50.03
	15:00	16:00	17.54	63.23	50.09
	16:00	17:00	17.74	132.58	49.81
	17:00	18:00	19.64	134.96	50.01
	18:00	19:00	15.18	134.21	50.14
	19:00	20:00	19.44	131.89	0.00
	20:00	21:00	21.52	133.20	50.02
	21:00	22:00	16.39	133.41	50.19
	22:00	23:00	11.87	132.93	50.14
	23:00	0:00	8.32	132.74	50.14
2022-07-23	0:00	1:00	13.68	132.13	50.15
	1:00	2:00	13.61	132.86	50.02
	2:00	3:00	12.39	134.57	50.06
	3:00	4:00	9.51	134.40	50.03
	4:00	5:00	11.67	135.33	50.03
	5:00	6:00	11.53	134.44	50.08
	6:00	7:00	9.35	133.42	50.00
	7:00	8:00	12.79	129.13	50.03
	8:00	9:00	18.97	130.38	49.97
	9:00	10:00	18.78	133.33	50.07
	10:00	11:00	17.13	132.95	49.99
	11:00	12:00	17.93	134.00	49.94
	12:00	13:00	19.10	135.73	50.10
	13:00	14:00	20.10	133.73	50.14
	14:00	15:00	19.62	131.56	50.16
	15:00	16:00	18.72	133.02	49.96
	16:00	17:00	17.98	135.44	49.93
	17:00	18:00	14.81	131.29	50.07

	18:00	19:00	-52.59	234.39	50.13
	19:00	20:00	-64.93	228.69	50.12
	20:00	21:00	-93.20	230.46	50.17
	21:00	22:00	-90.85	232.10	50.20
	22:00	23:00	-82.82	231.34	50.19
	23:00	0:00	-71.70	231.37	50.14
2022-07-24	0:00	1:00	-63.73	233.91	50.13
	1:00	2:00	-59.28	234.73	50.19
	2:00	3:00	-55.37	232.11	50.11
	3:00	4:00	-53.57	233.03	50.15
	4:00	5:00	-51.42	234.11	50.19
	5:00	6:00	-53.16	234.46	50.23
	6:00	7:00	-55.69	232.58	50.19
	7:00	8:00	-62.70	229.69	50.10
	8:00	9:00	-66.17	225.46	49.92
	9:00	10:00	-61.70	220.29	50.01
	10:00	11:00	-57.83	220.65	50.24
	11:00	12:00	-46.04	224.93	50.19
	12:00	13:00	-23.96	232.18	50.11
	13:00	14:00	-24.39	235.20	50.15
	14:00	15:00	-23.64	232.98	49.93
	15:00	16:00	-17.17	232.08	50.09
	16:00	17:00	-16.85	231.89	49.98
	17:00	18:00	-16.59	232.16	49.95
	18:00	19:00	-32.95	226.15	50.05
	19:00	20:00	-57.84	226.90	49.93
	20:00	21:00	-66.82	226.43	50.06
	21:00	22:00	-79.27	231.19	50.13
	22:00	23:00	-76.45	235.45	50.26

	18:00	19:00	12.59	133.07	49.93
	19:00	20:00	22.09	129.91	50.08
	20:00	21:00	19.51	133.57	50.07
	21:00	22:00	16.56	135.17	50.12
	22:00	23:00	13.59	134.45	50.15
	23:00	0:00	8.97	133.78	50.14
2022-07-24	0:00	1:00	8.25	135.55	50.09
	1:00	2:00	8.57	136.18	50.08
	2:00	3:00	7.18	134.56	50.13
	3:00	4:00	6.67	135.16	50.06
	4:00	5:00	4.75	135.89	50.10
	5:00	6:00	7.56	136.16	50.14
	6:00	7:00	4.53	135.06	50.18
	7:00	8:00	9.95	132.57	50.14
	8:00	9:00	16.02	132.00	50.05
	9:00	10:00	18.13	128.98	49.87
	10:00	11:00	0.00	0.00	49.96
	11:00	12:00	0.00	0.00	50.19
	12:00	13:00	0.00	0.00	50.14
	13:00	14:00	0.00	0.00	50.06
	14:00	15:00	0.00	0.00	50.10
	15:00	16:00	0.00	0.00	49.88
	16:00	17:00	0.00	0.00	50.04
	17:00	18:00	0.00	0.00	49.93
	18:00	19:00	0.00	9.63	49.90
	19:00	20:00	15.42	133.34	50.00
	20:00	21:00	16.66	130.47	49.88
	21:00	22:00	17.55	133.59	50.01
	22:00	23:00	11.30	136.01	50.08

	23:00	0:00	-63.31	234.87	50.19
2022-07-25	0:00	1:00	-60.54	233.15	50.15
	1:00	2:00	-55.42	234.30	50.11
	2:00	3:00	-54.63	234.07	49.96
	3:00	4:00	-54.45	234.02	50.00
	4:00	5:00	-54.91	233.88	50.01
	5:00	6:00	-60.80	230.75	49.96
	6:00	7:00	-67.88	227.94	50.00
	7:00	8:00	-70.34	228.51	50.16
	8:00	9:00	-74.44	227.63	50.07
	9:00	10:00	-80.88	225.76	49.96
	10:00	11:00	-88.00	225.61	50.15
	11:00	12:00	-87.14	224.04	50.02
	12:00	13:00	-84.62	226.39	50.09
	13:00	14:00	-80.72	232.69	50.16
	14:00	15:00	-82.74	227.40	49.91
	15:00	16:00	-84.25	226.84	50.03
	16:00	17:00	-77.35	229.18	50.04
	17:00	18:00	-66.53	229.47	50.17
	18:00	19:00	-74.43	231.86	50.07
	19:00	20:00	-94.78	225.82	50.10
	20:00	21:00	-97.68	231.28	50.07
	21:00	22:00	-94.82	230.23	50.14
	22:00	23:00	-83.11	227.50	50.17
	23:00	0:00	-71.69	227.58	50.14
2022-07-26	0:00	1:00	-63.95	229.47	50.05
	1:00	2:00	-61.62	230.84	50.15
	2:00	3:00	-59.77	231.39	49.97

	23:00	0:00	8.57	136.63	50.20
2022-07-25	0:00	1:00	11.75	135.36	50.14
	1:00	2:00	10.52	135.85	50.10
	2:00	3:00	10.14	135.73	50.06
	3:00	4:00	10.32	135.55	49.91
	4:00	5:00	9.58	135.58	49.95
	5:00	6:00	11.75	133.55	49.96
	6:00	7:00	12.89	130.88	49.91
	7:00	8:00	14.58	131.19	49.95
	8:00	9:00	14.32	130.18	50.11
	9:00	10:00	15.82	129.90	50.02
	10:00	11:00	16.62	130.76	49.91
	11:00	12:00	21.15	130.23	50.10
	12:00	13:00	21.83	132.72	49.97
	13:00	14:00	19.06	137.27	50.04
	14:00	15:00	17.24	133.68	50.11
	15:00	16:00	18.74	133.14	49.86
	16:00	17:00	19.41	134.76	49.98
	17:00	18:00	19.57	135.27	49.99
	18:00	19:00	15.38	136.25	50.12
	19:00	20:00	18.97	132.65	50.02
	20:00	21:00	20.06	136.85	50.05
	21:00	22:00	18.28	135.27	50.02
	22:00	23:00	11.61	132.59	50.09
	23:00	0:00	7.42	132.29	50.12
2022-07-26	0:00	1:00	13.01	132.86	50.09
	1:00	2:00	13.29	133.80	50.00
	2:00	3:00	10.15	134.50	50.10

	3:00	4:00	-58.79	231.59	49.98
	4:00	5:00	-61.54	230.13	49.92
	5:00	6:00	-66.22	228.04	49.92
	6:00	7:00	-74.50	226.98	50.07
	7:00	8:00	-80.49	225.52	50.07
	8:00	9:00	-76.57	226.93	49.89
	9:00	10:00	-77.75	226.66	50.11
	10:00	11:00	-90.06	224.67	50.04
	11:00	12:00	-93.83	225.04	50.09
	12:00	13:00	-91.96	228.84	50.11
	13:00	14:00	-85.95	228.46	50.22
	14:00	15:00	-85.31	226.01	49.95
	15:00	16:00	-85.87	227.10	50.06
	16:00	17:00	-87.18	229.87	50.17
	17:00	18:00	-88.14	231.58	50.09
	18:00	19:00	-69.20	234.47	50.04
	19:00	20:00	-71.92	228.53	50.00
	20:00	21:00	-73.26	234.78	50.34
	21:00	22:00	-82.63	230.06	50.20
	22:00	23:00	-78.06	232.29	50.21
	23:00	0:00	-66.80	232.99	50.16
2022-07-27	0:00	1:00	-61.04	230.30	50.07
	1:00	2:00	-58.23	231.27	50.09
	2:00	3:00	-60.20	231.63	49.96
	3:00	4:00	-59.60	232.61	50.04
	4:00	5:00	-60.47	232.56	50.06
	5:00	6:00	-64.79	231.10	49.93
	6:00	7:00	-70.89	230.03	49.97
	7:00	8:00	-79.74	225.76	50.14

	3:00	4:00	8.76	134.61	49.92
	4:00	5:00	12.50	133.53	49.93
	5:00	6:00	12.08	131.98	49.87
	6:00	7:00	14.25	131.03	49.87
	7:00	8:00	18.98	131.21	50.02
	8:00	9:00	16.50	131.85	50.02
	9:00	10:00	18.29	132.22	49.84
	10:00	11:00	21.08	131.15	50.06
	11:00	12:00	24.98	131.68	49.99
	12:00	13:00	20.92	134.13	50.04
	13:00	14:00	17.67	131.68	50.06
	14:00	15:00	16.66	129.72	50.16
	15:00	16:00	20.00	131.42	49.90
	16:00	17:00	22.27	134.04	50.01
	17:00	18:00	22.67	135.08	50.12
	18:00	19:00	21.68	136.48	50.04
	19:00	20:00	25.08	131.52	49.99
	20:00	21:00	28.23	135.69	49.95
	21:00	22:00	18.63	133.75	50.29
	22:00	23:00	13.53	135.25	50.15
	23:00	0:00	9.44	135.73	50.16
2022-07-27	0:00	1:00	12.19	134.05	50.11
	1:00	2:00	12.14	134.63	50.02
	2:00	3:00	9.51	134.74	50.04
	3:00	4:00	9.43	135.35	49.91
	4:00	5:00	10.22	135.30	49.99
	5:00	6:00	12.39	134.40	50.01
	6:00	7:00	11.73	133.76	49.88
	7:00	8:00	16.51	130.21	49.92

	8:00	9:00	-78.88	229.01	50.01
	9:00	10:00	-76.40	225.79	50.05
	10:00	11:00	-89.89	228.11	50.15
	11:00	12:00	-90.34	228.01	50.08
	12:00	13:00	-89.54	229.59	50.12
	13:00	14:00	-87.70	232.71	50.12
	14:00	15:00	-89.21	230.66	49.98
	15:00	16:00	-67.79	226.19	50.07
	16:00	17:00	-67.57	226.38	50.06
	17:00	18:00	-66.72	229.13	50.00
	18:00	19:00	-65.61	231.69	50.02
	19:00	20:00	-70.97	228.57	49.95
	20:00	21:00	-75.70	232.52	50.36
	21:00	22:00	-95.63	232.67	50.22
	22:00	23:00	-87.34	234.05	50.18
	23:00	0:00	-77.05	233.49	50.12
2022-07-28	0:00	1:00	-70.05	233.70	50.16
	1:00	2:00	-66.21	233.93	50.19
	2:00	3:00	-62.48	234.20	50.07
	3:00	4:00	-59.28	235.16	50.13
	4:00	5:00	-58.91	235.19	50.06
	5:00	6:00	-62.68	232.93	49.83
	6:00	7:00	-71.99	230.91	50.01
	7:00	8:00	-78.99	228.76	50.22
	8:00	9:00	-86.84	225.50	50.15
	9:00	10:00	-93.31	227.34	50.05
	10:00	11:00	-94.41	225.82	50.08
	11:00	12:00	-94.26	225.93	50.08
	12:00	13:00	-92.18	228.97	50.19

	8:00	9:00	16.19	132.15	50.09
	9:00	10:00	19.12	131.17	49.96
	10:00	11:00	20.46	133.14	50.00
	11:00	12:00	21.06	133.27	50.10
	12:00	13:00	20.49	134.19	50.03
	13:00	14:00	20.10	136.41	50.07
	14:00	15:00	18.02	135.54	50.07
	15:00	16:00	20.11	131.47	49.93
	16:00	17:00	19.50	131.65	50.02
	17:00	18:00	20.62	133.53	50.01
	18:00	19:00	22.84	134.56	49.95
	19:00	20:00	23.58	132.59	49.97
	20:00	21:00	24.40	134.14	49.90
	21:00	22:00	22.64	134.59	50.30
	22:00	23:00	16.95	135.88	50.17
	23:00	0:00	11.22	135.87	50.13
2022-07-28	0:00	1:00	13.75	135.99	50.07
	1:00	2:00	12.49	135.98	50.11
	2:00	3:00	12.68	135.94	50.14
	3:00	4:00	12.59	136.55	50.02
	4:00	5:00	12.10	136.53	50.08
	5:00	6:00	12.11	135.16	50.01
	6:00	7:00	15.08	134.01	49.78
	7:00	8:00	17.13	132.68	49.96
	8:00	9:00	18.40	130.17	50.17
	9:00	10:00	20.67	132.10	50.10
	10:00	11:00	18.89	132.13	50.00
	11:00	12:00	16.86	131.92	50.03
	12:00	13:00	17.04	133.77	50.03

	13:00	14:00	-86.09	233.26	50.07
	14:00	15:00	-89.06	228.64	50.07
	15:00	16:00	-87.57	228.99	50.08
	16:00	17:00	-87.58	227.83	49.91
	17:00	18:00	-89.18	231.11	50.12
	18:00	19:00	-69.51	231.97	50.01
	19:00	20:00	-84.71	230.28	49.82
	20:00	21:00	-90.68	231.56	50.18
	21:00	22:00	-88.97	226.23	50.20
	22:00	23:00	-81.44	228.33	50.14
	23:00	0:00	-71.29	226.99	50.09
2022-07-29	0:00	1:00	-66.91	228.84	50.04
	1:00	2:00	-61.99	228.44	49.94
	2:00	3:00	-58.47	230.45	50.14
	3:00	4:00	-58.79	229.63	50.01
	4:00	5:00	-58.09	229.83	49.99
	5:00	6:00	-62.33	227.46	49.89
	6:00	7:00	-67.44	227.74	50.15
	7:00	8:00	-73.22	226.42	50.08
	8:00	9:00	-85.21	225.96	50.00
	9:00	10:00	-89.01	228.55	50.13
	10:00	11:00	-91.95	231.51	50.21
	11:00	12:00	-87.36	228.17	50.05
	12:00	13:00	-87.95	228.74	50.03
	13:00	14:00	-85.05	234.54	50.12
	14:00	15:00	-81.00	235.05	50.10
	15:00	16:00	-80.97	234.97	50.22
	16:00	17:00	-67.37	230.07	50.02
	17:00	18:00	-60.67	231.37	50.02

	13:00	14:00	14.94	136.04	50.13
	14:00	15:00	14.49	132.72	50.02
	15:00	16:00	15.42	132.73	50.02
	16:00	17:00	14.42	132.22	50.03
	17:00	18:00	16.47	134.84	49.86
	18:00	19:00	14.68	134.50	50.07
	19:00	20:00	21.79	133.95	49.96
	20:00	21:00	18.87	134.47	49.77
	21:00	22:00	14.37	131.45	50.13
	22:00	23:00	8.75	132.91	50.15
	23:00	0:00	4.61	132.15	50.09
2022-07-29	0:00	1:00	10.82	132.88	50.04
	1:00	2:00	9.14	132.13	49.99
	2:00	3:00	5.10	133.46	49.89
	3:00	4:00	7.04	133.05	50.09
	4:00	5:00	6.82	133.23	49.96
	5:00	6:00	7.94	131.85	49.94
	6:00	7:00	7.72	131.85	49.85
	7:00	8:00	12.04	130.87	50.10
	8:00	9:00	17.59	129.96	50.03
	9:00	10:00	18.99	132.44	49.95
	10:00	11:00	16.99	134.43	50.08
	11:00	12:00	11.37	131.83	50.16
	12:00	13:00	9.11	132.31	50.00
	13:00	14:00	8.59	135.93	49.98
	14:00	15:00	6.94	136.36	50.07
	15:00	16:00	7.77	136.28	50.05
	16:00	17:00	11.69	133.27	50.17
	17:00	18:00	12.84	133.88	49.97

	18:00	19:00	-56.24	237.97	50.07
	19:00	20:00	-61.74	235.00	49.96
	20:00	21:00	-63.99	234.81	50.10
	21:00	22:00	-58.44	229.84	50.09
	22:00	23:00	-50.11	231.63	50.20
	23:00	0:00	-43.46	232.77	50.16
2022-07-30	0:00	1:00	-40.93	232.43	50.10
	1:00	2:00	-37.36	232.13	49.95
	2:00	3:00	-41.06	232.79	50.10
	3:00	4:00	-49.60	232.80	50.03
	4:00	5:00	-47.31	233.92	50.00
	5:00	6:00	-48.40	233.62	50.01
	6:00	7:00	-53.01	231.58	49.96
	7:00	8:00	-62.35	228.53	50.05
	8:00	9:00	-76.36	227.49	50.08
	9:00	10:00	-78.36	230.72	50.21
	10:00	11:00	-77.04	224.90	50.04
	11:00	12:00	-83.90	225.74	50.19
	12:00	13:00	-82.00	225.00	50.09
	13:00	14:00	-78.28	228.27	50.17
	14:00	15:00	-80.55	225.42	50.05
	15:00	16:00	-83.29	227.52	50.22
	16:00	17:00	-79.34	230.27	50.20
	17:00	18:00	-76.25	232.70	49.97
	18:00	19:00	-72.46	230.48	50.16
	19:00	20:00	-61.65	226.62	50.08
	20:00	21:00	-64.20	229.53	50.05
	21:00	22:00	-60.94	233.40	50.18
	22:00	23:00	-54.46	230.25	50.22

	18:00	19:00	10.08	138.05	49.97
	19:00	20:00	7.67	136.20	50.02
	20:00	21:00	5.07	136.77	49.91
	21:00	22:00	2.79	132.54	50.05
	22:00	23:00	-0.36	133.59	50.04
	23:00	0:00	-3.32	134.50	50.15
2022-07-30	0:00	1:00	-0.63	134.09	50.11
	1:00	2:00	-4.48	133.97	50.05
	2:00	3:00	-5.03	134.33	49.90
	3:00	4:00	-6.44	134.41	50.05
	4:00	5:00	-6.38	135.18	49.98
	5:00	6:00	-5.69	134.93	49.95
	6:00	7:00	-7.25	132.86	49.96
	7:00	8:00	-6.50	131.62	49.91
	8:00	9:00	11.15	132.12	50.00
	9:00	10:00	11.86	133.13	50.03
	10:00	11:00	3.62	129.18	50.16
	11:00	12:00	13.34	131.34	49.99
	12:00	13:00	9.07	130.97	50.14
	13:00	14:00	2.16	132.89	50.04
	14:00	15:00	5.20	131.23	50.12
	15:00	16:00	9.12	132.46	50.00
	16:00	17:00	4.62	134.77	50.17
	17:00	18:00	3.88	135.58	50.15
	18:00	19:00	-2.85	133.34	49.92
	19:00	20:00	-1.79	131.20	50.11
	20:00	21:00	-0.36	133.18	50.03
	21:00	22:00	-3.79	136.91	50.00
	22:00	23:00	-8.63	134.67	50.13

	23:00	0:00	-46.82	227.08	50.06
2022-07-31	0:00	1:00	-42.49	230.68	50.12
	1:00	2:00	-35.89	232.45	50.18
	2:00	3:00	-32.42	228.50	49.93
	3:00	4:00	-30.90	223.41	49.91
	4:00	5:00	-30.21	224.13	50.03
	5:00	6:00	-31.73	223.97	50.09
	6:00	7:00	-32.99	223.34	50.11
	7:00	8:00	-38.06	223.93	50.03
	8:00	9:00	-54.76	221.54	49.96
	9:00	10:00	-68.60	223.67	49.99
	10:00	11:00	-67.63	223.23	50.33
	11:00	12:00	-68.54	221.89	50.19
	12:00	13:00	-68.02	221.73	49.99
	13:00	14:00	-65.72	222.33	50.23
	14:00	15:00	-63.61	222.54	50.05
	15:00	16:00	-63.87	223.92	49.98
	16:00	17:00	-60.86	227.24	50.10
	17:00	18:00	-60.28	227.16	50.13
	18:00	19:00	-64.52	226.53	50.06
	19:00	20:00	-68.44	224.41	50.09
	20:00	21:00	-62.64	227.92	50.13
	21:00	22:00	-55.90	229.73	50.14
	22:00	23:00	-50.38	229.74	50.10
	23:00	0:00	-40.50	227.01	50.18

	23:00	0:00	-8.60	131.47	50.17
2022-07-31	0:00	1:00	-9.58	134.40	50.01
	1:00	2:00	-9.61	133.97	50.07
	2:00	3:00	-9.99	131.98	50.13
	3:00	4:00	-8.99	131.02	49.88
	4:00	5:00	-9.63	131.66	49.86
	5:00	6:00	-9.75	131.60	49.98
	6:00	7:00	-9.18	131.26	50.04
	7:00	8:00	-5.77	132.51	50.06
	8:00	9:00	-1.09	131.57	49.98
	9:00	10:00	-0.51	132.43	49.91
	10:00	11:00	0.00	129.80	49.94
	11:00	12:00	0.00	129.25	50.28
	12:00	13:00	0.00	129.18	50.14
	13:00	14:00	0.00	129.60	49.94
	14:00	15:00	0.00	129.36	50.18
	15:00	16:00	0.00	130.16	50.00
	16:00	17:00	0.00	132.27	49.93
	17:00	18:00	0.00	132.16	50.05
	18:00	19:00	0.00	131.94	50.08
	19:00	20:00	5.40	132.15	50.01
	20:00	21:00	4.93	135.31	50.04
	21:00	22:00	-0.55	135.13	50.08
	22:00	23:00	-1.74	134.05	50.09
	23:00	0:00	-6.07	132.40	50.05

Bujagali - Kawanda									
Nominal Voltage (kV)	**Route Length (km)**	**No. of circuits**	**Circuit Length (km)**	**No. of structures**	**Type**	**In service date**	**Line Age (yrs)**	**Line Rating (MVA) per circuit**	**Conductor Type**
220	72	2	144	212	Steel tower	2012	2021	205.8	DIN AAAC/

Masaka West - Mbarara North									
Nominal Voltage (kV)	**Route Length (km)**	**No. of circuits**	**Circuit Length (km)**	**No. of structures**	**Type**	**In service date**	**Line Age (yrs)**	**Line Rating (MVA) per circuit**	**Conductor Type**
132	130.5	1	130.5	407	tower	1995	58	151.6	ACSR Goat

APPENDIX X: EXPERIMENTAL ASSESSMENT PHOTOGRAPHS














DT9205A
42.4
HOLD
AUTO POWER OFF
COM
V/Ω
20A
mA


28.8
DIGITAL THERMOMETER
POWER
°C/°F/K
HOLD
MAX/MIN/AVG
T1/T2
T1−T2
Microprocessor


SOLAR POWER METER
801.0
W/B
HOLD
SM206-SOLAR


0.000
26.9
SMART SENSOR



